Development of a reference method based on the fast multipole boundary element method for sound propagation problems in urban environments : formalism, improvements & applications

Xavier Vuylsteke

UNIVERSITÉ PARIS-EST

École doctorale Sciences, Ingénierie et Environnement

Thèse de doctorat

Spécialité : Mécanique

Xavier VUYLSTEKE

Development of a reference method based on the fast multipole boundary element method for sound propagation problems in urban environments: formalism, optimizations & applications

---

Développement d'une méthode de référence basée sur la méthode par éléments de frontières multipolaires pour la propagation sonore en environnements urbains : formalisme, optimisations & applications

---

Soutenue publiquement le 10 décembre 2014 devant un jury composé de :

M. Marc BONNET	Président du jury
M. Philippe JEAN	Co-directeur
M. Thomas LEISSING	Encadrant
M. Martin OCHMANN	Rapporteur
M. Jean-François SEMBLAT	Directeur de thèse
M. Judicaël PICAUT	Rapporteur

Remerciements

- Je tenais tout d'abord à remercier Thomas Leissing et Philippe Jean ainsi que mon directeur de thÃ¨se Jean-François Semblat pour avoir cru en moi au début de se projet et m'avoir guidé durant ces 3 années de thèse.
- Merci également á Jérome Defrance de m'avoir accueilli au sein de sa division et pour sa disponibilité.
- Merci aussi à Pascal Ducruet, Catherine Guigou, Dirk Van Maercke, Julien Maillard, Isabelle Schmich et Pierre Verri pour leur accueil toujours convivial et leur bonne humeur.
- Merci à nos collaborateurs de Berlin: Martin Ochmann, Ralf Burgschweiger et Rafael Piscoya de nous avoir reçu très chaleureusement à chacun de nos déplacements.
- Merci à tous les membres du jury.
- Merci encore à mes amis Simon bailhache, Alexandre Jolibois, Jan Jagla, Nicolas Picart, Jérémy Rouch ainsi qu'à mon ancien co-burean Faouzi koussa et mon plus récent co-bureau Corentin Coguenanff pour leurs convivialités et les nombreuses soirées passées en leur compagnie.
- Merci de même à mes anciens collègues de promo de l'université du Maine: Baptiste Bergeot et Mathieu Rupin pour le souvenir des soirées *pizza-pinard*.
- Merci à mes amis de Grenoble: Louis, Martin, Jan, Konstantin, Lou, Ronan et Ronan, Nicolas et Adrien.
- Merci de plus à tous mes amis de Nantes: Baptiste, Julien, Juliette, Thibaud, Kevin, Sylvain, Bruno, Mathieu et à ceux un peu moins de Nantes: Baptiste, Armelle et Gabin, Clair et Simon, Clément.
- Enfin merci à mes parents qui m'ont permis d'arriver jusqu'ici et à mes deux petits frères Sylvain et Yann.
- À Amandine . . .

Development of a reference method based on the fast multipole boundary element method for sound propagation problems in urban environments: formalism, optimizations & applications

Described as one of the best ten algorithms of the 20th century, the fast multipole formalism applied to the boundary element method allows to handle large problems which were inconceivable only a few years ago. Thus, the motivation of the present work is to assess the ability, as well as the benefits in term of computational resources provided by the application of this formalism to the boundary element method, for solving sound propagation problems and providing reference solutions, in three dimensional dense urban environments, in the aim of assessing or improving fast engineering tools.

We first introduce the mathematical background required for the derivation of the boundary integral equation, for solving sound propagation problems in unbounded domains. We discuss the conventional and hyper-singular boundary integral equation to overcome the numerical artifact of fictitious eigen-frequencies, when solving exterior problems. We then make a brief historical and technical overview of the fast multipole principle and introduce the mathematical tools required to expand the elementary solution of the Helmholtz equation and describe the main steps, from a numerical viewpoint, of fast multipole calculations.

A sound propagation problem in a city block made of 5 buildings allows us to highlight instabilities in the recursive computation of translation matrices, resulting in discontinuities of the surface pressure and a no convergence of the iterative solver. This observation leads us to consider the very recent work of Gumerov & Duraiswamy, related to a "stable" recursive computation of rotation matrices coefficients in the RCR decomposition. This new improved algorithm has been subsequently assessed successfully on a multi scattering problem up to a dimensionless domain size equal to 207 wavelengths.

We finally performed comparisons between a BEM algorithm, *Micado3D*, the FMBEM algorithm and a ray tracing algorithm, Icare®, for the calculation of averaged pressure levels in an opened and closed court yards. The fast multipole algorithm allowed to validate the results computed with Icare in the opened court yard up to 300 Hz, (i.e. 100 wavelengths), while in the closed court yard, a very sensitive area without direct or reflective fields, further investigations related to the preconditioning seem required to ensure reliable solutions provided by iterative solver based algorithms.

Keywords: Boundary element method, fast multipole method, urban acoustics, wave propagation, Helmholtz equation, computational acoustics.

Développement d'une méthode de référence basée sur la méthode par éléments de frontières multipolaires rapides pour la propagation sonore en environnements urbains : formalisme, optimisations & applications

Décrit comme l'un des algorithmes les plus prometteurs du 20ème siècle, le formalisme multipolaire appliqué à la méthode des éléments de frontière, permet de nos jours de traiter de larges problèmes encore inconcevables il y a quelques années. La motivation de ce travail de thèse est d'évaluer la capacité, ainsi que les avantages concernant les ressources numériques, de ce formalisme pour apporter une solution de référence aux problèmes de propagation sonore tri-dimensionnels en environnement urbain, dans l'objectif d'améliorer les algorithmes plus rapides déjà existants.

Nous présentons la théorie nécessaire à l'obtention de l'équation intégrale de frontière pour la résolution de problèmes non bornés. Nous discutons également de l'équation intégrale de frontière conventionnelle et hyper-singulière pour traiter les artefacts numériques liés aux fréquences fictives, lorsque l'on résout des problèmes extérieurs. Nous présentons par la suite un bref aperçu historique et technique du formalisme multipolaire rapide et des outils mathématiques requis pour représenter la solution élémentaire de l'équation de Helmholtz. Nous décrivons les principales étapes, d'un point de vue numérique, du calcul multipolaire.

Un problème de propagation sonore dans un quartier, composé de 5 bâtiments, nous a permis de mettre en évidence des problèmes d'instabilités dans le calcul par récursion des matrices de translations, se traduisant par des discontinuités sur le champ de pression de surface et une non convergence du solveur. Ceci nous a conduit à considérer le travail très récent de Gumerov et Duraiswamy en lien avec un processus récursif stable pour le calcul des coefficients des matrices de rotation. Cette version améliorée a ensuite été testée avec succès sur un cas de multi diffraction jusqu'à une taille adimensionnelle de problème de 207 longueur d'ondes.

Nous effectuons finalement une comparaison entre un algorithme d'élément de frontière, *Micado3D*, un algorithme multipolaire et un algorithme basé sur le tir de rayons, Icare®, pour le calcul de niveaux de pression moyennés dans une cour ouverte et fermée. L'algorithme multipolaire permet de valider les résultats obtenus par tir de rayons dans la cour ouverte jusqu'à 300 Hz (i.e. 100 longueur d'ondes), tandis que concernant la cour fermée, zone très sensible par l'absence de contributions directes ou réfléchies, des études complémentaires sur le préconditionnement de la matrice semblent requises afin de s'assurer de la pertinence des résultats obtenus à l'aide de solveurs itératifs.

Mots-clés : Méthode des éléments de frontière, méthode multipolaire rapide, acoustique urbaine, propagation des ondes, Équation d'Helmholtz, acoustique numérique.

Résumé étendu

Avec l'augmentation de la population dans les zones urbaines, la réduction du bruit dans les villes est devenue un enjeu majeur du 21ème siècle. Un individu sur trois se dit gêné pendant la journée et une sur cinq a un sommeil perturbé (la nuit) à cause du bruit de circulation. En France, l'exposition au bruit représente la principale perturbation dans les zones urbaines et la première cause de plaintes. Selon l'Organisation Mondiale de la Santé (OMS), cette tendance va continuer à croître, avec plus de 70% de la population mondiale vivant en zone urbaine d'ici 2050. Le problème du bruit est donc, plus que jamais d'actualité, dans l'objectif d'une ville durable.

L'exposition au bruit est reconnue comme un problème de santé publique. Son impact sur les facultés auditives, le stress, les maladies cardiovasculaires, les troubles du sommeil doit être une question importante, car les dommages induits par le bruit peuvent être irréversibles. L'exposition au bruit a également une influence sur le comportement et les habitudes des riverains. Cela comprend, par exemple, l'ouverture et la fermeture des fenêtres, l'utilisation de somnifères, l'utilisation d'un balcon ou d'un jardin, ou de fuir la ville pendant le week-end. Les effets économiques du bruit ont également été étudiés, en particulier son impact sur la valeur d'une propriété. Un indice de la dépréciation des prix des logements par rapport à l'exposition au bruit a été développé. Basé sur une série d'études de cas, des relations ont été établies entre augmentation du niveau d'exposition au bruit et diminution des prix des logements.

Le Journal officiel des Communautés européennes reconnaît un grand nombre de citoyens européens affectés par le bruit, soutenu par le Comité des Régions qui souligne le besoin urgent d'une stratégie commune de lutte contre le bruit. Le Parlement européen et le Conseil ont adopté la directive relative à l'évaluation et à la gestion du bruit ambiant, le 25 Juin 2002. La directive sur le bruit ambiant s'applique au bruit auquel sont exposés les humains, en particulier dans les zones bâties, dans les parcs publics ou d'autres lieux calmes d'une agglomération, à proximité des écoles, des hôpitaux et d'autres bâtiments et zones sensibles au bruit (article 2.1), comme cela peut être le cas pour d'autres facteurs environnementaux (pollution de l'air / eau ou la gestion des déchets).

Ainsi, le bruit ambiant est officiellement considéré comme un grave problème, du point de vue de la santé sociale, environnementale et publique. L'importance de l'environnement sonore ainsi que sa conception a été largement reconnue, ce qui représente un grand pas en avant dans un objectif de limitation du niveau de bruit en milieu urbain. En termes de politiques et de réglementations environnementales, la

problématique de bruit a été l'objet d'une grande attention à différents niveaux, en particulier en Europe, conduisant à une série de mesures importantes pour lutter contre le bruit. Toutefois, l'évaluation du bruit est un problème complexe, et est liée à un certain nombre de disciplines, dont l'acoustique, la physiologie, la sociologie, la psychologie et les statistiques.

Les améliorations en termes de réduction du bruit, dans le cadre du paysage sonore urbain, impliquent un contrôle de la puissance sonore des sources, des protections appropriées au niveau des récepteurs (humains ou animaux) et une meilleure compréhension des voies de propagation dans un environnement donné. Dans ce cadre, bien que les mesures in situ fournissent des preuves irréfutables d'un niveau de pression acoustique quantifiée, les simulations numériques sont encore la meilleure (et la seule) façon d'évaluer l'influence d'un futur dispositif de réduction du bruit ou de l'influence, sur un immeuble résidentiel, d'une future infrastructure de transport. L'évaluation du paysage sonore implique la prise en compte de la complexité des sources sonores et du milieu de propagation. Les algorithmes de cartographie du bruit ont été mis au point et largement appliqués dans la pratique avec l'augmentation des ressources informatiques. Diverses méthodes de prévision pour la propagation du son dans les zones urbaines à l'échelle micro ou macroscopique ont également été explorées.

Il n'est pas réaliste d'imaginer un algorithme simple qui pourrait inclure tous les avantages des méthodes numériques utilisées en acoustique. En effet, chaque algorithme de calcule possède ses propres avantages et domaine de validité. La théorie modale est attrayante à basse fréquence pour des géométries canoniques. Les méthodes basées sur l'approche asymptotique sont jugées fiables en champ diffus et peuvent faire face à des propriétés de propagation complexes qui peuvent avoir des effets importants sur la propagation sonore en espace extérieur. Les méthodes numériques basées sur les équations aux dérivées partielles sont reconnues comme extrêmement fiable et peuvent gérer des géométries très complexes, mais sont inutilisables à des fréquences élevées en raison de temps de calcul prohibitifs. Cependant, la plupart des méthodes numériques utilisées en propagation extérieur doivent d'abord être évalués et un algorithme de référence est nécessaire. L'objectif de cette thèse est de fournir un outil de référence, afin d'évaluer et d'améliorer les algorithmes numériques plus rapides déjà existants pour résoudre les problèmes de propagation du son en espace urbains denses et dans ce cadre, la méthode des éléments de frontière semble appropriée.

Fondamentalement, la formulation intégrale de frontière, sur laquelle la méthode des éléments de frontière est basée, est très attrayante en espace extérieur puisque celle ci: (i) élimine la nécessité de considérer le domaine infini normalement associé à des problèmes de rayonnement; (ii) réduit la dimension du problème par une (par exemple, partant d'une équation différentielle partielle en trois dimensions vers une équation intégrale de surface à deux dimensions); (iii) peut facilement gérer des géométries arbitraires et les conditions aux limites. Les deux premières propriétés réduisent considérablement les besoins de stockage informatique pour les problèmes extérieurs de propagation d'ondes. Pour ces raisons, les algorithmes basés sur la BEM sont couramment utilisés pour fournir des solutions de référence pour les problèmes régis par des équations linéaires aux dérivées partielles en milieux homogènes, comprenant un large éventail d'application en physique : problèmes de Laplace ou de Poisson, les équations d'ondes fréquentielles ou

temporelles, équations élastostatique ou élastodynamique. . . L'inconvénient majeur de ce formalisme est le système d'équation dense généré, le conduisant à une forte dépendance en ressources de calcul (temps de calcul et mémoire de stockage), qui, jusqu'ici, a limité l'application de la méthode des éléments de frontière à un faible nombre de degrés de liberté.

Néanmoins, la croissance exponentielle des capacités informatiques, selon les lois de Moore, double tous les 18 mois. En effet, si une station de travail classique, au début des années 80, n'était capable que de gérer des systèmes matriciels denses ne comprenant seulement que quelques dizaines d'éléments, de nos jours quelques minutes sont suffisantes pour inverser des systèmes matriciels denses contenant plusieurs dizaines de milliers d'éléments. En outre, une autre récente amélioration spectaculaire, à savoir la méthode multipolaire rapide, provenant de travaux de Greengard et Rokhlin sera le sujet de ce manuscrit. Décrit comme l'un des dix algorithmes les plus prometteurs du 20^{eme} siècle, il permet d'accélérer la multiplication de matrices diminuant ainsi la complexité des algorithmes basés sur les éléments de frontière d'un ordre de grandeur. Ainsi, la manipulation de plusieurs centaines de milliers ou de millions de degrés de liberté sur une station de travail commune est maintenant possible. Les développements récents sur un cluster de calcul dans le domaine électromagnétique ont même permis de travailler sur des problèmes contenant des centaines de millions d'éléments.

L'application du formalisme multipolaire rapide sur la méthode des éléments de frontière permet donc de traiter des modèles encore impensables il y a quelques années. Ainsi, la motivation de ce travail est d'évaluer la capacité, ainsi que les avantages en termes de ressources de calcul fournies par l'application de ce formalisme, pour résoudre les problèmes de propagation sonore et fournir une solution de référence, dans les environnements urbains denses tri-dimensionels, dans le but d'évaluer ou d'améliorer les outils numériques existant plus rapides.

La première partie de ce travail de thèse est dédiée à l'élaboration de l'équation intégrale de frontière sur laquelle la méthode des éléments de frontière est basée. Nous étudions, dans cette partie, la capacité de la formulation intégrale de frontière classique et hyper-singulière à résoudre un problème de diffraction par un corps sphérique, et ce même aux fréquences propres fictives, pour des conditions aux limites rigides et impédantes.

Cependant, le système matriciel obtenu par le formalisme BEM est dense, non-symétrique et peut également être mal conditionné. Il s'ensuit que la solution du système, par l'utilisation d'un solveur direct telle que la quadrature de Gauss nécessite un nombre d'opération $O(N^3)$, de par la forme générale du système, avec N le nombre de degré de liberté. Même avec l'aide d'un solveur itératif pour approcher la solution, le formalisme BEM requiert une quantité de mémoire de stockage $O(N^2)$ et une dépendance temporelle $O(N^2)$ pour calculer les données de la matrice. D'un point de vue pratique, cette dépendance implique un temps de calcul élevé pour un modèle à grande échelle, puisque pour un critère de discrétisation spatial donné en termes de fréquence f, $N \propto f^2$ et le temps de calcul $O(f^6)$ (ou $O(f^4)$ avec un solveur itératif). Une telle dépendance conduit à des temps de calcul prohibitifs lorsque la fréquence augmente et met en évidence l'intérêt de la recherche liée au développement de méthodes rapides et efficaces pour l'amélioration

des algorithmes existants. Améliorer le coût de calcul des algorithmes BEM d'un ordre de grandeur à travers le formalisme multipolaire rapide sera le sujet de la deuxième partie (II), l'algorithme d'éléments de frontière ayant été jugée fiable, dans une première partie, pour calculer les interactions proches dans le cadre de l'algorithme multipolaire rapide des éléments de frontière.

La méthode des éléments de frontière (BEM), comme décrit dans la première partie, produit des matrices denses et non-symétriques nécessitant $O(N^2)$ opérations pour calculer les coefficients de la matrice et $O(N^3)$ opérations pour la résolution du système par solveurs directs. En conséquence, l'application de cette méthode sur de grands modèles conduit à des temps de calcul prohibitifs. Depuis quelques années, la méthode des éléments de frontière a profité d'une optimisation majeure à travers le formalisme multipolaire rapide, utilisé pour diminuer la complexité du temps de calcul des algorithmes basés sur des éléments de frontière. Ainsi, le but de la deuxième partie (II) a été de présenter le principe multipolaire rapide ainsi que les outils mathématiques nécessaires. En cohérence avec la première partie, nous avons évalué la capacité et la précision de la méthode multipolaire rapide, pour résoudre un problème de diffraction par un corps sphérique.

Dans le troisième chapitre (3), nous donnons un aperçu général du principe multipolaire rapide. Nous présentons les séries de base sphérique requises pour le développement des noyaux. Nous avons également introduit la décomposition RCR sur laquelle notre algorithme est basé ainsi que la formulation haute fréquence. Nous décrivons plus précisément toutes les étapes du calcul, à savoir le développement multipolaire, l'étape Moment à Moment (M2M), l'étape Moment à Local (M2L), l'étape Local à Local (L2L) et l'étape de sommation finale. Enfin, nous avons évalué la complexité théorique de calcul de l'algorithme multipolaire rapide comme étant $O(N) \approx O(p^2)$. Le quatrième chapitre (4) est consacré à l'évaluation du formalisme multipolaire rapide pour résoudre des problèmes de diffraction par un corps sphérique. Ainsi, nous prouvons l'exactitude du formalisme multipolaire pour deux conditions limites, rigides et impédants, par comparaison avec la solution analytique à des fréquences régulières. Nous avons également évalué la formulation intégrale frontière conventionnelle et hyper-singulière pour lutter contre le problème de fréquence fictive. Nous montrons tout d'abord, comme pour l'algorithme BEM, que la formulation conventionnelle et hyper-singulière réduit considérablement le nombre d'itérations à mesure que la fréquence augmente, quel que soit les conditions aux limites. Nous avons également démontré l'efficacité de cette formulation pour fournir des solutions fiables pour les conditions aux limites fortement absorbantes et rigides. Elle conduit à une perte de précision avec l'augmentation du nombre de niveaux à basse fréquence. Ainsi, cette formulation ne semble pas être recommandée pour les modèles basses fréquences, et des études complémentaires portées sur cette observation seraient souhaitables afin de garantir une fiabilité optimale de l'algorithme. Nous remarquons cependant que la formulation de Burton & Miller sera appliquée avec succès dans le cadre de modèles de propagation à grande échelle dans la partie III. La présence d'un sol en milieu urbain, par l'intermédiaire du principe de source image, implique la nécessité de considérer et de mailler le domaine image, conduisant à un nombre deux fois plus important d'éléments. Cet inconvénient peut être résolu par la mise en oeuvre du problème du demi espace grâce à l'ajout d'un baffle rigide infini, apportant un gain en termes de temps de calcul et de mémoire de stockage, par rapport à un problème

équivalent traité en espace libre. Ce formalisme de demi espace est utilisé dans la partie III de ce document dans un contexte urbain.

Nous nous concentrons dans cette partie sur l'application de l'algorithme multipolaire rapide des éléments de frontière sur des cas concrets. La première application est un cas de diffraction par une barrière anti-bruit située en amont d'une façade de bâtiment. Nous avons effectué des comparaisons entre le niveau de pression moyen calculé par un algorithme de référence BEM et l'algorithme FMBEM pour deux gammes de fréquence. Il s'en suit que 98% des récepteurs qui se trouvent sur le sol ont une différence inférieure à 3 dB dans la première plage de fréquences (90 à 100 Hz), tandis que 96% des récepteurs ont un écart inférieur à 3 dB dans la deuxième plage fréquentielle (170 à 190 Hz). Nous étudions également un problème de propagation dans un quartier de ville composé de 5 bâtiments. Une étude sur le paramètre de pondération de la formulation CHBIE fournit une valeur adéquate pour minimiser le problème de fréquence propre fictive ainsi que le nombre d'itérations. Nous étudions également l'influence de la valeur du résidu relatif du solveur itératif par rapport à la précision de la solution. Une valeur égale à 10^{-2} semble suffisante pour une évaluation rapide du niveau de pression dans ce contexte, à l'exception de certaines zones sensibles où une valeur de 10^{-3} semble nécessaire pour assurer une solution fiable. Ce problème est résolu avec une complexité en temps de calcul $O(Nlog(N))$, alors qu'un algorithme BEM standard basé sur un solveur itératif nécessite un temps de calcul $O(N^2)$. Ce temps de calcul peut, en outre, être amélioré en effectuant les calculs d'interactions directes de manière parallèle, facilement réalisé à l'aide de la librairie OpenMP (Open Multi-Processing). On observe un très bon accord entre les deux calculs (c'est à dire de l'algorithme BEM de référence et l'algorithme FMBEM) jusqu'à une taille de domaine adimensionnelle égale à 32 longueurs d'onde. Pour des tailles supérieures de domaine, nous mettons en évidence des discontinuités du champ de pression de surface et une absence de convergence du solveur itératif provenant d'instabilités dans le processus récursif de calcul des matrices de translation. Cette observation nous amène à envisager un processus récursif «stable», présenté par Gumerov & Duraiswamy, pour le calcul des coefficients des matrices de rotation au sein de la décomposition RCR. Nous décrivons comment un schéma récursif «rapide et stable» peut être garanti pour le calcul des composants des matrices de rotation et montrons les bénéfices apportés dans le cas d'un problème de propagation sonore en zone urbaine. Cet algorithme amélioré est ensuite évalué avec succès sur un problème de diffraction multiple par des cubes jusqu'à une taille adimensionnelle de domaine égale à 207 longueurs d'onde. Ce problème est résolu, pour 621 000 éléments, 750 fois plus rapidement avec l'algorithme FMBEM que si il était résolu par un algorithme BEM de collocation standard utilisant un solveur itératif, tout en réduisant la mémoire de stockage par 477. Enfin, nous avons effectué des comparaisons entre un algorithme BEM, Micado3D, prit comme référence, l'algorithme FMBEM et un algorithme basé sur le tir de rayon, le logiciel Icare®, pour calculer des niveaux de pression moyens dans des cours ouvertes et fermées. L'algorithme multipolaire rapide a permis de valider les résultats calculés avec Icare® dans la cour ouvertes jusqu'à 300 Hz ($\approx 100\lambda$), tandis que dans la cour fermée, c'est à dire une zone très sensible, des études complémentaires portant sur le préconditionnement de la matrice semblent nécessaires pour assurer une solution fiable obtenue par solveurs itératifs.

Contents

Remerciements iii

Abstract / Résumé iv

Résumé étendu vii

Table of contents xiii

List of Figures xvii

List of Tables xix

General introduction 1
- Noise issue in cities . . . 1
- Motivation of the thesis . . . 2
- Organization of the document . . . 6

I Boundary Element Method for solving three dimensional acoustic waves propagation problems: Theory & verification 9

Part I: Introduction 11

1 Boundary Integral Equation formulation 13
- 1.1 From the wave equation to the Helmholtz equation . . . 13
- 1.2 Boundary conditions . . . 14
- 1.3 Conventional Boundary Integral Equation (CBIE) formulation . . . 15
- 1.4 Conventional & Hypersingular Boundary Integral Equation (CHBIE) formulation . . . 18
- 1.5 Discretization of the boundary integral equation . . . 20
- 1.6 In summary . . . 22

2 Verification of the boundary element algorithm with a scattering problem by a spherical body 23
- 2.1 Analytical solution of the scattering problem by a spherical body . . . 23
- 2.2 Validation of the algorithm for regular frequencies . . . 24
- 2.3 Treatment of the fictitious eigenfrequency problem . . . 28
- 2.4 Analytical angular integration on a singular element . . . 34
- 2.5 In summary . . . 35

Part I: Conclusion 37

II Fast Multipole formalism for acoustic waves: Theory & verification 39

Part II: Introduction 41

3 The fast multipole formalism applied to the boundary element method for acoustic waves 43
3.1 A general overview of the fast multipole method principle . . . 43
3.1.1 Brief review of the method . . . 43
3.1.2 Overview of the method . . . 44
3.2 Field representation through the fast multipole formalism . . . 45
3.2.1 Spherical basis functions . . . 46
3.2.2 Field decomposition by the multipole expansion coefficients . . . 47
3.2.3 Translation of the multipole expansion coefficients . . . 48
3.2.4 High Frequency translation . . . 50
3.2.5 Field reconstruction by the multipole coefficients reexpansion . . . 50
3.3 Description of the fast multipole method algorithm . . . 51
3.3.1 Hierarchical tree construction . . . 52
3.3.2 Multipole expansion stage . . . 53
3.3.3 Moment to Moment (M2M) stage : Upward pass . . . 53
3.3.4 Moment to Local (M2L) stage : Transfer pass . . . 55
3.3.5 Local to Local (L2L) stage : Downward pass . . . 56
3.3.6 Final summation : Multipole coefficients reexpansion . . . 57
3.4 Numerical aspects . . . 57
3.4.1 Level-dependent truncation number . . . 58
3.4.2 Theoretical error bounds of the multipole expansion . . . 59
3.4.3 Estimation of the computational complexity . . . 59
3.5 In summary . . . 62

4 Validation of the fast multipole BEM with a scattering problem by a spherical body 63
4.1 Validation of the algorithm for regular frequencies . . . 63
4.1.1 Algorithm parameters . . . 63
4.1.2 Comparison of the surface sound pressure levels . . . 64
4.1.3 Number of iterations for a frequency sweep . . . 65
4.2 Treatment of the fictitious eigenfrequency problem . . . 68
4.2.1 Convergence of the iterative solver . . . 68
4.2.2 Comparison of the surface sound pressure level . . . 69
4.3 Validation of a half-space propagation problem . . . 73
4.3.1 The half-space principle . . . 73
4.3.2 Comparison with the full-space problem . . . 74
4.4 In summary . . . 76

Part II: Conclusion 77

III Application on realistic cases & improvements of the fast multipole algorithm 79

Part III: Introduction 81

5 Applications of the FMBEM for acoustic wave problems in urban environments 83
5.1 Scattering problem by a noise barrier in front of a building . . . 83
5.1.1 Description of the studied geometry . . . 83
5.1.2 Sound pressure level on a receivers' map . . . 84
5.2 Sound propagation in a city block . . . 88
5.2.1 Description of the studied geometry . . . 88
5.2.2 Influence of the weighting parameter on the iterative solver . . . 88
5.2.3 Influence of the relative residual on the noise map . . . 89
5.2.4 Sound pressure level in the city block . . . 93
5.2.5 Computational resources . . . 94
5.3 Consequence of unstable recursive computations . . . 98
5.3.1 Influence on the convergence of the solver . . . 99
5.3.2 Impact on the accuracy of the solution . . . 99
5.3.3 Improvement of the stability of recursive calculations . . . 100
5.4 Discussion about the current limitations . . . 101

6 Stable recursive computation of translation matrices 103
6.1 Stable recursion for large expansion orders . . . 104
6.2 Improvements in the case of the sound propagation in the city block . . . 106
6.3 The new limitations of the algorithm: A multi scattering problem . . . 108
6.3.1 Bi-dimensional array of cubic scatterers: square frame . . . 109
6.3.2 Bi-dimensional array of cubic scatterers: rectangular frame . . . 110
6.4 Conclusion on the stable recursive computations of the rotational matrices . . . 113

7 Comparison between a BEM, a FMBEM and a beam tracing algorithm 115
7.1 Brief overview of the beam tracing algorithm principle . . . 116
7.2 Comparison between algorithms: BEM, FMBEM, beam tracing . . . 117
7.2.1 Description of calculation parameters . . . 117
7.2.2 Comparison of pressure levels . . . 119
7.3 Influence of the iterative solver in sensitive areas . . . 120
7.4 Comparisons between the FMBEM algorithm and ray tracing method . . . 121
7.5 Conclusion . . . 121

Part III: Conclusion 125

Conclusion of this work 127
Summary of results . . . 127
Perspectives of this work . . . 129

A RCR decomposition **131**
A.1 Rotation Matrices coefficients 131
A.2 Coaxial translation coefficients 132
A.3 Inverse rotation Matrices coefficients 132

B Appendixes related to the spherical body **133**

C Appendixes related to the sound barrier **135**

D Appendixes related to the city block **137**

E Benefits provided by a parallelization process **139**

F Multi scattering problem by cubic bodies **141**

Bibliography **145**

Publication lists **157**

Résumé/Abstract **158**

List of Figures

1.1 *Schema of an interior acoustic propagation problem within a domain Ω* 13
1.2 *Schema of discretization of the boundary S into constant elements dS* 21

2.1 *Schema of the studied problem: a sphere of radius a excited by a point source.* 24
2.2 *Analytical vs BEM pressure level for regular frequencies on the surface of the sphere* . . . 27
2.3 *BEM: Number of iterations for zero pressure vs zero velocity according to frequency* . . . 28
2.4 *Cut plane and surface pressure for 3 eigenfrequencies of the sphere.* 29
2.5 *Number of iterations: with vs without the B&M formulation according to frequency* 32
2.6 *Analytical vs BEM with and without the B&M formulation, rigid and impedance boundaries.* 33
2.7 *Definition of variables used for the evaluation of singular integrals in polar coordinates.* . 34
2.8 *Number of iterations: zero pressure vs zero velocity according to frequency* 36
2.9 *Surface sound pressure level computed with the Gaussian quadrature vs the polar integration.* 36

3.1 *Interactions for straightforward method, Single-Level FMM and Multi-Level FMM* 45
3.2 *RCR decomposition principle.* 49
3.3 *Interactions between well separated sources and receivers through the FMM principle.* . . 51
3.4 *The procedure to construct the hierarchical tree.* 52
3.5 *The moment computation step.* 54
3.6 *The Moment to Moment (M2M) step.* 54
3.7 *The Moment to Local (M2L) transfer step.* 55
3.8 *The Local to Local (L2L) step.* 56
3.9 *The final summation step.* 57

4.1 *Analytical vs FastBEM pressure level for regular frequencies on the surface of the sphere* . 66
4.2 *FMBEM: Number of iterations: zero pressure vs zero velocity according to the frequency* . 67
4.3 *Difference of the number of iterations required with the BEM and the FMBEM algorithms.* 67
4.4 *Number of iterations: with vs without the B&M formulation according to the frequency* . . 71
4.5 *Analytical vs FastBEM surface pressure levels with and without the B&M formulation.* . . 72
4.6 *A sphere of radius a excited by a point source, full-space and half-space cases.* 73
4.7 *Half-space problem: definition of the real and virtual objects by the FMBEM.* 74
4.8 *Analytical vs FastBEM pressure level for regular frequencies on the surface of the sphere* . 75

5.1 *Overview of the studied geometry: a sound barrier located in front of a building.* 84
5.2 *Scattering by a noise barrier 100Hz: Intermediate results for a single frequency of 100 Hz.* 85
5.3 *Scattering by a noise barrier 100 Hz: Differences between Micado3D and FMBEM.* 86
5.4 *Scattering by a noise barrier 180 Hz: Logarithmic summation on the range (170-190 Hz).* 86
5.5 *Scattering by a noise barrier 180 Hz: Differences between Micado3D and FMBEM.* 87
5.6 *Overview of the studied geometry: A city block made of 5 buildings.* 89

5.7 *Propagation in a city block: convergence of the solver in terms of the weighting parameter* 90
5.8 *Propagation in a city block 100 Hz: Convergence of the solution for a relative residual* 10^{-4}. 91
5.9 *Propagation in a city block: Influence of the relative residual on the receivers' map.* 92
5.10 *Propagation in a city block: Comparison Micado3D vs FMBEM of the receivers' map* . . 93
5.11 *Propagation in a city block: Comparison Micado3D vs FMBEM along three receivers' lines* 95
5.12 *Propagation in a city block: CPU in terms of frequency with the FMBEM algorithm* 96
5.13 *Propagation in a city block: memory storage in terms of frequency with the FMBEM algorithm* 97
5.14 *Propagation in a city block: Benefits of multi-cores parallelization on direct interactions* . 99
5.15 *Propagation in a city block: Influence of unstable recursion on the convergence of the solver* 100
5.16 *Propagation in a city block: Influence of unstable recursion on the solution.* 101

6.1 *Stable recursive process for the construction of rotational matrices.* 104
6.2 *Solution on the mesh computed with the unstable recursive vs stable recursive scheme.* . . 106
6.3 *Sound pressure level computed with the unstable and the stable recursive scheme.* 107
6.4 *Number of iterations with the unstable and the stable recursive scheme* 108
6.5 *Sketch of a part of the array used to bring into light the limitation of the new FMM algorithm.* 109
6.6 *Overview of the mesh of the multi scattering problem in the squared array.* 110
6.7 *Sound pressure level within the squared array computed with Micado3D vs the FMM.* . . . 111
6.8 *Overview of the mesh of the multi scattering problem in the rectangular array.* 112
6.9 *Sound pressure level within the rectangular array computed with Micado3D vs the FMM.* . 112

7.1 *Overview of the studied geometry: A city block made of 5 buildings: Icare® calculation.* . 117
7.2 *Paths taken into account in the ray tracing calculation.* 118
7.3 *Averaged pressure levels computed by Micado3D, the FMBEM and Icare® software.* . . . 119
7.4 *Averaged pressure levels computed by Micado3D, the FMBEM and Icare® software.* . . . 120
7.5 *Pressure levels with Micado3D (GMRes), Micado3D (direct) and the FMBEM (GMRes).* . 122
7.6 *Pressure levels with Micado3D (GMRes), Micado3D (direct) and the FMBEM (GMRes).* . 123

B.1 *spherical body discretized with 7932 constant planar triangular elements.* 133
B.2 *Spherical body discretized with 31696 constant planar triangular elements.* 133
B.3 *Space partitionning for a spherical body at the* 2^{nd} *level.* 134
B.4 *Space partitionning for a spherical body at the* 4^{th} *level.* 134

C.1 *Space partitionning for the sound barrier at the* 4^{th} *level.* 135

D.1 *Space partitionning for the city block at the* 6^{th} *level.* 137

E.1 *Benefits of the computational time provided by a parallelization process.* 139

F.1 *Multi scattering problem for a dimensionless domain size equal to* 16.5λ, 33.9λ and 52λ. 142
F.2 *Sound pressure level for a dimensionless domain size equal to* 16.5λ, 33.9λ *and* 52λ. . . . 143

List of Tables

4.1 *Scattering problem by a spherical body: Computation data related to the FMBEM.* 65
4.2 *Numerical data for the half-space and the full-space FMBEM.* 75

5.1 *Computing resources of the main computation stages for the FastBEM calculations at 100 Hz.* 93

6.1 *Cubic frame: Expansion orders with respect to level and number of iterations, 52λ.* 110
6.2 *Rectangular frame: Expansion orders with respect to level and number of iterations, 207λ.* 113
6.3 *Rectangular frame: Expansion orders with respect to level and number of iterations, 275λ.* 113

General introduction

Noise issue in cities

With the increase of population in urban areas, noise abatement in cities has become a major challenge of the 21^{st} century. One in three individuals is annoyed during daytime and one in five has a disturbed sleep (at night) because of the traffic noise [WHO 2011]. In France, noise exposures represent the main disturbance in urban areas and the first cause of complaints. According to the World Health Organization [WHO 2014] (WHO), this trend will continue to grow, with over 70% of the world's population living in cities by 2050. The noise issue is therefore, more relevant than ever, in the objective of sustainable cities.

The noise exposure is recognized as a public health problem. Its impact on auditory faculties, stress, cardiovascular diseases, sleep disturbances [Alves-Pereira 2007] must be a significant issue, since the damages induced by noise can be irreversible. Behavior and habit are another important aspects which can be affected by noise exposures. This includes, for instance, opening and closing windows [Bertoni 1993, Lercher 1998], using sleeping pills, using balconies or gardens, having a sound insulated home, or frequently leaving the town during the weekends [Lambert 1984]. Economic effects of noise have also been studied, especially from the viewpoint of compensation payable on depreciation in property value that can be attributed to noise. A noise sensitivity depreciation index in house prices with respect to dB noise has been developed [Walters 1975, Nelson 1980, Nelson 1982]. Based on a series of case studies, some relationships have been established between dB increase and house price decrease [Bristow 2005].

The Official Journal of the European Communities [2001/C 148/02] recognizes a large number of European citizens affected by noise, supported by the Committee of the Regions which highlights the urgent need for a common strategy against noise pollution. The European Parliament and Council adopted Directive [Directive 2002/49/EC] [1] related to the assessment and management of environmental noise on 25 June 2002. The Environmental Noise Directive applies to noise to which humans are exposed, particularly in built-up areas, in public parks or other quiet areas in an agglomeration, near schools, hospitals and other noise-sensitive buildings and areas (Article 2.1).

[1] http://eur-lex.europa.eu/legal-content/EN/TXT/HTML/?uri=CELEX:32002L0049&from=EN

The principles of the Directive are similar to those overarching environment policies (such as air or waste), i.e.:

- monitoring the environmental problem,
- informing and consulting the public,
- addressing local noise issues,
- developing a long-term EU strategy.

Hence, environmental noise is officially considered as a serious issue, from a social, environmental and public health perspective. The importance of soundscape and sound environment design has been widely recognized and represents a major step forward from reducing the urban noise level. In terms of environmental policies and regulations, noise problems have been paid great attention at various levels, especially in Europe, leading to a series of substantial actions in noise abatement. However, the evaluation of noise is a complex problem, and is related to a number of disciplines including acoustics, physiology, sociology, psychology and statistics [Marquis-Favre 2005].

Motivation of the thesis

The improvements in term of noise abatement, within the scope of urban soundscape, involve a control of source radiated powers, implying a better design of sound sources, suitable protections of receivers (humans or animals) to noise exposure and a better understanding of propagation paths in a given environment. In this framework, although full scale measurements provide irrefutable evidences of a quantified sound pressure level, numerical simulations are still the better (and the only) way to assess the influence of an upcoming noise abatement device or the influence of a future transport infrastructure, on a residential building. The evaluation of soundscape involves accounting for the complexity of sound sources and propagation media. Noise mapping algorithms have been extensively developed and applied in practice with the improvement of computing resources. Various prediction methods for sound propagation in micro or macro scale urban areas have also been explored. We try in the following section to give a brief overview of numerical tools commonly used in engineering or research.

Numerical predictions of noise levels in urban environments

We do not claim to perform, in this section, a complete overview of the numerical methods used in acoustics, but rather to briefly introduce the underlying theory as well as the benefits and the drawbacks of these methods and the main motivations for our choice. For a more exhaustive overview of the numerical methods commonly used in acoustics, we recommend the reader to turn to dedicated literature [Salomons 2001], [Attenborough 2006], [Picaut 2006], [Kang 2007].

MORSE's work, carried during the 30's, [Morse 1936] provided a complete mathematical solution for sound behavior in a rectangular room. In contrast to all previous approaches, it was able to take into account the wave nature of sound and provided the basis for the study of many aspects of room acoustics. Lying on the decomposition of the acoustic field on an orthogonal basis of elementary solutions of the wave equation, the analytical **modal theory** [Morse 1968, Berman 1975, Markovic 1998] is therefore commonly and only applied for enclosed media of simple geometries (spherical or rectangular). However, the density of appearance of modes grows as the frequency increases and the modal theory is thus limited to low and medium frequencies. Furthermore, the application of a prediction method based upon the modal theory for sound propagation in urban environments [Bullen 1977] requires the knowledge of the averaged mode number of the sound field in street turning out to be very difficult to find in practice.

Asymptotic approaches

First developed for the study of radiant heat transfers in simple configurations [Siegel 2001], **the radiosity model** has then been adapted to three dimensional illumination rendering algorithms. The radiosity method divides the propagation domain boundaries into a number of elements. The sound propagation in the domain can then be simulated by an energy exchange between the nodes through form factors. This method assumes that all scattered fields are perfectly diffuse, according to the heat radiation principle. The radiosity model has also been applied in the field of room acoustics [Lewers 1993, Kang 2002b] and environmental acoustics in urban cases for cross streets [Kang 2001] and urban squares [Kang 2005]. A modified version of this method allows to consider a geometrically reflecting ground [Kang 2002a], through the image source principle and comparison with measurements [Picaut 2005] appears to be very promising [Kang 2007]. However, this method was only applied to ideal street shapes (canyons or squares) and the extension to more usual geometries seems compromised by prohibitive computation times.

Beside all other methods commonly used in room acoustics or environmental acoustics, **the particular approach** is a probabilistic method [Joyce 1974], based on sound particles, *the phonon*. The acoustic field is decomposed on elementary particles, without mutual interaction, carrying an infinitesimal energy. The energy distribution is deducted from the space repartition of sound particles. The sound particles travel in straight lines, at the sound velocity and can be either absorbed or reflected, following a specified law, at each collision. This approach appears to be very suited for the prediction of reverberation times and sound attenuation for diffusely reflecting boundaries [Picaut 1997]. The particular approach can easily handle the complexity of sound reflection on facades [Picaut 1998] or in diffuse rooms [Picaut 1999]. Furthermore the diffusion model may also deal with atmospheric absorption or meteorological effects. This approach has also been compared with full scale model measurements in a narrow street and has supplied good agreement [Le Pollès 2003, Picaut 2005]. Thus, through the numerical method of particles launching, it can be possible to consider complex behaviors of the propagation domain such as partially diffusely reflecting building facades, scattering by urban objects, atmospheric attenuation and wind effects.

The ray tracing approach consists in emitting a large number of rays from the source and following their propagation. Ray tracing algorithms are all based upon an analogy between optics and acoustics where the propagation of sound is analyzed by the mean of acoustical rays. Most evolved algorithms can account for reflections on curved surfaces, multiple reflections and diffractions [Jean 2008]. One of the problems with this method is the continuity of the solution and an artificial width is usually added to each ray [Van Maercke 1993]. However, aliasing problems still remain. An alternative is to employ beam tracing where emitted rays are replaced by beams. Reflections on plane surfaces or elements can then be derived analytically.

However, one must keep in mind that all asymptotic approaches make the assumption of incoherent sources, and do not allow account for phase relations and are, in theory, only valid at high frequencies when the acoustic wavelengths become smaller than geometrical details.

Partial differential equation based method

The Parabolic Equation (PE) [Gilbert 1989, White 1989] is a numerical method allowing to describe sound propagation in inhomogeneous media. The solution is built, step by step, from the source to the receiver and it is therefore possible to take into account the local physical properties of the computational domain (sound velocity, ground impedance, atmospheric disturbance, etc). Indeed, the PE based methods seem to be very attractive because of their ability to solve outdoor sound propagation problems above a mixed ground with topographic irregularities in both refractive and turbulent atmospheres [Aballéa 2004]. Furthermore, the application of the split-step Padé solution [Collins 1993] appears to be more convenient in the framework of traffic noise propagation because of the good compromise between CPU time and accuracy in heterogeneous media [Gauvreau 2002, Lihoreau 2006]. Thus, despite the fact that the PE based methods allow to deal with the complexity of an outdoor sound propagation problem and seem to be very suitable for solving long range propagation problems, it seems not specially recommended in a dense urban medium, where the macro and micro scale perturbations can be, at first order, neglected. Furthermore its application on arbitrary three dimensional shapes seems, so far, a difficult task.

The Finite Difference Time Domain (FDTD), is a numerical method for solving the linearized form of Euler equations in the time domain [Bottledooren 1994, Van Renterghem 2003]. The FDTD is used to deal with unsteady state problems and appears to be well-suited to take into account complex propagations in outdoor inhomogeneous media [Salomons 2002]. This model can account for combined effect of multiple reflections, multiple diffractions, inhomogeneous absorbing and partly diffusely reflecting surfaces or wind effect [Heimann 2007]. Some publications relate a cross FDTD-PE [Van Renterghem 2005, Van Renterghem 2006] method where the FDTD is applied in the complex source region and the PE for the propagation to a distant receiver.

The well known **Finite Element Method** (FEM) is commonly used in engineering problems to provide reliable solutions in frequency or time domains. Based on a space discretization of the studied problem,

this method proved to be an effective tool for bounded domains. Regarding the outdoor sound propagation problems, this method would require an infinite mesh which is unrealistic from a numerical viewpoint. The coupled finite/infinite element method or the use of absorbing layers methods have been developed to tackle this latter drawback [Autrique 2006] but its efficiency on general geometry is still a purpose of investigations.

It is unrealistic to imagine a simple algorithm that could include all benefits of the numerical methods presented above. Indeed, they have all their own advantages and domain of validity. The modal theory is attractive at low frequency for canonical geometries. The asymptotic approach based methods are found to be reliable for incoherent sources and can deal with complex propagation properties which can have significant effects in outdoor sound propagation. The numerical methods based on the partial differential equations appear to be extremely reliable and can handle very complex geometries but are useless at high frequencies due to prohibitive computation times. However most of the numerical methods used in outdoor sound propagation have first to be assessed and a reference algorithm is required. The aim of this thesis is rather to provide a reference tool, to assess and improve faster numerical algorithms for sound propagation in outdoor dense urban applications and, within this scope, the boundary element method seems suitable.

Why the Boundary Element Method?

Basically, the boundary integral formulation, which the boundary element method is based on, appears to be very attractive in free space as it:

(i) eliminates the need to discretize the infinite domain usually associated with radiation problems;

(ii) reduces the dimensionality of the problem by one (i.e., from a three dimensional partial differential equation to a two dimensional surface integral equation);

(iii) can readily handle arbitrary geometries and boundary conditions.

All these three properties are very attractive from a computational viewpoint as the first two significantly reduce the computer storage requirement for outdoor wave propagation problems. For these reasons, the BEM based algorithms are commonly used to provide reference solutions for problems governed by partial differential linear equations in homogeneous media including a broad scope in physics: Laplace's or Poisson's problems, frequency or time wave equations, elastostatics or elastodynamics... The major drawback of this formalism is the dense system of equations generated, leading to a heavy computational resources dependency (time and memory), which so far limited the application of the boundary element method to a low number of degrees of freedom.

Nevertheless, the exponential growth of the capabilities of technology, according to Moore's laws, doubles every 18 months. Indeed, while a classical workstation, during the 80's, could handle dense matrix systems with several tens of elements [Terai 1980], nowadays few minutes appear to be sufficient to

work out dense matrix systems containing several tens of thousands of elements. In addition, another recent dramatic improvement, namely the fast multipole method, comes from GREENGARD & ROKHLIN's work [Greengard 1987] and will be the topic of this manuscript. Described as one of the best ten algorithms of the 20th century [Dongarra 2000], it allows to accelerate the multiplication of $N \times N$ matrices and decreases the complexity of boundary element based algorithms by an order of magnitude. So, handling several hundreds of thousands or millions of degrees of freedom on a common workstation is now possible. Recent applications on a cluster in the electromagnetic domain allowed even to work out problems consisting in hundreds of millions of elements [2] in few hours [Ergül 2008].

The application of the fast multipole formalism to the boundary element algorithm allowed to handle larger scale models which was inconceivable a few years ago. Thus the motivation of the present work is to assess the ability, as well as the benefits in terms of computational resources provided by the application of this formalism, for solving sound propagation problems and providing reference solutions, in three dimensional dense urban environment, with the aim of assessing or improving faster numerical tools.

Organization of the document

The fast multipole formalism can be seen as an essential optimization of the boundary element method. Although it is already used as a reference algorithm in other physical domains (as in electromagnetics), this powerful improvement is not systematically applied in the acoustics. Thus, we intend, throughout this manuscript, to evaluate and optimize the fast multipole boundary element method on urban acoustic issues.

The first part (I) of this manuscript is dedicated to the boundary element method. First (chapter 1), we introduce the mathematical background required for the derivation of the boundary integral equation for solving sound propagation problems in unbounded domains. We also talk about the conventional and hyper-singular boundary integral equation (also known as the Burton & Miller formulation) to overcome the numerical artifact of the fictitious eigen-frequencies, when solving problems at certain characteristic frequencies. Problems related to the hyper-singularities will be circumvented thanks to the subtraction technique. We finally consider the boundary element formalism from a numerical viewpoint, leading to the boundary element method. In a second time (chapter 2), we investigate a verification process of the accuracy of our boundary element algorithm to solve scattering problems by a spherical body, by comparison with the analytical solution at regular frequencies. Both rigid and impedance boundary conditions will be considered. We also check the accuracy of the conventional and hyper-singular boundary integral equation to overcome the fictitious eigen-frequency problem and evaluate its influence in terms of iterations on the iterative solver. All these verifications are required since the boundary element method will be subsequently used to evaluate the *near interactions* in the framework of the fast multipole method.

[2] http://abakus.computing.technology/world_record

The second part (II) of this manuscript is dedicated to the fast multipole boundary element method. First of all (chapter 3), we present a brief historical and technical overview of the fast multipole principle. Afterwards, we detail the mathematical tools required to represent the acoustic field through the fast multipole formalism. We also describe the RCR-decomposition principle, introduced by Gumerov & Duraiswamy, which our fast multipole algorithm is based on, as well as details regarding the high frequency formulation. We detail more precisely, step by step, how to perform fast multipole calculations. We also provide a theoretical estimation of the complexity of the fast multipole method. Then, consistently with the first part of this manuscript, we investigate (chapter 4) a verification process to evidence the reliability and the accuracy of a fast multipole algorithm for both rigid and impedance boundary conditions, by comparison with the analytical solution. We also describe how to take into account the reflections on the ground through the implementation of the infinite rigid baffle in the framework of the fast multipole method, which will be subsequently used in the cases of urban applications.

The third part (III) of this manuscript represents, as far as the author knows, the most original work of this PhD thesis. The purpose of this part is to deal with realistic cases such as encountered in urban environments. The first considered realistic case (chapter 5) is a scattering problem by a sound barrier located in front of a building. The second larger realistic case is a sound propagation problem in a city block made of 5 buildings. This geometry implies sound propagation in streets as well as propagation in sensitive areas, i.e. opened and closed court yards. Through this problem, we investigate parametric studies with respect to (i) the weighting parameter of the conventional and hyper-singular boundary integral equation and (ii) the iterative solver relative residual. We subsequently focus on the computing requirements, i.e. computation time and memory, of the fast multipole boundary element method for solving this problem according to frequency and on the benefits provided by a parallelization process of the *near interactions*. This study allows to highlight some instabilities which occur for expansion orders above a hundred, leading to discontinuities on the surface pressure field and a failed convergence of the iterative solver. These issues led us to consider (chapter 6) the very recent Gumerov & Duraiswamy's work, related to the stability of the recursive process to compute the rotation matrices coefficients. A successful implementation of the "stable" process allows then to consider higher scale models such as multi scattering problems by cubic bodies, the largest scale model that we have considered in the scope of this thesis. Finally, in the last chapter 7, we perform comparisons in the case of the city block inside an opened and a closed court yards, between three different algorithms, for two different frequency ranges. In a low frequency range, we compare the sound pressure levels computed with the BEM algorithm, the FMBEM algorithm and a ray tracing based algorithm, Icare® software, while in a higher frequency range, only a comparison between the FMBEM algorithm and Icare® is possible.

This manuscript will end with a synthesis on the applications of the fast multipole boundary element method for solving sound propagation problems in dense urban environments and open the field on investigations which have not been considered in the framework of this thesis.

Part I

Boundary Element Method for solving three dimensional acoustic waves propagation problems: Theory & verification

Part I: Introduction

The Boundary Element Method (BEM) is a numerical method for solving the discretized form of the Boundary Integral Equation (BIE). This equation can be obtained after the reformulation to boundaries of a given problem of a certain class of Partial Differential Equations (PDE) and is hence not widely applicable when compared to the adaptability of the Finite Element Method (FEM) or finite difference methods. Basically, the BEM provides a numerical solution for problems governed by partial differential linear equations in homogeneous media. The boundary element formulation has been first proposed during the $60's$ by Jaswon [Jaswon 1963] and Symm [Symm 1963] to solve two dimensional potential problems. Some applications in elastostatic domain have subsequently been implemented [Rizzo 1967, Cruse 1969]. The BIE formulation has then been applied more generally, during the $70's$ for solving stress problems [Cruse 1974, Rizzo 1977, Wilson 1978, Kupradze 1979], and the name of the BEM is given by analogy with the FEM. Regarding the application of the BEM in the framework of acoustics, first applied to solve two dimensional scattering problems governed by the Helmholtz equation for an arbitrary body [Banaugh 1963], the application in three dimensions came at the end of the $60's$ [Schenck 1967]. Burton & Miller introduced a formulation [Burton 1971] to overcome the fictitious eigenfrequency problem which appears when solving exterior propagation problems. This formulation has been implemented at the end of the $70's$ in [Meyer 1978] and the static subtraction technique has been proposed in order to deal with the singularity problems of hypersingular integrals. Since then, the BEM has been extensively covered in dedicated books including several domains in applied mechanics [Brebbia 1978, Banerjee 1981, Chen 1992, Bonnet 1999, Kirkup 2007] providing a general insight of the application of the BEM in physics.

The purpose of this first part is to introduce the physical variables as well as deriving the Boundary Integral Equation which the boundary element method is based on. We also assess the accuracy of the BEM algorithm for solving scattering problems in free space. This validation step is a crucial aspect of the fast multipole algorithm since the boundary element formalism will be subsequently used to perform the *near interactions* in the framework of the fast multipole boundary element method.

We recall, in the first chapter (1), the mathematical background required to construct the boundary integral formulation. Starting from the wave equation, we first introduce the Helmholtz equation assuming a harmonic time dependency (section 1.1). Then, we introduce the boundary conditions satisfied by the Helmholtz equation (section 1.2) and the main theorems required to express and build the Boundary Integral Equation (section 1.3). We also describe the Burton & Miller (B&M) formulation used in outdoor sound

propagation to overcome the fictitious eigenfrequency problem (section 1.4). Finally, we come to the BEM by the discretization of the BIE.

In the second chapter (2), by comparison with analytical solutions (section 2.1), we assess the accuracy of the BEM for scattering problems by a spherical body (section 2.2). We also study the behavior of the iterative solver in terms of boundary conditions and frequency. We emphasize the fictitious eigenfrequency problem and assess the robustness of the B&M formulation to avoid this difficulty in section (2.3) as well as its influence on the iterative solver. Finally, as the use of constant elements allows the analytical integration in polar coordinates of singular integrals (weakly or hyper-singular), we emphasize the influence of this implementation on the number of iterations in section (2.4).

Chapter 1

Boundary Integral Equation formulation

1.1 From the wave equation to the Helmholtz equation

For a three dimensional propagation problem in a homogeneous isotropic domain Ω (figure 1.1), the wave equation can be written as:

$$\nabla^2\varphi(\mathbf{x},t) - \frac{1}{c^2}\frac{\partial^2\varphi(\mathbf{x},t)}{\partial t^2} = 0, \qquad \forall \mathbf{x} \in \Omega, \tag{1.1}$$

in which $\varphi(\mathbf{x},t)$ is the acoustic pressure field at point $\mathbf{x}$ at time t, ∇ is the nabla operator, $\nabla^2(.) = \partial^2(.)/\partial x^2 + \partial^2(.)/\partial y^2 + \partial^2(.)/\partial z^2$ for Cartesian coordinates, c is the sound velocity in the medium (e.g. 343 m/s in the air at 20 °C). For one dimensional propagation along the x axis, the solution of this equation is the sum of two arbitrary functions:

$$\varphi(x,t) = f(x-ct) + g(x+ct) \tag{1.2}$$

The former function f describes a right-traveling wave (towards +x direction) and the latter function g describes a left-traveling wave (towards -x direction). Indeed the right-traveling wave phase can be characterized by some constant value of f, which is realized at $x = ct + const$, and so the wavefronts travel towards

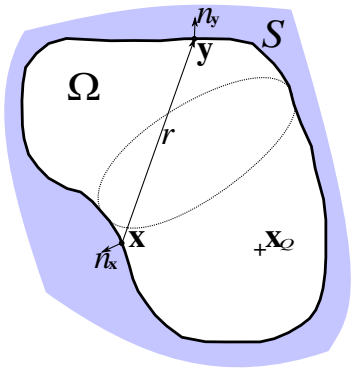

FIGURE 1.1: *Schema of an interior acoustic propagation problem within a domain Ω. The shaded area represents the unexamined domain.*

the +x direction as t grows. Inversely, the left-traveling wave phase is characterized by some constant value of g, which is realized at $x = -ct + const$ and so the wavefronts travel towards the $-x$ direction as t increases.

We also introduce some other useful quantities in wave analysis related to the frequency f:

$$\omega = 2\pi f \quad \text{(angular frequency)}; \qquad k = \frac{2\pi f}{c} \quad \text{(wave number)}; \qquad \lambda = \frac{c}{f} \quad \text{(wave length)}. \tag{1.3}$$

Only time-harmonic solutions to the wave equation are considered, thus the solution to the wave equation can be written, assuming a time convention factor $e^{-i\omega t}$, $\varphi(\mathbf{x}, t) = \phi(\mathbf{x})e^{-i\omega t}, \forall \mathbf{x} \in \Omega$, with ϕ being the complex acoustic pressure at point $\mathbf{x}$ in the frequency domain and i, the unit imaginary number ($i^2 = -1$). Thus the acoustic wave equation (1.1) becomes, in steady state condition :

$$\nabla^2\phi(\mathbf{x}) + k^2\phi(\mathbf{x}) = 0, \qquad \forall \mathbf{x} \in \Omega \tag{1.4}$$

This equation is the well known Helmholtz equation, it is a wave analog (in the frequency domain) of the Poisson equation (the case $k = 0$), for a three dimensional propagation problem in a homogeneous isotropic domain Ω.

1.2 Boundary conditions

The Helmholtz equation is an equation for which it is usual to consider boundary value problems. The Boundary conditions (BC) follow from particular physical laws (conservation equations) formulated on the boundaries S of the domain for which a solution is required. There are two specific types of problems in acoustic wave analysis. One corresponds to the case of imposed pressure ϕ on the boundary referred to as Dirichlet's problem:

$$(Dirichlet\ BC) \qquad \phi(\mathbf{x}) = \bar{\phi}(\mathbf{x}), \qquad \forall \mathbf{x} \in S, \tag{1.5}$$

the other corresponding to the case of an imposed normal velocity q on the boundary referred to as Neumann's problem:

$$(Neumann\ BC) \qquad q(\mathbf{x}) = \frac{\partial\phi}{\partial\vec{n}_{\mathbf{x}}} = \bar{q}(\mathbf{x}), \qquad \forall \mathbf{x} \in S \tag{1.6}$$

and is thus proportional to the normal derivative of the surface pressure, according to the unit normal $\vec{n}_{\mathbf{x}}$ at the point $\mathbf{x}$. We can also define a mixed (impedance or Robin's) boundary condition linking both previous quantities with the specific acoustic impedance Z:

$$i\omega\rho_{air}\phi(\mathbf{x}) = Z(\mathbf{x})q(\mathbf{x}), \qquad \forall \mathbf{x} \in S \tag{1.7}$$

with the air density ρ_{air}. We denote that the quantities with overbars indicate imposed values on the boundary S.

An additional boundary condition, which will be suitable for exterior acoustic propagation problems (i.e. in an infinite or semi infinite domain) can be introduced. This is the Sommerfeld radiation condition, resulting from the fact that all outgoing waves, scattered or radiated, vanish at infinity:

$$\lim_{r\to+\infty} r\left(\frac{\partial\phi}{\partial r} - ik\phi\right) = 0 \tag{1.8}$$

where r is the distance from a fixed origin to a general field point and ϕ is the total acoustic wave (velocity potential or acoustic pressure).

1.3 Conventional Boundary Integral Equation (CBIE) formulation

We will see in this section the establishment of the Conventional Boundary Integral Equation (CBIE) applied in three dimensional outdoor sound propagation. We first have to introduce some fundamental identities required in the framework of the integral representation formalism.

The fundamental solution in infinite domain

Starting from the homogeneous Helmholtz equation (1.4):

$$\nabla^2\phi(\mathbf{x}) + k^2\phi(\mathbf{x}) = 0, \qquad \forall \mathbf{x} \in \Omega, \tag{1.9}$$

we can introduce the Green's function G as the free-space fundamental solution of the previous equation in three dimensions:

$$G(\mathbf{x},\mathbf{y}) = \frac{e^{ikr}}{4\pi r}, \quad \text{with} \quad r = |\mathbf{x}-\mathbf{y}| \quad , \tag{1.10}$$

where r is the distance between two arbitrary points $\mathbf{x}$ and $\mathbf{y}$. It follows from the previous definition that G is a symmetrical function:

$$G(\mathbf{x},\mathbf{y}) \equiv G(\mathbf{y},\mathbf{x}). \tag{1.11}$$

This impulse response of a free-space propagation problem, is the fundamental solution of the Helmholtz equation (1.9) for a point source of amplitude Q, located at $\mathbf{x}_Q$:

$$\nabla^2 G + k^2 G = -Q\delta(\mathbf{x}-\mathbf{x}_Q), \qquad \forall \mathbf{x} \in \Omega, \tag{1.12}$$

where $\delta(\mathbf{x}-\mathbf{y})$ refers to the Dirac delta function which is defined for an arbitrary function $f(\mathbf{x})$ as:

$$\int_\Omega f(\mathbf{x})\delta(\mathbf{x}-\mathbf{y})d\Omega = \begin{cases} f(\mathbf{y}), & for\ \mathbf{y} \in \Omega, \\ 0, & otherwise. \end{cases} \tag{1.13}$$

The divergence theorem

The divergence theorem, coming from the Gauss theorem, relates an integral over a domain $\Omega \in \mathbb{R}^3$ to the

surface integral over the boundary S of this domain:

$$\int_{\Omega}(\nabla\cdot\mathbf{A})d\Omega=\int_{\partial\Omega}(\vec{n}\cdot\mathbf{A})dS, \tag{1.14}$$

where $\vec{n}$ is the normal vector to the surface S outgoing to the domain Ω and $\mathbf{A}$ a scalar or vector quantity for which the operator $\cdot$ is defined.

Green's integral theorem

Green's first integral theorem states that for a domain Ω with boundary S, given two functions $u(\mathbf{x})$ and $v(\mathbf{x})$, we can write:

$$\int_{\Omega}(u\nabla^2 v+\nabla u\cdot\nabla v)d\Omega=\int_{\Omega}\nabla\cdot(u\nabla v)d\Omega, \tag{1.15}$$

and taking back the divergence theorem (1.14) on the quantity $u\nabla v$:

$$\int_{\Omega}(u\nabla^2 v+\nabla u\cdot\nabla v)d\Omega=\int_{\partial\Omega}\vec{n}\cdot(u\nabla v)dS. \tag{1.16}$$

To obtain Green's second identity theorem, we write equation (1.16) by exchanging u and v and subtract it from (1.16), which yields:

$$\int_{\Omega}(u\nabla^2 v-v\nabla^2 u)d\Omega=\int_{S}\vec{n}\cdot(u\nabla v-v\nabla u)dS. \tag{1.17}$$

The Green's second integral theorem can also be written as:

$$\int_{\Omega}u\nabla^2 v d\Omega=\int_{\Omega}v\nabla^2 u d\Omega+\int_{S}\left(u\frac{\partial v}{\partial\vec{n}}-v\frac{\partial u}{\partial\vec{n}}\right)dS, \tag{1.18}$$

where we use $\partial(\cdot)/\partial\vec{n}=\vec{n}\cdot\nabla(\cdot)$.

Conventional Boundary Integral Equation (CBIE)

Let us consider a domain Ω with its boundary S. Using the property of the delta function (1.13) for a given function ϕ at a point $\mathbf{x}\in\Omega$:

$$\int_{\Omega}\phi(\mathbf{y})\delta(\mathbf{y}-\mathbf{x})d\Omega=\phi(\mathbf{x}),\qquad \mathbf{x}\in\Omega, \tag{1.19}$$

$$\phi(\mathbf{x})=-\int_{\Omega}\phi_(\mathbf{y})\left[\nabla^2_{\mathbf{y}}G(\mathbf{x},\mathbf{y})+k^2G(\mathbf{x},\mathbf{y})\right]d\Omega(\mathbf{y}), \tag{1.20}$$

where $\nabla_{\mathbf{y}}$ is the nabla operator with respect to variable $\mathbf{y}$. Using Green's second integral theorem (1.18), where we set $u=\phi$ and $v=G$, the above equation can be written:

$$\phi(\mathbf{x})=-\int_{\Omega}k^2\phi(\mathbf{y})G(\mathbf{x},\mathbf{y})d\Omega_{\mathbf{y}}-\int_{\Omega}G(\mathbf{x},\mathbf{y})(\nabla^2_{\mathbf{y}}\phi)d\Omega_{\mathbf{y}}-\int_{S}\left[\phi(\mathbf{y})\frac{\partial G(\mathbf{x},\mathbf{y})}{\partial\vec{n}_{\mathbf{y}}}-G(\mathbf{x},\mathbf{y})\frac{\partial\phi(\mathbf{y})}{\partial\vec{n}_{\mathbf{y}}}\right]dS_{\mathbf{y}}, \tag{1.21}$$

$$\phi(\mathbf{x})=-\int_{\Omega}\left[\nabla^2_{\mathbf{y}}\phi(\mathbf{y})+k^2\phi(\mathbf{y})\right]G(\mathbf{x},\mathbf{y})d\Omega_{\mathbf{y}}-\int_{S}\left[\phi(\mathbf{y})\frac{\partial G(\mathbf{x},\mathbf{y})}{\partial\vec{n}_{\mathbf{y}}}-G(\mathbf{x},\mathbf{y})\frac{\partial\phi(\mathbf{y})}{\partial\vec{n}_{\mathbf{y}}}\right]dS_{\mathbf{y}}. \tag{1.22}$$

Let us consider the case of a function ϕ in the domain Ω which fulfills the Helmholtz equation (1.9), then the first integral in the above equation becomes:

$$\int_\Omega \left[\nabla^2_{\mathbf{y}}\phi(\mathbf{y}) + k^2\phi(\mathbf{y})\right] G(\mathbf{x},\mathbf{y}) d\Omega_{\mathbf{y}} = -Q\int_\Omega \delta(\mathbf{x},\mathbf{x}_Q)G(\mathbf{x},\mathbf{y})d\Omega_{\mathbf{y}} = -QG(\mathbf{x},\mathbf{x}_Q). \tag{1.23}$$

Thus, relation (1.22) leads to:

$$\phi(\mathbf{x}) = \int_S \left[-\frac{\partial G(\mathbf{x},\mathbf{y})}{\partial \vec{n}_{\mathbf{y}}}\phi(\mathbf{y}) + G(\mathbf{x},\mathbf{y})q(\mathbf{y})\right] dS_{\mathbf{y}} + \phi_{in}(\mathbf{x}), \qquad \forall \mathbf{x}\in\Omega, \forall \mathbf{y}\in S, \tag{1.24}$$

with $QG(\mathbf{x},\mathbf{x}_Q) = \phi_{in}(\mathbf{x})$, the incident pressure at $\mathbf{x}$ due to a point source located at $\mathbf{x}_Q$.

Equation (1.24) is the integral representation of the solution ϕ inside the domain Ω of the Helmholtz Equation (1.9). Regarding the case of an exterior propagation problem, the opposite direction of $\vec{n}_{\mathbf{y}}$ is usually used since it is defined as the outward normal to the propagation domain at $\mathbf{y}$, that is to say turned inward the scattering body. Furthermore, in order to determine the pressure potential ϕ everywhere in the domain using equation (1.24), both ϕ and q are needed on the boundary. Even though this equation is valid for both exterior or interior problems, it is not valid when $\mathbf{x}$ coincides with the boundary. Let the collocation point $\mathbf{x}$ approach the boundary S, the previous equation leads to the following Conventional Boundary Integral Equation (CBIE) for exterior propagation problems:

$$C(\mathbf{x})\phi(\mathbf{x}) = \int_S \left[\frac{\partial G(\mathbf{x},\mathbf{y})}{\partial \vec{n}_{\mathbf{y}}}\phi(\mathbf{y}) - G(\mathbf{x},\mathbf{y})q(\mathbf{y})\right] dS_{\mathbf{y}} + \phi_{in}(\mathbf{x}), \qquad \forall \mathbf{x},\mathbf{y}\in S. \tag{1.25}$$

The coefficient $C(\mathbf{x})$ is related to the fraction of local volume determined by the solid angle γ, included in the domain Ω at point $\mathbf{x}$,

$$C(\mathbf{x}) = \begin{cases} 1/2, & \mathbf{x} \textit{ on a smooth part of the boundary,} \\ \gamma/4\pi, & \mathbf{x} \textit{ at a corner of the boundary,} \\ 1, & \mathbf{x} \textit{ inside the domain.} \end{cases} \tag{1.26}$$

For the sake of readability, we will use throughout the rest of the document, for both kernels G and F, the following notations :

$$G(\mathbf{x},\mathbf{y}) = \frac{e^{ikr}}{4\pi r}, \tag{1.27}$$

$$F(\mathbf{x},\mathbf{y}) = \frac{\partial G(\mathbf{x},\mathbf{y})}{\partial \vec{n}_{\mathbf{y}}} \equiv \frac{\partial G(\mathbf{x},\mathbf{y})}{\partial r}\frac{\partial r}{\partial \vec{n}_{\mathbf{y}}} \quad \Longrightarrow \quad F(\mathbf{x},\mathbf{y}) = (ikr-1)\frac{e^{ikr}}{4\pi r^2}\frac{\partial r}{\partial \vec{n}_{\mathbf{y}}}. \tag{1.28}$$

In the case of a free space problem, all outgoing waves vanish at infinity which is implicitly satisfied by the boundary integral formalism since it fulfills the Sommerfeld radiation condition (eq. (1.8)), thus the CBIE is valid at any point $\mathbf{x}$ in the domain Ω and on the surface S, allowing to determine ϕ at any point in Ω, once the values ϕ and q are known on the boundary.

1.4 Conventional & Hypersingular Boundary Integral Equation (CHBIE) formulation

Equation (1.25) has a major drawback when applied to exterior acoustic propagation problems. Indeed it does not lead to a unique solution at certain characteristic frequencies corresponding to the eigenfrequencies of the corresponding interior problem. This difficulty is referred to as the fictitious eigenfrequency problem [Bonnet 1999]. Several methods and formulations have been proposed over the last 3-4 decades for overcoming this non-uniqueness problem [Rego Silva 1994, Ochmann 2002, Osetrov 2005]. The CHIEF method performs well at low frequencies, but a reliable solution can never be guaranteed. The method of Rosen and al. [Rosen 1995] has already been tested and is not recommended since it performs even less reliably than the conventional CHIEF. One of the most effective, and recommended method [Rosen 1995, Marburg 2005], is the Burton & Miller (B&M) formulation. It consists in a linear combination of the CBIE formulation and its normal derivative. Burton and Miller have proved in [Burton 1971] that this formulation yields to unique solutions at all frequencies for exterior acoustic problems.

Let $\mathbf{x}$ approach S and let us take the derivative of equation (1.25) with respect to the outward normal to the domain Ω at the collocation point $\mathbf{x}$. It leads to the following Hyper-singular Boundary Integral Equation (HBIE):

$$C(\mathbf{x})\frac{\partial\phi(\mathbf{x})}{\partial\vec{n}_{\mathbf{x}}} = \int_S \left[\frac{\partial^2 G(\mathbf{x},\mathbf{y})}{\partial\vec{n}_{\mathbf{y}}\partial\vec{n}_{\mathbf{x}}}\phi(\mathbf{y}) - \frac{\partial G(\mathbf{x},\mathbf{y})}{\partial\vec{n}_{\mathbf{x}}}\frac{\partial\phi(\mathbf{y})}{\partial\vec{n}_{\mathbf{y}}}\right] dS_{\mathbf{y}} + \frac{\partial\phi_{in}(\mathbf{x})}{\partial\vec{n}_{\mathbf{x}}}, \qquad \forall\mathbf{x}\in S, \tag{1.29}$$

according to the constant $C(\mathbf{x})$ defined in (1.26). Consistent with definitions (1.27) and (1.28), the two new kernels K and H are defined as follows [Kirkup 2007]:

$$K(\mathbf{x},\mathbf{y}) = \frac{\partial G(\mathbf{x},\mathbf{y})}{\partial\vec{n}_{\mathbf{x}}} \equiv \frac{\partial G(\mathbf{x},\mathbf{y})}{\partial r}\frac{\partial r}{\partial\vec{n}_{\mathbf{x}}} \quad\Longrightarrow\quad K(\mathbf{x},\mathbf{y}) = (ikr-1)\frac{e^{ikr}}{4\pi r^2}\frac{\partial r}{\partial\vec{n}_{\mathbf{x}}}, \tag{1.30}$$

$$H(\mathbf{x},\mathbf{y}) = \frac{\partial^2 G(\mathbf{x},\mathbf{y})}{\partial\vec{n}_{\mathbf{y}}\partial\vec{n}_{\mathbf{x}}} \equiv \frac{\partial G(\mathbf{x},\mathbf{y})}{\partial r}\frac{\partial^2 r}{\partial\vec{n}_{\mathbf{y}}\partial\vec{n}_{\mathbf{x}}} + \frac{\partial G(\mathbf{x},\mathbf{y})}{\partial r^2}\frac{\partial r}{\partial\vec{n}_{\mathbf{y}}}\frac{\partial r}{\partial\vec{n}_{\mathbf{x}}}$$

$$\Longrightarrow\quad H(\mathbf{x},\mathbf{y}) = (ikr-1)\frac{e^{ikr}}{4\pi r^2}\frac{\partial^2 r}{\partial\vec{n}_{\mathbf{y}}\partial\vec{n}_{\mathbf{x}}} + (2-2ikr-k^2r^2)\frac{e^{ikr}}{4\pi r^3}\frac{\partial r}{\partial\vec{n}_{\mathbf{y}}}\frac{\partial r}{\partial\vec{n}_{\mathbf{x}}}. \tag{1.31}$$

According to the CBIE (equation (1.25)) and the HBIE (equation (1.29)), Burton and Miller have introduced a linear combination of both equations with a non-zero imaginary part coupling constant α, leading to the following Conventional & Hyper-singular Boundary Integral Equation (CHBIE):

$$CBIE + \alpha\, HBIE = 0,$$

$$C(\mathbf{x})\left[\phi(\mathbf{x}) + \alpha q(\mathbf{x})\right] = \int_S \left[\left(F(\mathbf{x},\mathbf{y}) + \alpha H(\mathbf{x},\mathbf{y})\right)\phi(\mathbf{y}) - \left(G(\mathbf{x},\mathbf{y}) + \alpha K(\mathbf{x},\mathbf{y})\right)q(\mathbf{y})\right] dS_{\mathbf{y}} + \phi_{in}(\mathbf{x}) + \alpha q_{in}(\mathbf{y}). \tag{1.32}$$

It has been proven in [Burton 1971] that the Conventional & Hypersingular Boundary Integral Equation (CHBIE) Eq. (1.32) yields unique solutions for $\Im(\alpha) \neq 0$ at all frequencies when applied to exterior acoustic problems. One possible, and subsequently used, value of the parameter α may be $\alpha = i/k$ (cf. [Meyer 1978]). However, it has then been proven that such a value of the coupling parameter almost minimizes the condition number of the operators on the left and the right hand sides of equation (1.32), when the boundary is a sphere (cf. [Amini 1990a]), so we will prefer using the following expression:

$$(1-\eta)CBIE + \eta\frac{i}{k}HBIE = 0 \quad \text{with} \quad 0 \leq \eta \leq 1. \tag{1.33}$$

Even if this equation is not the usual CHBIE, by choosing a proper value of the weighting factor, η, it allows a better control of the fictitious eigenfrequency problem and appears to be more suitable for urban geometries. It is noteworthy that the CBIE is obtained for $\eta = 0$, the HBIE for $\eta = 1$ and the commonly used CHBIE, i.e. the one introduced by Burton and Miller in [Burton 1971], corresponds to $\eta = 0.5$. Furthermore, for impedance boundary conditions, even if this equation leads to a slower convergence for low frequency problems (thus it is not recommended at low frequency), it will be shown in the following (section 2.3) that the CHBIE allows a stable convergence of the iterative solver as the frequency increases. Yasuda and al. [Yasuda 2007] provide very detailed information about the behavior of several iterative solvers for both interior and exterior propagation cases. However, as far as the author knows, the behavior of the CHBIE formulation with respect to the frequency seems to be still a topic of investigation and will be studied in section (2.3).

Weakly singular form of the Hypersingular Boundary Integral Equation

The major drawback of the CHBIE (equation (1.32)), according to the definitions of kernels G, F, K and H, equations (1.27), (1.28), (1.30) and (1.31) respectively, is that singularity problems occur when r tends towards zero. Regarding the integration of the kernel G, the $O(1/r)$ dependency does not introduce difficulties from a numerical point of view and can be readily handled with a standard Gaussian quadrature. We will see in section (2.4) that this integral can even be computed analytically in the particular case of zero interpolation order to discretize the boundary by using polar coordinates. Even though both kernels F and K include a $1/r^2$ term, it can be proved that their integration behaves actually only as weakly singular integrals and can also be readily handled by using standard numerical integration techniques such as the Gauss quadrature. Furthermore, by using zero numerical interpolation order (*i.e.* constant elements) to discretize the boundary, the singular behavior, when two points are on top of each other (*i.e.* $\mathbf{x} \equiv \mathbf{y}$), of the integration of both kernels F and K disappears. Indeed when $\mathbf{x}$ and $\mathbf{y}$ are in the same element, the dot product, $\vec{r}\cdot\vec{n} = 0$ and it follows:

$$\frac{\partial r}{\partial \vec{n}_\mathbf{y}} = \frac{\vec{r}\cdot\vec{n}_\mathbf{y}}{r} = 0 \qquad \text{thus} \qquad F(\mathbf{x},\mathbf{y}) = (ikr-1)\frac{e^{ikr}}{4\pi r^2}\frac{\partial r}{\partial \vec{n}_\mathbf{y}} = 0. \tag{1.34}$$

Likewise for the singular kernel K in the HBIE, when $\mathbf{x}$ and $\mathbf{y}$ are in the same element:

$$\frac{\partial r}{\partial \vec{n}_\mathbf{x}} = \frac{\vec{r}\cdot\vec{n}_\mathbf{x}}{r} = 0 \qquad \text{and thus} \qquad K(\mathbf{x},\mathbf{y}) = (ikr-1)\frac{e^{ikr}}{4\pi r^2}\frac{\partial r}{\partial \vec{n}_\mathbf{x}} = 0. \tag{1.35}$$

The HBIE, however, still introduces a hyper-singularity due to the presence of the $1/r^3$ term appearing in the kernel H (eq. 1.31):

$$\frac{\partial^2 G(\mathbf{x},\mathbf{y})}{\partial \vec{n}_\mathbf{y} \partial \vec{n}_\mathbf{x}} \propto \frac{1}{r^3}. \tag{1.36}$$

However it is possible to write a weakly singular form using a singularity subtraction technique, first reported in a physical review in [Meyer 1978] and detailed in [Liu 1991] and [Li 2010]:

$$\begin{aligned}\int_S \phi(\mathbf{y}) \frac{\partial^2 G(\mathbf{x},\mathbf{y})}{\partial \vec{n}_\mathbf{y} \partial \vec{n}_\mathbf{x}} dS_\mathbf{y} = \int_S \phi(\mathbf{y}) \left[\frac{\partial^2 G(\mathbf{x},\mathbf{y})}{\partial \vec{n}_\mathbf{y} \partial \vec{n}_\mathbf{x}} - \frac{\partial^2 G_0(\mathbf{x},\mathbf{y})}{\partial \vec{n}_\mathbf{y} \partial \vec{n}_\mathbf{x}} \right] dS_\mathbf{y} + \int_S \nabla\phi(\mathbf{x}) \vec{n}_\mathbf{y} \frac{\partial G_0(\mathbf{x},\mathbf{y})}{\partial \vec{n}_\mathbf{x}} dS_\mathbf{y} \\ - \frac{1}{2} \nabla\phi(\mathbf{x}) \cdot \vec{n}_\mathbf{x} + \int_S \left[\phi(\mathbf{y}) - \phi(\mathbf{x}) - \nabla\phi(\mathbf{x})(\mathbf{y}-\mathbf{x}) \right] \frac{\partial^2 G_0(\mathbf{x},\mathbf{y})}{\partial \vec{n}_\mathbf{y} \partial \vec{n}_\mathbf{x}} dS_\mathbf{y}\end{aligned} \tag{1.37}$$

with the static Green's function $G_0(\mathbf{x},\mathbf{y}) = \frac{1}{4\pi r}$. It has been proved that all integrals in the right-hand side are at most weakly singular. Hence, the hyper-singular integral is reformulated into an improved form involving boundary integrals that are only weakly singular. This weakly singular integral (eq. 1.37) is valid for an arbitrary interpolation order and can be readily handled by standard numerical integration techniques such as the Gauss quadrature. Furthermore, when applied with constant elements, the gradient appearing in equation (1.37) may reasonably be considered as null, $\nabla\phi(\mathbf{x}) = \nabla\phi(\mathbf{y}) \approx 0$, and the previous equation yields:

$$\int_S \phi(\mathbf{y}) \frac{\partial^2 G(\mathbf{x},\mathbf{y})}{\partial \vec{n}_\mathbf{y} \partial \vec{n}_\mathbf{x}} dS_\mathbf{y} \approx \int_S \phi(\mathbf{y}) \left[\frac{\partial^2 G(\mathbf{x},\mathbf{y})}{\partial \vec{n}_\mathbf{y} \partial \vec{n}_\mathbf{x}} - \frac{\partial^2 G_0(\mathbf{x},\mathbf{y})}{\partial \vec{n}_\mathbf{y} \partial \vec{n}_\mathbf{x}} \right] dS_\mathbf{y} + \int_S \left[\phi(\mathbf{y}) - \phi(\mathbf{x}) \right] \frac{\partial^2 G_0(\mathbf{x},\mathbf{y})}{\partial \vec{n}_\mathbf{y} \partial \vec{n}_\mathbf{x}} dS_\mathbf{y}. \tag{1.38}$$

This latter assumption could represent a rough approximation therefore, before being used in the framework of the fast multipole formalism, has first to be validated. This point will be discussed in the next chapter related to the validation of the boundary element algorithm.

1.5 Discretization of the boundary integral equation

We propose to focus in this section on the BIE from a numerical point of view. We first discretize the boundary S into elementary constant elements dS as displayed in figure 1.2.

Since we deal with 3 dimensional propagation problems and to ease the numerical implementation, the boundary shape is approached with planar triangles. The functions ϕ and q are then replaced by constant values on each triangle, leading to a number of unknowns equal to the number of elements N. The CBIE (equation (1.25)) becomes:

$$\frac{1}{2}\phi(\mathbf{x}_i) = \sum_{j=1}^{N} \left[\phi(\mathbf{y}_j) \int_{dS_j} F(\mathbf{x}_i,\mathbf{y}_j) dS - q(\mathbf{y}_j) \int_{dS_j} G(\mathbf{x}_i,\mathbf{y}_j) dS \right] + \phi_{in}(\mathbf{x}_i), \tag{1.39}$$

$$\forall \mathbf{x}_i, \mathbf{y}_j \in S \quad for \quad i,j = 1,2,\cdots,N.$$

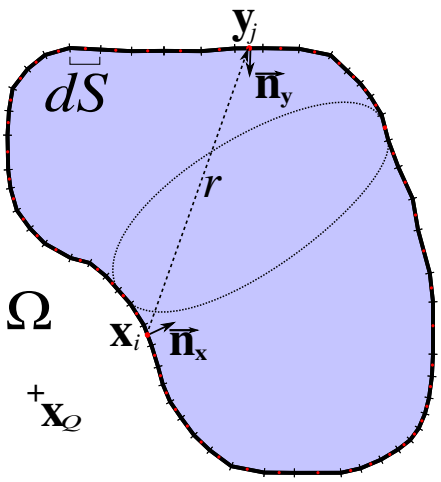

FIGURE 1.2: *Schema of discretization of the boundary S into constant elements dS. The shaded area represents the unexamined domain.*

Re-arranging each term, that is, moving the unknown terms to the left-hand side and known terms to the right-hand side, leads to the following linear system of equations which can take the following matrix form $\left[A\right]\left(\lambda\right) = \left(b\right)$ or :

$$\begin{bmatrix} A_{11} & A_{12} & \dots & A_{1N} \\ A_{21} & A_{22} & \dots & A_{2N} \\ \vdots & \vdots & \ddots & \vdots \\ A_{N1} & A_{N2} & \dots & A_{NN} \end{bmatrix} \begin{pmatrix} \lambda_1 \\ \lambda_2 \\ \vdots \\ \lambda_N \end{pmatrix} = \begin{pmatrix} b_1 \\ b_2 \\ \vdots \\ b_N \end{pmatrix} \tag{1.40}$$

where:

$$A_{ij} = \frac{1}{2}\delta_{ij} \begin{cases} -\int_{dS_j} G(\mathbf{x}_i, \mathbf{y}_j) dS, & \text{(for Dirichlet BC)} \\ +\int_{dS_j} F(\mathbf{x}_i, \mathbf{y}_j) dS, & \text{(for Neumann BC)} \end{cases}$$

$$\lambda_i = \begin{cases} \phi(\mathbf{x}_i), & \text{(for Neumann BC)} \\ q(\mathbf{x}_i), & \text{(for Dirichlet BC)} \end{cases} \tag{1.41}$$

$$b_i = \phi_{in}(\mathbf{x}_i) \begin{cases} -\bar{q}(\mathbf{y}_i) \int_{dS_j} G(\mathbf{x}_i, \mathbf{y}_j) dS & \text{(for Neumann BC)} \\ +\bar{\phi}(\mathbf{y}_i) \int_{dS_j} F(\mathbf{x}_i, \mathbf{y}_j) dS, & \text{(for Dirichlet BC)} \end{cases}$$

A_{ij} are the components of the matrix, the vector λ is the unknown pressure ϕ or velocity q on each node i, and the vector b, the known right hand side consists of the incident pressure field and the product of the imposed boundary pressure value $\bar{\phi}$ or imposed boundary velocity value $\bar{q}$ by the corresponding integral.

According to the previous definitions (equations (1.39) and (1.41)), the HBIE leads to a similar linear system of equations obtained by exchanging G and F with K and H respectively.

$$\frac{1}{2}\phi(\mathbf{x}_i) = \sum_{j=1}^{N} \left[\phi(\mathbf{y}_j) \int_{dS_j} H(\mathbf{x}_i, \mathbf{y}_j) dS - q(\mathbf{y}_j) \int_{dS_j} K(\mathbf{x}_i, \mathbf{y}_j) dS \right] + \phi_{in}(\mathbf{x}_i), \tag{1.42}$$

$$\forall \mathbf{x}_i, \mathbf{y}_j \in S \qquad for \qquad i, j = 1, 2, \cdots, N.$$

It is noteworthy that the use of the CBIE (equations (1.39)) only requires the evaluation of two integrals while the weakly singular form of the B&M formulation (equations (1.39) and (1.42)), consistent with the definition (1.38), is more time consuming since it requires the evaluation of five integrals for impedance boundary conditions. We have only described here the numerical features of the boundary integral equation with constant elements; however the use of constant elements to discretized the surface usually requires more elements to reach the same accuracy as compared with the use of linear or quadratic elements.

1.6 In summary

This chapter has been dedicated to the underlying theory of the boundary integral formalism in order to derive, from a numerical point of view, the Boundary Element Method (BEM). We introduce the Conventional and Hyper-singular Boundary Integral Equation (CHBIE), also called the Burton & Miller formulation, to tackle the drawback of the well-known fictitious eigen-frequency problem which occurs at resonance frequencies of the adjoint interior problem. Using the static subtraction technique, we finally derive the weakly singular form of the hyper-singular boundary integral equation which can be handled numerically by standard Gauss quadrature. The following chapter is dedicated to the numerical validation of the formalism we described in this chapter, a necessary step to ensure a reliable computation of the *near interactions* in the framework of the subsequently fast multipole formalism.

Chapter 2

Verification of the boundary element algorithm with a scattering problem by a spherical body

The purpose of this section is the verification of the accuracy of the boundary element method through a scattering problem by a spherical body. The verification of the reliability of the boundary element method is an important step since it will subsequently be used in the framework of the fast multipole formalism to compute the direct interactions (see chapter 3.3). Thus, we study the case of a spherical incident wave scattered by a spherical body with a radius a equal to 1 m (see figure 2.1). The analytical solution described in the following section (2.1) is taken as a reference solution throughout the validation of the BEM algorithm. First, we compare the surface potential pressure level for regular frequencies with rigid and impedance boundary conditions as well as the number of iterations required to solve for the problem (section 2.2). Then, we deal with the fictitious eigenfrequency problem with the use of the Burton & Miller (B&M) formulation and the static subtraction technique (section 2.3). Finally, since the mesh is made of planar triangular elements, we will see how the singularity problem occurring on a singular element can be solved by an angular analytical integration in polar coordinates (section 2.4).

2.1 Analytical solution of the scattering problem by a spherical body

We consider the case of a spherical body of radius a excited by a spherical wave generated by a point source of amplitude Q located at a distance d of the sphere center (cf. figure 2.1).

The acoustical surface potential $\phi|_S$ and its normal derivative corresponding to the normal velocity $\left.\frac{\partial\phi}{\partial n}\right|_S$ in this case can be written as:

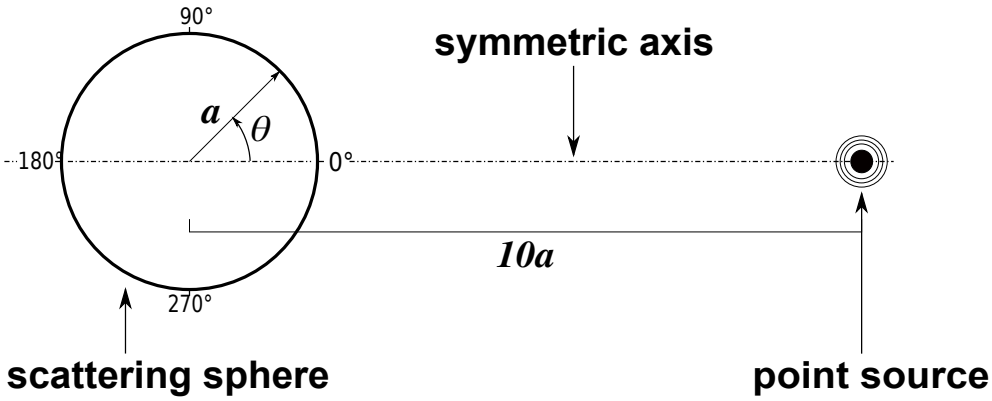

FIGURE 2.1: *Schema of the studied problem: a sphere of radius a excited by a point source.*

$$\phi|_S = -\frac{Q}{4\pi k a^2}\sum_{n=0}^{\infty}\frac{(2n+1)h_n(kd)P_n(cos\theta)}{h_n'(ka)+\sigma h_n(ka)}, \qquad \left.\frac{\partial\phi}{\partial n}\right|_S = i\sigma\,\phi|_S\,, \tag{2.1}$$

where σ is the complex admittance and the azimuthal angle θ, is the angle between the radius vector of the surface point and the direction of the incident wave. Note that the surface potential and its normal derivative are only related to θ, which means that this problem is axi-symmetrical (see figure 2.1), implying that only the solution for $\theta \in [0, \pi]$ needs to be computed in order to know the solution on the whole surface. Both equations bring into play Legendre polynomials $P_n(\mu)$ defined in the range $[-1, 1]$, spherical Hankel functions of the first kind h_n (often denoted $h_n^{(1)}$) and their derivatives h_n'. Further information about the relations between Bessel's functions can be found in [Abramowitz 1964].

Note that equations (2.1) can also be simplified into the limit solution of a rigid body ($\sigma = 0$) and the limit solution of a soft body ($\sigma = \infty$) published previously in [Hanish 1981]. We also notice that the solution of the plane wave scattering by a rigid sphere was published by Lord Rayleigh a century ago [Rayleigh 1904].

2.2 Validation of the algorithm for regular frequencies

The linear system of equations is solved by using the Generalized Minimum RESidual method, [Saad 1986]. Iterative techniques have been investigated in quite a number of papers by AMINI and al. [Amini 1987, Amini 1990b] who investigated the application of different iterative methods for exterior acoustic problems, in particular for the Burton & Miller formulation. Since an iterative technique will be subsequently used in the framework of the FMBEM, we first propose to check its accuracy and its reliability for solving exterior acoustical problems through the boundary element method.

Comparison of the surface sound pressure level

The verification tests are made for a sphere of radius a, whose surface is meshed with 31696 planar triangular elements to keep a very good continuity on the curved surface since it corresponds to a space discretization criterion equal to 10 elements per λ for the highest considered frequency (see results in appendix B.2). 360 receivers are evenly distributed on the surface of the sphere in a vertical plane. Figure 2.2 shows the comparisons of the sound pressure level in decibels, in terms of azimuthal angle in degrees, between the analytical solution (blue line) and the solution computed with BEM algorithm using a collocation approach (dashed red line). The comparisons are performed for six dimensionless wave numbers: $2ka = kD = 0.1$, 1.0, 2.0, 5.0, 10 and 20, corresponding to frequencies equal to 5.4, 54, 108, 271, 541 and 1082 Hz respectively. In order to ensure that both kernels G and F are properly computed, we consider a rigid case for which only the kernel F is involved, and also an impedance case for which both kernels G and F are involved. The impedance has been chosen to study the limit cases of a rigid body (*i.e.* $\sigma = 0$), and a soft body with a normalized complex impedance (compared with the air) $Z/Z_A = \sigma_A/\sigma = 1.22 + 1.22i$.

The source has a unit amplitude Q = 1 and the reference pressure chosen is 20 μPa, *i.e.* reference of the dB (SPL) (Sound Pressure Level). We have chosen to use the iterative solver GMRES with the BEM algorithm even though it is not justified according to the expensive computation time. Indeed the computation time involved by the iterative process with the BEM in this case leads to a more expensive computation time than a direct solver such as Gauss elimination since the matrix vector product needs to be computed at each iteration. However, since we will use the GMRES solver in our FMBEM code, it is suitable to use this solver now. The GMRES solver stops when the residue is below the relative tolerance 1.10^{-3} without using a restart condition, since a small number of iterations is required in these verification procedures.

We can see a very satisfactory consistency between the analytical (equation 2.1) and the BEM solutions (see figure 2.2) for both cases, rigid and impedance (solid lines and dashed lines are superposed), meaning that the kernels F and G are properly computed. Thus the BEM algorithm is relevant to subsequently be used to take into account the *near interactions* for regular frequencies in the framework of the FMBEM formalism. We point out that the considered frequencies have been chosen in order to avoid the well known fictitious eigenfrequency problems which will be treated in a following section (2.3).

Number of iterations for a frequency range

Since we have checked the accuracy of the BEM for discrete frequencies, we focus on the behavior of the iterative solver for a frequency range. We study a range of frequencies starting from the dimensionless frequency $2ka = kD = 0.09$ or 0.03λ to $2ka = kD = 20.3$ or 6.5λ corresponding to 5 and 1100 Hz respectively with a 1 Hz step. We are still considering the case of the scattering sphere excited by a point source (see figure 2.1). Due to the large number of calculations involved by the fine frequency step (*i.e.* 1 Hz) and in order to emphasize what happens for each frequency, we set the number of constant triangular

element to 7932 (5 elements per λ at 1100 Hz, see results in appendix B.1). In figure 2.3 we can see the total number of iterations required by the GMRES to approach the solution of the system under the prescribed tolerance for every frequency.

We can see the behavior of the convergence for both kernels F (rigid case in blue line) and G (sound soft case in red line), in figure 2.3 for zero velocity and zero pressure conditions on the boundary respectively. A zero pressure boundary condition requires more iterations to converge than a zero velocity boundary condition, most likely because of the computation of the singular integral kernel G when the source point and the collocation point are on top of each other. We emphasize through this section, the fluctuating increase of the number of iterations with frequency. Indeed we can see sharp peaks occurring around specific frequencies. These frequencies, the so-called eigenfrequencies, do actually correspond to the resonance frequencies of the associated interior problem of the scattering sphere. This difficulty is referred to as the fictitious eigenfrequency problem and is a pure numerical artifact since it can be proved that the matrix system does not possess a unique solution at these characteristic frequencies. As a result the exterior pressure field will be disturbed even for rigid boundary condition which does not have physical meaning. The density of appearance of eigenfrequencies increases with the frequency and causes the instability of the iterative solver (starting from $ka = 5\pi$) leading to an inefficiency of the iterative solver at higher frequency. Some of these frequencies are highlighted in dashed black lines in figure 2.3. Resonances occur with a dimensionless frequency $ka \propto n\pi$ corresponding to pure radial mode (*i.e.* eigen modes of the pulsating sphere). We focus more specifically in the following section on three eigenfrequencies for $ka = \pi, 6.98$ and 15.04 (emphasized in figure 2.3).

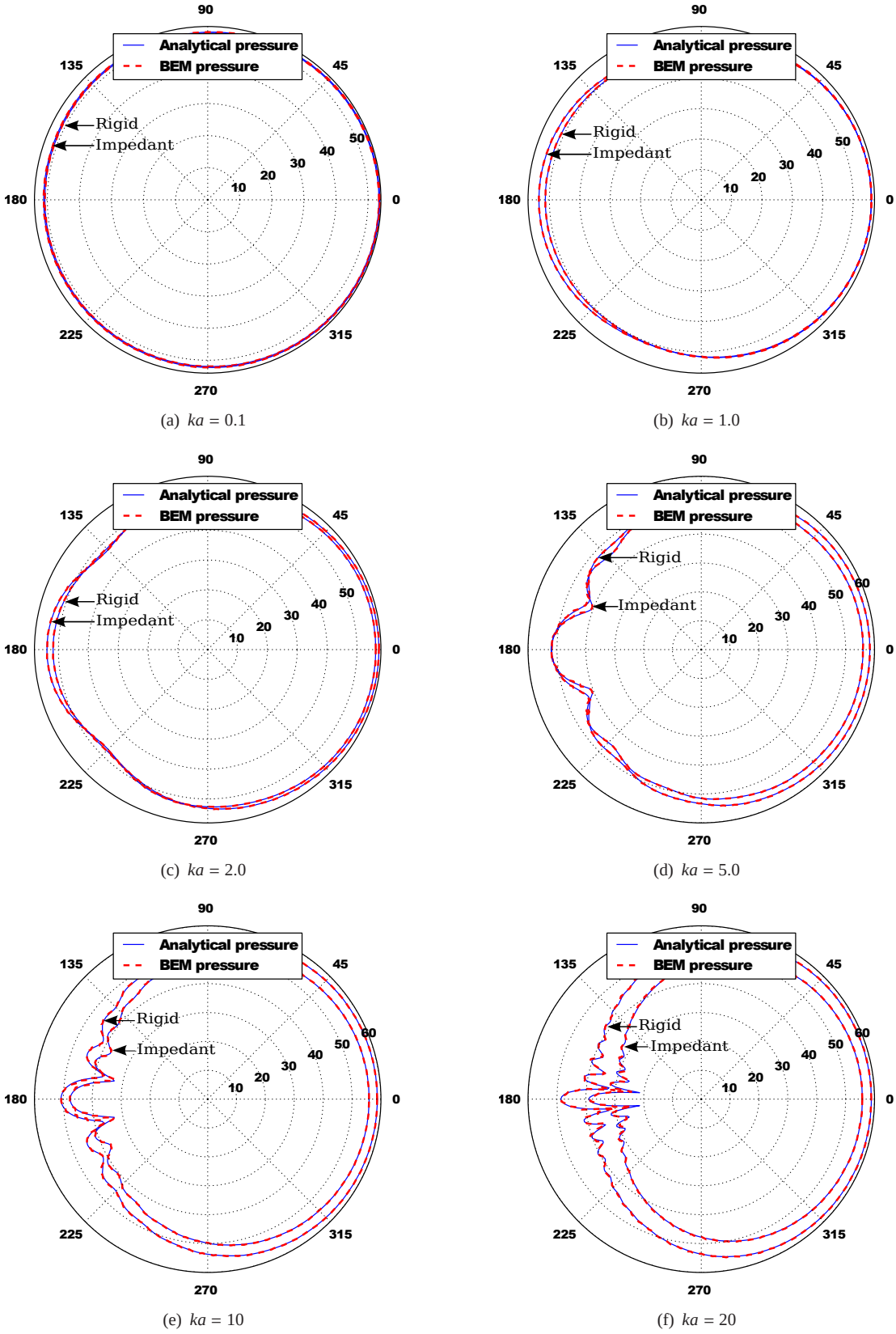

(a) $ka = 0.1$ (b) $ka = 1.0$

(c) $ka = 2.0$ (d) $ka = 5.0$

(e) $ka = 10$ (f) $ka = 20$

FIGURE 2.2: *Comparison between the analytical solution (blue lines) and the BEM solution (dashed red lines) of the sound pressure level in dB (SPL) on the surface of the sphere excited by a point source of unit amplitude $Q = 1$. The reference pressure is 20 μPa. The source is located at* 10*a from the sphere center (a = radius).*

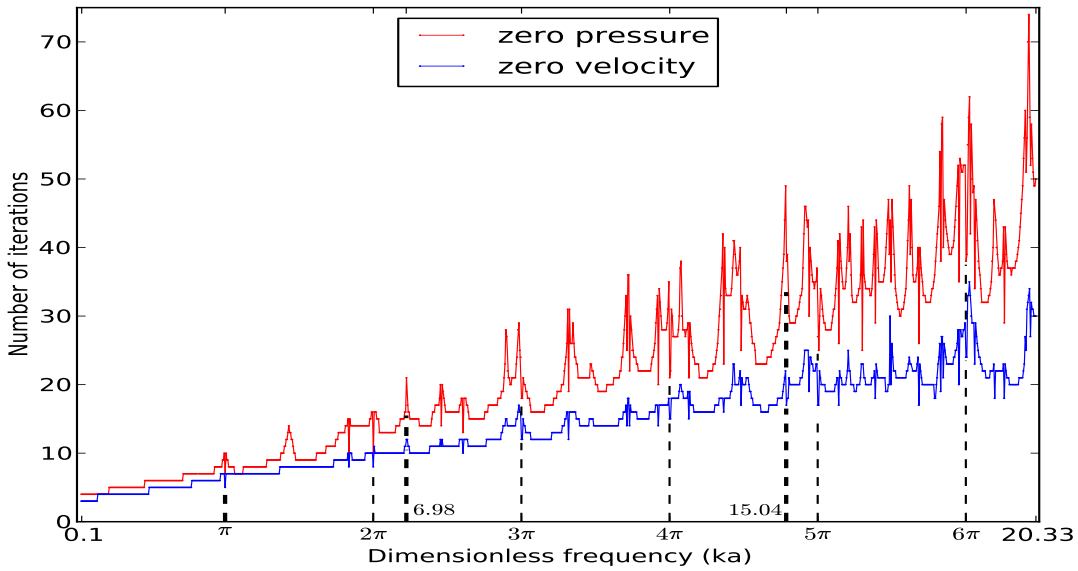

FIGURE 2.3: *Number of iterations required for GMRES to converge below the prescribed tolerance (i.e.*10^{-3}*) for zero pressure boundary condition in red line and zero velocity boundary condition in blue line. The dashed black lines indicate some fictitious eigenfrequencies.*

2.3 Treatment of the fictitious eigenfrequency problem

The pulsating sphere has been extensively used in the literature to show the effect of irregular frequencies. Often, the only irregular frequencies observed in this case correspond to zeros of $j_0(ka)$, that is $ka = n\pi$, with $n = 1, 2, 3, ...$ corresponding to pure radial modes. The problem of the scattering sphere involves in addition all ortho-radial and combined modes (see figure 2.3). As the density of irregular frequencies increases with increasing values of the wavenumber k and causes the instability of the iterative solver, an effective solution to overcome this problem seems to be required.

We focus in this section on 3 eigenfrequencies, *i.e.* $ka = \pi$, 6.98 and 15.04 denoted by the thick dashed black lines in figure 2.3. The number of constant elements is set to 31696 to keep a good continuity of the pressure field on the mesh. To prove the resonant behavior, we draw an internal noise map at each eigenfrequency (see figures 2.4(a), 2.4(c) and 2.4(e)) and distinctly see three eigenmodes of the sphere. $ka = \pi$ is the first radial mode, 6.98 is the third orthoradial mode and 15.04 corresponding to a complex combined mode. It turns out that for these three resonances the BEM algorithm fails in properly computing the correct solution as we can see in figures 2.4(b), 2.4(d) and 2.4(f). This is a well-known conclusion that the classical BEM does not possess a unique solution at certain characteristic frequencies for exterior acoustic propagation problems.

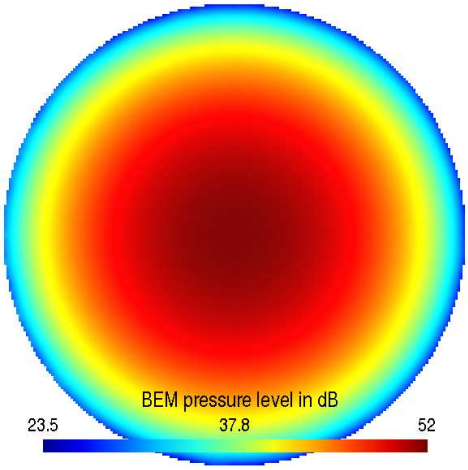

(a) internal pressure, $ka = \pi$

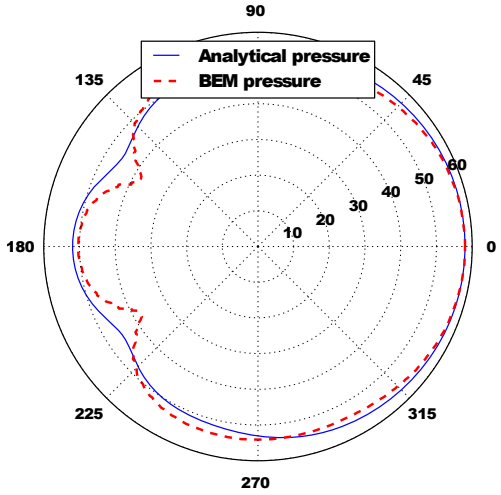

(b) surface pressure, $ka = \pi$

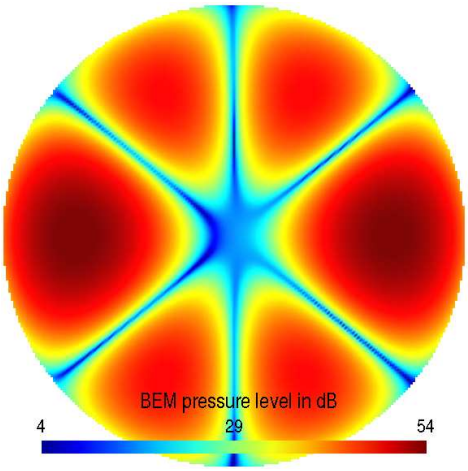

(c) internal pressure, $ka = 6.98$

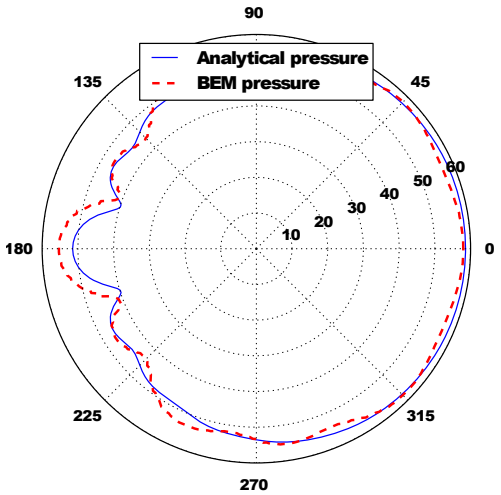

(d) surface pressure, $ka = 6.98$

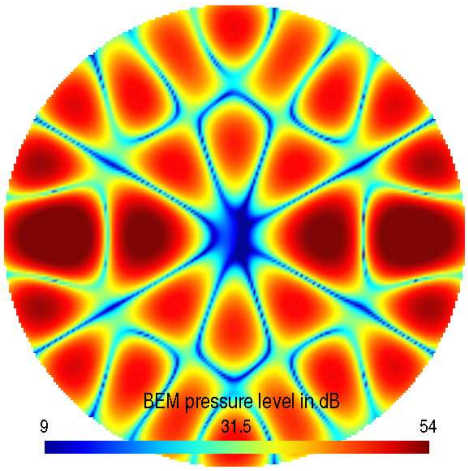

(e) internal pressure, $ka = 15.04$

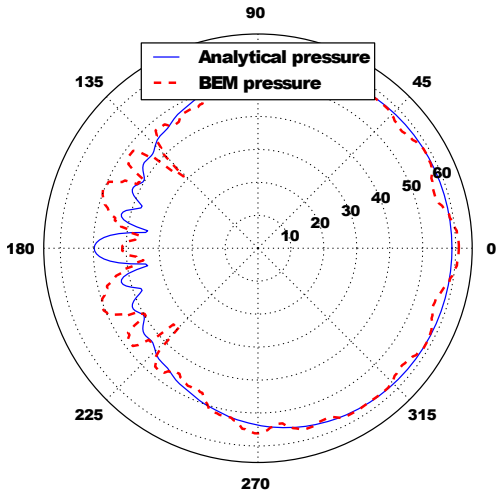

(f) surface pressure, $ka = 15.04$

FIGURE 2.4: *Cut plane along the symmetric axis of the sound pressure level in dB (SPL) within the scattering sphere on the left side and surface pressure in dB (SPL) ($p_0 = 20\ \mu Pa$) on the right side for 3 eigenfrequencies. The BEM (dashed red lines) fails to properly computing the correct solution (blue lines).*

In the following section, we solve the scattering sphere problem for irregular frequencies with the Burton & Miller formulation (CHBIE). It has been proved [Burton 1971] that the linear combination with a complex coupling constant of the BIE and its normal derivative yields a unique solution for all frequencies. We remind that the hypersingularity problem occurring with the integration of the H kernel will be overcome through the static subtraction technique (see eq. (1.38) in section 1.4). We first focus on the iterative solver behavior with the use of the B&M formulation for the same range of frequency as in section 2.2 (*i.e.* from $ka = 0.09$ to $ka = 20.3$) and subsequently provide the proof of the robustness and accuracy of the B&M formulation applied to the problem of the scattering sphere. The number of constant elements is once again set to 7932 (see results in appendix B.1) for the study of the iterations and 31696 (see results in appendix B.2) for the study of the pressure field on the mesh.

Influence of the B&M formulation on the convergence of the iterative solver

We first focus in this section on the behavior of the iterative solver with the B&M formulation. We compare the total number of iterations obtained for each frequency with the classical formulation of the BIE previously studied in section 2.2, with the B&M formulation of the BIE (*i.e.* equation (1.33) with a weighting parameter $\eta = 0.5$). We show the differences for both formulations for the limit case of an imposed zero pressure ($Z = 0$) boundary condition in figure 2.5(a) and the limit case of an imposed zero velocity ($Z \mapsto \infty$) boundary condition in figure 2.5(b). This study allows us to emphasize the influence of contributions of the kernel K ($Z = 0$) and the kernel H ($Z \mapsto \infty$) of the B&M formulation.

Figure 2.5(a) shows the benefit for a zero pressure boundary condition of the B&M formulation for the whole frequency range. Indeed, while the classical BIE has an unpredictable behavior, the B&M formulation seems to provide a better conditioning of the matrix system and yields a very slow increase of the number of iterations with respect to frequency. Thus we can say that the addition of the derivative of the kernel G, K, which takes part in the B&M formulation stabilizes the number of iterations and allows a decrease of computation time even though the evaluation of two additional integrals are required at each iteration. Figure 2.5(b) shows the decrease of the number of iterations with respect to frequency for a zero velocity boundary condition. For a dimensionless frequency inferior to 3π more iterations with the B&M formulation are required than with the classical BIE, but less iterations starting from 3π to the end of the range. Thus, the derivative of the kernel F, H, allows a decrease of the number of iterations as the frequency increases.

We point out that the B&M formulation leads to a stable dependency of the number of iterations on the whole frequency range regardless of the boundary conditions (*i.e.* absence of peaks and fluctuating behavior). In the next section, we will see if the B&M formulation is relevant to provide a satisfactory accuracy specifically for several fictitious eigenfrequencies of the problem.

Application of the B&M formulation at singular frequencies

In the previous section, the efficiency of the B&M formulation has been shown through the convergence of the iterative solver. We now focus on its efficiency to solve a scattering problem by a spherical body. We compare, in figure 2.6, the surface pressure computed on the sphere for the same three eigenfrequencies as in section (2.3), $ka = \pi$, 6.98 and 15.04 for rigid boundary conditions ($Z \mapsto \infty$) on the left hand side and complex impedance boundary conditions ($Z = 1.22 + 1.22i$) on the right hand side. The analytical solution is displayed in blue line and the BIE with the B&M formulation in dashed red line. The unsatisfactory solutions obtained with the classical BEM are also recalled for the rigid case, on the right hand side (see section 2.2) and for impedance boundary conditions on the left hand side.

The very good agreement between the analytical solution and the solution obtained with the B&M formulation, on the left side (figure 2.6), proves the efficiency of the kernel H to overcome the eigenfrequency problem for rigid boundary conditions. While the very good agreement between the analytical solution and the solution obtained with the B&M formulation, on the right side (figure 2.6), proves the efficiency of both kernels H and K to overcome the eigenfrequency problems for impedance boundary conditions. It follows that the derivated kernels H and K are properly computed and the B&M formulation is relevant to overcome the fictitious eigenfrequency problems for mixed boundary conditions for the case of the scattering sphere.

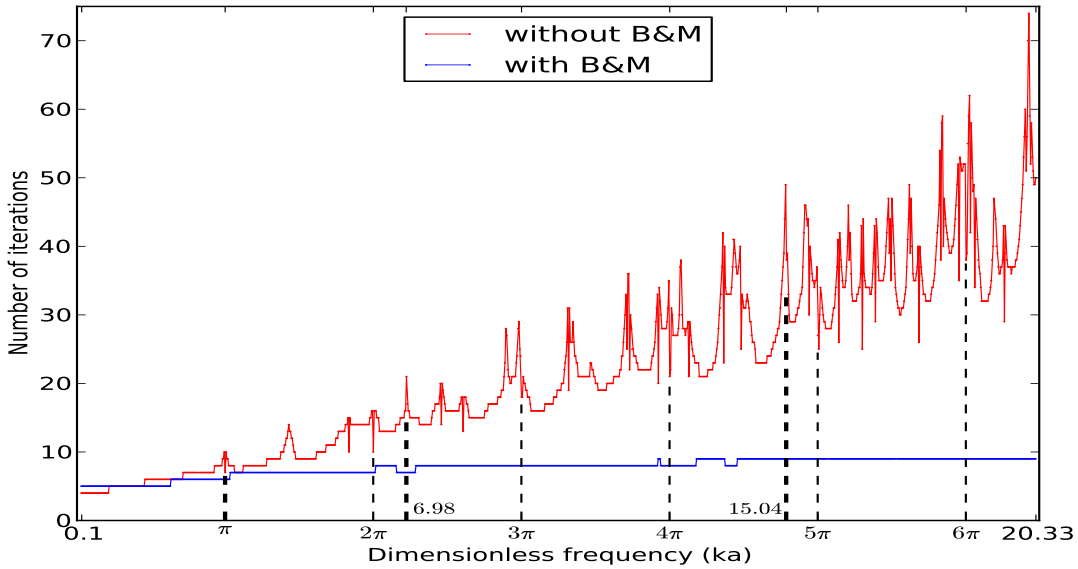

(a) number of iterations required for zero pressure boundary condition without B&M formulation (red line) and with B&M formulation (blue line).

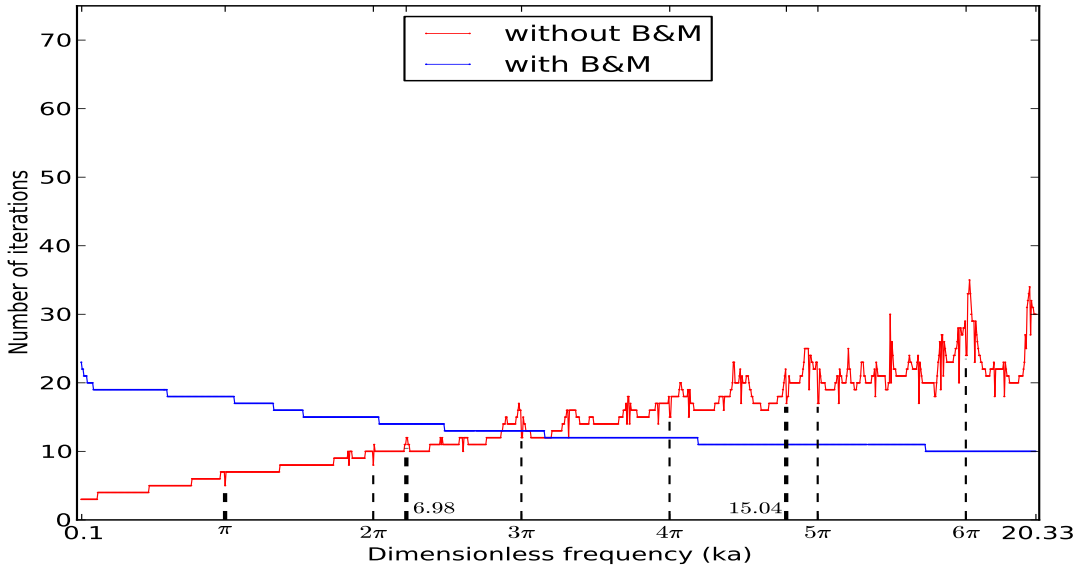

(b) number of iterations required for zero velocity boundary condition without B&M formulation (red line) and with B&M formulation (blue line).

FIGURE 2.5: *Number of iterations required for GMRES to converge below the prescribed tolerance (i.e.*10^{-3}*) for zero pressure (a) and zero velocity (b) boundary condition. The dashed black lines indicate some fictitious eigenfrequencies.*

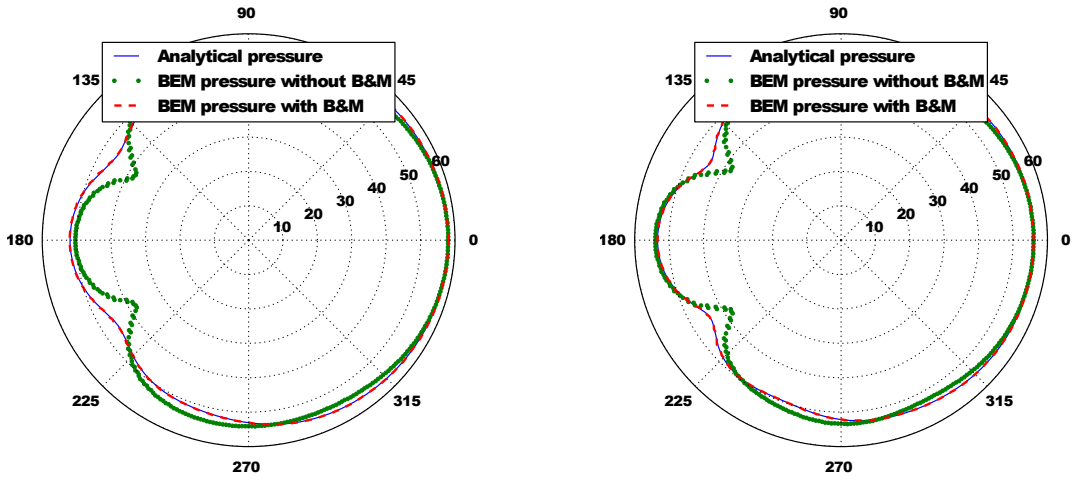

(a) $ka = \pi, Z \mapsto \infty$ (b) $ka = \pi, Z/Z_A = 1.22 + 1.22i$

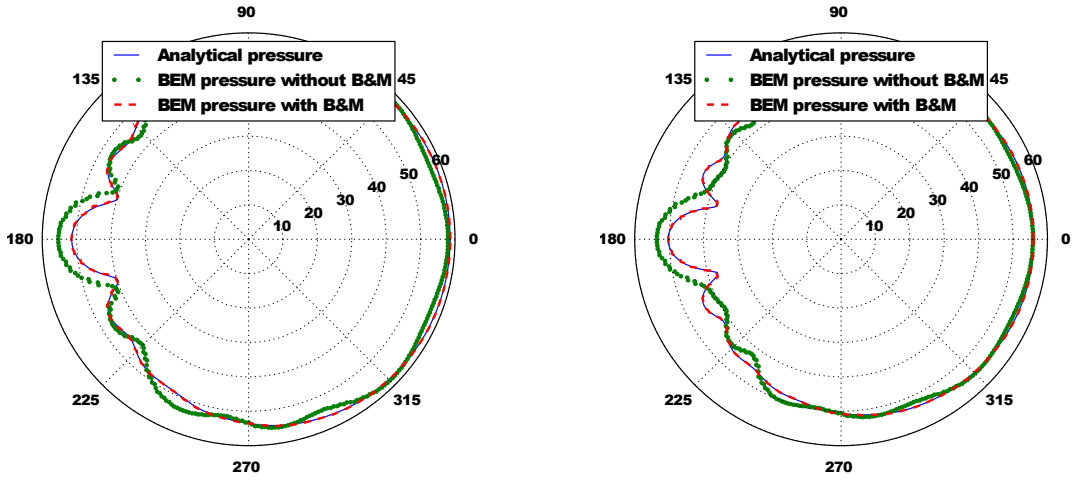

(c) $ka = 6.98, Z \mapsto \infty$ (d) $ka = 6.98, Z/Z_A = 1.22 + 1.22i$

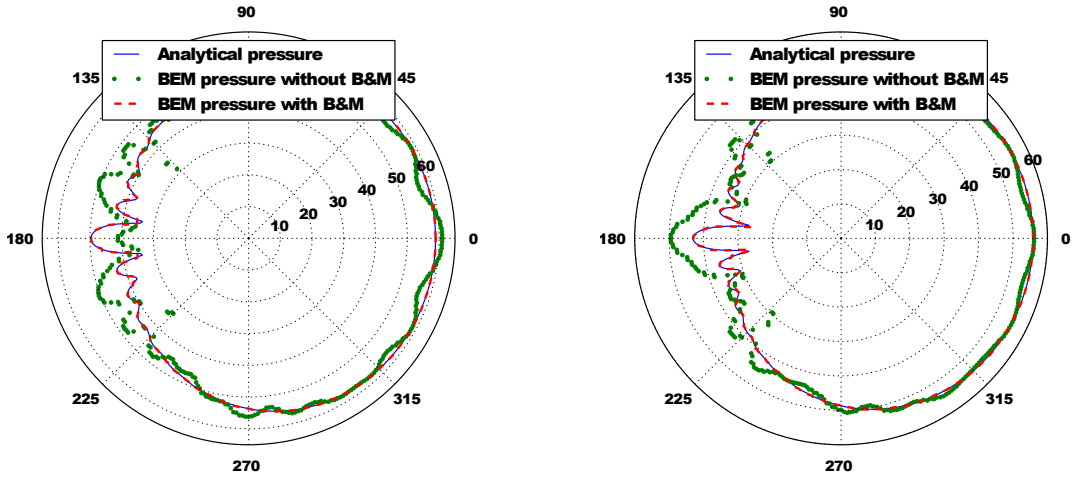

(e) $ka = 15.04, Z \mapsto \infty$ (f) $ka = 15.04, Z/Z_A = 1.22 + 1.22i$

FIGURE 2.6: *Comparison between the analytical solution (blue lines) and the BEM solution with and without the B&M formulation (dashed red lines and green dots respectively) of the surface pressure level in dB (SPL) ($p_0 = 20\mu Pa$). The 3 fictitious eigenfrequencies are studied for rigid (left side) and impedance (right side) boundary conditions. The sphere is excited by a point source of unit amplitude $Q = 1$ located at $10a$ from the sphere center.*

2.4 Analytical angular integration on a singular element

The main difficulty occurring with the CHBIE formulation is related to the evaluation of singular integrals. However, the singular integrals (weak or hyper singular) can be evaluated analytically in the sense of finite-part [Dangla 2005, Matsumoto 2010] when the mesh is discretized with constant elements. The obtained boundary integral expression includes neither the fundamental solution of Laplace's equation nor the tangential derivative of the sound pressure, which exist in the formulation based on regularization, and can be easily implemented in the BEM. We proceed as follows: the integral of the surface in which the collocation point is located is evaluated in polar coordinates (r, θ) by dividing the element into three parts as shown in figure (2.7).

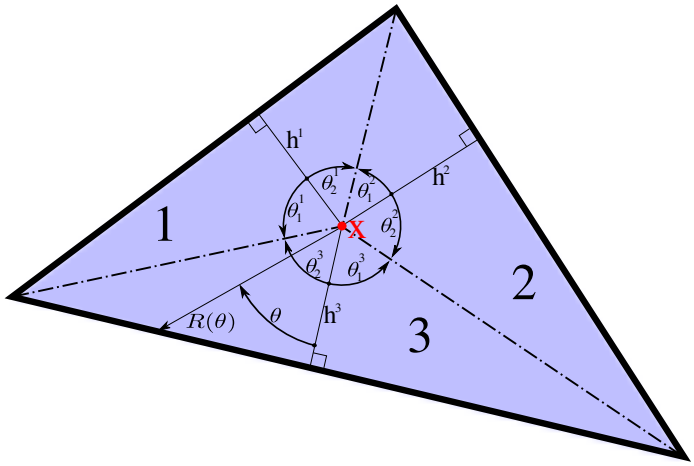

FIGURE 2.7: *Definition of variables used for the evaluation of singular integrals in polar coordinates.*

According to the definition of the Green's function G and assuming constant triangular elements, the contribution of the integral of the G kernel leads to calculate the following expression:

$$\int_S G(\mathbf{x},\mathbf{y})q(\mathbf{y})dS = \int_{S/dS_\mathbf{x}} G(\mathbf{x},\mathbf{y})q(\mathbf{y})dS + \frac{i}{2k}\left(1 - \frac{i}{2\pi}\sum_{m=1}^{3}\int_{\theta_1^m}^{\theta_2^m} \mathrm{e}^{ikR(\theta)}d\theta\right)q(\mathbf{x}), \tag{2.2}$$

where S/dS_x denotes the boundary S excluding the boundary element dS_x in which the collocation point x is located, m is related to the triangle $m = 1, 2$ and 3. For a detailed calculation, the reader may refer to [Matsumoto 2010]. A similar development can be carried out on the hypersingular integral (H kernel), involving a double normal derivative of the fundamental solution which appears in the CHBIE formulation. Its evaluation in polar coordinates leads to calculate the following expression:

$$\int_S H(\mathbf{x},\mathbf{y})\phi(\mathbf{y})dS = \int_{S/dS_\mathbf{x}} H(\mathbf{x},\mathbf{y})\phi(\mathbf{y})dS - \frac{i}{k}\left(\frac{ik}{2} - \sum_{m=1}^{3}\int_{\theta_1^m}^{\theta_2^m} \frac{\mathrm{e}^{ikR(\theta)}}{4\pi R(\theta)}d\theta\right)\phi(\mathbf{x}). \tag{2.3}$$

The resulting CHBIE only consists of integrals of regular functions of angular variables and can be evaluated numerically directly by means of the standard Gaussian quadrature.

However, this latter expression (2.3) has not been implemented successfully in the algorithm in the framework of this thesis, thus the study of the influence on the convergence of the iterative solver of the analytical integration on singular elements, will be only carried on the weakly singular integral (*i.e.* integral of G kernel equation (2.2)).

Influence on the iterative solver

We study the same frequency range as studied in previous sections, starting from the dimensionless frequency $2ka = kD = 0.09$ or 0.03λ to $2ka = kD = 20.3$ or 6.5λ corresponding to 5 and 1100 Hz respectively with 1 Hz step. We are still considering the case of the scattering sphere excited by a point source (see figure 2.1). Due to the large number of computations involved by the fine step (*i.e.* 1 Hz) in order to emphasize what happens for each frequency, we set the number of constant triangular elements to 7932 ($5elmts/\lambda$ at 1100 Hz, see results in appendix B.1) . As mentioned above, we only focus on the integration of the G kernel, that is to say for sound soft values on the boundary $Z/Z_A = \sigma_A/\sigma = 1.22 + 1.22i$. In figure 2.8, we can see the total number of iterations required by GMRES to approach the solution of the system under the prescribed tolerance 10^{-3} for every frequencies without the angular integration (in dotted blue line) and with the angular integration described in this section (in red line). The discrepancy between both integrations are displayed in cyan line.

The average deviation between both integration techniques is 0.64. This means that even if the number of iterations of the analytical integration leads to the same fluctuating behavior than the integration with the Gaussian quadrature, it seems nevertheless to improve the convergence at some discrete frequencies, while keeping the same accuracy as shown in figure 2.9 for the two frequencies 5 Hz and 541 Hz, on the left and right hand side respectively. For these reasons the analytical integration of G kernel on the singular element will be used for the upcoming calculations.

2.5 In summary

This chapter (2) has been dedicted to the validation of the reliability of the BEM algorithm. Thus we have checked the accuracy of the BEM algorithm to solve a scattering problem by a spherical body by performing comparisons with the analytical solution for both rigid and impedance cases. We also ensure the reliability of the weakly form of the conventional and hypersingular boundary integral equation to overcome the fictitious eigenfrequency problems and investigate on the influence of this formulation on the behavior of the iterative solver. Indeed, a prior assessement of the successful implementation of the BEM is a crucial aspect of the fast multipole formalism since the BEM calculation will be subsequently used for the evaluation of the direction interactions.

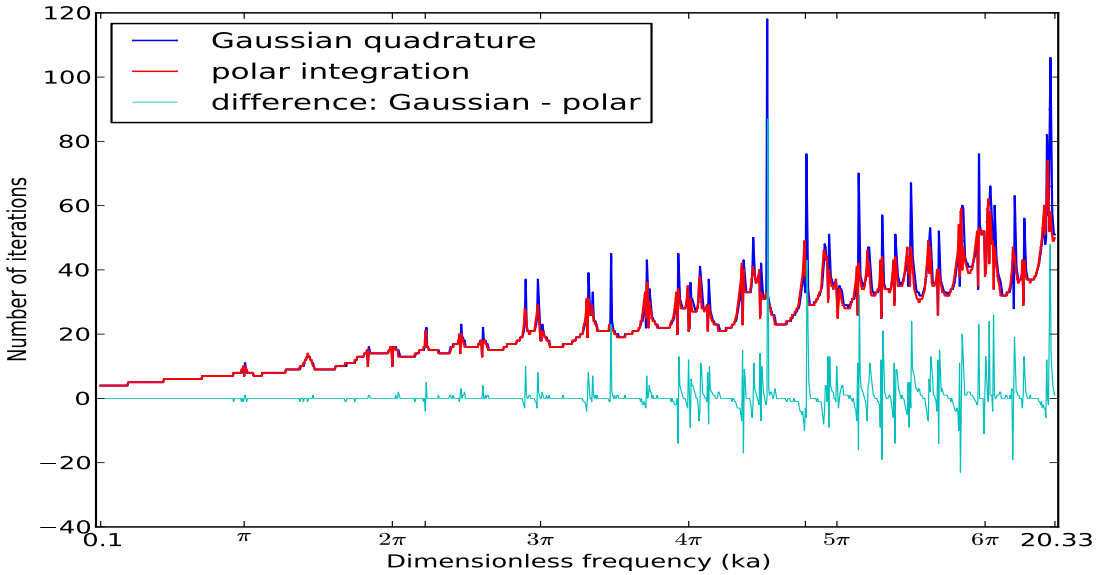

FIGURE 2.8: *Number of iterations required for GMRES to converge below the prescribed tolerance (i.e.*10^{-3}*) for zero pressure boundary condition considering a standard Gaussian quadrature (blue line) and polar (red line) integrations. Difference between both integrations are displayed in cyan line.*

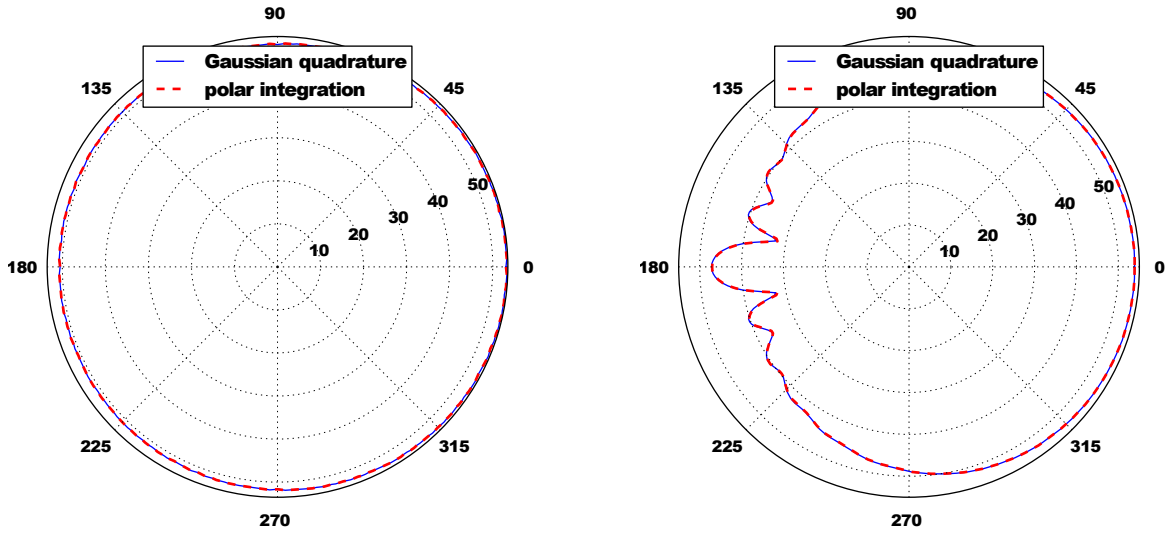

(a) $ka = 0.1$ (b) $ka = 10$

FIGURE 2.9: *Comparison between the surface sound pressure in dB (SPL) level computed with the Gaussian quadrature integration and the polar analytical integration on the singular element for a sound soft scattering sphere* ($Z/Z_A = \sigma_A/\sigma = 1.22 + 1.22i$) *excited by a spherical wave located* $10a$ *away from the sphere center.*

Part I: Conclusion

The boundary element method: (i) eliminates the need to consider the infinite domains usually associated with radiation problems; (ii) reduces the dimensionality of the problem by one leading to a two dimensional surface integral equation for three dimensional partial differential equation and (iii) can readily handle arbitrary geometries and boundary conditions. However, the matrix system derived by the previously described BEM formalism is fully-populated, non-symmetrical and can also be ill-conditioned. It follows that the solution of the system (1.40), by the use of a direct solver such as Gauss elimination requires $O(N^3)$ operations because of the general form of the matrix system. Even with the help of an iterative solver to approach the solution, the BEM formalism still requires an amount of storage memory $O(N^2)$ and a time dependency $O(N^2)$ for computing the matrix entries. From a practical viewpoint, this feature involves an expensive computation time for a large scale model, since for a given space discretization criterion in terms of frequency f, $N \propto f^2$ and the computation time dependency is $O(f^6)$ ($O(f^4)$ with an iterative solver). Such a dependency leads to prohibitive computation times as frequency increases and highlights the interest of research related to the development of fast and efficient methods for the improvement of existing algorithms. Improving the computational cost of the BEM by an order of magnitude through the fast multipole formalism will be the scope of the following part (II). We investigated, in this part, the ability of the conventional & hyper-singular boundary integral formulation to successfully solve a scattering problem by a spherical body, even at fictitious eigen-frequencies, for both rigid and impedance boundary conditions. As a result, the boundary element algorithm is found to be reliable to compute the direct interactions in the framework of the fast multipole boundary element algorithm.

Part II

Fast Multipole formalism for acoustic waves: Theory & verification

Part II: Introduction

The conventional Boundary Element Method (BEM), as described in the previous chapter, produces dense and non-symmetric matrices which require $O(N^2)$ operations to compute the matrix coefficients and $O(N^3)$ operations to solve for the system through direct solvers, N being the number of equations of the linear system. Many methods have been proposed to counter this drawback. One of the most widely used is the combination of the BEM with an iterative solver such as Generalized Minimal Residual (GMRES) [Saad 1986]. The computation time is, in such a way, dictated by the time required to store the matrix entries. This leads to a decrease of solution cost from $O(N^3)$ to $O(N^2)$. Regarding the storage memory, the $O(N^2)$ dependency can be reduced to a linear dependency by storing only the matrix-vector product and never explicitly built the entire dense matrix. However, this requires the evaluation of $O(N^2)$ interactions at each iterative solver step. However, through the fast multipole formalism the evaluations of interactions can be performed at each step of the iterative process, with a $O(N)$ dependency. This point is the topic of this part.

The purpose of this second part is to introduce the fast multipole principle as well as the mathematical background required to perform calculations. Consistently with the previous part, we also assess the ability and the accuracy of the fast multipole method for solving a scattering problem by a spherical body. This validation will allow subsequently to solve more realistic propagation problems in the next part.

The third chapter (3) is dedicated to the introduction of the fast multipole formalism applied to the Boundary Element Method. After presenting a brief overview of the fast multipole principle, we introduce the mathematical background required by a fast multipole algorithm. Thus, we detail the spherical harmonic series, the RCR-decomposition and the high frequency formulation which the algorithm is based on. A more precised description of the algorithm stages is also realized i.e. the multipole expansion step, the translation of the multipole expansion coefficient and the final summation step. Finally, we provided a rapid assessment of the error bound as well as the theoretical computational complexity.

The fourth chapter (4) is dedicated to the validation of the fast multipole boundary element method. We assess the fast multipole for solving three dimensional scattering problem for both rigid and impedance boundary conditions by comparison with the analytical solution. We also focus on the infuence of the conventional and hypersingular boundary integral equation on the iterative solver. Finally, we discuss how ground reflections can be taken into account, from a fast multipole point of view, through the infinite rigid

baffle. Indeed the half space propagation problem will be subsequently used in an urban context.

Chapter 3

The fast multipole formalism applied to the boundary element method for acoustic waves

3.1 A general overview of the fast multipole method principle

3.1.1 Brief review of the method

The Fast Multipole Method (FMM) comes from Rokhlin and Greengard's work [Rokhlin 1985], [Greengard 1987]. While it was first formulated for the rapid evaluation of the potential or gravitational fields governed by Laplace equation including a large number of particles in two and three dimensions, it was more generally extended later for the multiplication of $N \times N$ matrices. Thus, the FMM has subsequently been applied to electromagnetism problems [Coifman 1993, Song 1997, Chew 1997, Sylvand 2002], acoustical problems [Gumerov 2004], elastodynamics problems [Chaillat 2008, Chaillat 2013], Stokes flow [Gomez 1997, Liu 2008], etc. For a complete overview of the FMBEM and its application in physics, the reader may refer to [Liu 2009]. Coupled with the advances in iterative methods for the rapid solution of linear systems, the FMBEM can efficiently reduce complexity of the computational time and memory to a linear dependency, $O(N)$ or $O(NlogN)$. The term "iterative methods" refers to a wide range of techniques using, at each step, more accurate successive approximation of the linear system solution. Several of them are described in [Barrett 1994] and applications in the framework of the boundary element method for both external and internal acoustic problems have been investigated in [Amini 1987, Amini 1990b], [Yasuda 2007]. Among them, the Generalized Minimum RESidual (GMRES) [Saad 1986], has become a reliable tool for the efficient solution of large scale acoustic problems as shown in some papers [Marburg 2003, Schneider 2003]. For extremely large problems, the gain in efficiency and memory can be very significant, and enables the use of more sophisticated modeling approaches that, while known to be better, may have been discarded as computationally unfeasible so far.

Since the early 1990's, the FMM algorithm for solving Helmholtz equation has been widely covered in the literature. A very detailed description of the application of FMM to the Helmholtz equation was introduced by Epton & Dembart [Epton 1995]. Because of the $O(p^5)$ nature of the standard formulation, with p related to the precision of the method, using the Wigner 3-j symbols, the number of operations can be reduced to $O(p^4)$ by the use of various recursive relations, but the computing time can still increase quickly with the increase of the value of p. Based on a *direct Rotation-Coaxial translation-inverse Rotation* decomposition (RCR-decomposition) [Gumerov 2004], Gumerov & Duraiswami have developed a formulation using a set of coefficients which can be computed recursively and does not introduce the Wigner 3-j symbol [Gumerov 2001, Gumerov 2003]. This latter $O(p^3)$ formalism has been considered in the implementation of our FMBEM algorithm and is described in the following.

Furthermore, to counter the instability problem of the FMM in its original version at high frequency, Rokhlin developed a high frequency formulation using a diagonal translation [Rokhlin 1993] and fast spherical transforms [Swarztrauber 2000], [Sakuma 2002, Schneider 2003]. This formulation has subsequently led to a broadband/wide-band FMBEM algorithm including both low and high frequency formulations [Cheng 2006], [Gumerov 2009] and has also been applied to a Galerkin boundary element method [Fischer 2004].

3.1.2 Overview of the method

The first key idea is the application of an iterative solver such as GMRES to approach the solution of the matrix system and accelerate the matrix-vector product required at each iteration through the fast multipole principle. This principle consists in grouping sources' contributions around a common referential which can be seen as a single source in order to subsequently calculate this unique influence to well separated receivers. The simplest form of the FMM, also known under the name of the Middleman method can only be applied when sources and receivers are located in well separated areas, actually useless in the framework of the BEM since the nodes of the boundary can be seen as sources and receivers alternatively and so are not well separated. To overcome this limitation, the Middleman principle can nevertheless be applied with the use of a space partitioning. Figure 3.1 illustrates how computational savings appear through this space partitioning. Instead of the evaluation of all pairwise interactions between the sources and evaluation points (figure 3.1(a)), as it is realized in the framework of the standard BEM, we can evaluate the interactions between sources and expansion centers, between expansion centers and expansion centers and finally between the expansion centers and evaluation points. This constitutes the Single Level Fast Multipole Method SLFMM principle [Coifman 1993] (figure 3.1(b)). Following the development of the previous idea, for the fast evaluation of a potential due to a large number of sources, it leads to the Multi Levels Fast Multipole Method MLFMM and results in the organization of a hierarchical space partitioning (figure 3.1(c)). In a such a way, the interactions will be then performed between boxes and groups of boxes allowing that the evaluation areas can now be next to each other.

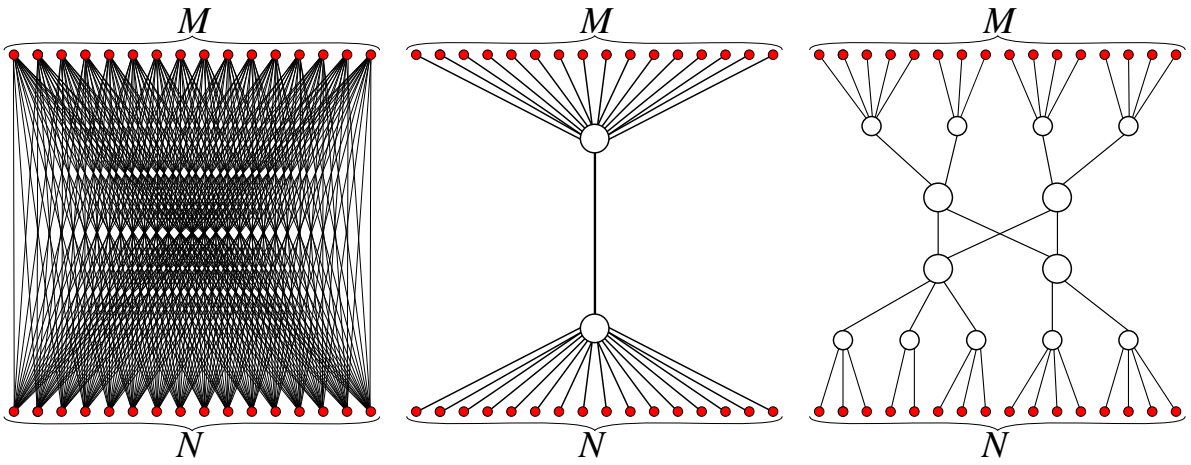

(a) straightforward method: number of interactions $O(N \times M)$.

(b) Single Level FMM $O(N + M)$

(c) Multi-Level FMM: number of interactions $O(N + M)$.

FIGURE 3.1: *Comparison of the number of interactions between N sources and M receivers for (a): the straightforward method (classical BEM), (b): the Single Level FMM and (c): the Multi Level Fast Multipole Method. The lines show the interactions for each method, the red circles symbolize the elements and the black circles represent the expansion centers.*

We introduce in this chapter the formalism for the fast multipole method and assess the efficiency of our algorithm to solve basic scattering problems. First, we make a general overview of the FMBEM formalism and introduce the mathematical background related to the FMBEM and the RCR decomposition. We also describe more practically each step required by a fast multipole algorithm. Then, we assess the algorithm with the analytical solution of a scattering problem by a spherical body in order to prove its efficiency. We also study the behavior of the iterative solver in terms of boundary conditions and frequency. Next, we describe how reflections on a rigid ground can be accounted for in the framework of the FMBEM, using the image source principle. Finally, we deal with the half-space problem through the infinite fictitious rigid baffle which will be subsequently used in the next part to take into account the reflection in a more realistic urban acoustic application.

3.2 Field representation through the fast multipole formalism

The Boundary Integral Equation (BIE) coming from the 3 dimensional Helmholtz equation (1.25) which has been established in the previous chapter can be written as:

$$C(\mathbf{x})\phi(\mathbf{x}) = \int_S \left[F(\mathbf{x},\mathbf{y})\phi(\mathbf{y}) - G(\mathbf{x},\mathbf{y})q(\mathbf{y})\right] dS + \phi_{in}(\mathbf{x}), \qquad \forall \mathbf{x} \in \Omega, \mathbf{y} \in S. \tag{3.1}$$

It describes the pressure field ϕ at any point $\mathbf{x}$ in terms of the boundary S delimiting the domain Ω. The two kernels G and F correspond to the Green's function and its outward normal derivative respectively, between the source point $\mathbf{y}$ and the receiver point $\mathbf{x}$. ϕ_{in} is the incident pressure field. $\phi(\mathbf{y})$ and $q(\mathbf{y})$ are the pressure

and velocity values at the boundary point **y** :

$$(Dirichlet\ BCs)\ \phi(\mathbf{y}) = \bar{\phi}(\mathbf{y}), \qquad (Neumann\ BCs)\ q(\mathbf{y}) = \frac{\partial \phi}{\partial n} = \bar{q}(\mathbf{y}), \qquad \forall \mathbf{y} \in S. \tag{3.2}$$

The quantities with over bars indicate initial prescribed values on the boundary S.

3.2.1 Spherical basis functions

The main idea of the Fast Multipole Method is the expansion of the fundamental solution of the Helmholtz equation on spherical basis functions. We introduce a regular basis R and a singular basis S based upon the spherical harmonics series Y_n^m of degree n and order m, as:

$$R_n^m(\vec{r}) = j_n(kr)Y_n^m(\theta,\varphi), \qquad S_n^m(\vec{r}) = h_n(kr)Y_n^m(\theta,\varphi), \tag{3.3}$$

$$n = 0, 1, 2, \ldots, \qquad m = -n, \ldots, +n,$$

with the wavenumber k and $\vec{r}$, a translation vector in spherical coordinates (r, θ, φ). j_n and h_n denote the spherical Bessel functions and Hankel functions of the first kind respectively. The spherical harmonic series is defined by:

$$Y_n^m(\theta,\varphi) = (-1)^m \sqrt{\frac{2n+1}{4\pi}\frac{(n-|m|)!}{(n+|m|)!}} P_n^{|m|}(\cos\theta) e^{im\varphi} \tag{3.4}$$

$$n = 0, 1, 2, \ldots, \qquad m = -n, \ldots, +n$$

where $P_n^m(\mu)$ are the associated Legendre functions consistent with [Abramowitz 1964] and Rodrigues' formulas:

$$P_n^m(\mu) = (-1)^m (1-\mu^2)^{m/2} \frac{d^m}{d\mu^m} P_n(\mu), \qquad n \geq 0, \qquad m \geq 0, \tag{3.5}$$

with

$$P_n^0(\mu) = \frac{1}{2^n n!}\frac{d^n}{d\mu^n}(\mu^2-1)^n, \qquad n \geq 0. \tag{3.6}$$

The definition of these spherical harmonics (eq 3.4), according to the definition of Gumerov & al., coincides with that of Epton & Dembart [Epton 1995] except for a factor $\sqrt{2n+1/4\pi}$. This spherical harmonics series define a complete orthonormal system over the unit sphere and can thus form a basis for expanding other functions. Note that these spherical harmonics functions are even for even $n+m$ and odd for odd $n+m$.

3.2.2 Field decomposition by the multipole expansion coefficients

According to the previous definition of the spherical basis, the Green's function (or the kernel G) in the BIE (3.1) can now be expanded under the following form:

$$G(\mathbf{x},\mathbf{y}) = ik\sum_{n=0}^{\infty}\sum_{m=-n}^{n} S_n^m(\mathbf{x}-\mathbf{y}^c)R_n^{-m}(\mathbf{y}-\mathbf{y}^c). \tag{3.7}$$

This expansion is theoretically an infinite sum of spherical basis functions calculated between two points $\mathbf{x}$ and $\mathbf{y}$ and an intermediate point, an expansion center $\mathbf{y}^c$, which fulfills the far field condition:

$$|\mathbf{y}-\mathbf{y}^c| \ll |\mathbf{x}-\mathbf{y}^c|. \tag{3.8}$$

The integral representation of G can now be evaluated with the following multipole expansion:

$$\int_S G(\mathbf{x},\mathbf{y})q(\mathbf{y})dS_y = ik\sum_{n=0}^{\infty}\sum_{m=-n}^{n} S_n^m(\mathbf{x}-\mathbf{y}_c)\int_S R_n^{-m}(\mathbf{y}-\mathbf{y}_c)q(\mathbf{y})dS_y, \tag{3.9}$$

$$\int_S G(\mathbf{x},\mathbf{y})q(\mathbf{y})dS_y = ik\sum_{n=0}^{\infty}\sum_{m=-n}^{n} S_n^m(\mathbf{x}-\mathbf{y}_c)M_n^m(\mathbf{y}_c), \tag{3.10}$$

where $M_n^m(\mathbf{y}_c)$ are the multipole expansion coefficients of all the contributions coming from elements of the boundary S, which fulfill the far field condition (equation (3.8)), centered around the expansion center $\mathbf{y}_c$,

$$M_n^m(\mathbf{y}_c) = \int_S R_n^{-m}(\mathbf{y}-\mathbf{y}_c)q(\mathbf{y})dS_y. \tag{3.11}$$

Consistently with the definitions (3.1) and (3.7), the integral representation of the Green's function derivative (or the kernel F) which appears in the BIE can also be expanded in 3 dimensions as:

$$\int_S F(\mathbf{x},\mathbf{y})\phi(\mathbf{y})dS_y = ik\sum_{n=0}^{\infty}\sum_{m=-n}^{n} S_n^m(\mathbf{x}-\mathbf{y}_c)\tilde{M}_n^m(\mathbf{y}_c), \tag{3.12}$$

$$\text{with} \qquad \tilde{M}_n^m(\mathbf{y}_c) = \int_S \frac{\partial R_n^{-m}(\mathbf{y}-\mathbf{y}^c)}{\partial \vec{n}_\mathbf{y}}\phi(\mathbf{y})dS_y, \tag{3.13}$$

where the y points fulfill the far field criteria (eq. (3.8)). The theory of translation and rotation operators for the Helmholtz equation presented in [Gumerov 2004] is based on the differential properties of elementary solutions. These properties presumably first reported by [Chew 1992] and calculated independently by [Gumerov 2001] serve as a basis for recurrence relations which can be employed for the resolution of the Helmholtz equation. It turns out that the normal derivative $\frac{\partial R_n^{-m}(\mathbf{y}-\mathbf{y}^c)}{\partial \vec{n}_\mathbf{y}}$ can be computed recursively by the use of properties of differentiation theorems for the spherical basis functions in an arbitrary direction specified

by the unit vector $\vec{n} = (n_1, n_2, n_3)$:

$$\frac{\partial R_n^{-m}}{\partial \vec{n}_{\mathbf{y}}} = \frac{1}{2}\left[(n_1 + in_2)\left(b_n^m R_{n-1}^{m+1} - b_{n+1}^{-m-1} R_{n+1}^{m+1}\right) + (n_1 - in_2)\left(b_n^{-m} R_{n-1}^{m-1} - b_{n+1}^{m-1} R_{n+1}^{m-1}\right)\right] + n_z\left(a_n^m R_{n+1}^m - a_{n-1}^m R_{n-1}^m\right), \tag{3.14}$$

$$m = 0, \pm 1, \pm 2, \cdots, \qquad n = |m|, |m| + 1, \cdots,$$

where R_n^m is equivalent to $R_n^m(\mathbf{y} - \mathbf{y}^c)$ and a_n^m and b_n^m are the differentiation coefficients computed as follows,

$$a_n^m = a_n^{-m} = \sqrt{\frac{(n+1+m)(n+1-m)}{(2n+1)(2n+3)}}, \qquad for \quad n \geq |m|, \tag{3.15}$$

$$a_n^m = b_n^m = 0, \qquad for \quad n < |m|, \tag{3.16}$$

$$b_n^m = \sqrt{\frac{(n-m-1)(n-m)}{(2n-1)(2n+1)}}, \qquad for \quad 0 \leq m \leq n, \tag{3.17}$$

$$b_n^m = -\sqrt{\frac{(n-m-1)(n-m)}{(2n-1)(2n+1)}}, \qquad for \quad - \leq m \leq 0. \tag{3.18}$$

The infinite summation on spherical basis functions of expressions (3.7) and (3.12) are only theoretical and must be in fact, for obvious numerical reasons, truncated. The suitable truncation expansion order p will be determined thanks to an analysis of theoretical error bounds of Bessel and Hankel functions and will be the purpose of a latter section 3.4, dedicated to the numerical aspects of the fast multipole algorithm. One will see before, the mathematical tools required to perform the translations through the translation operators as well as a detailed description of the fast multipole algorithm.

3.2.3 Translation of the multipole expansion coefficients

Once the expansion coefficients are known around an expansion center, we need to transfer the information toward another expansion center, that is to say change the origin of the reference center. These translations are performed through the translation operators. Basically two multipole translation techniques are commonly used. The use of the *Wigner 3j symbol* is adequate for low frequencies because of the $O(p^5)$ nature of the formulation. Although the number of operations can be reduced to $O(p^4)$ by the use of various recursive relations, the computation time can still increase quickly with the increase of the value of p and lead to a prohibitive storage memory if the translation coefficients are stored. The second one, coming from Gumerov & Duraiswami's work, which is actually used in our fast multipole algorithm, is based on the decomposition of the translation operators into rotation and coaxial translation parts, the RCR-decomposition: rotation-coaxial translation-inverse rotation, summarized in figure 3.2. Each of these operations can be performed with a complexity $O(p^3)$ using a recursive computation of matrices components [Gumerov 2003]:

$$(\mathbf{E}|\mathbf{F})(t) M_n^m = \mathbf{Rot}(Q^{-1})(\mathbf{E}|\mathbf{F})_{coax}(t)\mathbf{Rot}(Q) M_n^m, \qquad \mathbf{E}, \mathbf{F} = \mathbf{S}, \mathbf{R} \tag{3.19}$$

with **Rot**(Q), a rotation matrix transform which provides the expansion coefficients of a reference frame rotated by some rotation matrix $Q(\alpha,\beta,\gamma)$ specified by three angles of rotation α,β,γ. The operator $(\mathbf{E}|\mathbf{F})_{coax}(t)$ denotes an arbitrary (subsequently specified) coaxial translation along the vector t, a translation along the z-axis oriented towards the target expansion center and **Rot**(Q^{-1}), the backward rotation which brings the reference frame to its initial rotation. For an overview of numerical procedures to compute the RCR-decomposition matrices, the reader can first refer to the appendix A.

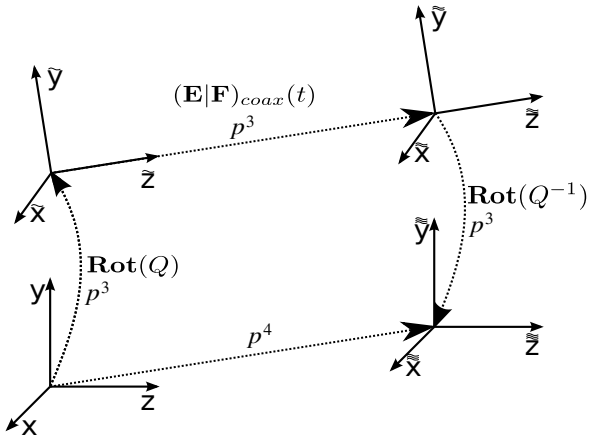

FIGURE 3.2: *RCR decomposition principle.*

There are three types of translation operators, the Moment to Moment (M2M), the Moment to Local (M2L) and the Local to Local (L2L), directly related to the location of the new expansion center. The coaxial translation matrix $(\mathbf{E}|\mathbf{F})_{coax}(t)$ can thus take the following forms:

$$\text{M2M:} \quad (\mathbf{E}|\mathbf{F})_{coax}(t) \equiv (R|R)^{m',m}_{n',n}(|\mathbf{y}'_c - \mathbf{y}_c|) \quad \text{for} \quad |\mathbf{x} - \mathbf{y}'_c| \gg |\mathbf{y}'_c - \mathbf{y}_c| \tag{3.20}$$

$$\text{M2L:} \quad (\mathbf{E}|\mathbf{F})_{coax}(t) \equiv (S|R)^{m,m}_{n,n}(|\mathbf{x}'_c - \mathbf{y}'_c|) \quad \text{for} \quad |\mathbf{x}'_c - \mathbf{y}'_c| \gg |\mathbf{x} - \mathbf{x}'_c| \tag{3.21}$$

$$\text{L2L:} \quad (\mathbf{E}|\mathbf{F})_{coax}(t) \equiv (S|S)^{m',m}_{n',n}(|\mathbf{x}_c - \mathbf{x}'_c|) \quad \text{for} \quad |\mathbf{y} - \mathbf{x}'_c| \gg |\mathbf{x}_c - \mathbf{x}'_c| \tag{3.22}$$

The overall summary (figure 3.3) provides a clearer overview of the translations principle of multipole coefficients through these translation operators (dotted black lines). The M2L translation leads to a set of local expansion coefficients L^m_n including all the contributions of far sources translated at a local expansion center $\mathbf{x}_c$ located close to the receiver point $\mathbf{x}$. For the sake of brevity the computational procedures are described in appendix A.

However, the standard fast multipole formalism, as described in its original form, involves some instabilities as the frequency increases as well as prohibitive memory storage requirements. In order to counter this drawbacks at high frequency, the M2L translation operator can be replaced by its diagonal form, introduced by ROKHLIN in [Rokhlin 1993], which can be used in a higher frequency range. The so-called High Frequency (HF) translation is detailed in the following section.

3.2.4 High Frequency translation

The high frequency formulation of the M2L translation operator is based on Rokhlin's works [Rokhlin 1993] which introduces the following decomposition of the translation matrix :

$$(\mathbf{S}|\mathbf{R})(t)M_n^m = \mathbf{Sp}^{-1}\Lambda_s(t)\mathbf{Sp}\ M_n^m, \tag{3.23}$$

which brings into play the forward discrete spherical transform **Sp** (and the backward transform $\mathbf{Sp}^{-1}$), and the diagonal form of the translation operator $\Lambda(s)$ which is defined as follows:

$$\Lambda_{jj}(t) = \sum_{n=0}^{2p-2} i^n(2n+1)h_n(kt)P_n\left(\frac{s_j \cdot t}{|t|}\right). \tag{3.24}$$

The forward transform **Sp** is a projection on a unit spherical space of p^2 expansion coefficients. The distribution of the sampling nodes on the unit sphere depends on the truncation number p and it is sufficient to take $(2p-1)$ points on the elevation angle and $(4p-3)$ points on the azimuthal angle. It implies that Λ_s is a matrix of size $(2p-1)(4p-3)\times(2p-1)(4p-3)$ and thus $\mathbf{Sp}^{-1}$ is a matrix of size $(2p-1)(4p-3)\times p^2$ which provides a backward transform to the space of coefficients. The operator **Sp** can be decomposed into the Legendre transform with respect to elevation angle (since it depends on the cosines of the angle) followed by a Fourier transform with respect to the azimuthal angle (equispaced abscissas). Consistently with the definition of **Sp**, $\mathbf{Sp}^{-1}$ can be decomposed into a inverse Fourier transform followed by a inverse Legendre transform. There exists a number of papers dedicated to the fast spherical transform (*e.g.* see references [Driscoll 1994], [Jakob-Chien 1997], [Swarztrauber 2000]). The fast spherical transform is used to accelerate the translations for high frequencies [Sakuma 2002, Schneider 2003]. This formulation has subsequently led to a broadband/wide-band FMBEM algorithm including both low and high frequency formulations [Cheng 2006], [Gumerov 2009] and has also been applied to a Galerkin boundary element method [Fischer 2004].

3.2.5 Field reconstruction by the multipole coefficients reexpansion

The local expansion coefficients can finally be translated from an expansion center $\mathbf{x}_c$ to a receiver point $\mathbf{x}$, in blue in figure 3.3, using an analogous formula as for the multipole expansion:

$$\int_S G|F(\mathbf{x},\mathbf{y})\ q|\phi(\mathbf{y})\ dS_y = ik\sum_{n=0}^{\infty}\sum_{m=-n}^{n} R_n^m(\mathbf{x}-\mathbf{x}_c)L_n^m(\mathbf{x}_c), \tag{3.25}$$

regardless the kernels G or F, while the kernels K or H lead to a local expansion:

$$\int_S K|H(\mathbf{x},\mathbf{y})\ q|\phi(\mathbf{y})\ dS_y = ik\sum_{n=0}^{\infty}\sum_{m=-n}^{n} \frac{\partial R_n^m(\mathbf{x}-\mathbf{x}^c)}{\partial \vec{n}_{\mathbf{x}}} L_n^m(\mathbf{x}_c), \tag{3.26}$$

in agreement with the definition (1.29). We note that the kernel H, from a fast multipole point of view, is not hyper-singular, as it was the case in the framework of the standard BEM and thus this expansion does not introduce additional difficulties. However this assumption will be discussed in the paragraph dedicated to the assessment of the Burton & Miller formulation (section 4.2).

The following drawing summarizes the usage of translation operators required to accelerate point to point interactions. One can see the multipole expansions, expressions (3.11) and (3.13), between red source points $\mathbf{y}$ and the expansion center $\mathbf{y}_c$, the multipole coefficient translations through the translator operators, expressions (3.20) - (3.22) between the expansion centers $\mathbf{y}_c$, $\mathbf{y'}_c$, $\mathbf{x'}_c$ and $\mathbf{x}_c$ and the final reexpansion of multipole coefficients, expressions (3.25) and (3.26), between the local expansion center $\mathbf{x}_c$ and receiver blue points $\mathbf{x}$.

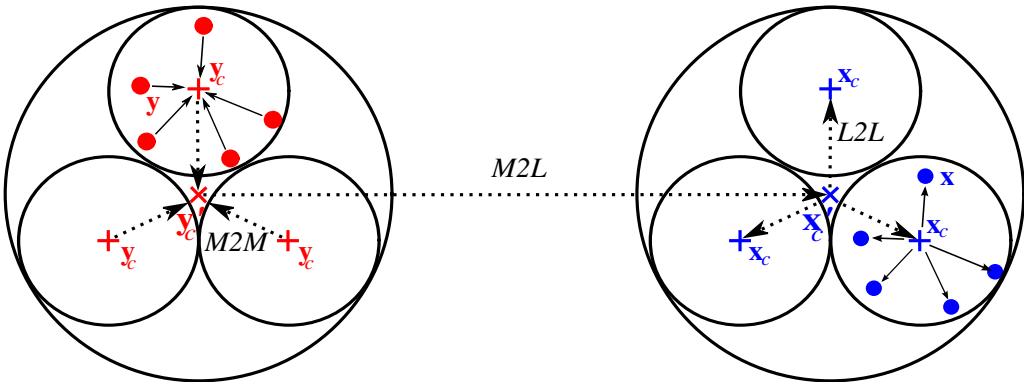

FIGURE 3.3: *General overview of interactions between well separated sources (red points) and receivers (blue points) through the multipole expansion principle. The dotted lines is related to the multipole coefficients translations.*

This section has described the mathematical background which the fast multipole method is based upon. The following section will detail more precisely each step of the fast multipole algorithm we developed in this work.

3.3 Description of the fast multipole method algorithm

Even if all the numerical tools have their own specifications depending on the development language (C++, Fortran ...) or computer programmer habits, basically the fast multipole formalism requires several important steps which we intend to describe in this section. First of all, we need to include the whole discretized geometry in a cubic box from which a hierarchical tree is constructed. Then all the multipole coefficients are computed (multipole expansion) before being translated through the translation operators i.e. Moment to Moment (M2M), Moment to Local (M2L) and Local to Local (L2L) often referred to as upward pass, far translations and downward pass respectively. Finally, we evaluate the integrals of kernels G and F by the summation of direct contributions of *close elements* (BEM contribution) with the local multipole coefficients coming from *far elements* (FMBEM contribution). All these steps are detailed below.

3.3.1 Hierarchical tree construction

The discretized geometry is first embedded in a three dimensional cubic box for a three dimensional mesh (two dimensional square on the illustration 3.4) including all elements. This bounding cell corresponds to the *level* 0, the highest *level* of the hierarchical tree and has a length L_0. We subsequently start to divide this *parent* cell into 8 identical *children* cells (4 in two dimensions in figure 3.4) of *level* 1. Then we create *level* 2 by splitting the *cells* located on *level* 1. This is the minimum number of *levels* required in the fast multipole formalism (we will see the reason thereafter). Starting from *level* 2, we need to divide the *cells*, and so add a new *level*, if and only if at least one *cell* contains more elements than the *cellsize* number, i.e. the maximum number of elements allowed within a *cell* at the lowest *level* l_{max}. Thus at the lowest *level*, all *cells* include a maximum of a prescribed number of elements determined by the *cellsize* parameter. It follows that a *level* l contains a maximum number of *cells* equal to 8^l (4^l in two dimensions) and have a $L_0/2^l$ length. We denote that an element is considered to be inside a given *cell* if its center is inside this *cell* and a *cell* is removed (considered as *dead*) if it does not contain any element. We can see the building process of the hierarchical tree for a two dimensional case and a *cellsize* criterion equal to 2 (for the sake of readability) in figure 3.4.

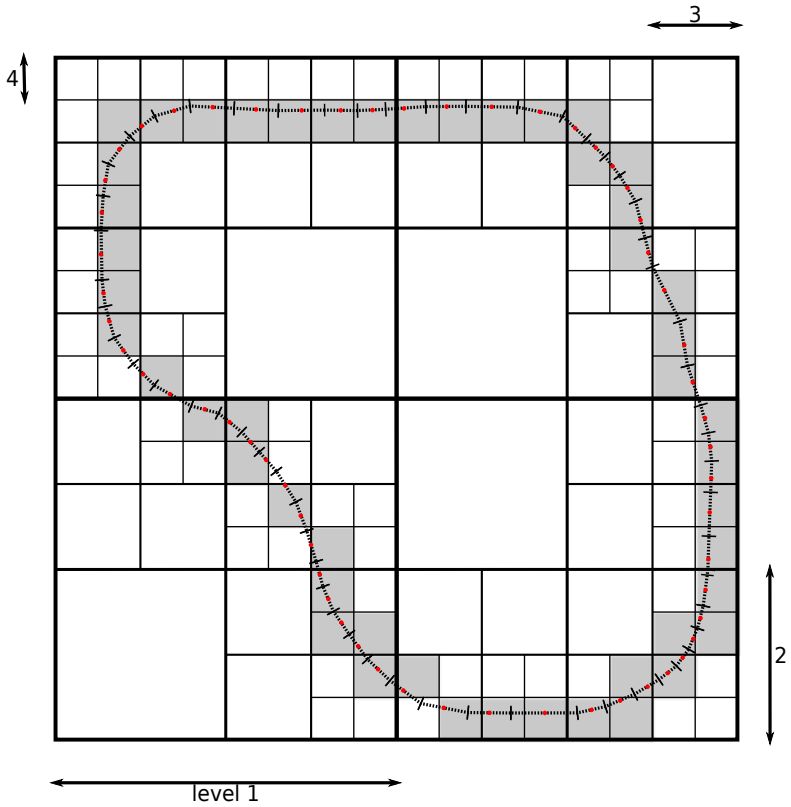

FIGURE 3.4: *Recursive process to construct the hierarchical tree. The dashed black line represents the discretized geometry and the shaded cells, the leaves. All cells without elements are removed from the tree.*

Thus this hierarchical space partitioning has introduced some definitions which will be used in the following:

leaf: Each *cell* (not removed) located at the lowest level, l_{max}, is called a *leaf* (shaded in figure 3.4). For a specific problem, the theoretical, but hardly ever reached, maximum number of *leaves* is $8^{l_{max}}$ in 3 dimensions.

parent, child: Each *cell* divided are *parent cells* and produce a maximum of 8 *child cells*. Consistent with this definition, the *parent cells* are located between level 2 and level $l_{max} - 1$ and the *child cells* are located between level 3 and level l_{max}.

adjacent cell: Each *cell* has an *adjacent cells* list containing *cells* located at the same *level*, sharing at least a boundary point. According to this definition a *cell* has a maximum of 26 *adjacent cells* in 3 dimensions.

interaction list: Each *cell* at a *level* ≥ 2 has an *interaction cell* list containing *children* of *adjacent cells* to the *parent* of the considered *cell*, and which does not belong to the *adjacent list* of the considered *cell*. As a result an *interaction list* has a maximum of 189 *cells* in 3 dimensions.

far cell: A *far cell* is a *cell* on the same *level* of the considered *cell* belonging neither to its *adjacent list* nor to its *interaction list*. It is noteworthy that a *cell* located at *level* 2 has no *far cells* since its *adjacent list* and its *interaction list* cover all the points of the boundary. For this reason we do not have to consider *levels* higher than 2. The active levels in the fast multipole formalism are thus located between *levels* 2 and l_{max}.

3.3.2 Multipole expansion stage

This stage will be executed for all the leaves of the hierarchical tree. Thus, all the contributions of elements $\mathbf{y}$ belonging to the same leaf will be computed under the form of multipole coefficients and subsequently summed around the same expansion center of the *leaf* $\mathbf{y}_c$. Consistently with the definitions (3.7) and (3.12), we can compute the m, n multipole coefficients for both kernels G and F respectively:

$$M_n^m(\mathbf{y}_c) = \sum_{i=1}^{i_{max}} R_n^{-m}(\mathbf{y}_i - \mathbf{y}_c) q(\mathbf{y}_i) \qquad \text{and} \qquad \tilde{M}_n^m(\mathbf{y}_c) = \sum_{i=1}^{i_{max}} \frac{\partial R_n^{-m}(\mathbf{y}_i - \mathbf{y}_c)}{\partial \vec{n}_{\mathbf{y}_i}} \phi(\mathbf{y}_i). \tag{3.27}$$

The subscript i refers to each element within the considered *leaf* which contains a maximum of i_{max} elements. The partial derivative is computed recursively according to expression (3.14). At the end of this stage, each expansion center at the lowest *level* contains a set of multipole coefficients coming from all the contributions of elements included into its corresponding *leaf*. The principle of the multipole expansion stage is summarized in figure 3.5.

3.3.3 Moment to Moment (M2M) stage : Upward pass

This stage will be performed for all *children cells*, i.e. for all *cells* of *level* > 2. The multipole coefficients of *child cell* computed at the previous step are translated from their own expansion center y_c^l and summed

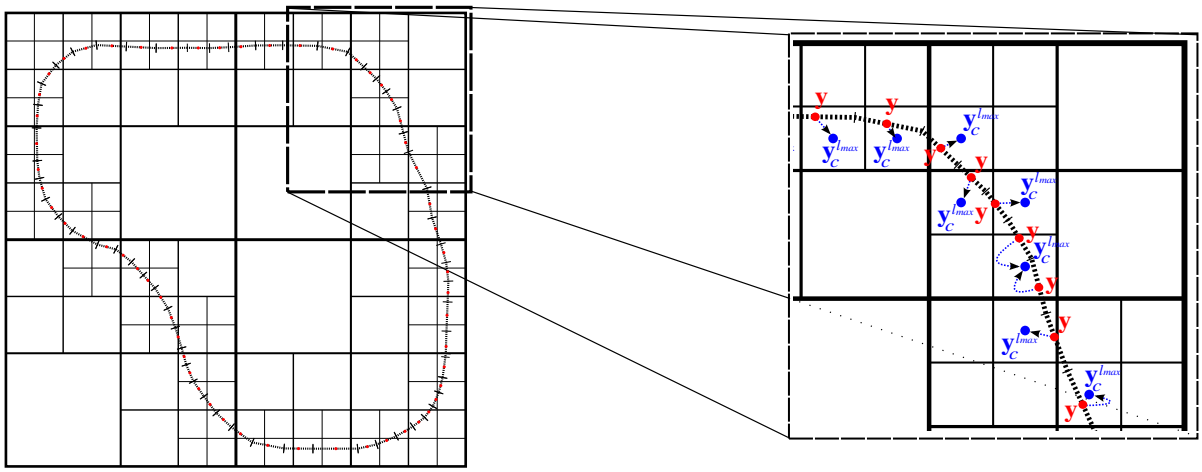

FIGURE 3.5: *The computation of the moment at the lowest level (l_{max}) is performed for each leaves of the hierarchical tree. The expansion coefficients of leaves are the sum of moments of each point* $\mathbf{y}$ *included into it, expressed at the expansion center* $\mathbf{y}_c^{l_{max}}$.

at the expansion center of their *parent cell* y_c^{l-1}, according to the RCR-decomposition (3.19) and (3.20):

$$(\mathbf{R}|\mathbf{R})(\mathbf{y}_c^{l-1} - \mathbf{y}_c^{l})M_n^m = \mathbf{Rot}(Q^{-1})(\mathbf{R}|\mathbf{R})_{coax}(|\mathbf{y}_c^{l-1} - \mathbf{y}_c^{l}|)\mathbf{Rot}(Q)M_n^m, \qquad \forall\ l_{max} \geq l \geq 3 \qquad (3.28)$$

Obviously this process must start at *level* l_{max} in order to transfer the informations toward the higher *levels* as described in figure 3.6. In a such a way at the end of this stage all *parent cells* will possess all the contributions coming from their own *children cells*.

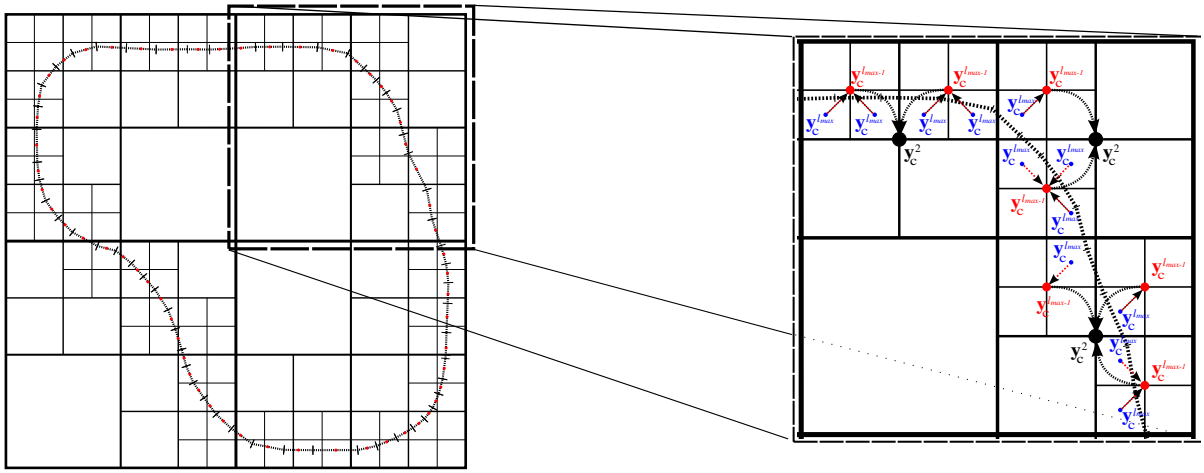

FIGURE 3.6: *During the Moment to Moment (M2M) step, the expansion coefficients of children at a level* l *are translated towards the expansion center of their parents* $\mathbf{y}_c^{l-1}$ *and summed. This step is performed until the level* $l = 3$.

3.3.4 Moment to Local (M2L) stage : Transfer pass

This step will be applied to all the *cells* of the hierarchical tree i.e. from *level* 2 to *level* l_{max} included. For a given *cell* located at *level* l, we translate and sum all the expansion coefficients coming from the expansion center $\mathbf{y}_c^l$ of *cells* belonging to its *interaction list* thanks to the M2L translation operator according to expressions 3.19 and 3.21 for low frequency *levels*:

$$(\mathbf{S}|\mathbf{R})(\mathbf{x}_c^l - \mathbf{y}_c^l)M_n^m = \mathbf{Rot}(Q^{-1})(\mathbf{S}|\mathbf{R})_{coax}(|\mathbf{x}_c^l - \mathbf{y}_c^l|)\mathbf{Rot}(Q)M_n^m \qquad 2 \leq l \leq l_{max} \tag{3.29}$$

or the diagonal form of the M2L translation operator according to expressions (3.19) and (3.23) for high frequency *levels*:

$$(\mathbf{S}|\mathbf{R})(\mathbf{x}_c^l - \mathbf{y}_c^l)M_n^m = \mathbf{Sp}^{-1}\Lambda_s(\mathbf{x}_c^l - \mathbf{y}_c^l)\mathbf{Sp}\ M_n^m \tag{3.30}$$

In figure 3.7, let us take the example of an element located inside the dotted blue *leaf*. One can see the interactions coming from expansion centers of the *interaction list cells*, corresponding to *level* 2 (in gray), 3 (in red) and 4 (in blue) and translated to the expansion centers x_c^2, x_c^3 and x_c^4 respectively. At the end of this stage all cells of the hierarchical tree include the contributions of its own *interaction list cells*.

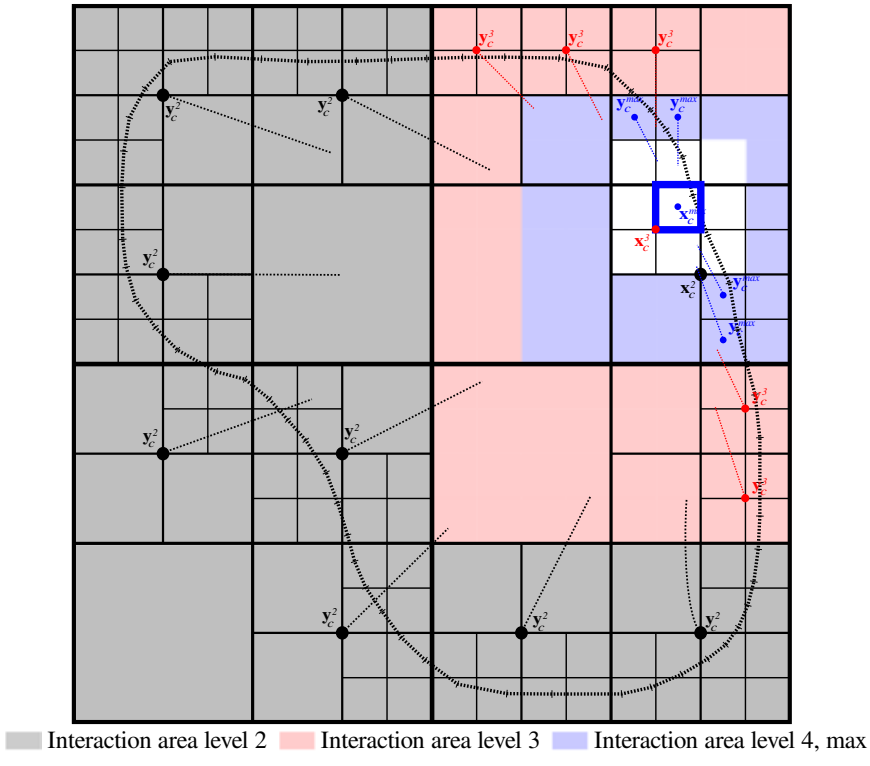

FIGURE 3.7: *The Moment to Local (M2L) transfer step. The dotted black lines correspond to an arbitrary M2L transfer at level 2, the dotted red lines to an arbitrary M2L transfer at level 3, and the dotted blue lines to an arbitrary M2L transfer at level 4 (the lowest level on this example). The target element is located in the leaf emphasizes by the blue box.*

3.3.5 Local to Local (L2L) stage : Downward pass

This step is analogous to the *Upward* step or M2M step. The Local to Local (L2L) step is executed for each *parent cell*, i.e. *cells* located between *levels* 2 and $l_{max} - 1$. Starting from *level* 2 to *level* $l_{max} - 1$, the expansion coefficients coming from *parent cells* are translated to the expansion center of their *children cells* (see figure 3.8) by the mean of the L2L translation operator (equation (3.22)):

$$(\mathbf{R}|\mathbf{R})(\mathbf{x}_c^{l+1} - \mathbf{x}_c^l)M_n^m = \mathbf{Rot}(Q^{-1})(\mathbf{R}|\mathbf{R})_{coax}(|\mathbf{x}_c^{l+1} - \mathbf{x}_c^l|)\mathbf{Rot}(Q)M_n^m, \qquad 2 \leq l \leq l_{max} - 1 \quad (3.31)$$

and summed up to the multipole coefficients calculated at the previous step. At this point of the algorithm, all the expansion centers contain the information from their own *interaction list* and also the information coming from the interaction list of their parent cell which contains itself the information coming from their own *parent cell* and so on... It follows that, at the lowest *level* l_{max}, the expansion centers take into account all the interactions of the boundary, except the elements contained in the *cells* of its *adjacent list* (white area figure 3.7).

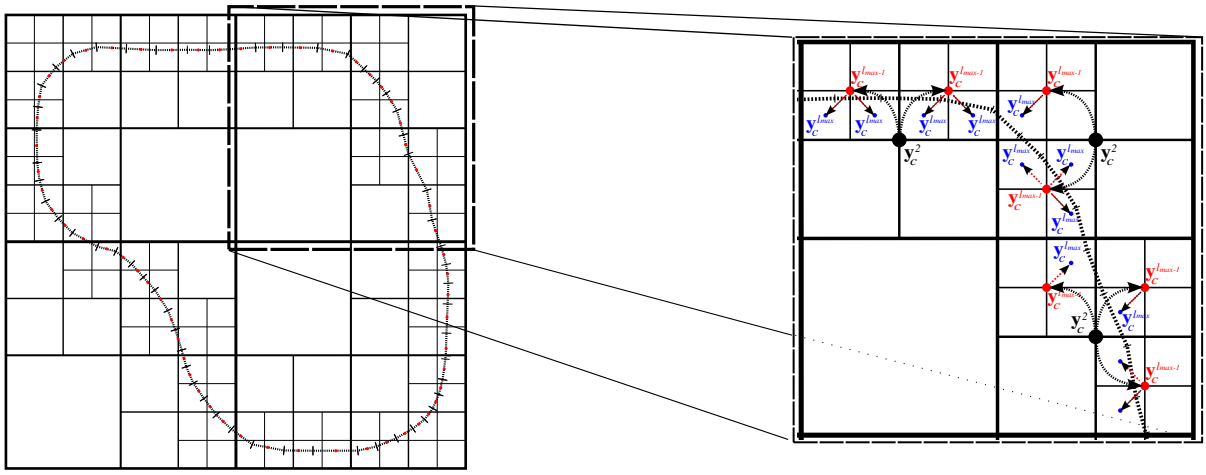

FIGURE 3.8: *During the Local to Local (L2L) step, the expansion coefficients of parents at a level l are translated towards the expansion centers of their children* $\mathbf{x}_c^{l+1}$ *and summed up. This step is performed until the level* $l_{max} - 1$.

3.3.6 Final summation : Multipole coefficients reexpansion

The final summation on an element $\mathbf{x}_i$ at the lowest level consists in the summation of:

- the contribution coming from the expansion center $\mathbf{x}_c^{l_{max}}$ of its leaf (in blue line in figure 3.9) thanks to the local multipole coefficients reexpansion, in analogy with the moment expansion step:

$$\int_{S_{far}} (G/F)(\mathbf{x},\mathbf{y})(q/\phi)(\mathbf{y})dS_{far} \backsimeq ik \sum_{n=0}^{p_{l_{max}}} \sum_{m=-n}^{n} R_n^m(\mathbf{x}_i - \mathbf{x}_c) L_n^m(\mathbf{x}_c), \quad \forall\ \mathbf{x}_i \in S \tag{3.32}$$

- with the direct contributions from near elements in the adjacent leaves (in red lines figure 3.9) directly as in the conventional BEM:

$$\int_S (G/F)(\mathbf{x},\mathbf{y})(q/\phi)(\mathbf{y})dS_y = \underbrace{\int_{S_{far}} (G/F)(\mathbf{x},\mathbf{y})(q/\phi)(\mathbf{y})dS_{far}}_{\boxed{\textit{Fast BEM part}}} + \underbrace{\int_{S_{near}} (G/F)(\mathbf{x},\mathbf{y})(q/\phi)(\mathbf{y})dS_{near}}_{\boxed{\textit{classical BEM part}}} \tag{3.33}$$

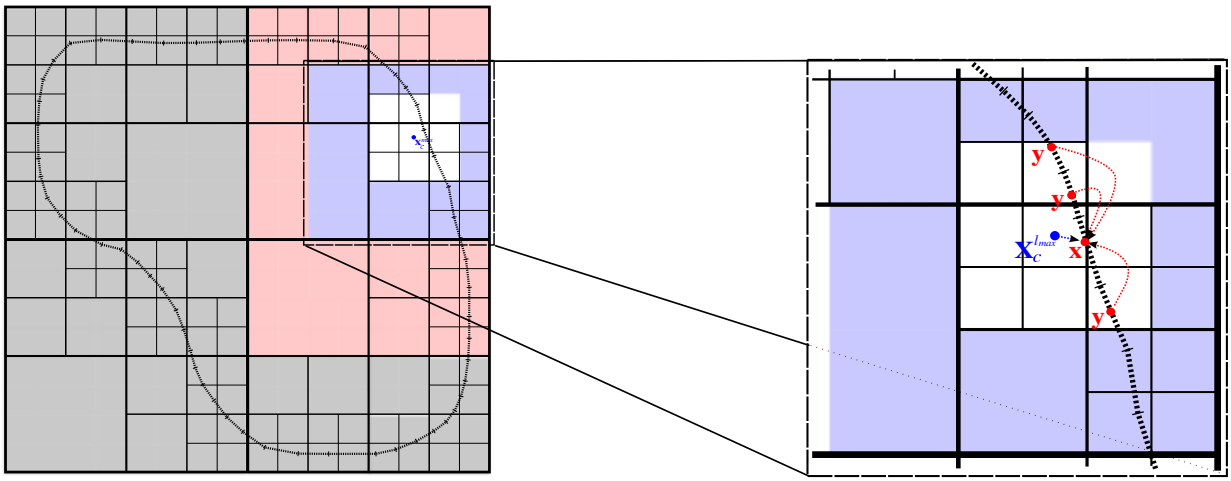

FIGURE 3.9: *The direct contributions of near elements* $\mathbf{y}$ *are summed with the multipole coefficients contribution coming from the expansion center* $\mathbf{x}_c^{l_{max}}$. *We execute this step for each leaf of the hierarchical tree.*

3.4 Numerical aspects

We intended in the previous section to describe more specifically each step of the fast multipole formalism from a computational point of view. Due to the truncation of the spherical harmonics series, the multipole expansion induces approximations of integral operators involving errors which can be controlled through the expansion order p. This section will describe how this foremost parameter will be properly chosen thanks

to a theoretical error bound analysis. We also provide an estimation of the computational complexity of the developed algorithm.

3.4.1 Level-dependent truncation number

The expansions of kernels G (equation (3.7)) and F (equation (3.12)) are theoretically an infinite sum based upon the spherical basis functions (3.3). Obviously, from a numerical point of view, these summations need to be truncated. Our algorithm includes both low and high frequency formulations and a switch between low and high frequency *levels* (whose expansion order are p_{low} and p_{high} respectively) is performed. Consistent with the definition of [Gumerov 2009], this is dictated by the estimation of the threshold at which the magnitude of the smallest truncated term in the translation kernel starts growing exponentially. An analysis of the theoretical error bound allows to validate these expressions of expansion orders for each *level* depending on a characteristic size of this *level* which is the radius a_l of a cubic box at *level* l. The number of *levels* is determined by the *cellsize* parameter, defining the maximum number of elements allowed in a *leaf*, a *cell* at the lowest *level* l_{max}. It results that the *cells* at l_{max} include a maximum of *cellsize* elements. Thus, the smaller this parameter is, the larger the number of *levels* will be. It follows that the *cellsize* criterion determines the ratio between the contributions coming from the direct integrations (the *near area*) and the fast multipole integrations (the *far area*). The following expressions are used to estimate the suitable expansions orders p for each *level* coming from an analysis of theoretical error bounds studied in detail in [Gumerov 2004, chapter 9]:

$$p_{low} = 1 - \frac{\log \epsilon \left(1 - \delta^{-1}\right)^{3/2}}{\log \delta}, \quad p_{high} = ka_l + \frac{\left(3 \log \epsilon^{-1}\right)^{2/3}}{2} ka_l^{1/3} \quad \text{and} \quad p_l = \left(p_{low}^4 + p_{high}^4\right)^{1/4}. \tag{3.34}$$

Thus $p_l = p(ka_l, \epsilon, \delta)$ with a_l being the largest radius of a cell at *level* l, ϵ, the prescribed iterative stopping criterion and $\delta = 2$. This expression (3.34) combines both low and high frequencies approximations. Thus, for low and high frequencies (or ka), it coincides asymptotically with limiting cases, while in the transition region, it is also acceptable for the estimation of the expansion order. We denote that the formalism introduced by Gumerov & Duraiswamy leads to the computation of spherical basis functions at an order up to $2p_l - 2$. This expansion order is a crucial parameter of the FMBEM formalism since it determines the error bound [Darve 2000] due to the truncation of the spherical basis series. Thus it is possible to reduce this parameter in order to accelerate the computations but it leads to a loss of accuracy.

3.4.2 Theoretical error bounds of the multipole expansion

We consider the errors associated with the expansion and translation of multipole coefficients. The representation of the Green's function is theoretically an infinite sum on the spherical basis functions:

$$\int_S G(\mathbf{x},\mathbf{y})q(\mathbf{y})dS_y = ik\sum_{n=0}^{\infty}\sum_{m=-n}^{n} S_n^m(\mathbf{x}-\mathbf{y}_c)\int_S R_n^{-m}(\mathbf{y}-\mathbf{y}_c)q(\mathbf{y})dS_y. \tag{3.35}$$

However, from a numerical point of view, this series needs to be truncated up to the order p involving an error on the truncated expansion

$$\int_S G(\mathbf{x},\mathbf{y})q(\mathbf{y})dS_y = ik\sum_{n=0}^{p}\sum_{m=-n}^{n} S_n^m(\mathbf{x}-\mathbf{y}_c)\int_S R_n^{-m}(\mathbf{y}-\mathbf{y}_c)q(\mathbf{y})dS_y + ik\sum_{n=p+1}^{\infty}\sum_{m=-n}^{n} S_n^m(\mathbf{x}-\mathbf{y}_c)\int_S R_n^{-m}(\mathbf{y}-\mathbf{y}_c)q(\mathbf{y})dS_y. \tag{3.36}$$

The theoretical error bound $\varepsilon(p)$ can thus be estimated by:

$$\varepsilon(p) = \left| ik\sum_{n=p+1}^{\infty}\sum_{m=-n}^{n} S_n^m(\mathbf{x}-\mathbf{y}_c)\int_S R_n^{-m}(\mathbf{y}-\mathbf{y}_c)q(\mathbf{y})dS_y \right|. \tag{3.37}$$

Based on the error obtained for the zero-order spherical Hankel function, the errors bound of the computation of Green's function corresponding to the low frequency region can be written:

$$\varepsilon_p < \frac{1}{4\pi a}\frac{\sigma^{-p-1}}{(1-\sigma^{-1})^{3/2}} \tag{3.38}$$

and the errors bound of the computation of Green's function corresponding to the high frequency region can be written as:

$$\varepsilon_p < \frac{k}{4\pi\sigma(ka)^{1/3}}\exp\left[-\frac{1}{3}\left(\frac{2(p-ka)}{(ka)^{1/3}}\right)^{3/2}\right], \tag{3.39}$$

corresponding with p_{low} and p_{high} in expression (3.34) respectively. We do not claim to do here an exhaustive explanation of the derivation of both previous equations. We recommend the interested readers to refer to [Gumerov 2004, chapter 9] for more details related to the geometrical parameters a, b and σ required for the establishment of both previous relations. This reference also provides quantitative numerical experiments showing that both previous expressions overestimate the actual errors which are in practical much smaller than predicted theoretically for a given p. Gumerov & Duraiswami have showed absolute and uniform convergence of series for the three regions where the behavior of the expansion is qualitatively different corresponding to the low, transition and high frequency regions.

3.4.3 Estimation of the computational complexity

The estimation of the complexity of such an algorithm is not so easily determined, because of the large number of steps involved, as well as the large number of parameters in the numerical implementation of the

fast multipole formalism. Nevertheless, we try here to evaluate the complexity of each step of the FMBEM, in order to provide a general insight of the algorithm complexity.

The computational complexity of an algorithm is directly dictated by the number of operations to perform. The actual number of operations in the fast multipole formalism is related to the spatial distribution of sources and evaluation points. The worst case in terms of computation time would be the case of a uniform three dimensional distribution of sources and receivers. This hypothetical case would involve only non-empty leaves, that is to say $8^{l_{max}}$ leaves at the lowest level l_{max} including *cellsize* elements. However in the framework of the application of the fast multipole method to the boundary element, we reasonably assumed a uniform distribution of elements over the surfaces and an identical number of sources and receivers N. Thus the theoretical maximum number of leaves $N_{cells,l}$ at each level will be $4^{l_{max}}$. Below, we describe the computational complexity of each step mentioned in the previous section. We assume the worst case which could be encountered in the framework of the BEM, each leaf contains *cellsize* elements.

Basically the computational cost will be dictated by the most consuming step among the following:

The tree construction This step only consists in reading the mesh file and can be considered as independent of the number of elements or the expansion order:

$$Cost(TreeConstruction) = O(1) \tag{3.40}$$

Computation of direct contributions We compute and store all the contributions coming from adjacent elements in the adjacent cells for a computational cost:

$$Cost(DirectContribution) = O(27 \times cellsize \times N) = O(N) \tag{3.41}$$

We denote that this step actually has a linear dependency with N only if the cellsize criterion is small enough. In practice, the linear dependency will only be reached with an increasing number of levels which can be controlled through the *cellsize* criterion.

Computation of multipole coefficients The time required to compute all the expansion coefficients for each element is directly related to the length, $p_{l_{max}}$, of the representing vector at *level* l_{max} and leads to the the following complexity:

$$Cost(MultipoleExpansion) = O(N \times p_{l_{max}}) = O(N) \qquad \text{since} \qquad p_{l_{max}} \ll N \tag{3.42}$$

Upward pass The translation operators **Rot**, (**R**|**R**) and $\mathbf{Rot}^{-1}$ which appear in the RCR-decomposition, allow to translate the coefficients from a *level* l to a *level* $l-1$, leading respectively to a complexity in $O(p_l^2)$,

$O(p_{l-1}^2)$ and $O(p_{l-1}^2)$. Thus the total cost of this step which will be performed for each child cells is:

$$Cost(UpwardPass) = O\left(\sum_{l=l_{max}}^{3} N_{cells,l}^{l} \times (p_l^2 + p_{l-1}^2 + p_{l-1}^2)\right) = O(N) \times O(p_2^2). \tag{3.43}$$

As a result, the complexity of this step depends on N and the maximum required value of p which will be reached at *level* 2, p_2^2. Assuming $p_2^2 \ll N$, the cost of this step is determined by N.

Transfer pass: low frequency region The $O(p^3)$ translation complexity of the RCR decomposition (figure 3.2) is performed for each *interaction list cells* of each *cell* at each *level l* leading to:

$$Cost(Transfert/LF) = O\left(\sum_{l_{max}}^{2} N_{cells,l}^{l} \times 189 \times p_l^3\right) = O(N) \times O(p_2^3). \tag{3.44}$$

For moderate values of p, i.e. $p_{max}^3 \ll N$, the computational cost is mainly dictated by the number of *cells* at *level l*, i.e. 4^l, and so on by N through the *cellsize* criterion. We denote that the number of cells in the interactions list, 189, is only theoretical and practically never reached. As a result, because of the $O(p^3)$ dependency of the complexity of the RCR-decomposition, the total complexity will be heavily affected by the complexity of a single translation when $p_2^3 \sim N$ or higher. Finally, such a dependency is not acceptable in an algorithm developed to circumvent the N^2 dependency of a BEM algorithm. This explains the development of the diagonal form of the operator in the high frequency region.

Transfer pass: high frequency region The computation of the translation operator Λ in equation (3.2.4) requires $O(p^3)$ operations [Cheng 2006]. However, all these entries can be precomputed and stored, so no computations are needed during the iterative process of the algorithm. The spherical transform requires $O(p^2)$ operations due to the fast Fourier transform and it follows that the $O(p^2)$ complexity of the diagonal translation is performed for each *cell* on each high frequency *level l*, leading to:

$$Cost(Transfert/HF) = O\left(\sum_{l=l_{max}}^{2} N_{cells,l}^{l} \times 189 \times p_l^2\right) = O(N) \times O\left(p_2^2\right). \tag{3.45}$$

Downward step The complexity of this step is executed for each *parent cells* of the tree and has an identical complexity than the *Upward pass* which can be estimated as:

$$Cost(DownwardPass) = O\left(\sum_{l=2}^{l_{max}-1} N_{cells,l}^{l} \times (p_l^2 + p_l^2 + p_{l+1}^2)\right) = O(N) \times O\left(p_2^2\right). \tag{3.46}$$

We can make the same remark as for the upward pass that is to say that the computational complexity of this step is mainly dictated by N assuming $p_2^2 \ll N$.

Multipole coefficient reexpansion The coefficient reexpansion pass has an identical behavior than the multipole expansion pass, which gives:

$$Cost(Coefficient Reexpansion) = O(N \times p_{l_{max}}) = O(N) \qquad \text{since} \qquad p_{l_{max}} \ll N. \tag{3.47}$$

Since the complexity described above will be executed for each step of the iterative process, we reasonably assumed that the number of iteration is small enough compared to the number of elements N. It results in a competition between the number of elements N and the expansion order at *level* 2 p_2^2. Actually, it can be shown that these two parameters are linked. Indeed, the number of elements N leads to a quadratic dependency on frequency $N = O(f^2)$, assuming a constant space discretization criterion, while the expansion order leads to a linear dependency with the frequency $p = O(kD)$. In practical, this optimum $O(N)$ or $O(p^2)$ complexity is hardly ever reached for a realistic study. Indeed as we will show in a latter section (chapter 5) related to the application of this algorithm for urban propagation problems, the more usual complexity reached is actually $NlogN$.

3.5 In summary

This chapter has been dedidacted to the introduction of the fast multipole principle. We detailed the spherical harmonic series which the kernels are expanded on. We also present the rotation-coaxial translation-back rotation decomposition coming from Gumerov & Duraiswamy's work as well as the high frequency formulation based on the diagonal translation introduced by Rokhlin. We detailed more precisely a common fast mutlipole calculation that is to say the multipole expansion step, the translation of multipole coefficient and the final summation of the *near* and *far interactions* and finally provide a theoretical estimation of the complexity of such a fast multipole algorithm.

Chapter 4

Validation of the fast multipole BEM with a scattering problem by a spherical body

We just had, in previous sections, a general insight of the fast multipole formalism applied to the boundary element method, the different steps and the main related operators. The purpose of this section is the verification of the efficiency of the fast multipole algorithm to solve scattering problems. We will focus, throughout this verification stage, on the same problem than for the validation of the BEM algorithm, that is to say, the case of a spherical incident wave scattered by a spherical body with a radius a equal to 1 m (see figure 2.1), for which an analytical solution exists, already described in a previous section 2.1. After detailing some useful parameters required from a numerical point of view in the framework of the FMBEM formalism, the analytical solution is taken as a reference solution to demonstrate the accuracy of the FMBEM for both rigid and mixed boundary conditions (section 4.1) at regular frequencies. We also emphasize the influence of the fast multipole formalism on the behavior of the iterative solver. Next, we more precisely focus on fictitious eigenfrequencies of the scattering sphere to study the ability of the B&M formalism to overcome this problem as well as its influence on the iterative solver (section 4.2). The algorithm is finally used as a reference method to validate the half-space formalism, starting from its associated full-space problem, section 4.3, half space propagation which will be subsequently used in the next chapter in a urban context to take into account the reflections on the ground.

4.1 Validation of the algorithm for regular frequencies

4.1.1 Algorithm parameters

The verification tests are made for a sphere of radius a, whose surface is meshed with 31694 constant triangular elements representing a space discretization of almost 10 elements per wavelength at $ka = 20$ (see result in appendix B.2). The maximum number of elements authorized at the lowest *level* is 50, which

involves a tree consisting of 6 *levels* (4 useful *levels*). We supply overviews in appendices B.3 and B.4 of the space partionning related to the 2^{nd} and the 4^{th} *level* respectively used in the framework of the fast multipole formalism. The level-dependent truncation number p, used for the expansion of kernels, is chosen to keep a very good accuracy, according to its definition (section 3.4.1). In order to validate the two formulations (low and high frequency formulations), we have performed several tests with both formulations: pure LF and HF tests in which only LF formalism or HF formalism are used and also tests with a LF/HF switch, occurring between two *levels*. Considering the GMRES solver, we do not use any preconditioner and the stopping criterion (the relative residual) is set to 10^{-3}. Since a small number of iterations is required in these verification procedures, the memory storage related to the Krylov subspace is small and we do not have to use the restart parameters (set to 200).

4.1.2 Comparison of the surface sound pressure levels

The analytical solution (see section 2.1) is taken as the reference solution for the verification of the FMBEM algorithm. We study the case of a spherical incident wave scattered by a spherical body with a radius a equal to 1 m (see figure 2.1). We compare the surface pressure field levels. The source has a unit amplitude $Q = 1$ and the reference pressure chosen is 20μ Pa. 360 receivers are evenly distributed on the surface of the sphere. Figure 4.1 shows the comparisons of the sound pressure level in decibels, in terms of azimuth in degrees, between the analytical solution (blue line) and the solution computed with the FMBEM algorithm (dashed line). The comparison is performed for six dimensionless wave numbers: ka = 0.1, 1.0, 2.0, 5.0, 10.0 and 20, obtained for frequencies equal to 5.4, 54, 108, 271, 541 and 1082 Hz respectively. Since the studied frequencies do not involve fictitious eigenfrequency problems, the CHBIE formulation is not required in this study and the weighting parameter η in CHBIE formulation (equation (1.33)) can be set to 0 (pure CBIE formulation). In order to ensure that both kernels G and F are properly computed, we treat a rigid case ($\overline{q} = 0$) for which only the computation of the kernel F is required, and also an impedance case for which both kernels G and F are required. The impedances have been chosen to study the limit cases of a rigid body (i.e. $\sigma = 0$), and a soft body with a normalized complex impedance (compared with the air) $Z/Z_A = \sigma_A/\sigma = 1.22 + 1.22i$.

Each graph of figure 4.1 shows a comparison of both solutions (analitycal pressure and FMBEM pressure) for both boundary conditions (rigid and impedance). One can see a very satisfactory agreement between both solutions (see figure 4.1), the two curves (blue line and red dotted line) are actually superposed, meaning that the FMBEM algorithm succeeds in working out the solution for the considered ka. Hence, the expansion of the kernel G (equation (3.7)) and its normal derivative F (equation (3.12)) on the spherical basis functions are relevant to keep a satisfactory accuracy. The considered frequencies have been chosen in order to avoid the fictitious eigenfrequency problems which will be covered later in section 4.2. We also provide in table 4.1 some useful data in the framework of the fast multipole formalism obtained for solving this scattering problem.

TABLE 4.1: *Computation data related to the FMBEM : dimensionless domain size ka, number of levels in the tree structure l_{max}, maximum expansion order used p_{max}, levels in LF and HF formulation, iteration number, total memory and computation time required.*

ka	l_{max}	p_2	LF *levels*	HF *levels*	iterations	Memory (MB)	Time (s)
0.1	5	5	all	none	3	212	18
1.0	5	5	3-4-5	2	4	206	21
2.0	5	6	4-5	2-3	5	301	23
5.0	5	10	none	all	8	332	30
10.0	5	15	none	all	13	523	52
20.0	5	24	none	all	21	1112	145

4.1.3 Number of iterations for a frequency sweep

We focus in this section on the behavior of the iterative solver as function of frequency. We study a range of frequencies starting from the dimensionless frequency $2ka = kD = 0.09$ or 0.03λ to $2ka = kD = 20.3$ or 6.5λ corresponding to 5 and 1100 Hz respectively with a 1 Hz step. We are still considering the case of the scattering sphere excited by a point source (see figure **??**). This study is similar to the one performed with the BEM algorithm in the previous chapter. This will allow us to emphasize more precisely the behavior of the iterative solver with the fast multipole formalism. Due to the large number of calculations involved by the fine frequency resolution (*i.e.* 1 Hz) and, in order to emphasize what happens for each frequency, we set the number of elements to 7932 (see results in appendix B.1).

In figure 4.2, one can see the number of iterations required by GMRES to converge below the prescribed tolerance for a zero pressure (in red line) and a zero velocity (in blue line) boundary condition. As for the case of the BEM algorithm, the iterative solver has a fluctuating behavior meaning a close dependency on the frequency. In figure 4.3, we also provide the difference between the number of iterations required for GMRES with the BEM and the FMBEM algorithm for a zero pressure (left hand side), and a zero velocity (right hand side), boundary conditions. A positive value denotes that the FMBEM algorithm requires more iterations than the BEM algorithm. It seems that the FMBEM algorithm would require slightly more iterations than a similar problem solved with the BEM algorithm. Obviously the convergence of the iterative solver to solve problems through the FMBEM algorithm is slightly related to the expansion order p. Furthermore, the fictitious eigenfrequencies (highlighted in figure 4.2 in dashed black lines) seems also to impact the convergence of the FMBEM algorithm. Thus the following section is dedicated to the application of the B&M formulation on the fast multipole formalism to tackle the fictitious eigenfrequency problem.

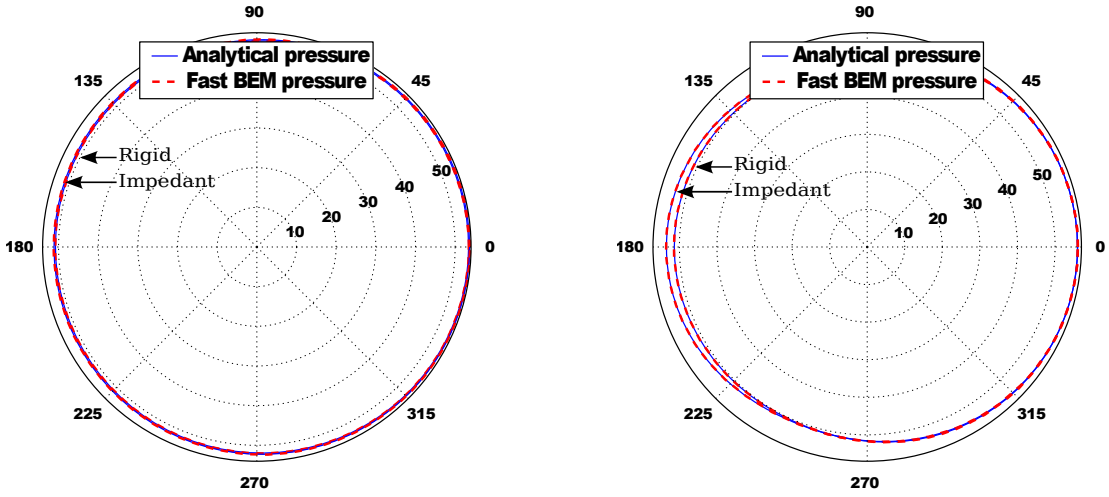

(a) $ka = 0.1$

(b) $ka = 1.0$

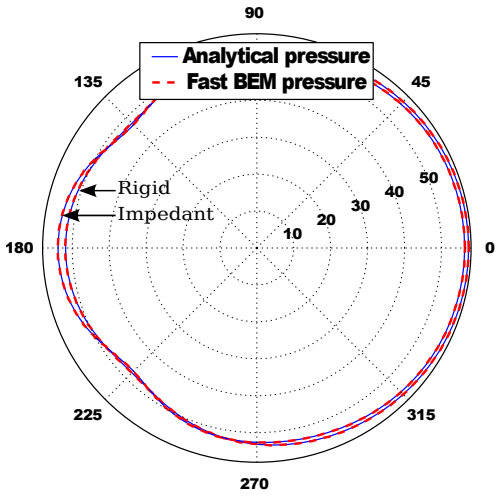

(c) $ka = 2.0$

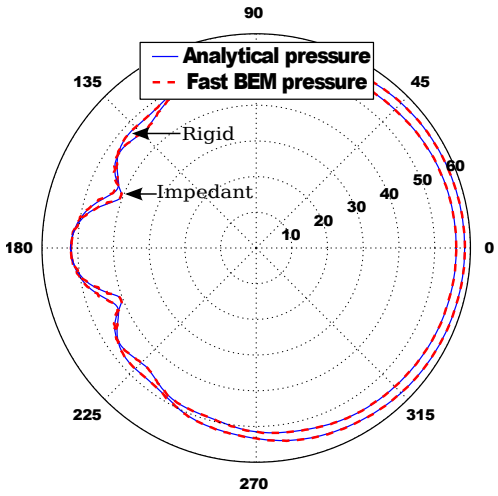

(d) $ka = 5.0$

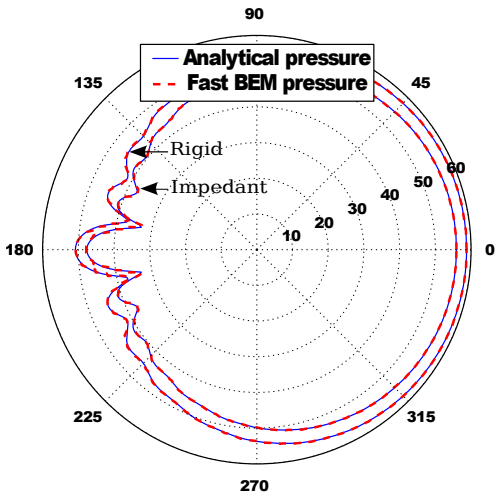

(e) $ka = 10$

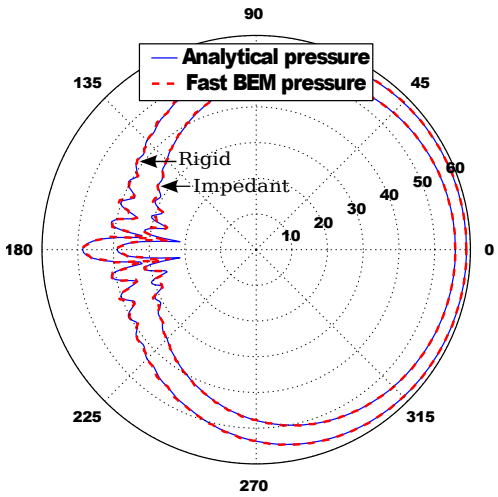

(f) $ka = 20$

FIGURE 4.1: *Comparison between the analytical solution (blue lines) and the FMBEM solution (dashed red lines) of the sound pressure level in dB (SPL) on the surface of the sphere excited by a spherical source of unit amplitude $Q = 1$. The reference pressure is 20 μ Pa. The source is located at* $10a$ *from the sphere center (a = radius).*

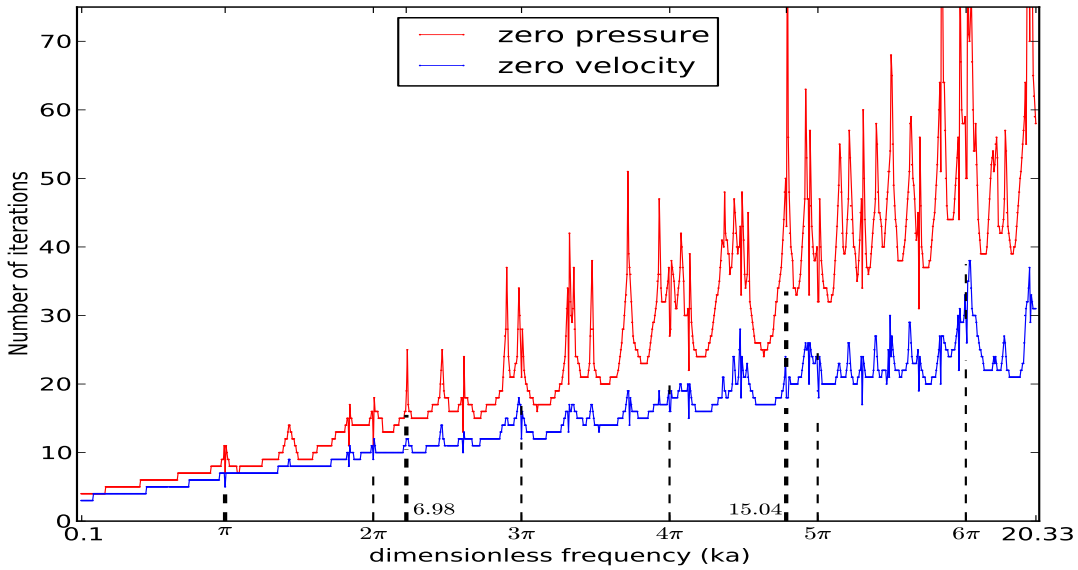

FIGURE 4.2: *Number of iterations required for GMRES to converge below the prescribed tolerance (i.e.*10^{-3}*) for a zero pressure boundary condition in red line and a zero velocity boundary condition in blue line. The dashed black lines correspond to fictitious eigenfrequencies.*

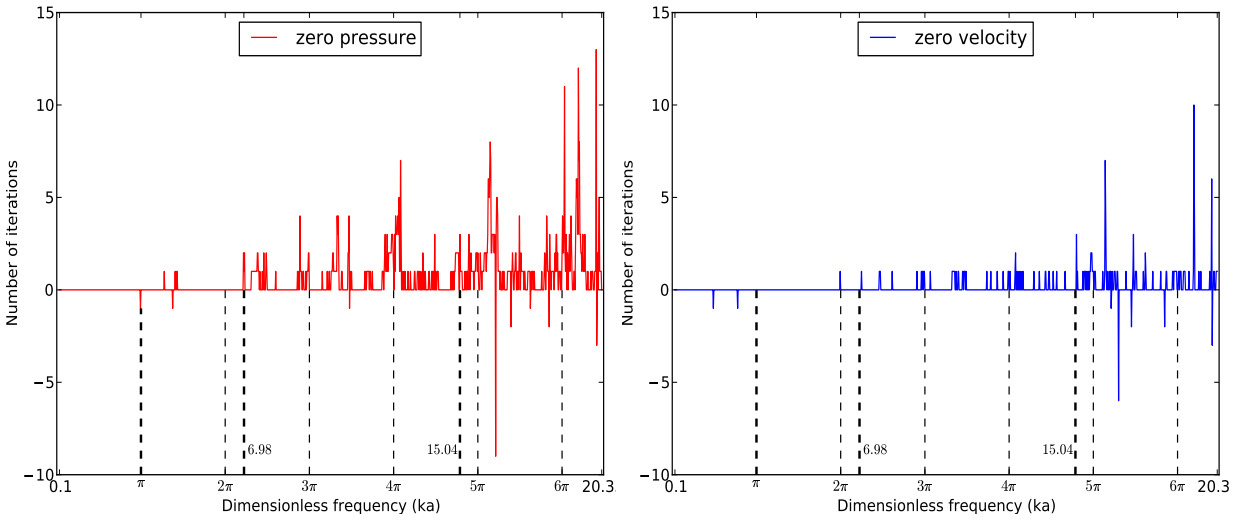

(a) difference for zero pressure boundary condition.

(b) difference for zero velocity boundary condition.

FIGURE 4.3: *Difference between the number of iterations required for GMRES to converge below the prescribed tolerance (i.e.*10^{-3}*) with the BEM and the FMBEM algorithms for a zero pressure (a) and a zero velocity (b) boundary conditions. A positive value denotes that the FMBEM algorithm requires more iterations than the BEM algorithm.*

4.2 Treatment of the fictitious eigenfrequency problem

The fast multipole method applied to the BEM appears to be also sensitive to fictitious eigenfrequency problems (see section 1.4 and section 2.3). Indeed, this sensitivity, which can be emphasized by drawing the sound pressure level on interior receivers' maps (see figures 2.4(a), 2.4(c), 2.4(e)), results in the disturbance of the exterior pressure field, as it has been emphasized for the BEM. Since in the previous chapter, the B&M formulation has been found to be relevant to overcome this drawback in the framework of the BEM, one will see, in this section, the influence of the B&M formulation when applied to the FMBEM since, theoretically, it does not involve numerical difficulties (see section 3.2.5). Consistently with section 2.3, one will first see the influence of the B&M formulation on the convergence of the iterative solver for both sound soft and rigid boundary conditions and then its efficiency to overcome the fictitious eigenfrequency problem.

4.2.1 Convergence of the iterative solver

The section 2.3 in chapter 2 has been dedicated to the influence of the B&M formulation (equation (1.32)) applied to the BEM, we now focus on the influence of this formulation applied to the FMBEM. This study is still carried out on the same range of frequency, from $ka = 0.09$ to $ka = 20.3$. The number of elements, 7932, is kept constant for the whole range involving $5elmts/\lambda$ at 1100 Hz (see results in appendix B.1). On the one hand we study the number of iterations required to converge below the relative residual 10^{-3} for sound soft boundary conditions $Z/Z_A = 10^{-3} + 10^{-3}i$ (figure 4.4(a)) to assess the computation of kernels G and K and on the other hand for rigid boundary conditions $Z \mapsto \infty$ (figure 4.4(b)) to assess the computation of kernels F and H.

We can make the same conclusion as for the case of the application of the B&M formulation to the boundary element method (see figure 4.4): the B&M formulation provides a better convergence of the iterative solver than in the absence of this formalism as frequency increases for both sound soft and rigid boundary conditions. It results in a stable dependency of the number of iterations in the whole frequency range and the B&M formulation also seems to bring a better conditioning when applied to the fast multipole formalism. However, regarding the convergence of the iterative solver for rigid boundary conditions (figure 4.4(b)), the use of the B&M formalism leads to a larger number of iterations, at low frequencies, than without it, as it was also emphasized for the standard BEM in the previous chapter (section 2.3). It is noteworthy that the red and blue curves intersect around the same abscissa, 3π, as for the boundary element method. For this reason the use of the B&M could not be recommended when ka is too small ($ka < 3\pi$, *i.e.* 510 Hz in this scattering sphere problem), since the eigenfrequency density is low.

4.2.2 Comparison of the surface sound pressure level

Regarding the sound soft boundary conditions (right hand side in figure 4.5), the discrepancy between the reference solution (blue lines), i.e. the BEM with the B&M formulation already validated in the previous chapter section 2.3 and the FMBEM with the B&M formulation, (red dashed lines), is only of several tenth of decibels (blue lines and red dashed lines are on top of each other). Thus, the B&M formulation applied to the FMM seems to provide a much better consistency with the reference solution than results obtained without the use of the B&M formulation (green dashed line). Thus the B&M formulation appears to be efficient to properly solve a scattering problem by a spherical body for sound soft boundary conditions regardless the frequency. From a numerical point of view, this means that the kernel K which appears in the B&M formalism is properly computed in the framework of the FMBEM. We point out that the B&M formalism was only assessed in this section for fictitious eigenfrequencies but we ensure that the B&M formalism has the same reliability for all the frequency range for sound soft boundary condition. It results that the B&M formulation (i.e. weighting parameter in equation 1.33, $\eta = 0.5$) succeeds in properly computing both kernels G and K and is found to be relevant in this case of the scattering sphere problem.

Regarding the rigid boundary conditions, left hand side figures in 4.5, we highlight the behavior of the surface pressure level for two different numbers of *levels*; 2 (red dashed lines) and 4 (black dashed lines). Compared to the reference solution (in blue line), already validated in the previous chapter (section 2.3), it is regrettable that the use of the B&M formalism leads to a unreliable solution in the low frequency range, for instance $ka = \pi$ (figure 4.5(a)) for 4 *levels*, than when it is not applied (green dashed line), while the use of this formulation provided a good agreement when the FMBEM is only carried on 2 *levels*. This means that additional *levels* in the framework of the fast multipole formalism lead to a loss of accuracy as the number of *levels* increases in the low frequency range. However as frequency increases, even for 4 *levels*, the application of the B&M formulation seems to provide a much better agreement with the reference solution than without it, as for instance for $ka = 15.04$ (i.e. 810 Hz), figure 4.5(e). Since the computation of kernels F and H has been validated in the previous chapter for the BEM as well as the computation of the kernel F has been validated in the framework of the fast multipole formalism in the previous section, this loss of accuracy may only be due to the computation of kernel H. From a theoretical point of view the use of the B&M formulation in the framework of the fast multipole method should not introduce numerical difficulties since the singularity problems of the H kernel only occurs in the BEM part. Thus, this inaccuracy may result from an implementation problem and the relevance of the application of the B&M formulation will be discussed in the following.

As already emphasized when applied to the BEM, the B&M formulation dramatically reduces the number of iterations to a stable dependency for the whole frequency range, when applied to the FMBEM, regardless of the boundary conditions. However the accuracy of the B&M formulation through the fast multipole formalism to solve scattering problems by a spherical body has not been evidenced. Since both efficiency and accuracy of the B&M formulation applied to the BEM have been validated in the previous chapter, these discrepancies seem to be due to the application of the B&M formulation in the framework

of the fast multipole formalism. More precisely since the proper computation of the kernel K has been previously evidenced, this loss of accuracy seems to be due to the computation of the kernel H. This observation is not in agreement with the theoretical results (see section 3.2.5) and the B&M formulation should not introduce numerical difficulties in the framework of the fast multipole formalism. We will see in the following section, dedicated to the application of the FMBEM for sound propagation problems in urban environments, that the inaccuracy of the B&M formulation allows nevertheless to compute noise maps with a sufficient precision, while providing a better conditioning. However, further research is needed to work out this problem in order to guarantee an optimum reliability of the algorithm. We nevertheless notice that other investigations which can been found in the literature report a slight loss of accuracy when solving problem at interior eigenfrequencies [Li 2010, Li 2011a] and certain authors advise against the use of the B&M formulation except at fictitious eigenfrequencies [FastBEM software 2014].

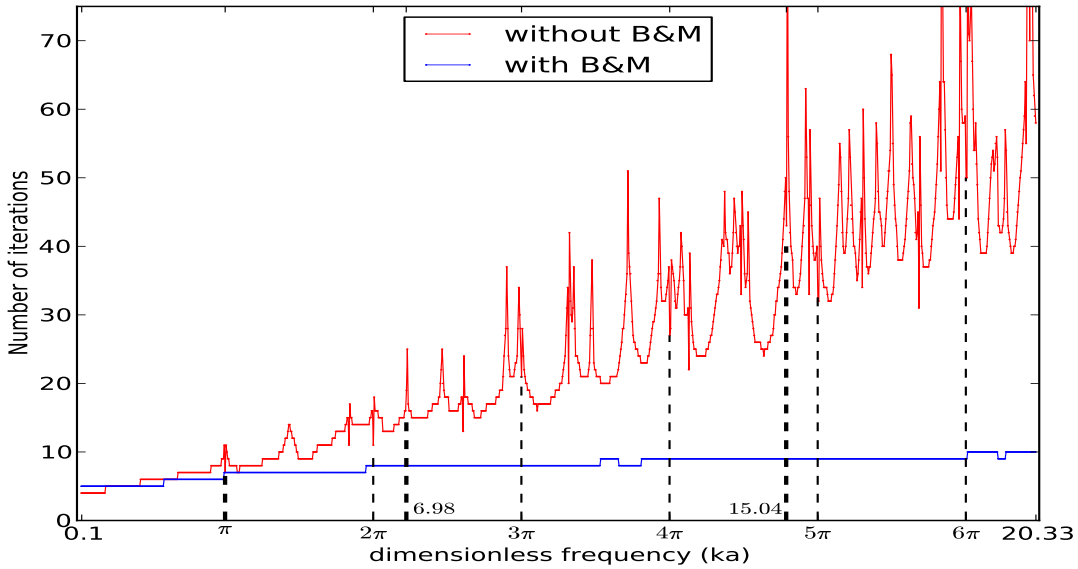

(a) number of iterations required for zero pressure boundary condition without B&M formulation (red line) and with B&M formulation (blue line).

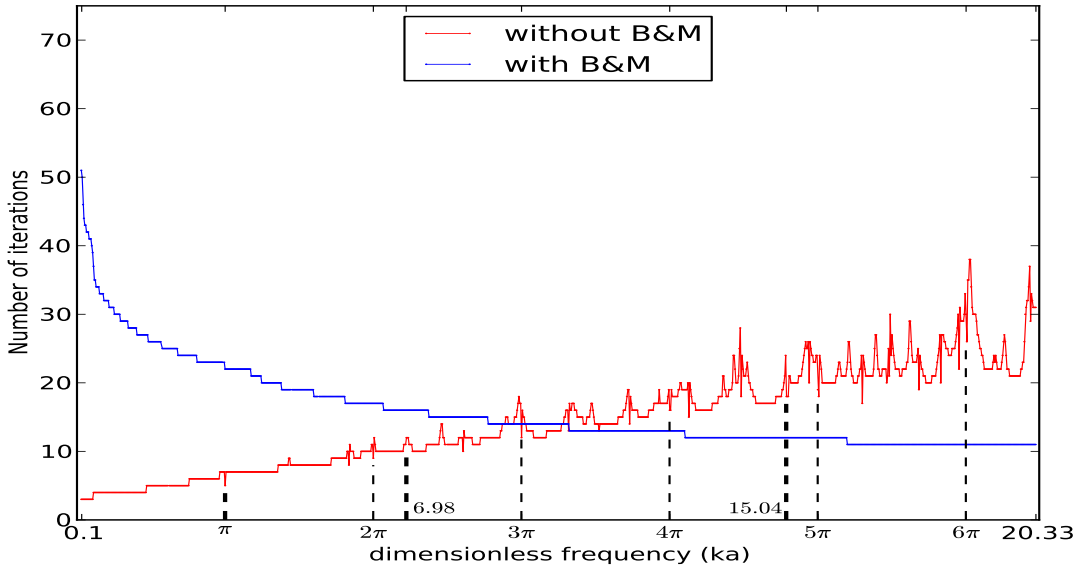

(b) number of iterations required for zero velocity boundary condition without B&M formulation (red line) and with B&M formulation (blue line).

FIGURE 4.4: *Number of iterations required for GMRES to converge below the prescribed tolerance (i.e.*10^{-3}*) for zero pressure (a) and zero velocity (b) boundary condition. The dashed black lines correspond to fictitious eigenfrequencies.*

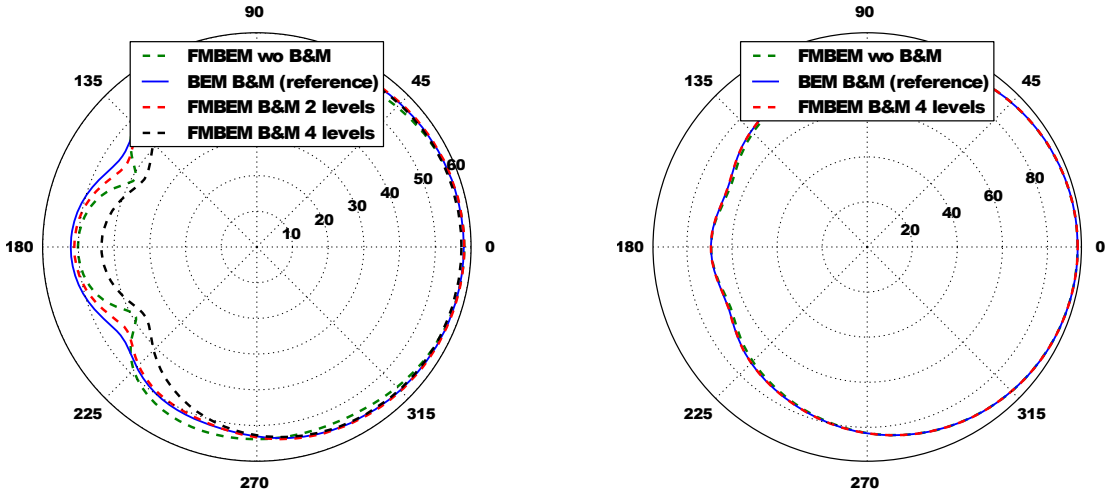

(a) $ka = \pi, Z \mapsto \infty$

(b) $ka = \pi, Z/Z_A = 10^{-3} + 10^{-3}i$

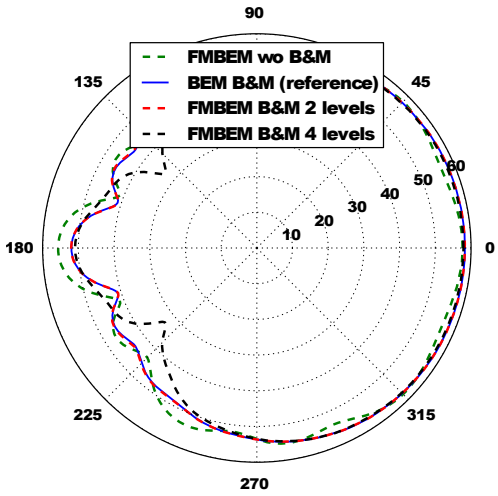

(c) $ka = 6.98, Z \mapsto \infty$

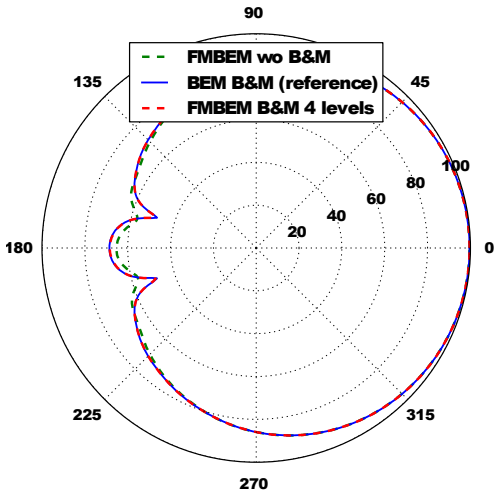

(d) $ka = 6.98, Z/Z_A = 10^{-3} + 10^{-3}i$

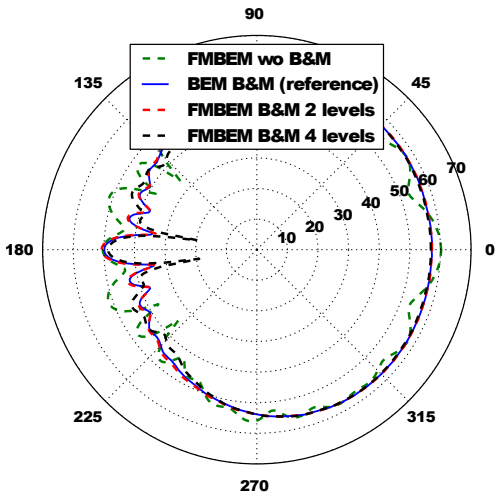

(e) $ka = 15.04, Z \mapsto \infty$

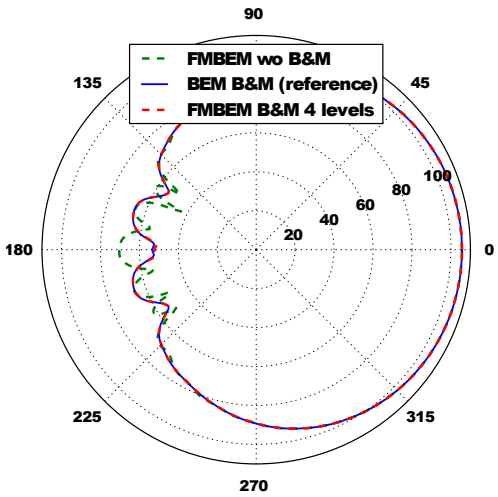

(f) $ka = 15.04, Z/Z_A = 10^{-3} + 10^{-3}i$

FIGURE 4.5: *Comparison between the BEM solution (blue lines) and the FMBEM solution for 2 levels (dashed red lines) and 4 levels (dashed black lines) of the surface sound pressure level in dB (SPL) for a spherical source located at* $10a$ *from the sphere center (*a *= radius) of unit amplitude* $Q = 1$*. We also provide the unsatisfactory results obtained by the FMBEM without the application of the B&M formalism (in green dotted lines). The reference pressure is 20* μ*Pa for the rigid cases, left side and the reference velocity is* 50.10^{-10} ms^{-1} *for the soft cases, right side.*

4.3 Validation of a half-space propagation problem

The full-space acoustic problem studied in the previous section is actually unusable in urban acoustic. Indeed, due to the presence of the ground, the problems encountered in urban acoustic can be seen as semi-infinite problems. Thus, a half-space problem can be solved either by meshing the geometry in the mirror domain (for a rigid plane ground) or by taking into account the acoustic reflection on the ground thanks to a fictitious rigid baffle. One will see in this section how to deal with a half-space problem in the framework of the FMBEM, starting from its corresponding full-space problem. The half-space formalism introduced in this section has already been the purpose of previous dedicated publications in two dimensions [Li 2011b] and in three dimensions, first in [Yasuda 2005] and then in [Bapat 2009]. Even though it is possible to deal with an impedance plane as introduced in [Ochmann 2004, Sarabandi 2004] and in [Ochmann 2008, chapter 17], we only consider here the case of a rigid symmetrical plane. The problem of a whole rigid sphere, studied in the previous section, corresponding to the full-space problem, will be used as a reference solution. We will compare it to the half-space problem in which only a half-sphere, lying on a fictitious infinite rigid plane, needs to be meshed. The contributions of the image domain, which corresponds to the ground reflections, will be added through the fictitious rigid baffle. The half-space problem is depicted in figure 4.6(b) and its corresponding full-space problem in figure 4.6(a).

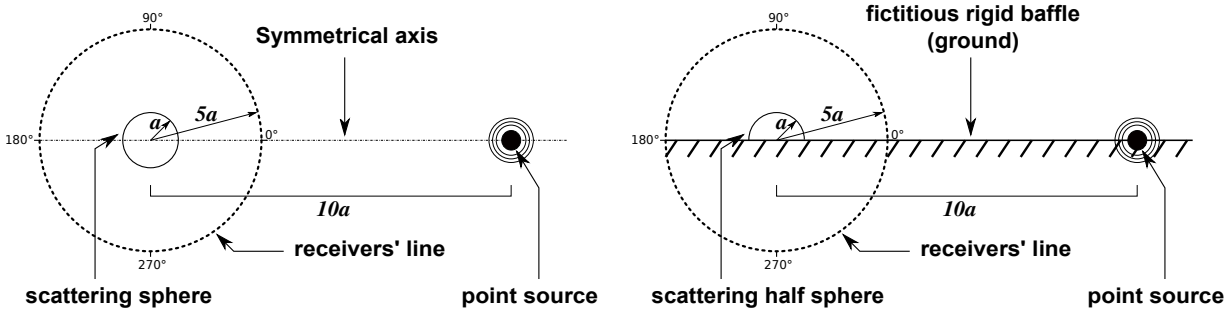

(a) Full-space problem

(b) Corresponding half-space problem

FIGURE 4.6: *A sphere of radius a excited by a point source, full-space and half-space cases.*

4.3.1 The half-space principle

We introduce in this section the method to deal with a half-space problem starting from its associated full-space problem and we describe its implementation in the FMBEM algorithm. Since the urban ground can be considered in a first approach as a rigid plane, the implementation of the baffle is actually based upon the image source principle. As for the full-space problem, for each cell, the oct-tree structure is divided in two areas. The first area corresponds to the *near* elements and the second area corresponds to the *far* elements.

The contribution of the *near* elements is computed directly using the boundary integral equation. For each contribution from a *near* source element $\mathbf{y}$, towards a receiver element $\mathbf{x}$, we add the contribution

coming from the image source element $\mathbf{y}'$ and thus the free space solution G becomes:

$$G(\mathbf{x},\mathbf{y}) \equiv G(\mathbf{x},\mathbf{y},\mathbf{y}') = \frac{e^{ikr}}{4\pi r} + \frac{e^{ikr'}}{4\pi r'}, \tag{4.1}$$

with r and r' being the distance from $\mathbf{x}$ and $\mathbf{y}$ to $\mathbf{y}'$ respectively.

The contribution of the far elements is computed using the fast multipole principle, described in a previous chapter 3. Each time that a translation is made in the moment step or in the moment to moment (M2M) step in the real space, from an expansion center to another one, a symmetric translation is also made in the image domain (see [Li 2011a, Bapat 2009]). This involves two translation matrices, which will be added at the same expansion center in the moment to local (M2L) step. Afterwards, there is no distinction between these two translation matrices and the local to local (L2L) step and the final summation remain unchanged. The influence of the fictitious rigid baffle on the fast multipole principle is depicted in figure 4.7.

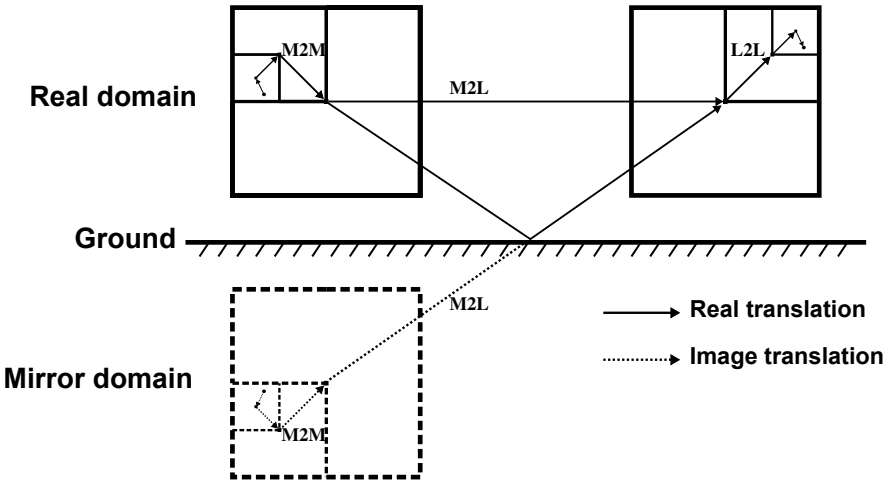

FIGURE 4.7: *Half-space problem: definition of the real and virtual objects by the FMBEM.*

Finally, for the calculation of acoustic pressure levels at a receiver point away from the boundaries (in the post-processing step), the contribution coming from the ground is taken into account through the image source principle (equation (4.1)) and added to the contribution of elements located in the real domain.

4.3.2 Comparison with the full-space problem

The solution of the full-space with its corresponding half-space problem is compared in this section. For the half-space problem, we only have to mesh a half sphere involving twice as less elements as for the full-space problem, 15846 (~31694/2) against 31694 elements respectively (or 10 elements per wavelength at $ka = 20$, see results in appendix B.2). As for the full-space problem, the studied frequencies do not involve fictitious eigenfrequency problems, and so the CHBIE formulation is not required in this study and the parameter η can be set to 0 (pure CBIE formulation). Solutions are both computed with the FMBEM

TABLE 4.2: *Numerical data for the half-space FMBEM and in parenthesis for the full-space FMBEM: dimensionless domain size ka, number of levels in tree structure l_{max}, maximum expansion order used p_{max}, levels in LF and HF formulation, iteration number, total memory and computation time required.*

ka	l_{max}	p_2	LF *levels*	HF *levels*	iterations	Memory (MB)	Time (s)
0.1	5	5	all	none	3 (3)	177 (212)	16 (18)
2.0	5	6	5	2-3-4	5 (5)	232 (301)	20 (23)
5.0	5	10	none	all	8 (8)	249 (332)	25 (30)
20.0	5	24	none	all	21 (21)	969 (1112)	123 (145)

algorithm in order to only highlight the differences due to the rigid baffle. We compare the potential pressure level taken on 360 receivers, evenly distributed on a circle of radius $r = 5a$ from the sphere center. The computations are done for two frequencies, which correspond to the dimensionless wave numbers $ka = 0.1$ and 20.0. Note that we have halved the amplitude of the source for the half-space problem since it is taken into account twice, once in the real domain and also in the image domain. Figure 4.8 shows the potential pressure in dB(SPL) taken on the receivers for the full-space problem (blue line) and for the half-space problem (red crosses). Table 4.2 summarizes some useful data, obtained at four different frequencies for the rigid case, related to the half-space computation and also data previously obtained for the full-space problem (in brackets). We keep the number of *level* l_{max} constant for all frequencies and both formulations (LF and HF) are assessed in these verification tests. Indeed, at $ka = 0.1$ only the LF formulation is required while a pure HF formulation is used starting from $ka = 5$. We point out a switch for $ka = 2$ between the *level* 5 and the *level* 4.

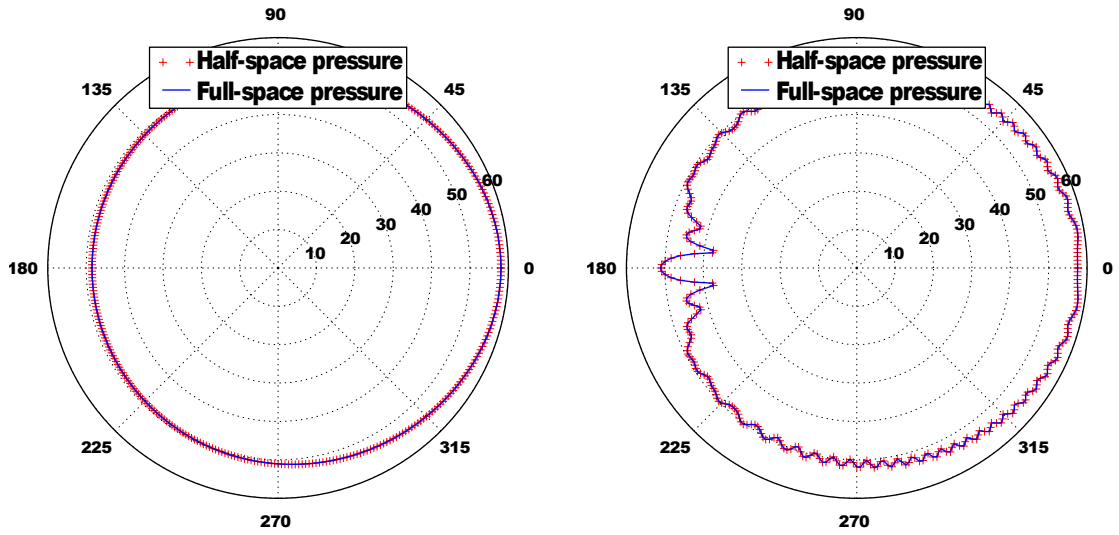

(a) $ka = 0.1$ (b) $ka = 20$

FIGURE 4.8: *Spherical wave of unit amplitude $Q = 1$ scattered by a rigid sphere ($\sigma = 0$). Comparison between the full-space solution (blue line) and the half-space solution (red crosses) of the sound pressure level in dB (SPL) on a curved line of radius $r = 5a$. The reference pressure is 20 μ Pa. The source is located at $10a$ from the sphere center (a = radius).*

Since one cannot see significant differences (maximum discrepancy of 0.02 dB) between the full-space and the half-space solutions, the half-space problem with the addition of the fictitious infinite rigid baffle is relevant to efficiently solve acoustic problems including the specular ground reflections without having to mesh the mirror object. We also notice that the half-space problem brings improvements in terms of computation time and required memory mainly due to the fact that the half-space problem requires only twice less elements as for its corresponding full-space problem (*cf.* table 4.2). Even if these improvements appear to be rather small for these simple verification cases, the benefit will become more significant as the complexity of the studied geometry increases. We note that YASUDA & al. introduced a more efficient technique for plane-symmetric acoustic problem dividing by 2 both computation time and required memory by planes of symmetry [Yasuda 2012].

4.4 In summary

We investigate in this chapter comparisons, for the scattering problem by a spherical body, between the analytical solution and the solution computed with the FMBEM algorithm. Thus the fast multipole algorithm is found to be relevant to properly compute the surface pressure of the studied case at regular frequencies, while at singular frequencies we noted a loss of accuracy for increasing number of *levels* for rigid boundary condition only. Finally, we detail how to deal with a half space problem to take into account the reflections on the ground starting from the full-space problem with the addition of the infinite rigid baffle.

Part II: Conclusion

The conventional Boundary Element Method (BEM), as described in the first part (I), produces dense and non-symmetric matrices which require $O(N^2)$ operations for computing the matrix coefficients and $O(N^3)$ operations for solving the system by using direct solvers, N being the number of equations of the linear system. As a consequence, applying this method on large scale models leads to prohibitive computation times. Since few years, the boundary element method profited from a major improvement through the fast multipole formalism, used to decrease the computation time complexity of boundary element based algorithms. Thus the purpose of this second part II has been to introduce the fast multipole principle as well as the mathematical background required to perform calculations. Consistently with the previous part, we also assessed the ability and the accuracy of the fast multipole method, for solving a scattering problem by a spherical body.

In the third chapter, we first provided a general overview of the fast multipole principle. We introduced the spherical basis series required for the kernel expansions. We also introduced the RCR decomposition which our algorithm is based on as well as the high frequency formulation. We described more precisely all steps of the calculation, i.e the multipole expansion, the Moment to Moment (M2M) step, the Moment to Local (M2L) step, the Local to Local (L2L) step and the final summation step. Finally, we have assessed the theoretical computational complexity of the fast multipole algorithm as $O(N) \simeq O(p^2)$.

The fourth chapter is dedicated to the assessment of the fast multipole formalism for solving a scattering problem by a spherical body. Thus, we proved the accuracy of the fast multipole formalism for both rigid and impedance boundary conditions by comparison with the analytical solution at regular frequencies. We also assessed the conventional & hyper-singular boundary integral formulation to tackle the fictitious eigenfrequency problem. We first emphasized, as for the BEM algorithm, that the B&M formulation dramatically reduces the number of iteration as the frequency increases, regardless the boundary conditions. We have also proved the efficiency of this formulation to provide reliable solutions for soft boundary conditions while for rigid cases, it leads to a loss of accuracy with increasing number of *levels* at low frequency. Thus this formulation seems not to be recommended for small scale models, and further investigations may be desirable to work out this problem in order to guarantee an optimum reliability of the algorithm. We however notice that the B&M formulation will be successfully applied in the framework of large scale propagation models in the next part III. Because of the presence of the ground in urban context, the full space problem requires to mesh the symmetrical geometry to simulate the reflections on the ground. This

drawback can be tackled by the implementation of the half space problem with the addition of the infinite rigid baffle, which provides improvements in terms of computation time and storage memory, compared to its equivalent problem in full space. This half space problem is subsequently used in an urban context in the next part III.

Part III

Application on realistic cases & improvements of the fast multipole algorithm

Part III: Introduction

In the previous section, we have checked both the efficiency and accuracy of the half-space FMBEM for solving scattering problems by a spherical body. We now focus on more realistic geometries such as encountered in urban environments. Although the fast multipole formalism applied to the Boundary Element Method has been the topic of many publications, its application in the framework of realistic sound propagation problems in dense urban environments has only been seldom studied and this part constitutes, as far as the author knows, an original work. We can, nevertheless, find some studies carried out, for instance, on a scattering problem by a noise barrier [Shen 2007] or in environmental acoustics [Bapat 2009]. A source-receiver transfer function for predicting pass by noise levels of automotive vehicles has also being evaluate numerically with the FMBEM [Huijssen 2012], however FMBEM algorithms in the domain of outdoor sound propagation are not systematically used for providing reference solutions of a specific problem. We attach importance, in this part, to show the applicability of the FMBEM algorithm on realistic geometries encountered in urban environment for the computation of reliable solutions, as well as improvements, in terms of both computation time and memory.

In the following chapter 5, the first application is a scattering case by a noise barrier in a front of building (section 5.1). The second one will be a sound propagation problem within a city block made of 5 buildings (section 5.2). We emphasized the benefits provided by the fast multipole formalism in terms of computational requirements, *i.e.* the computation time and storage memory. This latter application will highlight some instabilities which occur for expansion orders above around a hundred, leading to discontinuities on the surface pressure field and a no convergence of the iterative solver. We finally discuss (chapter 5.3) about the current limitations of the algorithm which led us to consider the very recent Gumerov & Duraiswamy's work (section 5.4), related to the stability of the recursive process to compute the rotation matrices coefficients.

We explain, (chapter 6), how a "fast and stable" recursive scheme can be guaranteed for the computation of the rotational matrices entries of large expansion orders (section 6.1). Then we apply this new improved version of the algorithm on the previous case of the sound propagation problem in the city block (section 6.2). Finally, we try to emphasize the new limitation of the algorithm through multi scattering problems by cubic scatterers (section 6.3).

In the last chapter (chapter 7), after having briefly introduced the outline of the ray tracing based

algorithms (section 7.1), we compare the pressure levels averaged within the opened and closed court yards through three different algorithms. In a first frequency range (1 - 150 Hz), section 7.2, we confront a BEM algorithm, the FMBEM algorithm and a ray tracing based algorithm Icare® software, while in a second frequency range (150 - 300 Hz), section 7.4, the comparison will be performed only between the FMBEM algorithm and the Icare®.

Chapter 5

Applications of the FMBEM for acoustic wave problems in urban environments

5.1 Scattering problem by a noise barrier in front of a building

We first deal, in this section, with the case of a quarter-circle impedance sound barrier located in front of a building. More precisely, we introduce the geometry of the problem and the numerical results are presented for two frequency bands centered on 100 Hz and 180 Hz, a regular and a singular frequency respectively.

5.1.1 Description of the studied geometry

We consider the case of a quarter-circle impedance sound barrier located between a point source with a unit amplitude and an impedance building. The sound barrier has a radius of 20 m ($\approx 11\lambda$ at a frequency of 180 Hz, λ being the wavelength) and is 6 m high. The building has a squared base of dimensions 8×8 m and is 16 m high. Both normalized impedances are set to $Z_{c/air} = 38$, corresponding to an absorption coefficient of approximately 0.1. This absorption coefficient is tuned to real value [Hornikx 2012] and [ISO 9613-2: 1996] and accounts for scattering by surface irregularities. The whole geometry (barrier + building) is discretized with 13182 constant triangular elements (see figure 5.1), corresponding to a space discretization criteria equal to $\lambda/5$ at 180 Hz (see figure 5.1). We perform (section 5.1.2.1) averaged pressure computations centered, in a first time, on 100 Hz (corresponding to a non-dimensional domain size of 11.8 λ), for a frequency range between 80 and 120 Hz with a 1 Hz step and in a second time (section 5.1.2.2) around a singular frequency of the building, i.e. 180 Hz (corresponding to a non-dimensional domain size of 21.3 λ), from 170 Hz to 190 Hz with a 1 Hz step. We finally average the sound pressure levels for each frequency on a receivers' grid (40×40 m i.e. $23\lambda \times 23\lambda$ at 180 Hz). The point source is located at coordinates (0,0,1).

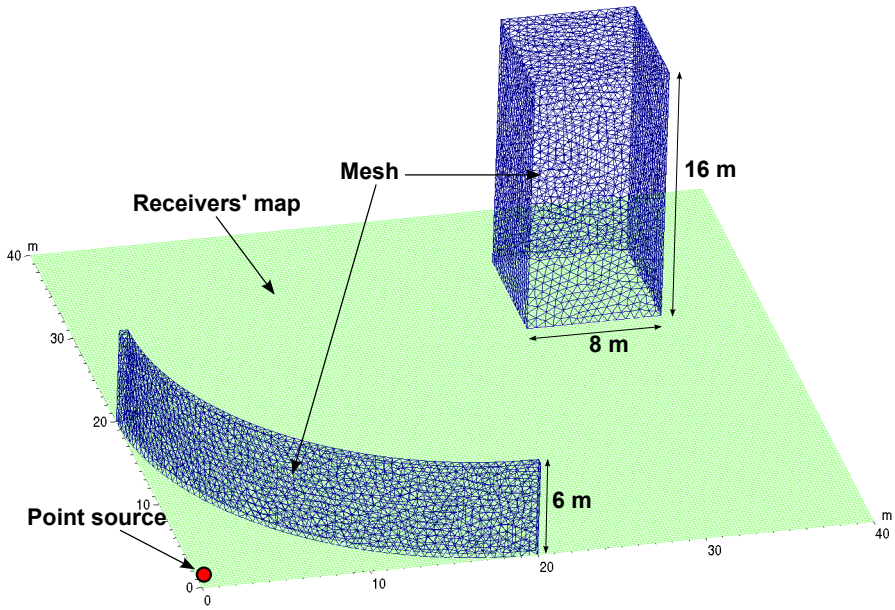

FIGURE 5.1: *Overview of the studied geometry: a sound barrier located in front of a building (13182 elements, in blue) excited by a point source and the receivers' map (40000 receivers, in green).*

Because of the high computation time involved by the standard BEM formalism, the comparison will be performed with an internal optimized BEM software, *Micado3D* (see [Jean 1998]). It is a 3 dimensional boundary element algorithm, using a direct approach, for the study of acoustical problems. It uses linear interpolation functions and is based on a variational approach [Hamdi 1982]. Since the variational approach does not suffer from the major drawback of the fictitious eigenfrequency problem, this algorithm will be taken as a reference. Indeed, even if the solution computed on the mesh could indicate a fictitious eigenfrequency behavior at certain characteristic frequencies, the solution does not radiate outside [Terrasse 2007, Thierry 2011]. It results that this inconvenience does not affect the pressure field on the receivers' grid. All the computations related to the *Micado3D* software run on a desktop PC with an Intel Xeon® E5645 processor at 2.40 GHz and 24 GB of memory storage.

5.1.2 Sound pressure level on a receivers' map

5.1.2.1 Around a regular frequency: 100Hz

The whole geometry (barrier + building) is discretized with 13162 constant triangular elements. The maximum number of elements allowed at the lowest level is set to 50 which involves 4 active *levels* from *level* 2 to 5. We supply an overview in appendix C.1 of the space partionning related to the 4^{th} level. We perform the computations for frequencies ranging between 80 Hz and 120 Hz with a 1 Hz step and finally average the pressure values obtained for each frequency, on a receivers' grid (40×40 m). In figure 5.2, we display the sound pressure levels obtained at a single frequency of 100 Hz for both *Micado3D* and FMBEM computations.

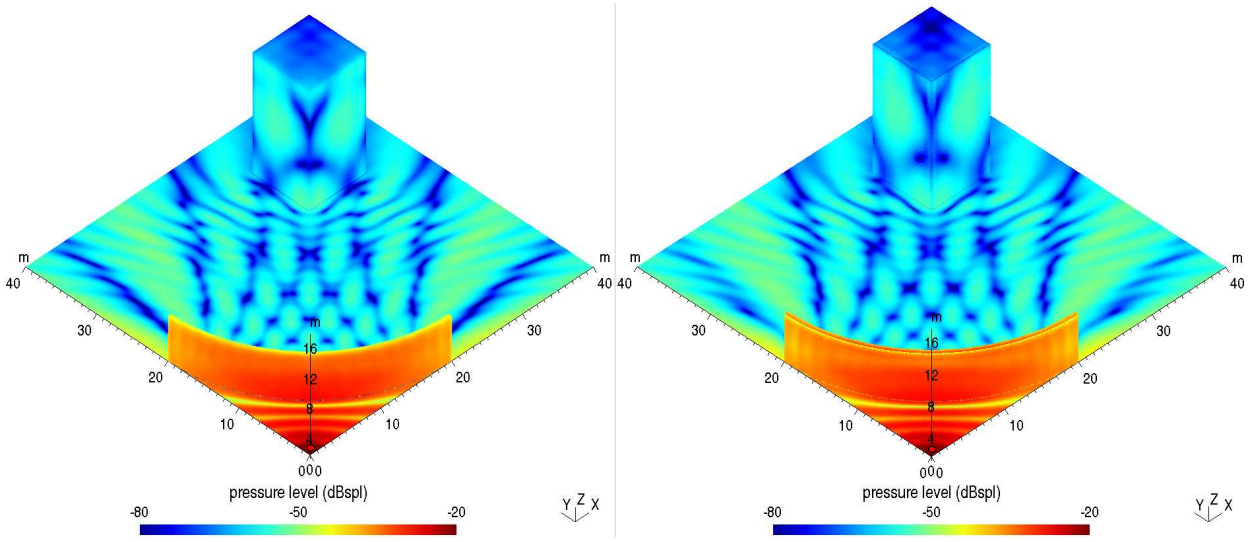

FIGURE 5.2: *Intermediate results for a single frequency of 100 Hz: on left with classical BEM (Micado3D), on right with the FMBEM algorithm.*

One can hardly see the differences between both computations on these views. To compare more precisely the differences between both computations, we display, in figure 5.3, the differences between the map obtained with the BEM algorithm *Micado3D* and the map obtained with FMBEM algorithm. The discrepancies are ranging between 0 and 3.6 dB with an average of 0.72 dB. We however denote that the maximum discrepancy is located on the destructive interference area, where the absolute pressure level is around 60 dB below the sound pressure level observed right in front of the sound barrier. We also note that 73% of pressure levels on the receivers are inferior to 1 dB, 93% < 2 dB and 98% < 3 dB. Thus we can say that both computations are in very good agreement meaning that the FMBEM can be relevant for solving urban acoustic propagation problems such as scattering problems.

5.1.2.2 Around a singular frequency: 180Hz

The whole geometry (barrier + building) is still discretized with 13162 constant triangular elements. The maximum number of elements allowed at the lowest level is set to 200 which involves 3 active levels. In order to overcome the fictitious eigenfrequency problem occurring around this frequency (i.e. 180 Hz), we assess the CHBIE formulation and set the weighting parameter, η to 0.98 (cf. eq. (1.33)), optimum value to overcome the fictitious eigenfrequency problem in this study.

We show the averaged sound pressure level obtained on both mesh and receivers map with the reference variational BEM solution (*i.e.* with *Micado3D* software) in figure 5.4 and the difference between the noise maps computed with *Micado3D* and our FMBEM algorithm including the CHBIE formulation (eq. (1.33)), in figure 5.5. On the 40000 receivers belonging to the map, 53 % of receivers show a discrepancy lower than 1 dB, 82 % < 2 dB and 96% < 3 dB. Thus, we can see that the CHBIE formulation proposed (eq. (1.33), $\eta = 0.98$) succeeds in overcoming the fictitious eigenfrequency problem with an acceptable accuracy.

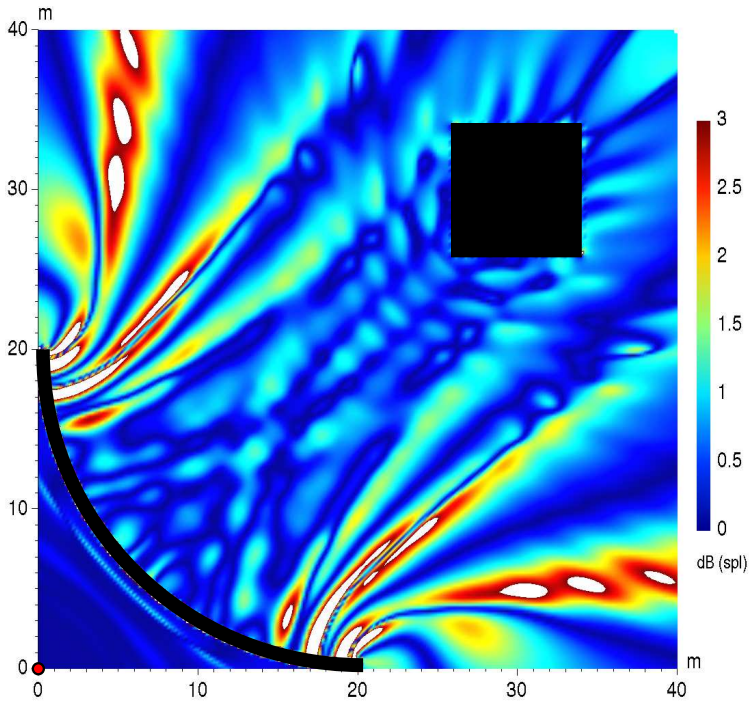

FIGURE 5.3: *Differences (in dB) between noise maps obtained with Micado3D and FMBEM (top view) for the frequency range (80 - 120 Hz). The pressure values obtained for each frequency are averaged. The sound barrier and the building are displayed in black.*

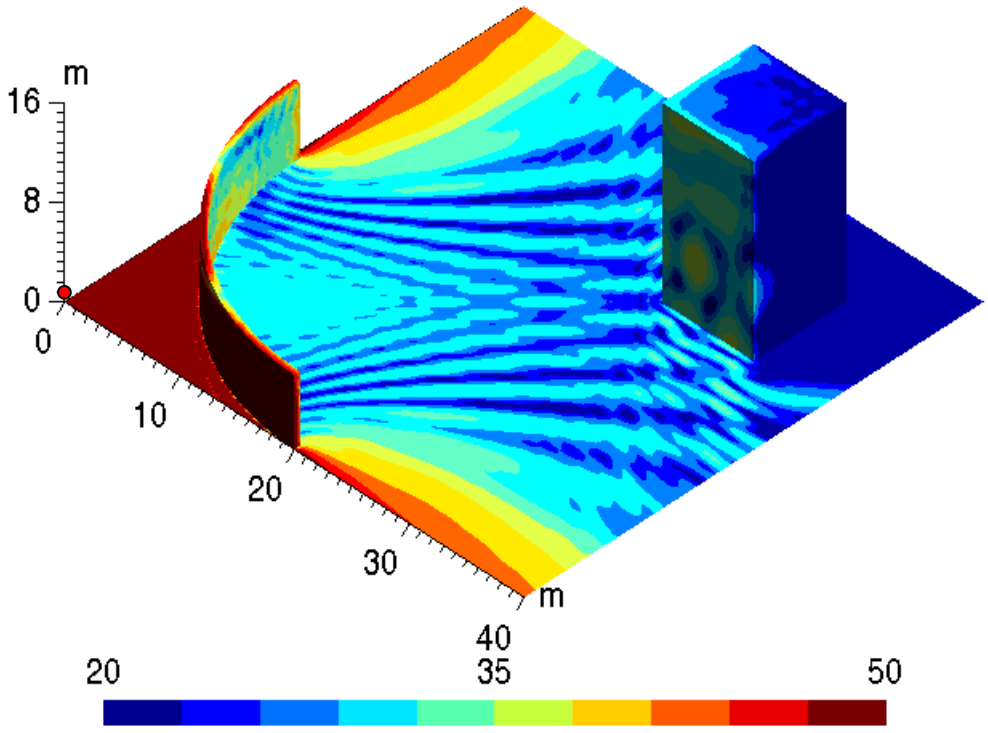

FIGURE 5.4: *Sound pressure level in dB(SPL) averaged on the studied frequency range (170-190 Hz) computed with our reference variational BEM algorithm for the mesh and on the receivers' map.*

Obviously this formulation requires the evaluation of five integrals for impedance boundary conditions and is more time-consuming than the CBIE (eq. (3.1)).

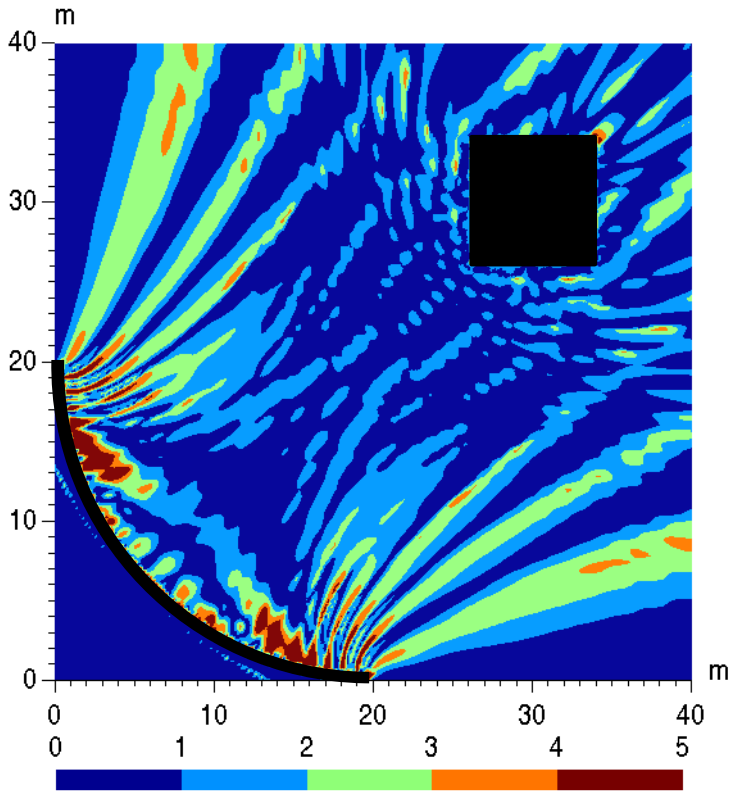

FIGURE 5.5: *Differences (in dB) between the noise maps obtained with Micado3D and the FMBEM for the frequency range (170-190 Hz). The sound barrier and the building are displayed in black (top view).*

Regarding the computing requirements, a standard BEM collocation approach would have needed 2700 Mo and around 1000 s (iterative solver) to solve this problem while the variational approach, (*Micado3D*), requires almost 700 Mo and 560 s (direct solver). The FMBEM algorithm needs 2800 Mo and 480 s to solve this same problem but it is noteworthy that the resources are mainly used by GMRES since it requires 1300 Mo to store the Krylov subspace and 320 s to converge. So, reducing the number of iterations with a suitable preconditioner seems to be an attractive solution to reduce both memory storage and CPU time [Chaillat 2012].

As a result, the fast multipole formalism applied to the BEM is found to be relevant for solving this scattering problem by a sound barrier. We performed investigations for a regular and a singular frequency and proved the accuracy of the algorithm by comparison with a reference algorithm *Micado3D* already validated in previous studies. Although the computational time benefits have not been emphasized in this studies due to the low number of elements, the next section will specifically bring to light the benefits in terms of CPU time as well as storage memory as the number of elements increases.

5.2 Sound propagation in a city block

We now deal with a larger scale model in order to emphasize the benefits of the FMBEM as the number of elements increases. We study the case of sound propagation in a city block made of 5 buildings. We first introduce the geometry characteristics of the studied mesh, we analyze the influence of the formulation (CBIE or CHBIE) on the convergence of the iterative solver by performing a parametric study on the weighting parameter η. This study allows us determining a suitable value of η which minimizes the CPU time by reducing the number of iterations as well as mitigating the fictitious eigenfrequencies problem. We subsequently focus on the influence of the iterative solver relative residual on the accuracy of the solution on a receivers' map. Then, we assess the accuracy of the FMBEM algorithm by comparison of the sound pressure levels on the receivers' map computed between the FMBEM algorithm and the reference software *Micado*3*D*. We also analyze the computational resources, as the CPU time or the memory storage, required to solve such an exterior sound propagation problem in an urban environment and the benefits provided by parallelized calculation of direct interactions. This study will allow us, in a last section, to discuss the current restrictions of the FMBEM algorithm due to unstable recursive properties and its influence on the accuracy of the solution. This discussion will lead us to focus, in the next chapter, on a recent investigation of a stable recursive calculation of the rotational operators.

Due to the unstable recursive calculations of the rotational matrices, we chose to truncate the multipole expansion series up to the order $p = 98$, since higher expansion orders involve instabilities in the recursive process. Obviously, such a choice implies a loss of accuracy, specifically in the more sensitive areas. According to section 5.1, the variational BEM solution will be taken as a reference solution and compared to the solution obtained with our FMBEM algorithm.

5.2.1 Description of the studied geometry

This larger scale model represents a city block, made of five, 15 meters high, buildings and a total length of 110×60 meters (i.e. $\approx 32\lambda \times 18\lambda$ at 100 Hz, λ being the wavelength). As for the case of the sound barrier, we set the normalized impedance to $Z_{c/air} = 38$ according to [Hornikx 2012] and [ISO 9613-2: 1996] and perform the computation for a frequency range between 90 and 100 Hz with a 1 Hz step, involving 66306 elements at 100 Hz with a space discretization criterion of $\lambda/4$. The mesh as well as the receivers' map is shown in figure 5.6. The point source is located at coordinates $(12, 45, 0)$ denoted by the red point on the map.

5.2.2 Influence of the weighting parameter on the iterative solver

The purpose of this section is the investigation of the influence of the weighting parameter on the convergence of the iterative solver. This study allows to determine a proper value of η to mitigate the fictitious eigenfrequency problem as well as a reduction of the computation time. Since a fast computation time will

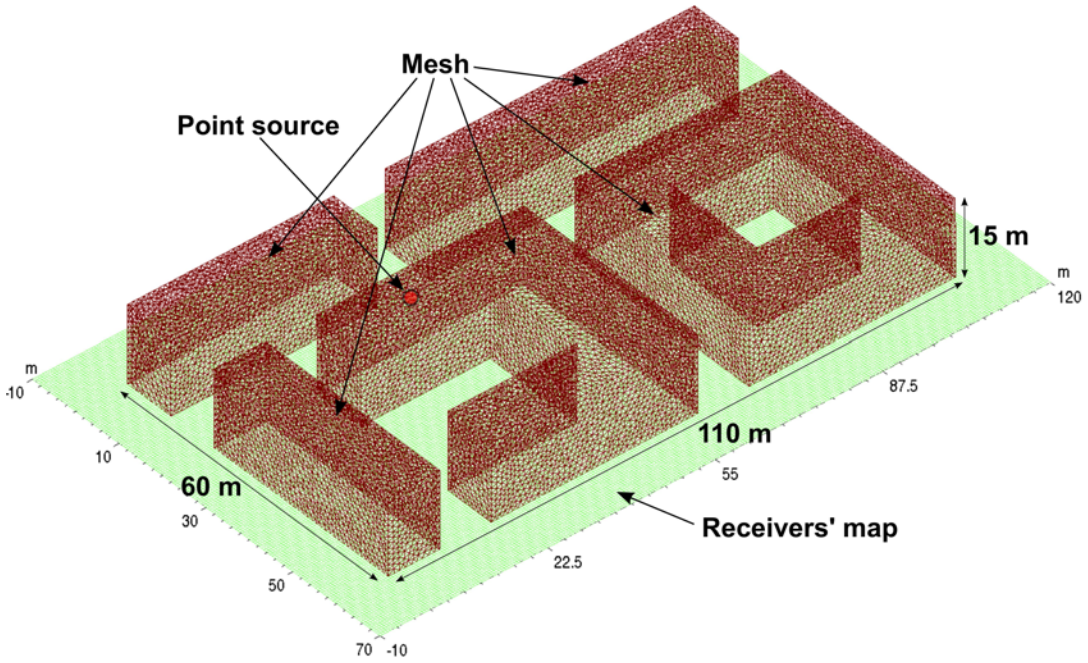

FIGURE 5.6: *Overview of the studied geometry: A city block made of 5 buildings excited by a point source (red point) of unit amplitude $Q = 1$. This overview contains 66306 mesh elements in red and 41600 receivers in green lying on the ground.*

be reached for a minimal number of iterations, we try to minimize the number of iterations with a suitable choice of the parameter η. The study frequency range is 30 and 100 Hz or in non-dimensional value between around 10 and 32 wavelengths. We set the iterative solver relative residual to 10^{-2} but precise that this criterion will be the subject of the following section. In Figure 5.7, one can see the influence of the parameter η on the number of iterations in terms of frequency. One can see that $\eta = 0.0$ (i.e. corresponding to a pure CBIE formulation) leads to a very large number of iterations meaning a very bad conditioning rending the iterative solver basically inefficient, while $\eta = 0.6$ leads to an optimum convergence rate. We reasonably assume that this value allows to mitigate the fictitious eigenfrequency problem and will be kept in the remainder of this section. Due to huge computational times involved by the pure CBIE formulation, the studied frequency range has been limited to 50 Hz for $\eta = 0.0$.

5.2.3 Influence of the relative residual on the noise map

One now see the influence of the relative residual on the reliability of the solution. We recall that this parameter is the iteration stopping criterion which needs to be reached by the approximate solution of the iterative solver. The mesh contains 33357 elements for a studied frequency of 100 Hz involving a space discretization criterion of 3.5 elements per wavelength. The aim of this parametric study is to determine a suitable value of the relative residual based on a compromise between speed of the iterative process and accuracy of the solution.

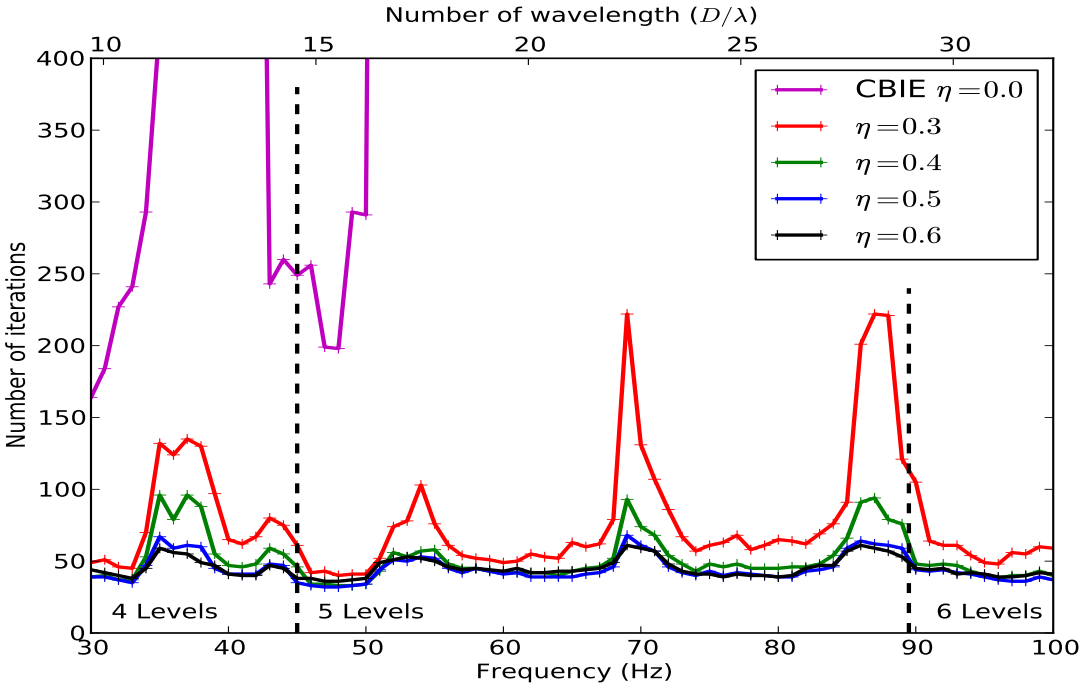

FIGURE 5.7: *Influence of the weighting parameter on the behavior of the iterative solver for a frequency range (30 - 100 Hz) with a 1 Hz step.*

Thus we analyze in figure 5.8 the relative residual obtained at each step of the iterative process for a relative residual stopping criterion equal to 10^{-4}. We also indicate the computation time required to converge below the values 10^{-1}, 10^{-2}, 10^{-3}, 10^{-4}, emphasized in red dotted lines.

In addition, we also carry on our study on the estimation of errors on the receiver map provided by relative residuals equal to 10^{-1}, 2.10^{-2}, 10^{-2}, 2.10^{-3} 10^{-3} and 2.10^{-4}. The comparison is performed with a receiver map obtained for a relative residual 10^{-4} (reference), assuming that the solution has converged (see figure 5.9). One can see that the more sensitive areas, as the opened or closed court yards required more iterations to ensure a reliable solution (see figures 5.9(d)). A value equal to 10^{-2} seems nevertheless sufficient for a rapid evaluation of the sound pressure on the receiver maps at the price of a slight loss of accuracy. For a converged and more precise solution (see figures 5.9(g)), one will prefer to set the relative residual to 1.10^{-3} which however requires a more important computation time (as emphasized in figures 5.8).

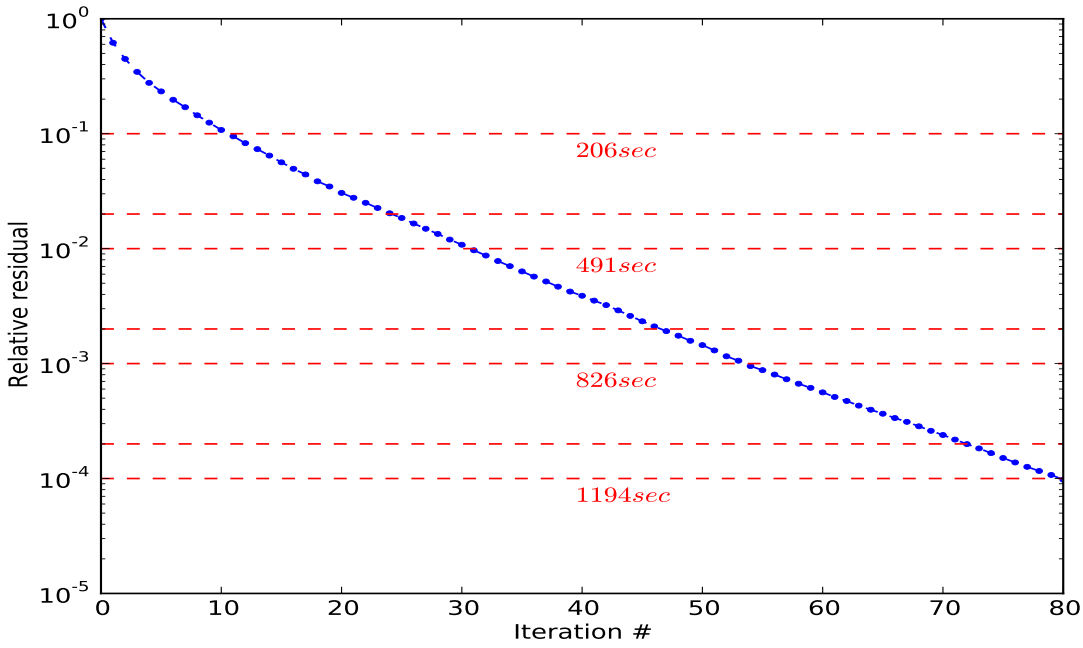

FIGURE 5.8: *Convergence of the approximation of the solution for a relative residual* 10^{-4} *for the city block at 100 Hz. We highlight in red dotted lines the computation time to converge below the relative residuals* 10^{-1}, 2.10^{-2}, 10^{-2}, 2.10^{-3}, 10^{-3}, 2.10^{-4} *and* 10^{-4}*, our reference in this study.*

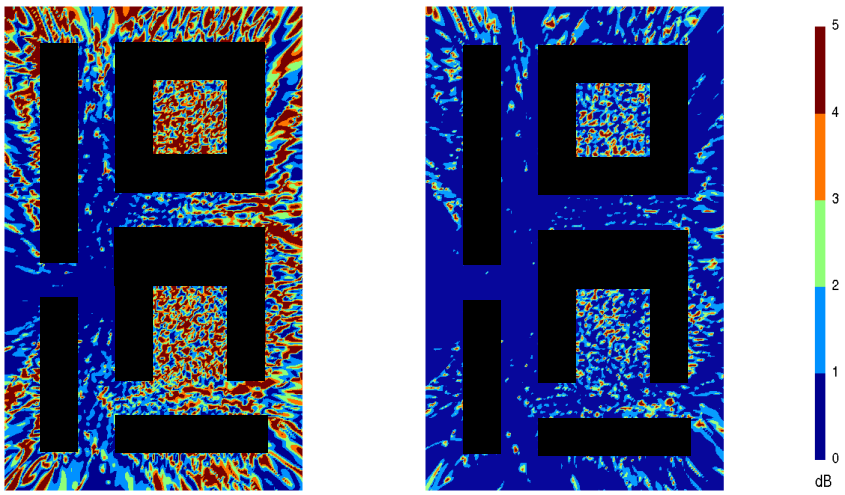

(a) residual = 1.10^{-1} (b) residual = 2.10^{-2}

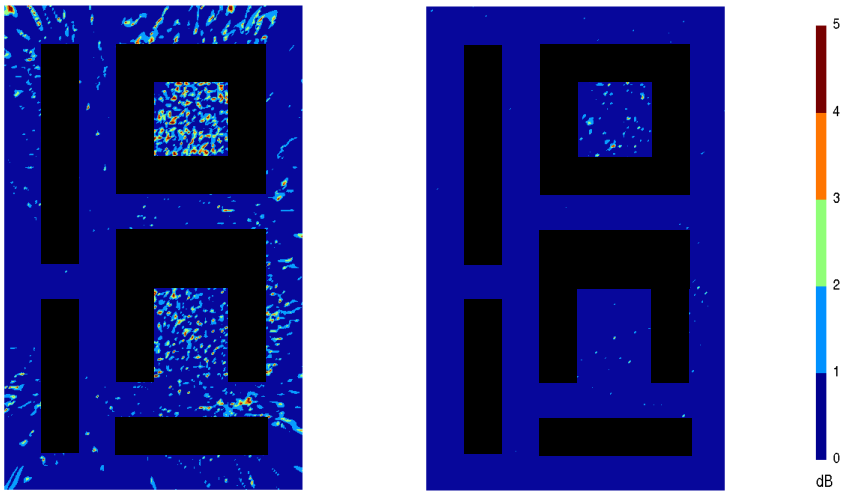

(d) residual = 1.10^{-2} (e) residual = 2.10^{-3}

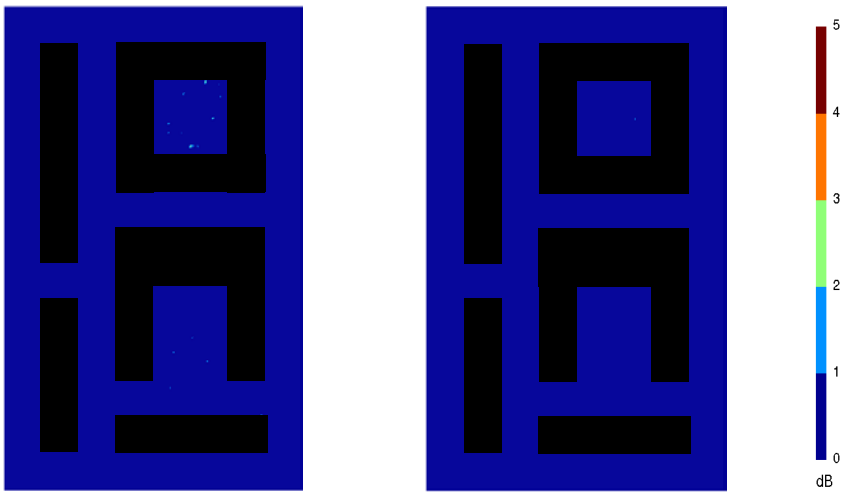

(g) residual = 1.10^{-3} (h) residual = 2.10^{-4}

FIGURE 5.9: *Influence of the relative residual on the solution on the receivers' map. Differences in dB on the receivers' map between several tested residuals and the reference* 1.10^{-4}.

5.2.4 Sound pressure level in the city block

In figure 5.10, the sound pressure level in dB (SPL) calculated on the receivers' map (total length: 70 m × 130 m, (i.e. $\approx 20\lambda \times 40\lambda$) for both variational BEM and the FMBEM algorithms is displayed. The reference pressure is $P_0 = 20\mu$ Pa. These two maps seem to be in good agreement. We provide, in table 5.1, only the details of the computing resources required by the FMBEM algorithm. Indeed, a comparison of the computing requirements between both algorithms would be meaningless since these computations have not been performed on the same computers and are not, furthermore, based on the same formalism. The benefit in terms of computation time brought by the fast multipole formalism will be specifically the topic of the next section.

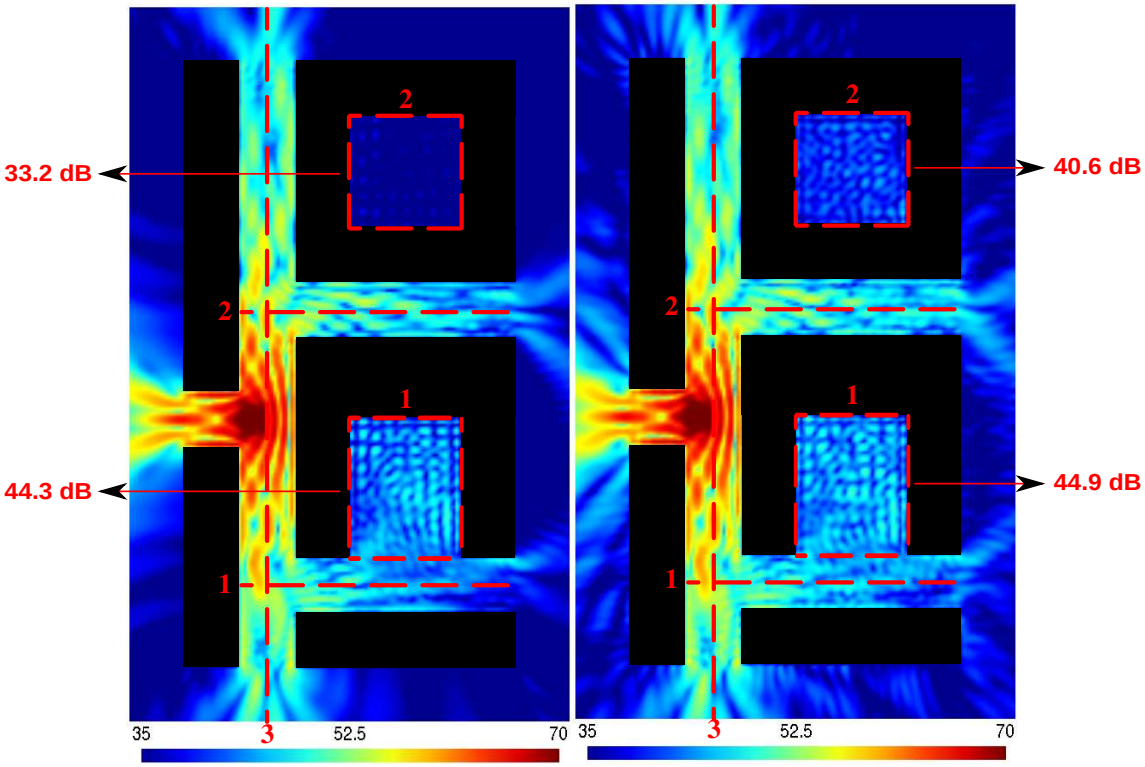

FIGURE 5.10: *Sound pressure level on the receivers' map computed with the Micado3D software (reference) on the left side and the FMBEM on the right side. The three receivers' lines and the two receivers' areas are displayed in red dotted lines.*

TABLE 5.1: *Computing resources related to the main computation stages for the FastBEM calculations for a frequency equal to 100 Hz.*

	Direct integrations		Translation matrices		Solver		Total	
	Time(s)	Mem(MB)	Time	Mem	Time	Mem	Time	Mem
Fast BEM (collocation)	84	510	136	806	1023	5171	1243	6487

It is noteworthy that the iterative solver appears to be the most expensive process in terms of computation time as well as for the required memory. We notice that no preconditioning has been used, thus a suitable preconditioner would reduce both computation time and memory storage.

In addition to these general results, we analyze more precisely the results for two sub-regions (two areas) of the map. We performed a logarithmic summation on receivers within the red dotted square (cf. figure 5.10) for the *area 1* (an opened court yard) and *area 2* (a closed court yard). The averaged sound pressure level calculated with the variational BEM and the FMBEM algorithm is 44.3 against 44.9 dB(SPL) in *area 1* respectively. In the *area 2*, the variational BEM calculates 33.2 dB(SPL), against 40.6 dB(SPL) with the FMBEM algorithm. This discrepancy is in fact mainly due to the truncated expansion order. The accuracy can nevertheless be improved with a stable recursive calculation of the translation matrices as it will be proven in the next chapter. It points out the fact that the computations in this area are very sensitive. Indeed, the pressure values only depend on the scattered field above the building and neither direct nor reflected field contribute.

We also compare, in figure 5.11, the sound pressure levels along the red dotted lines located in the middle of streets (cf. figure 5.10). There is a very good agreement on receivers under the influence of a direct contribution coming from the source (figure 5.11(c)) and an acceptable agreement in shaded areas (see figures 5.11(a) and 5.11(b)).

5.2.5 Computational resources

This section details more precisely the computational requirements needed to solve the previous studied case. We compare the computation times required with a standard collocation BEM algorithm with the one required through the Fast Multipole algorithm. We also show the requirements in terms of memory and finally focus on the improvement provided by parallelizing the process of direct interaction computations.

5.2.5.1 Computation time

We focus in this section on the computation times (CPU time) required by our FMBEM algorithm to solve the engineering problem of the sound propagation in the city block introduced in the previous section. In figure 5.12, we display the CPU time (blue line) obtained for each frequency between 30 and 100 Hz or as dimensionless values between 12 and 32 wavelengths. We use a meshing space criterion $\lambda/5$ (five elements per wavelength) for whole the frequency range involving around 7000 elements at a frequency of 30 Hz and around 78000 elements at 100 Hz. The cell-size criterion (*i.e.* the maximum number of elements allowed at the lowest level) is set to 100. We supply an overview in appendix D.1 of the space partitioning related to the 6^{th} level. Thus, when this cell-size criterion will be exceeded a supplementary level will be automatically added, decreasing the number of direct interactions.

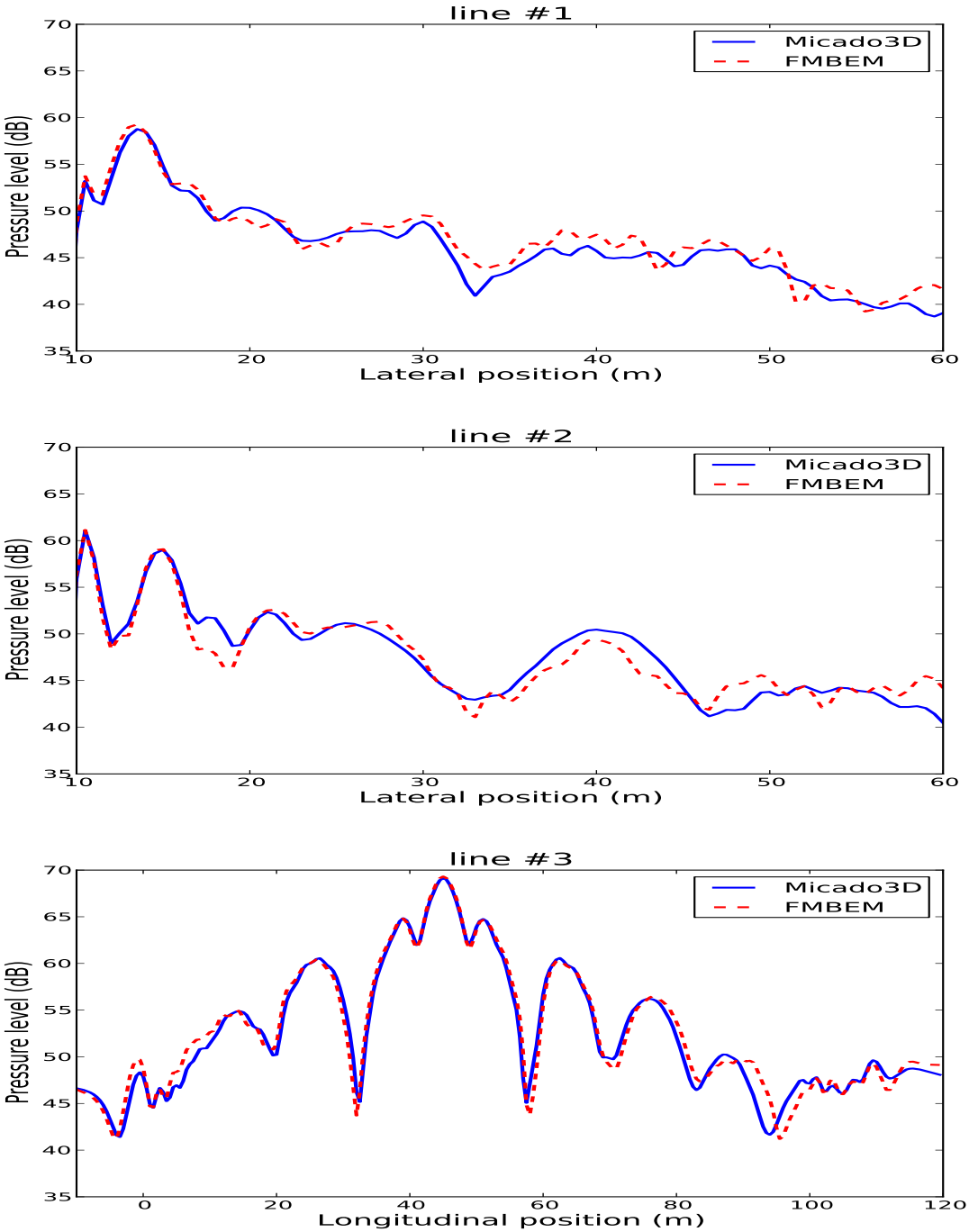

FIGURE 5.11: *Pressure level in dB taken along the 3 red dotted lines (cf. figure 5.10) with the variational BEM (reference) in blue lines and the FMBEM in red dotted lines.*

The benefit provided by an additional level, in terms of reduction of the CPU time, can be seen in figure 5.12. This reduction can be estimated to be around 33% of the total computation time. Besides, we can highlight the behavior of the computation time which seems to follow the theoretical law in $Nlog(N)$. For comparison, we also provide the CPU time required by the BEM to solve for this problem. We assume a standard boundary element algorithm and a matrix system solved with an iterative process. Thus the

CPU time is directly dictated by the time to compute and store the components of the matrix system. We notice that beyond almost 60000 elements, the CPU time seems to remain stable mainly due to the fact that the maximum allowed expansion order, to ensure stable recursive properties of rotation operators, is reached and kept constant beyond. However, a stable recursive computation process, recently introduced by Gumerov & al., allows to deal with higher expansion orders which are limited in this study to 98. We can also highlight a fluctuating CPU time according to the number of iterations required for solving the problem. Indeed the convergence of the iterative solver is closely related to the frequency. A method to tackle this drawback could be the use of a preconditioner. Indeed, both the efficiency and robustness of iterative techniques can be improved by using a preconditioner [Chaillat 2012]. Several options in the case of the GMRES are available (see chapter 9 in [Saad 2003]).

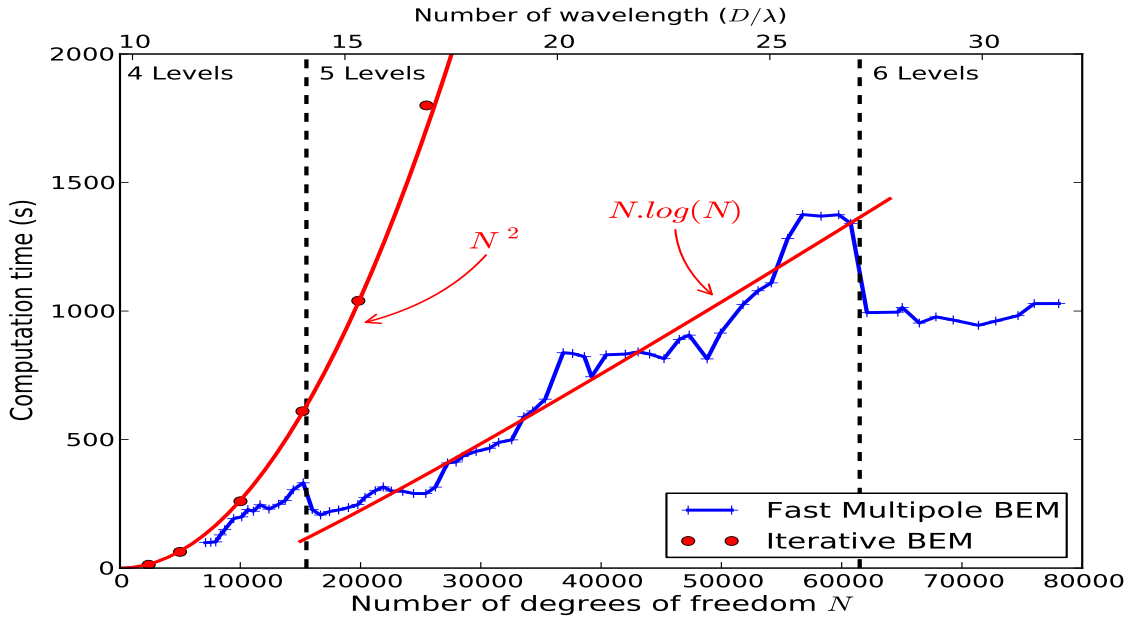

Figure 5.12: *Computation times required for the FMBEM algorithm in blue line and for the classical BEM in red points in terms of the number of elements with a space discretization of $\lambda/5$, D is equal to 110 m. Theoretical laws are displayed as red lines.*

As a conclusion on the results of the application of a FMBEM algorithm to a sound propagation problem in the city block, we can say that the fast multipole algorithm provides substantial benefits regarding the computational time compared to a standard BEM approach and becomes an essential optimization technique to calculate noise maps as the scale (frequency or dimension) of the model increases.

5.2.5.2 Memory storage

According to the previous section related to the benefits in terms of computation time, we now focus on the benefits regarding the memory storage required. This study is still carried out in a range of frequencies between 30 and 100 Hz or in terms of dimensionless values between 12 and 32 wavelengths. The cell-size

as well as the meshing space criteria are still set to 100 and $\lambda/5$ respectively. From a numerical point of view, the most consuming steps, regarding the memory storage in the fast multipole formalism, are the storage of direct contributions coming from *near areas*, the construction of the translation operators used for the contributions coming from *interaction list cells*, and the storage of Krylov's subspaces used by the iterative solver. We display in figure 5.13 the total memory (blue line) used by the algorithm including the required memory to store the direct contributions (red line), the translation operators (green line) and the Krylov's subspaces used by the iterative solver (cyan line). We also mention the memory used by the BEM for solving this problem. We assume a standard unsymmetrical boundary element formalism and a matrix system solved with an iterative process. Thus, the memory storage is mainly used to store the components of the matrix system.

We can highlight a fluctuating memory storage required by the iterative solver directly dictated by the number of iterations. The memory needed, with the increase of the frequency to store the direct interactions, is dictated by a quadratic law, in agreement with the boundary element formalism, while the memory required to set the translation operators seems to follow a linear law.

So, we have seen that the fast multipole formalism brought significant benefits regarding the required memory storage. The memory related to the direct interactions can be controlled through the number of levels. The weak point seems to appear in the use of an iterative solver as a "black box" and a suitable preconditioner seems to be recommended to avoid the close dependency with the frequency and thus the fluctuating number of iterations.

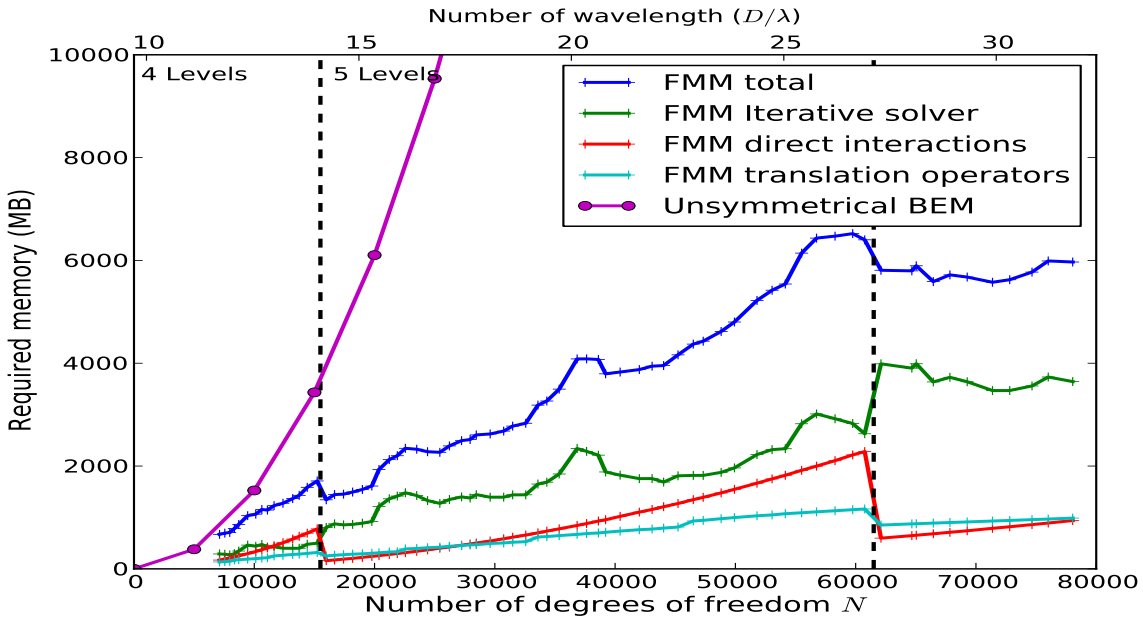

FIGURE 5.13: *Total memory storage required for the FMBEM algorithm (blue line) in terms of the number of elements. We also mention the memory allocated for the iterative solver (green line), for the direct contributions (red line) and for the translation matrices. For comparison, the memory storage required for a classical BEM using an unsymmetrical collocation formalism is also mentioned in purple. D is equal to 110 m.*

5.2.5.3 Benefit of multi-cores parallelization

All the fast multipole calculations performed in this manuscript have been realized without parallelization procedures on a desktop PC with a single Intel Xeon® X5675 processor at 3.07 GHz and 12 GB memory storage. However, the fast multipole method allows the parallelization of many process that can be realized simultaneously [Sylvand 2002]. With increasing power of computation clusters, it seems interesting to assess the benefits of the fast multipole algorithm through a parallelization procedure. Indeed, even if a suitable and efficient implementation of a parallel algorithm is not trivial because of the complicated structure of this algorithm, it can nevertheless dramatically improve its performances. A very detailed discussion can be found in the electromagnetic waves domain in [Ergül 2008] and [Ergül 2009]. The two most consuming steps, regarding the CPU time, are the computation of direct contributions coming from the *near areas* and the time required to solve the matrix system through the iterative solver. We propose, here, to assess the benefit of a parallelization procedure carried only on the computation of the direct interactions. Indeed, this step includes independent computations and does not require exchanges between the cores, which is suitable for parallel calculations. This parallelization is realized thanks to the OpenMP (Open Multi-Processing) library, enabling the creation of shared-memory parallel programs. The benefits provided by a parallelization procedure carrying out on the direct interactions can be seen in figure 5.14. We represent, in solid lines, the total CPU time and, in dotted lines, the CPU time allocated for the calculations of direct contributions. The colors represent the number of cores used to perform the calculations *i.e.* 1, 2 and 6 (the maximum number of physical cores available) in blue, red and green lines respectively. We provide, in complement (appendix E.1), the evolution of the gain factor with respect to the number of cores which the parallelization is carried out on. We note that the parallelization process has also been implemented for the calculation of the sound pressure level on the receivers' map.

Thus, we can observe a decrease of the CPU time according to the number of cores available to perform the calculations. This parallelization has been realized on the direct interactions which are independent calculations and then can be handled using the OpenMP library, a shared memory library which does not require deep knowledge in parallel programming.

5.3 Consequence of unstable recursive computations

Previous calculations in the case of sound propagation in the city block have been realized with a truncated expansion order $p_{max} = 98$, to ensure stable properties of the recursive process. This truncated expansion order allowed to perform calculations up to a non-dimensional domain size equal to almost 32 wavelengths with a satisfactory accuracy except in the closed court yard. We explain in this section the reasons of such a choice regarding the truncated expansion order and the impact on the convergence (in section 5.3.1) as well as on the loss of accuracy on the solution vector (in section 5.3.2) if the expansion order is not limited. We finally discuss (in section 5.3.3) a stabilized recursive calculation to compute rotational matrices coefficients which will be the topic of the following chapter.

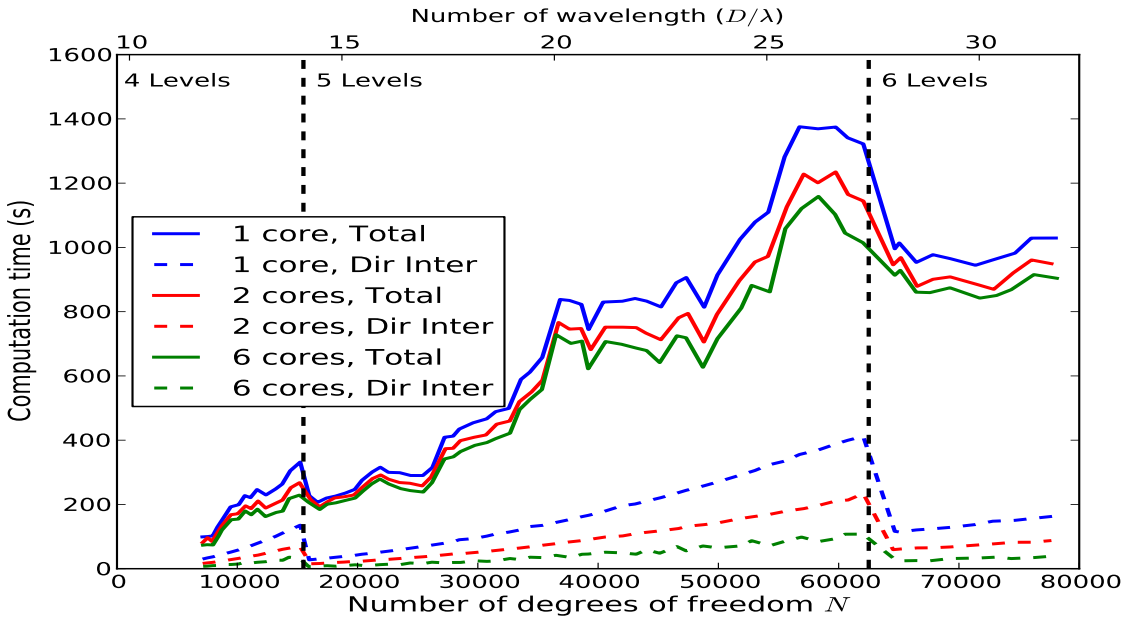

FIGURE 5.14: *Total CPU time required (solid lines) and CPU time allocated to calculate the direct interactions (dotted lines) in terms of the number of cores used to perform the calculations. D is equal to 110 m.*

5.3.1 Influence on the convergence of the solver

Consistently with the previous studied frequency range in the case of the sound propagation in the city block, we investigate in this section the behavior of the iterative solver with the unstable recursive scheme without limiting the maximum value of the expansion order p. In figure 5.15, one can see the number of iterations required to converge below the relative residual error 10^{-2} with the non truncated expansion order (red line) and with the truncated expansion order $p_{max} = 98$ which has been used so far. Differences in terms of the number of iterations occur starting from around 85 Hz, when the truncated expansion order is reached and an increased number of iterations is observed beyond 90 Hz leading to a very slow convergence of the solver around 100 Hz. This slow convergence justifies the choice of a truncated expansion order in the previous section since it nevertheless allows to keep an acceptable reliability on the receivers' map except in the more sensitive areas as in the close court yard.

5.3.2 Impact on the accuracy of the solution

As it has been previously emphasized in the previous section, instabilities in the recursive process lead to a difficult convergence of the iterative solver if the expansion order is not limited. The consequence of the numerical instability can also be emphasized by considering the sound presure level on the mesh. Indeed, as shown in figure 5.16 in red dotted circles, this generates a non physical solution on the surface pressure field and one can see discontinuities between two adjacent cells appearing. This discontinuity will obviously have an influence on the solution on a receiver map and an accurate solution will not be

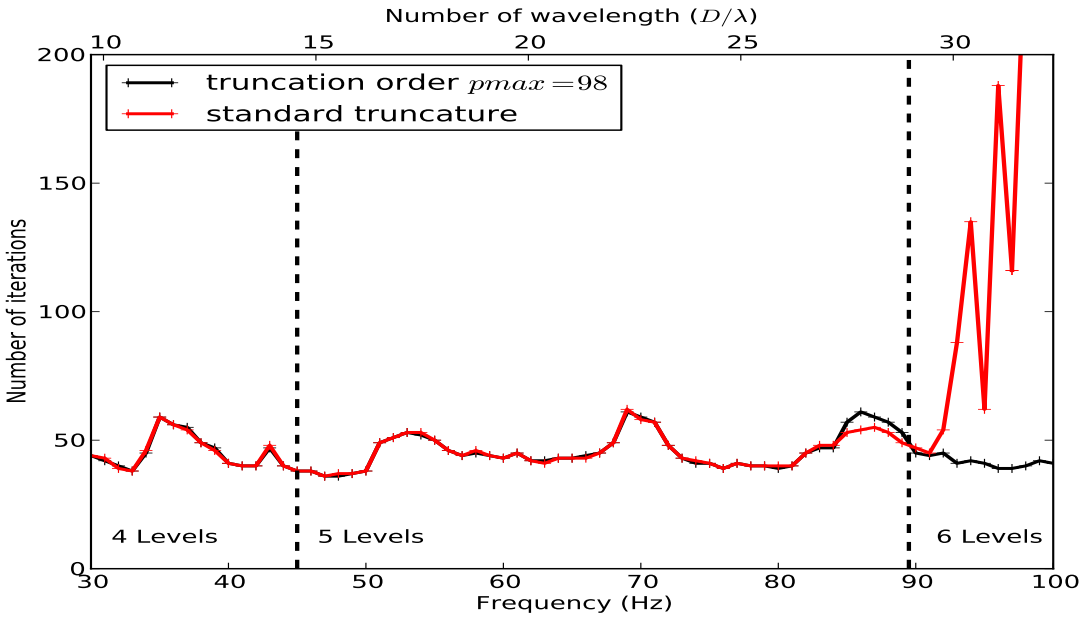

FIGURE 5.15: *Number of iterations to converge below the relative residual* 10^{-2} *with a truncated expansion order (black line) and with a non truncated expansion order previously defined (red line).*

guaranteed, specifically in the more sensitive area. This loss of accuracy has already led to discrepancies between our reference software *Micado3D* and the solution computed with the fast multipole algorithm in the closed court yard (see figure 5.10). Thus a stable recursive scheme is required to ensure reliable solution in a higher frequency range.

5.3.3 Improvement of the stability of recursive calculations

As a conclusion, it seems that our algorithm, and more generally algorithms based on the RCR decomposition, suffer from numerical instabilities for expansion orders up to a hundred, involving numerical inaccuracies, resulting in pressure field discontinuities between two adjacent cells. Indeed, it appears that the recursive process for the computation of rotation coefficients in the RCR decomposition becomes unstable for large p (around a hundred) if implemented without specific care. Thus, these recursive calculations have to be handled with care and a stable process is required to ensure stable recursion properties as described in [Gimbutas 2009]. GUMEROV & al. provide an improved process in [Gumerov 2012], which they found to be stable even for large p (several thousands) [Gumerov 2014]. This stable recursive computation has been recently implemented successfully in our algorithm and allows to deal with larger scale models. A study using a stable recursive process applied to urban acoustic propagation will be the purpose of the upcoming chapter. There also exists several publications devoted to the combination of the fast multipole formalism with other methods such as the Source Clustering Method (SCM) [Burgschweiger 2013] or the Fast Directional Algorithm (FDA) [Engquist 2007] which allow to deal with slightly larger scale models [Cao 2013] but are beyond the scope of the fast multipole method. The following chapter will be dedicated

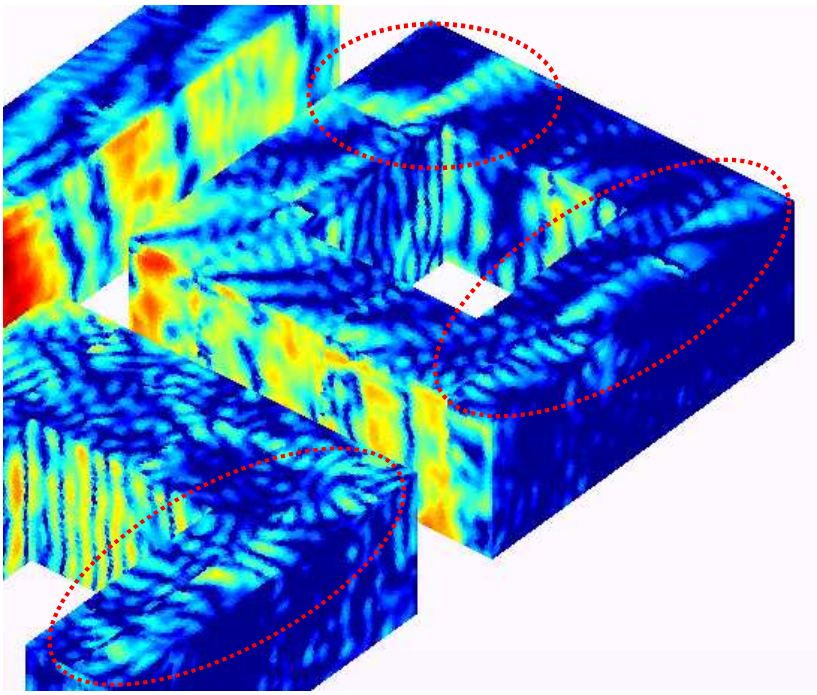

FIGURE 5.16: *Influence of unstable recursive scheme on the solution. Discontinuity of pressure field appears between two adjacent cells.*

to an explanation and application of a stable process to compute the rotational matrix coefficients required to perform the translations through the RCR decomposition.

5.4 Discussion about the current limitations

We investigated, throughout this chapter, the behavior of the fast multipole method applied to the boundary element method to deal with acoustic propagation problems for realistic urban geometries. It results that the fast multipole algorithm provides substantial benefits regarding the computation time as well as in terms of memory when compared to a standard BEM approach while keeping a sufficient accuracy to calculate noise maps and becomes an essential optimization as the scale (frequency or dimension) of the model increases. A parallelization process of the calculations of direct contributions has shown benefits, with respect to the number of calculation cores, in terms of computation times. Because of the very large cost in terms of memory requirement for the storage of Krylov subspaces for a large number of iterations, an appropriate preconditioner seems to be recommended but this point has not been investigated in the framework of this thesis. Thus the fast multipole formalism allowed us, so far, to perform calculations on domain sizes up to around 32 wavelengths.

However, from a numerical point of view, due to the high level of computational complexity of fast multipole algorithms, the recursive calculations must be handled with care, as for instance, the recursive computations of rotational matrices entries which should not be performed carelessly. Indeed, the recursive

process for the computation of rotation coefficients in the RCR decomposition formalism becomes unstable for large expansion orders (i.e. a hundred). A stable recursive scheme to compute the components of the rotational matrices required in the framework of the RCR decomposition has recently been the subject of Gumerov's & al. work [Gumerov 2014]. This stable recursive scheme has been successfully implemented in our fast multipole algorithm and allows to deal with larger scale models which will be the purpose of the next chapter.

Chapter 6

Stable recursive computation of translation matrices

The previous chapter was dedicated to the application of the fast multipole boundary element method on realistic geometries. These applications allowed us to bring into light some computational instabilities which restrict the current version of the algorithm to problems of maximum dimensionless domain sizes up to around 32 wavelengths. These numerical instabilities already highlighted by Gumerov & Duraiswamy [Gumerov 2012], result in a discontinuity of the sound pressure field between adjacent cells for expansion orders above around one hundred. The very recent Gumerov & Duraiswamy's research shows that this limitation comes actually from numerical instabilities if the recursive process of the computation of the rotational matrices entries is performed carelessly [Gumerov 2014]. To tackle this limitation, they proposed a recursive algorithm denoted as "fast and stable", based on an analysis of the Courant-Friedrichs-Lewy (CFL) criterion, tested for the computation of rotational matrix entries up to orders $p = 10^4$ [Gumerov 2014].

In the present chapter, we detail how a "fast and stable" recursive scheme can be guaranteed for the computation of the rotational matrix entries of large expansion orders (i.e. $p > 100$), which is numerically more "stable" than the one used in the previous chapters. This study is based on very recent Gumerov & Duraiswamy's research [Gumerov 2014]. We first detail (in section 6.1) the numerical implementation which allows us to ensure "stable" recursion properties in the computation of the rotational matrices entries. Then we apply this improved version of the algorithm on the previous case of the sound propagation in the city block and deal with higher frequency problems than it has been discussed in the previous chapter (see section 6.2). Finally, we try to emphasize the new limitation of the algorithm through multi scattering problems by cubic scatterers (section 6.3).

6.1 Stable recursion for large expansion orders

The recursive process which we use in this chapter comes from Gumerov & Duraiswamy's research [Gumerov 2014]. We describe how stable computations of the rotational matrices coefficients $H_n^{m',m}$ can be guaranteed. Analysis of the Courant-Friedrichs-Lewy (CFL) condition shows that, if the recursion is performed from $H_n^{m',m}$ to $H_n^{m',m+1}$, then the recursion will be absolutely unstable while the computation from $H_n^{m',m}$ value to $H_n^{m'+1,m}$ satisfies the necessary CFL stability condition. We however point out that some care may be needed for negative values of m' near the value $m = 0$. Figure 6.1 shows the "stable" and "unstable" directions of propagation of the absolute errors. By "stable" Gumerov & Duraiswamy mean that this recursive scheme leads to an absolute error equal to 10^2 above the numerical precision for expansion orders up to $p = 10^4$. This corresponds to an error equal to 10^{-13} when a numerical double precision is used to store the numerical data which is an acceptable accuracy for many practical problems.

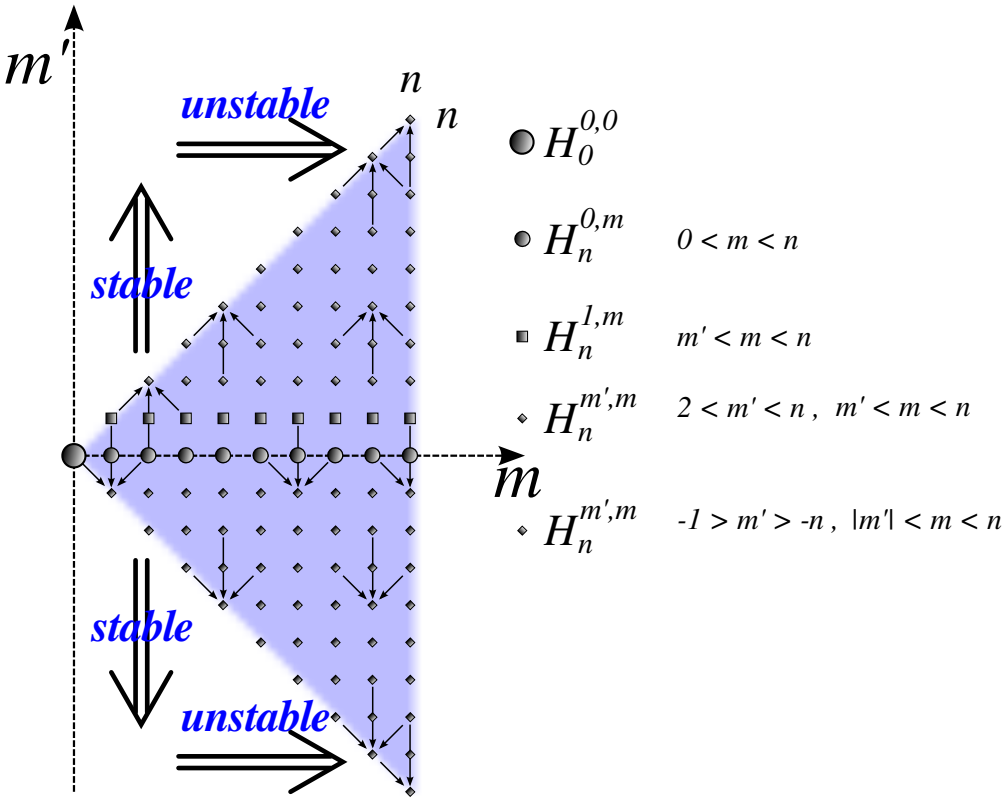

Figure 6.1: *Stable recursive process for the construction of rotational matrices. An order $n = 10^4$ leads to an absolute error of 10^2 above the numerical precision.*

Thus, the rotational matrices entries must be handled towards the high values of m' for $m' > 0$ and towards the low values of m' for $m' < 0$ since an important error growth occurs when the recursive relation is applied horizontally i.e. towards the increasing values of $m > 0$. We explicit below all the steps required to perform the "stable" recursive process of the rotational matrices coefficients in the sense of the CFL criterion.

1st step: Computation of $H_0^{0,0}$

The recursive process starts with the value for an arbitrary rotational angle β:

$$H_0^{0,0}(\beta) = 1, \qquad \text{for } n = m' = m = 0. \tag{6.1}$$

2nd step: Computation of $H_n^{0,m}$

For the other values of n ($n \neq 0$), we compute $H_n^{0,m}$ for $0 < m \leq n$ up to the order $n = p_{max} + 1$ thanks to a stable standard routine for computing the normalized associated Legendre functions P_n^m, usually based on the recursion:

$$H_n^{0,m}(\beta) = (-1)^m \sqrt{\frac{(n-|m|)!}{(n+|m|)!}} P_n^{|m|}(\cos\beta), \qquad \text{for } 0 < m \leq n, 1 \leq n \leq p_{max}+1. \tag{6.2}$$

3rd step: Computation of $H_n^{1,m}$

Use the following recursive relation, in which the values n up to $p_{max} + 1$ are required, to compute the $H_n^{1,m}$ values for $1 \leq m \leq n$:

$$H_n^{1,m}(\beta) = \frac{1}{b_{n+1}^0}\left\{\frac{1}{2}\left[b_{n+1}^{-m-1}(1-\cos\beta) H_{n+1}^{0,m+1} - b_{n+1}^{m-1}(1\cos\beta) H_{n+1}^{0,m-1}\right] - a_n^m \sin(\beta) H_{n+1}^{0,m}\right\}, \tag{6.3}$$

$$\text{for } 1 \leq n \leq p_{max}, \qquad \text{and } 1 \leq m \leq n.$$

with the values of coefficients a and b consistent with definitions (3.15) and (3.17) respectively.

4th step: Computation of $H_n^{m'>1,m}$

Recursively compute $H_n^{m'+1,m}$ using the following relation for $1 \leq m' \leq n-1$ and $m' \leq m \leq n$:

$$H_n^{m'+1,m} = \frac{1}{d_n^{m'}}\left\{d_n^{m'-1} H_n^{m'-1,m} - d_n^{m-1} H_n^{m',m-1} + d_n^m H_n^{m',m+1}\right\} \tag{6.4}$$

according to the definition of d_n^m:

$$d_n^m = \frac{\text{sgn}(m)}{2}\left[(n-m)(n+m+1)\right]^{1/2}.$$

We note that $d_n^n = 0$.

5th step: Computation of $H_n^{m'<0,m}$

In a similar way, recursively compute $H_n^{m'-1,m}$ coefficients for $0 \leq m' \leq -n+1$ and $1 \leq m \leq n$:

$$H_n^{m'-1,m} = \frac{1}{d_n^{m'-1}}\left\{d_n^{m'} H_n^{m'+1,m} + d_n^{m-1} H_n^{m',m-1} - d_n^m H_n^{m',m+1}\right\} \tag{6.5}$$

with the previous definition of coefficients d.

6th step: Symmetry properties

At this point of the recursive process all the coefficients in the gray area (see figure 6.1) are computed and stored. The other coefficients $-n \leq m' \leq n$ and $-n \leq m \leq n$ are computed using the following symmetry properties of rotational matrices:

$$H_n^{m',m} = H_n^{m,m'} \qquad \text{and} \qquad H_n^{m',m} = H_n^{-m',-m} \tag{6.6}$$

Thus at the end of this step, all the $H_n^{m',m}$ entries are known for all values $-n \leq m' \leq n$ and $-n \leq m \leq n$. We see in the next section the benefits provided by this recursive computation in the case of sound propagation in the city block .

6.2 Improvements in the case of the sound propagation in the city block

The improved recursive process described in the previous section is applied to the sound propagation in the city block studied in the section 5.2. The previous calculations were carried out with a truncated expansion order ($p_{max} = 98$) to ensure stability of the computation of rotational matrices entries. One has also seen that higher expansion orders involved, when the recursive process is computed carelessly, sound pressure discontinuities on the mesh between two adjacent *cells*. In figure 6.2, we compare the solution on the mesh previously computed with the unstable recursive scheme (left hand side) with the solution on the mesh computed with the new "stable" recursive scheme (right hand side). This comparison highlights the improvement provided by such an implementation on the solution computed on the mesh. Thus it seems that this recursive "stable" process has been implemented successfully in the fast multipole algorithm.

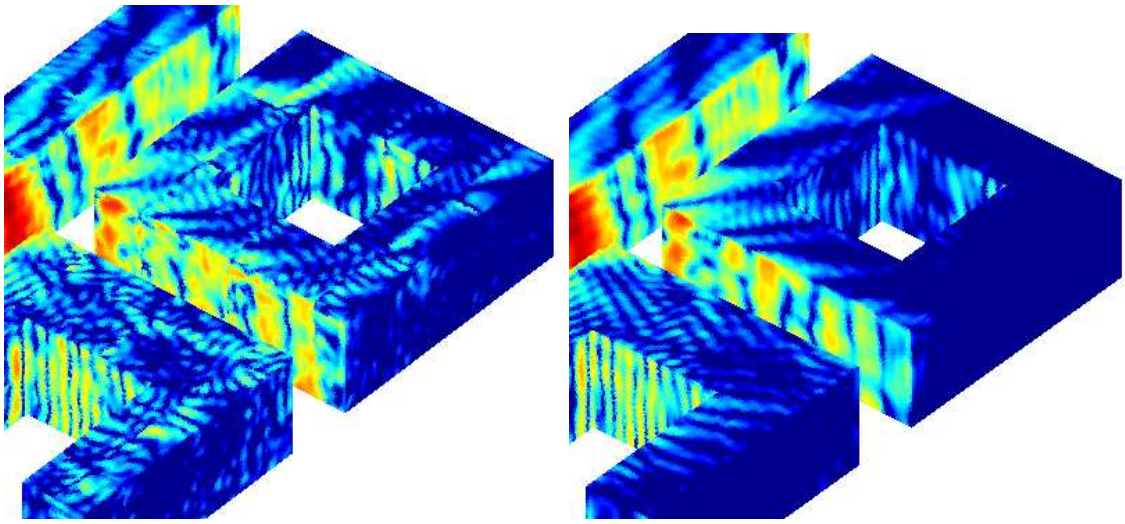

(a) with the unstable recursive scheme (b) with the stable recursive scheme

FIGURE 6.2: *A part of the solution on the mesh computed with (a) the unstable recursive scheme and (b) the stable recursive scheme.*

Thus it seems that the problems emphasized in the previous chapter (see figure 5.16) of sound pressure discontinuities between two adjacent *cells* disappear, resulting in a "more physical" solution of the sound pressure level (see figure 6.2). Furthermore, one can also see that this implementation seems to provide a more reliable sound pressure level on the mesh in the very sensitive areas as for instance within the court yards 1 and 2 (areas in red dotted line in figure 6.3). This observation is confirmed by computing the averaged sound pressure levels within the court yards (see figure 6.3) obtained from the logarithmic summation of the contribution of frequencies between 90 - 100 Hz (1 Hz step). Indeed we notice a reduction of 4.7 dB in the closed court yard while a decrease of 0.6 dB is observed in the opened court yard. With the "stable" recursive technique, the discrepancies with the reference *Micado3D* software are of 0.0 dB and 2.7 dB in the opened and closed court yards respectively.

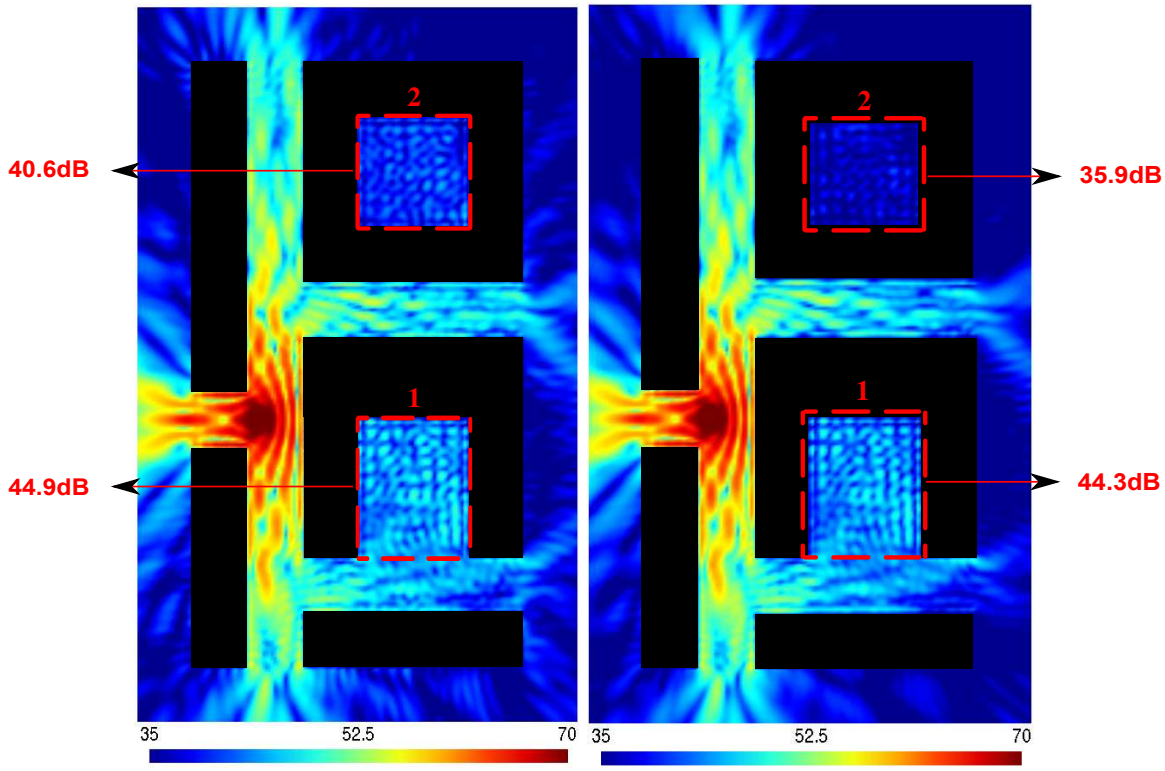

(a) with the unstable recursive scheme (b) with the stable recursive scheme

FIGURE 6.3: *Logarithmic summation of the sound pressure level on the receivers' map computed between 90 - 100 Hz (1 Hz step) with the unstable recursive scheme (same as in the previous section) on the left side and with the "stable" scheme on the right side.*

We can also assess the influence of the "stable" recursive computation on the number of iterations required to solve this sound propagation problem starting from a dimensionless domain size equal to 9.7λ (30 Hz). We set the iterative solver relative residual to 10^{-2} and compare, in figure 6.4, the number of iterations required with the unstable recursive scheme without truncating the expansion order with the number of iterations required with the "stable" scheme. The discrepancies between the unstable (red line) and the stable (blue line) recursive schemes appear above an expansion order around a hundred. While the unstable scheme leads to a non converging solution starting from $\approx 30\lambda$ (i.e. 98 - 99 Hz), leading to

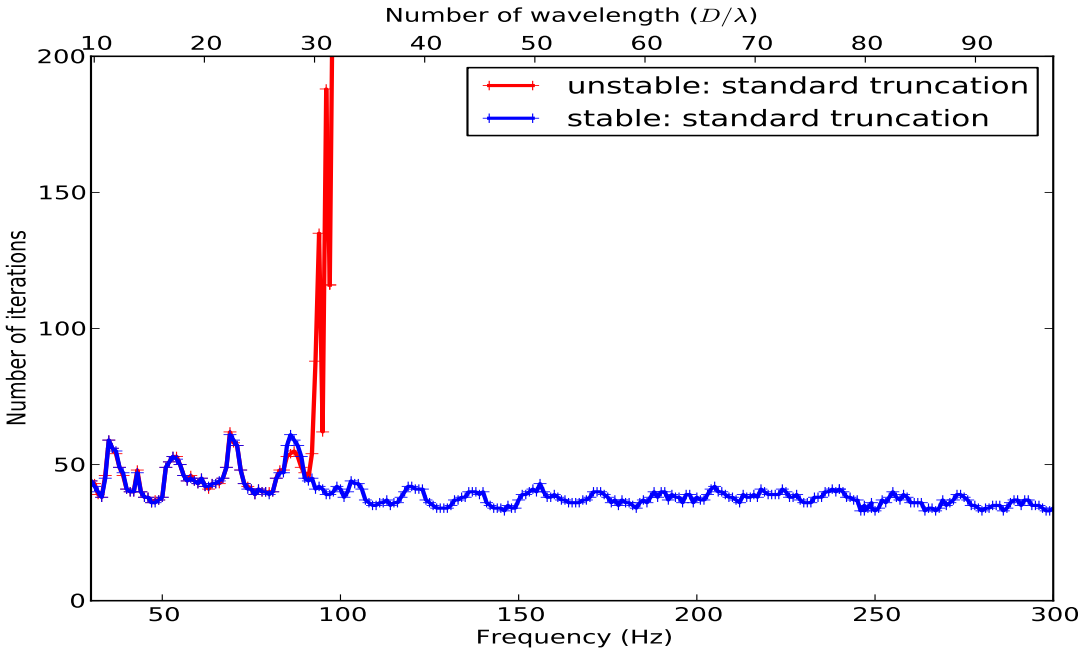

FIGURE 6.4: *Number of iterations required with the unstable recursive scheme (red line) and the stable recursive scheme (blue line) in terms of frequency.*

an inefficient convergence of the iterative solver at higher frequency, the "stable" scheme shows a steady number of iterations as frequency increases. As a conclusion, the analysis of the sound pressure levels on the receivers' map on one hand and the analysis of the behavior of the convergence of the iterative solver on the other hand seem to indicate a successful implementation of the "stable" recursive process and an efficiency of this latter scheme to tackle instabilities in the recursive calculation of rotational matrices coefficients. The calculations have been performed up to a dimensionless domain size value around 100 wavelengths due to memory limitations. Indeed for a calculation performed at around 100λ (i.e. 300 Hz), GMRES requires around 26 GB to store the Krylov's subspaces for 36 iterative steps. This result emphasizes once again the interest of a suitable preconditioner to deal with well conditioned matrix systems which can reduce the number of iterative steps, hence reducing the computation time and, at the same time, the memory storage. In the next section, we focus on a multi scattering problem by cubic bodies. The main idea is to deal with well conditioned problems to decrease the number of iterative steps and circumvent the problem of the prohibitive memory required by the iterative solver.

6.3 The new limitations of the algorithm: A multi scattering problem

The main idea of this section is to deal with problems which require a low number of iterations as well as to avoid the fictitious eigenfrequency problem. It allows us to focus only on problems related to expansion orders. Figure 6.5 provides a schematic overview in two dimensions of the studied geometry. It concerns a multi scattering problem by cubic scatterers distributed according to a square frame. The main geometrical

parameters are the length of the cubic scatterers 0.35λ, the distance between two successive scatterers $d\lambda$ and the maximal length of the problem $n\lambda$. All the computations are performed at the same frequency of 60 Hz (i.e. $\lambda = 5.67$ m), chosen to avoid the fictitious eigenfrequency problem allowing to solve for the problem only with the CBIE formulation ($\eta = 0.0$ in the CHBIE formulation). The first studied network is a square network and the second one a rectangular network used to increase the larger dimension of the problem $n\lambda$ while keeping a low number of elements allowing comparisons with the reference BEM algorithm *Micado3D*. Indeed the largest dimension of the problem will determine the highest expansion order in the framework of the fast multipole formalism. We note the symmetric properties of the geometry, for a point source located at the center of the network, which will be taken into account in our reference calculation while the whole geometry will be handled by the FMBEM algorithm, although planes of symmetry could nevertheless be considered.

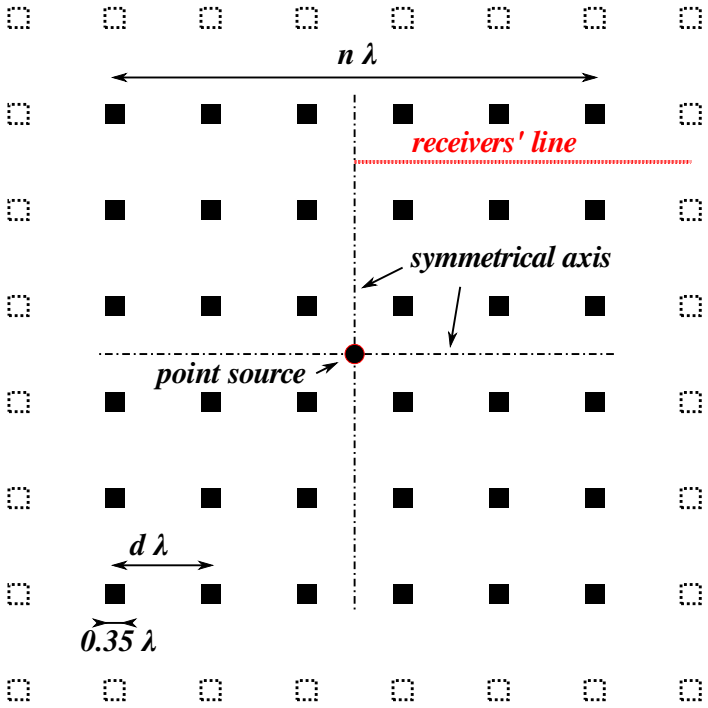

FIGURE 6.5: *Sketch of a part of the array used to bring into light the limitation of the new FMM algorithm. All the geometrical values depend on the wavelength at 60 Hz, $\lambda = 5.67$m.*

6.3.1 Bi-dimensional array of cubic scatterers: square frame

The mesh used to perform calculations is displayed in figure 6.6. It consists in 30×30 cubic scatterers for a total length equal to 300 m $\times$ 300 m. The studied geometry in this section has the following dimensionless parameters for calculations performed at 60 Hz ($\lambda = 5.67$ m): length of cubic scatterers of 0.35λ, $d = 1.75$ and $n = 52$. The infinite rigid baffle is used to take into account the reflections on the ground. We compare the sound pressure level taken along the red receivers' line. The location of the point source (black point) involves two planes of symmetry which are taken into account to reduce the computing requirements of the

reference BEM algorithm, *Micado3D*, while the whole geometry, involving 621000 elements, is handled by the FMBEM algorithm.

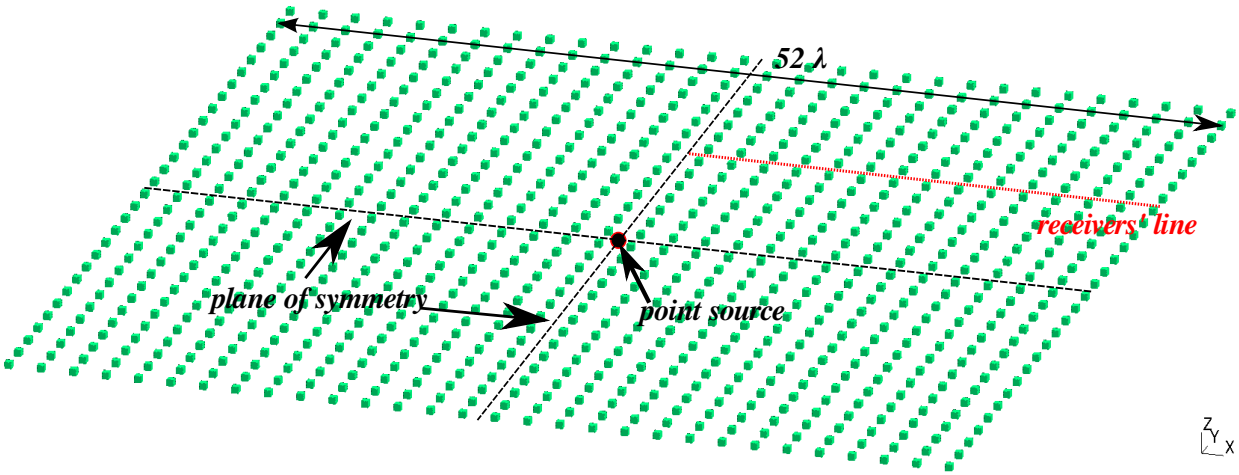

FIGURE 6.6: *Overview of the mesh (in green) of the multi scattering problem in the squared array made of* 30 × 30 *cubes of basis* 2*m* × 2*m, consisting each of 690 elements, for a total of 621000 elements. The planes of symmetry which are used in the BEM calculation are displayed in dashed black lines. The red dotted line indicates the receivers.*

The pressure level in dB (p_{ref} = 1 Pa) taken along the receivers' line (red dotted line in figure 6.6) is displayed in figure 6.7. We compare the solution computed by the *Micado3D* software (blue line) and the fast multipole algorithm (red line). We observe a very good agreement between the reference algorithm *Micado3D* and the FMBEM algorithm. We also provide in table 6.1 the expansion orders used with respect to the *level* in the *hierarchical tree*. We denote that this mesh is the biggest we have considered in the framework of this PhD thesis (621000 elements). Regarding the computing resources, the FMBEM algorithm solved this problem in about 20 minutes for 14 iterative steps and around 13 GB of memory has been required. If we had solved this problem with a classical collocation BEM algorithm, the calculation would have required almost 250 hours with an iterative solver and 6200 GB to store the matrix system (estimation) unavailable nowadays on classical workstations. It highlights the interest of the fast multipole method when few iterative steps are required.

TABLE 6.1: *Cubic frame: Expansion orders with respect to level for a hierarchical tree consisting of 8 active levels and number of iterations for a dimensionless domain size equal to* 52*λ.*

level #	2	3	4	5	6	7	8	9	iterations
expansion order	214	116	66	38	22	14	10	8	14

6.3.2 Bi-dimensional array of cubic scatterers: rectangular frame

Since the largest dimension of the problem determines the maximum expansion order of kernels on the spherical basis series, we chose now to deal with a rectangular frame. We wanted to reduce the number

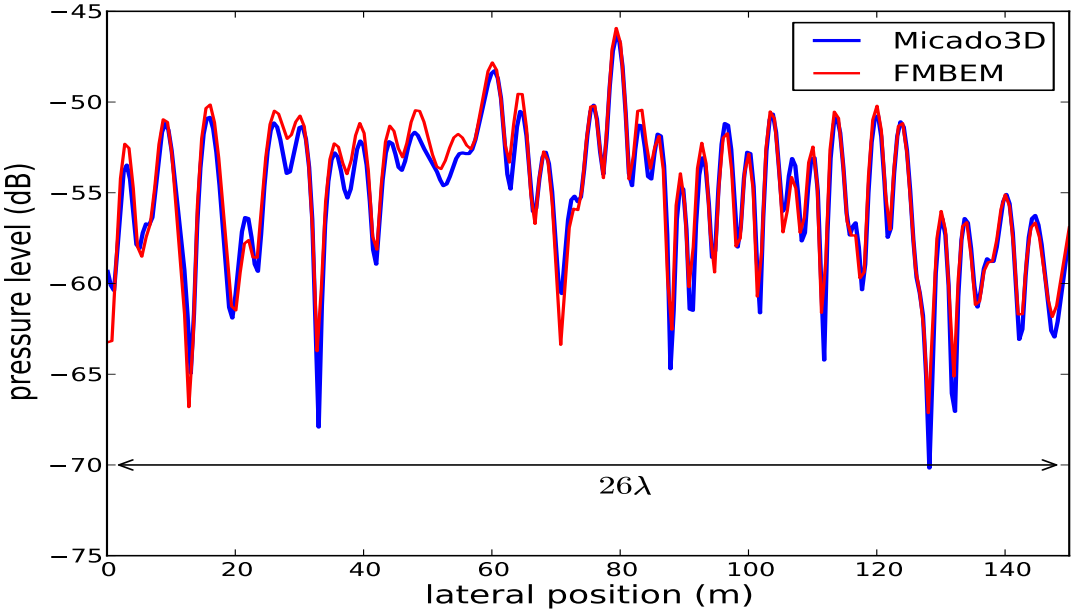

FIGURE 6.7: *Sound pressure level in dB along the receivers' line within the squared array computed with Micado3D software (blue line) and the FMM algorithm red line. The reference pressure level is* $p_{ref} = 1Pa$ *for a unit source amplitude.*

of elements and to keep *Micado3D* as the reference algorithm while increasing the problem dimensions $n\lambda$ and so the maximum expansion order. The mesh used to perform calculations is displayed in figure 6.8. It contains 40×20 cubic scatterers of a size of 0.35 λ and 5.25 λ apart for a studied frequency equal to 60 Hz ($\lambda = 5.67m$). This problem has a total length of 207 λ or 1200 m. The infinite rigid baffle is used to deal with a half space problem. We compare the sound pressure levels taken along the red receivers' line shown in figure 6.8. The location of the point source (black point) involves two planes of symmetry which are taken into account by the reference BEM algorithm *Micado3D* thus reducing the computing requirements while the whole geometry is considered (without planes of symmetry) by the FMBEM algorithm involving around 108000 elements.

The pressure level in dB ($p_{ref} = 1$ Pa), taken along the receivers' line, is compared in figure 6.9. The comparison is performed between the reference algorithm *Micado3D* (blue line) and the fast multipole algorithm (red line). We observe a very good agreement between both computations. The computing requirements by the FMBEM algorithm are 25 minutes to solve the matrix system and around 12 GB of memory. We also provide in table 6.2 the expansion orders used with respect to the *level* in the *hierarchical tree*. We note that this calculation is the highest we performed successfully during this PhD thesis in terms of expansion orders up to $p_{max} = 726$.

An additional calculation has been performed for a larger scale model for a dimensionless domain size equal to 275λ. This geometry is obtained with the following geometrical parameters, previously defined: length of the cubic scatterers 0.35λ, the distance between two successive scatterers is 7λ and the maximum

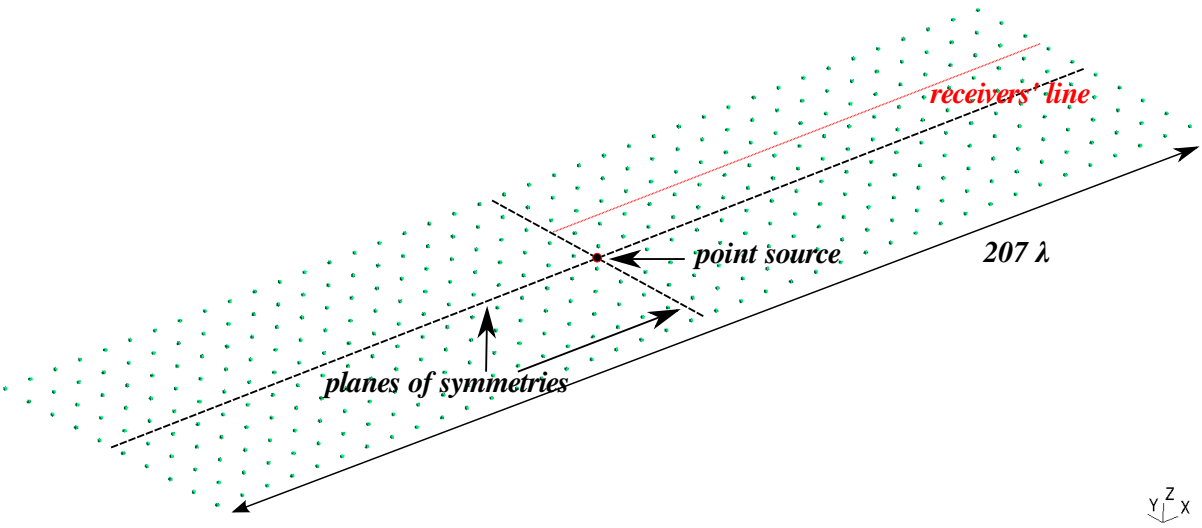

FIGURE 6.8: *Overview of the mesh (in green) of the multi scattering problem in the rectangular array made of* 40×10 *cubes of basis* $2m \times 2m$ *consisting each of 270 elements, for a total of 108000 elements. The planes of symmetry which are used in the BEM calculation are displayed in dashed black lines. The red line indicates the receivers.*

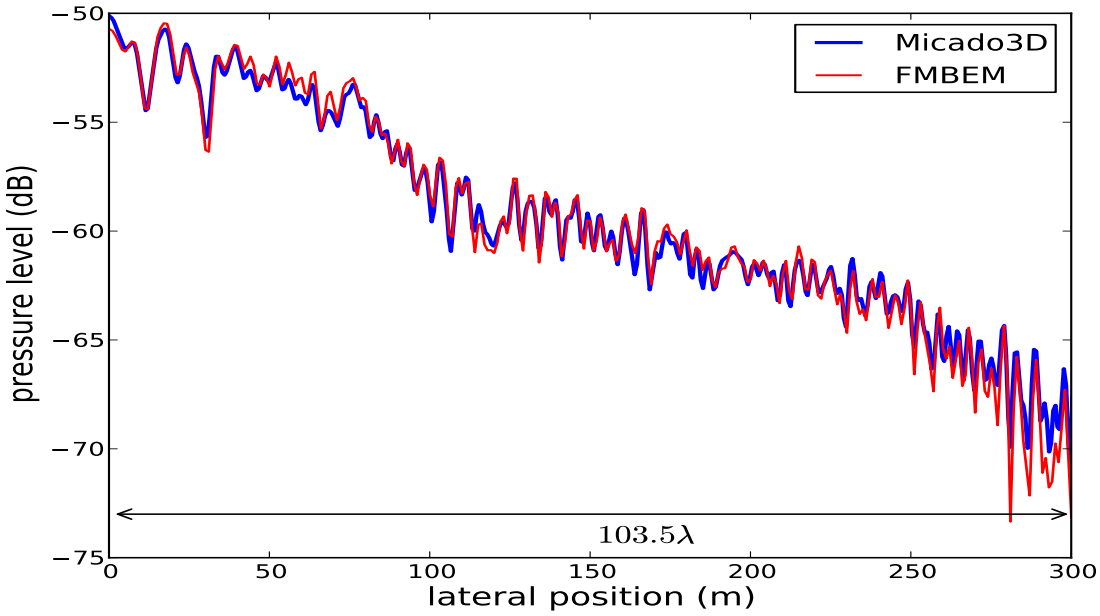

FIGURE 6.9: *Sound pressure level in dB along the receivers' line within the rectangular array computed with Micado3D software (blue line) and the fast multipole algorithm (red line). The reference pressure level is* $p = 1$ *Pa for a unit source amplitude.*

length of the problem is 1600 m (275λ). We detail below in table 6.3 the expansion orders with respect to the *level*. However this calculation does not lead to a convergence of the iterative solver most likely owing to the expansion order at *level* 2 (*i.e.* 956) involving instabilities in the recursive computation. Nevertheless, GUMEROV & DURAISWAMY proved the "stable" properties of the recursive scheme of the computation of

TABLE 6.2: *Rectangular frame: Expansion orders with respect to the level for a hierarchical tree consisting of 9 active levels and number of iterations for a dimensionless domain size equal to 207λ.*

level #	2	3	4	5	6	7	8	9	10	iterations
expansion order	726	378	200	108	62	36	22	14	10	8

rotational matrix coefficients up 10^4, thus this problem seems to be due to other instability sources. Because of the lack of time, this point has not been solved in the framework of this thesis and could be the topic of further research.

TABLE 6.3: *Rectangular frame: Expansion orders with respect to level for a hierarchical tree consisting of 9 active levels and number of iterations for a dimensionless domain size equal to 275λ.*

level #	2	3	4	5	6	7	8	9	10	iterations
expansion order	956	496	260	140	78	44	26	16	12	∞

6.4 Conclusion on the stable recursive computations of the rotational matrices

The stable recursive computation described in this section comes from GUMEROV & DURAISWAMY's works [Gumerov 2014]. After a brief overview of the numerical implementation which allows to ensure "stable" properties of the recursive computations of the rotational matrices coefficients, we evidence that the limitations emphasized in the previous chapter 5 can be solved by the implementation we discuss in this chapter. Indeed, it leads to a more reliable solution of the sound pressure field on the mesh in the case of the sound propagation problem in the city block while providing a stable number of iterations for a dimensionless domain size above 32λ. The average sound pressure levels in the sensitive areas are also improved by 0.6 dB and 4.7 dB in the opened and closed court yards respectively. The multi scattering problem by cubic bodies is solved successfully for 621000 elements 750 times faster with the FMBEM algorithm than if it was solved by a standard collocation BEM algorithm while reducing the required storage memory by 477. The multi scattering calculations are carried out successfully up to a dimensionless domain size of 207λ.

Chapter 7

Comparison between a BEM, a FMBEM and a beam tracing algorithm

Generally speaking, three dimensional BEM based algorithms are mostly used to provide reference solutions for wave propagation problems in homogeneous media. As it has been highlighted previously, the BEM formalism leads to prohibitive computation times as the number of elements increases, which limits the application of this numerical method to low frequencies, small scale models or two dimensional problems. Thus, with the development of the fast multipole formalism in others scientific domains, it seemed important to assess the applicability of this formalism to the BEM in the framework of urban acoustics. We recall that the first key idea of this thesis was to check the ability of FMBEM algorithms to deal with exterior sound propagation problems with the aim of providing reference solutions to assess or improve faster engineering algorithms.

An important class of algorithms commonly used in acoustics is based on asymptotic approaches, assuming high frequency approximations (ray tracing, beam tracing, particles launching . . .). We seek, in this chapter, to apply the FMBEM algorithm in a larger frequency range than what can nowadays be reached through classical BEM based algorithms. Thus, this last chapter is dedicated to the confrontation of different formalisms which possess their own advantages and domain of validity. We performed comparisons between a BEM algorithm (i.e. *Micado3D*), a fast multipole BEM algorithm and an asymptotic approach based software, Icare®[1], a ray tracing algorithm.

In a first section (7.1), we detail the main features of the Icare® software. Then (section 7.2), we check the reliability of the FMBEM algorithm and of the Icare® software to compute pressure levels in sensitive areas. To this end, we perform comparisons between the BEM algorithm, *Micado3D*, our reference in the first studied range of frequencies (1 - 150 Hz), the fast multipole algorithm and Icare® software. We discuss, section 7.3, the potential sources of inaccuracies through a study on an iterative solver used with our reference BEM algorithm, *Micado3D*. We highlight the particular attention necessary when solving

[1] http://www.cstb.fr/dae/en/nos-produits/logiciels/icare.html

problems in the more sensitive areas with an iterative solver. Finally, (section 7.4), in the second studied range of frequencies (150 - 300 Hz), the fast multipole algorithm is taken as reference algorithm to assess the reliability of Icare® software for computing the pressure level in the opened court yard.

7.1 Brief overview of the beam tracing algorithm principle

The mathematical background of the ray tracing algorithm has been developed during the first part of the 20^{th} century mainly in order to understand sound propagation in underwater acoustics. The wave propagation can be seen as a geometric construction of wave fronts, from which line flux can be obtained. The principles in geometrical acoustics have been developed by analogy with the light propagation, Snell-Descartes's law, Huygens principle, Fermat principle [Pierce 1981, Glassner 1989]... The computing software, Icare®, can also account for reflections on curved surfaces, multiple reflections and diffraction effects on edges [Jean 2008] as well as radiating surfaces.

The acoustic calculations are divided into two well-separated steps:

- **The geometric calculation step:** The aim of this step is to determine the geometrical paths between a source and a receiver, performed with a beam tracing, which take into account specular reflections and edges diffractions. The geometric calculation complexity will be determined by the number of reflections, as well as the number of diffractions allowed on edges during the path of each ray. Obviously, the larger these two parameters are, the higher the computation time will be. The diffraction edges must be chosen by the user. Successive diffractions can be defined. In practice, more than two successive diffractions are not recommended due to a very significant computation time. Thus, for reliable calculations, a compromise has to be found between accuracy of the results and computation time which can be difficult to determine for complex sound propagation problems.
- **The acoustic calculation step:** Once all the geometrical paths between a source and a receiver are known, the acoustic pressure associated to each ray is computed following the geometrical divergence, the impedance surface conditions and the acoustic phase. This step is generally much faster than the geometric calculation, and informations for a large frequency range can be obtained in a negligible computation time. This consists in the major strong point of the method.

The major drawback of the method is that these two steps must be performed for each pair of source and receiver and for a large number of sources or receivers, which can lead to prohibitive computation times. Thus the ray tracing method does not appear to be suitable to draw noise maps with a large number of receivers. For this reason, we only restrict the number of receivers in the next section to 361 (19×19). A more detailed description of the underlying theory of this approach can be found in [Noé 2011].

7.2 Comparison between algorithms: BEM, FMBEM, beam tracing

7.2.1 Description of calculation parameters

We seek to compare, in this section, the reliability of different algorithms to deal with the half space sound propagation problem in the city block, already described in the previous chapters. The comparison will be performed between the BEM approach (*Micado3D* software), the FMBEM algorithm and the ray tracing method (Icare® software). As a reminder, the geometry is displayed in figure 7.1. The computation of pressure levels will be compared in the more sensitive areas, that is to say within the opened and closed court yards (green areas in figure 7.1). The receivers' grids on each area contains 19 ×19 receivers, 1.5 meters above the ground. The source point is located on the plane of the ground. The normalized impedances of building facades are set to 38 which corresponds to an absorption coefficient equal to 0.1 [ISO 9613-2: 1996].

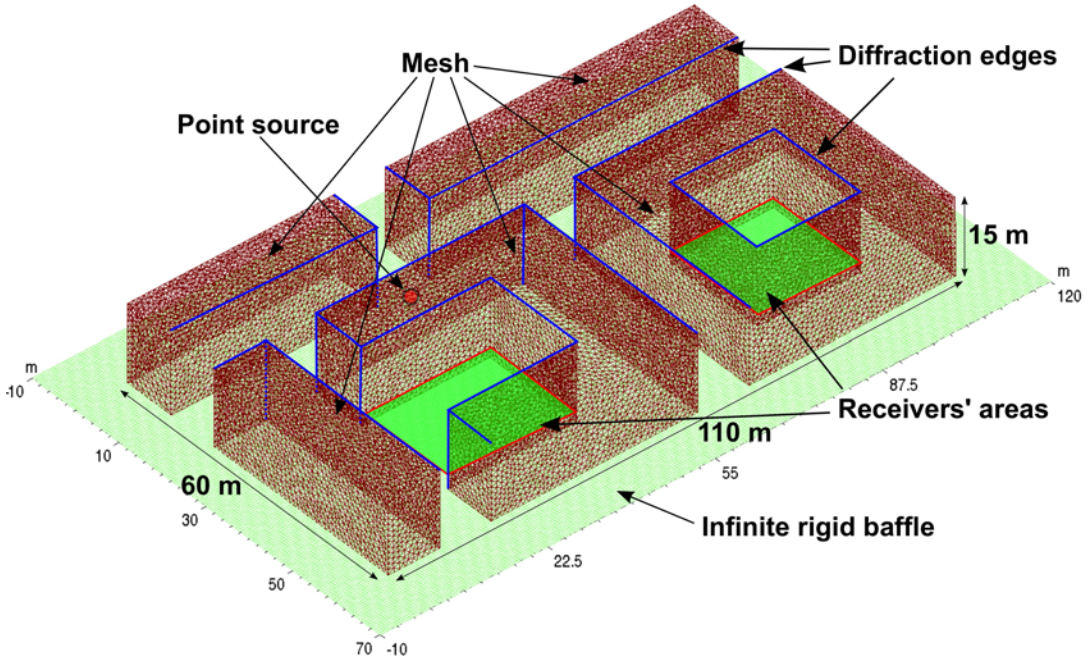

FIGURE 7.1: *Overview of the studied geometry: A city block made of 5 buildings excited by a point source (red point). This overview contains 66306 mesh elements in brown and the two receivers' areas, 1.5 m above the ground, contains each 19 × 19 receivers. The blue lines indicate the edges on which diffractions is allowed in the Icare® calculations.*

7.2.1.1 Ray tracing calculation

Regarding the geometrical calculation step in the Icare® software, the main parameters are the maximal number of reflections allowed during one ray path, including the number of diffractions on edges. These two latter parameters must be low to ensure acceptable computation time. Thus the maximum number of reflections is set to 8, including a maximum number of 2 diffractions on edges. The edges on which a

diffraction is authorized are displayed as blue lines in figure 7.1. These edges have been chosen to allow an energy diffusion in the streets and inside the court yards. We note that the addition of diffraction effect on edges (i.e. above the buildings) is necessary to perform a calculation of the pressure level in the close court yard.

We describe in this section the details of the computation carried by the Icare® software. We show in figure 7.2 an overview of the total number of paths found between the source position and two arbitrary receiver points, located in the closed and opened court yards. We recall that the maximal number of reflections is set to 8, including a maximal number of 2 successive diffractions on edges. As expected, the number of paths for a receiver located in the opened court yard is higher (1069 paths) than the number of paths found for a receiver located in the closed court yard (34 paths), within which only diffracted fields contribute. Regarding the source point, since this latter is located on the ground, we perform calculations with a hemispheric source and double its contribution to simulate the specular reflections on the ground.

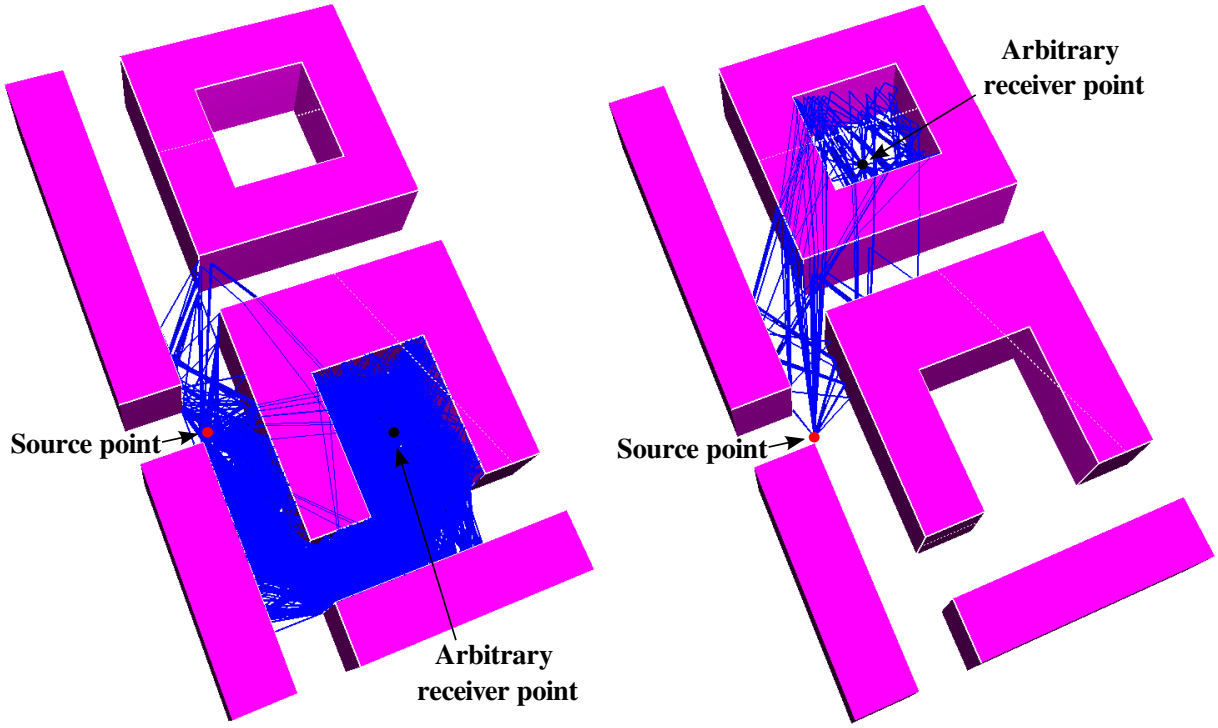

(a) (b)

FIGURE 7.2: *Paths taken into account for a ray tracing calculation, from the source position (red points) to an arbitrary receiver point (black points) located 7.2(a) in the opened court yard (1069 paths) and 7.2(b) in the closed court yard (34 paths).*

7.2.1.2 FMBEM algorithm calculation

The fast multipole calculations are performed with the improved “stable” version of the algorithm as described in the previous chapter. The space discretization criterion is equal to 5 elements per wavelength for

the frequency range 1 - 245 Hz (467434 elements at 245 Hz $\simeq 79.3\lambda$) and equal to 4 elements per wavelength above 245 Hz, because of limited memory storage. The cell size criterion is set to 100, involving a maximum of 7 levels in the hierarchical tree (i.e. 5 active levels). We solve the CHBIE formulation with a weighting parameter $\eta = 0.6$, which leads to an optimum convergence in this case (see the parametric study on the weighting parameter in chapter 5). The boundary normalized impedance $Z/(\rho_{air}c_{air})$ is set to 38, according to [ISO 9613-2: 1996].

7.2.2 Comparison of pressure levels

The first frequency range studied in this section is (1 - 150 Hz). In this frequency range the comparison between the three algorithms is performed even if we have limited the computation with the BEM algorithm to 138 Hz (45λ), owing to memory limitations. We can see in figures 7.3 and 7.4, the pressure level, averaged on the 19×19 receivers inside each court yards, normalized with the free field pressure level computed with: *Micado3D* software (blue lines), the FMBEM algorithm (red lines) and the Icare® software (green lines).

Regarding the pressure level within the opened court yard (see figure 7.3), despite local discrepancies, we note a good agreement between both BEM and FMBEM computations. The discrepancies between the Icare® software and BEM based algorithms seem to be reduced as the frequency increases, which is in agreement with the asymptotic approach which the ray tracing algorithm Icare® is based on. We will see in a latter section (7.4), a comparison performed in a higher frequency range (150 - 300 Hz) between the FMBEM algorithm, taken as reference and the Icare® software.

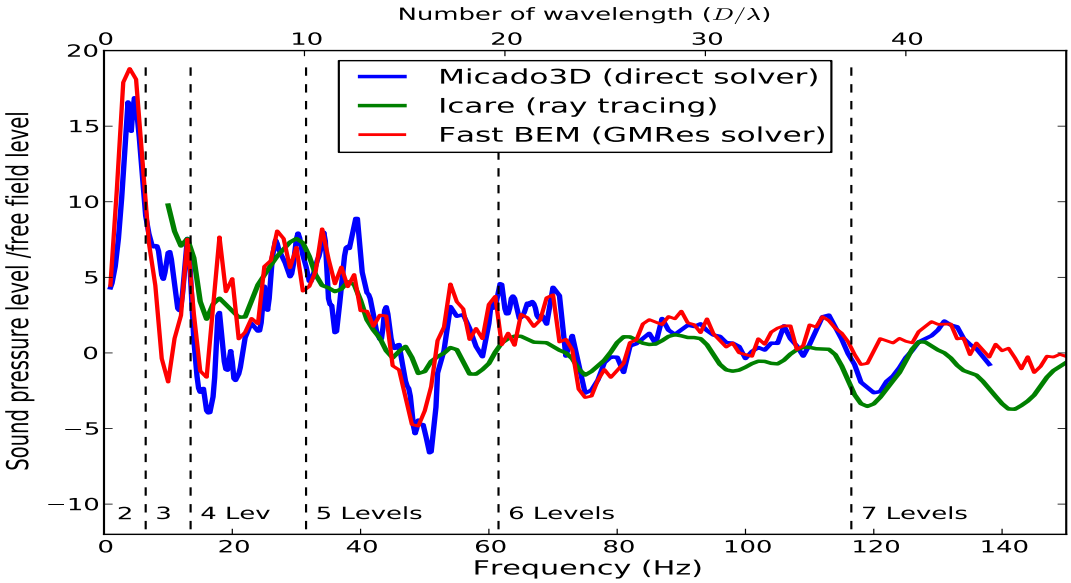

FIGURE 7.3: *Pressure levels averaged on the 19×19 receivers between 1 - 150 Hz in the opened court yard computed by Micado3D (blue line), the fast BEM (red line) and Icare® software (green line). The pressure levels are normalized by the free field pressure levels.*

Regarding the pressure level within the closed court yard (see results figure 7.4), the quality of the FMBEM computation is not as good as for the case of the opened court yard. Indeed, the discrepancy seems to increase with respect to frequency between the three tested algorithms. Furthermore, the ray tracing based algorithm, Icare® software, seems to provide more consistent results with the reference BEM algorithm than the FMBEM algorithm. We can also say that, the ray tracing method appears to underestimate the energy arriving in this sensitive area.

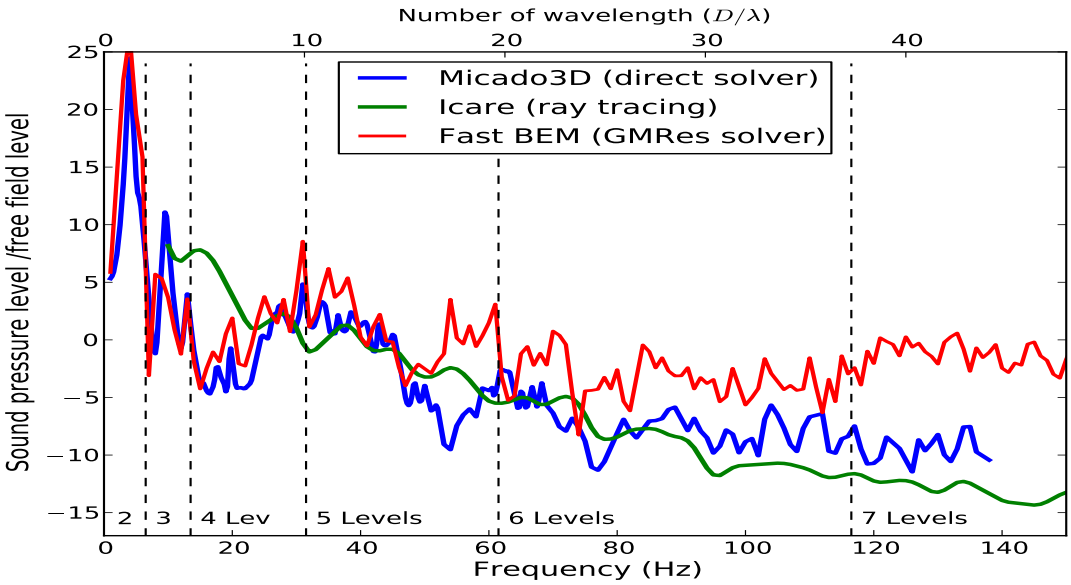

FIGURE 7.4: *Pressure levels averaged on the 19 × 19 receivers with respect to frequency between 1 - 150 Hz in the closed court yard computed by Micado3D (blue line), the fast BEM (red line) and Icare® (green line). The pressure levels are normalized by the free field pressure levels.*

Hence, the FMBEM does not show a good agreement with the reference BEM algorithm in the close court yard, while the results obtained in the opened court yard are satisfactory. In order to try to emphasize the possible sources of discrepancies between the BEM and the FMBEM calculations, an assessment of errors coming from the iterative solver, GMRes, seems to be required.

7.3 Influence of the iterative solver in sensitive areas

Several sources of errors may be responsible for discrepancies between the Micado3D and the FMBEM results. Indeed, Micado3D is based on a variational approach while our fast multipole algorithm is based on the collocation approach. The iterative solvers may also be a possible source of errors if used as a "black box". The iterative solver coming from a free software, the Petsc library [Balay 2014a, Balay 2014b, Balay 1997], used without preconditioner. In order to highlight the errors which may be due to the use of the iterative solver GMRes, we investigate comparisons with the BEM algorithm *Micado3D* for pressure levels obtained, on one hand by the direct solver, and on other hand by the iterative solver. Through the computations of pressure levels obtained with the BEM algorithm (direct solver in blue line and iterative

solver in cyan line) within the opened and within the closed court yard (figure 7.5), we can conclude that the iterative solver may be a possible source of errors if used as “a black box”. Indeed, while we can only highlight some slight discrepancies between both solvers (blue and cyan lines) in the case of the opened court yard 7.5(a), ensuring a reliable solution in the case of the closed court yard does not seem so trivial 7.5(b), since both solvers (direct and iterative) do not lead to the same solution and this, even after a stabilization of the relative residual. Thus, the accuracy of solutions is closely related to the observation area (as already emphasized in chapter 5) and guarantying accurate results in the more sensitive areas can be a very difficult task. We also recall the averaged pressure levels computed with the fast multipole algorithm (and so GMRes solver).

It may be concluded that using an iterative solver as “a black box” can be a possible source of inaccuracies, and further research may be needed to control the errors in the more sensitive areas to guarantee an optimum reliability of iterative solvers in the framework of the fast multipole formalism. More efficient convergence and so more reliable solutions in these sensitive areas could only be obtained with a preconditioning based on the elements located in these sensitive areas.

7.4 Comparisons between the FMBEM algorithm and ray tracing method

In the previous section, the accuracy of the FMBEM algorithm has been proved for the calculation of pressure levels within the opened court yard. We would like, in this section, to use this algorithm as a reference in a frequency range for which the BEM algorithm *Micado3D* can not provide solutions because of the prohibitive computational resources required (CPU and memory). Thus, the second frequency range studied in this section is (150 - 300 Hz). We can see in figure 7.6, the pressure level, averaged on the 19 $\times$ 19 receivers of the opened court yard, normalized with the free field pressure level computed with: the FMBEM algorithm (red line), and Icare® software (green line). A good agreement may be noticed between both algorithms and the ray tracing method (Icare® software) seems suitable to compute the pressure level in this opened court yard with an acceptable accuracy in the framework of urban acoustics.

7.5 Conclusion

We investigated in this last chapter comparisons between a BEM based algorithm *Micado3D*, the FMBEM algorithm and a ray tracing based method, Icare®, to compute averaged pressure levels in the opened and closed court yards. In the first frequency range (1 - 150 Hz), *Micado3D* is taken as the reference algorithm. It allows us to prove the accuracy of the FMBEM algorithm in the opened court yard but reveals, in the same time, a loss of accuracy with increasing frequency in the closed court yard. However the use of an iterative solver to perform calculations in very sensitive areas, such as the close court yard, requires further investigations to ensure reliable solutions. A preconditioning based on the elements located in the closed court yard could enhance the convergence and improve the accuracy. The FMBEM algorithm is

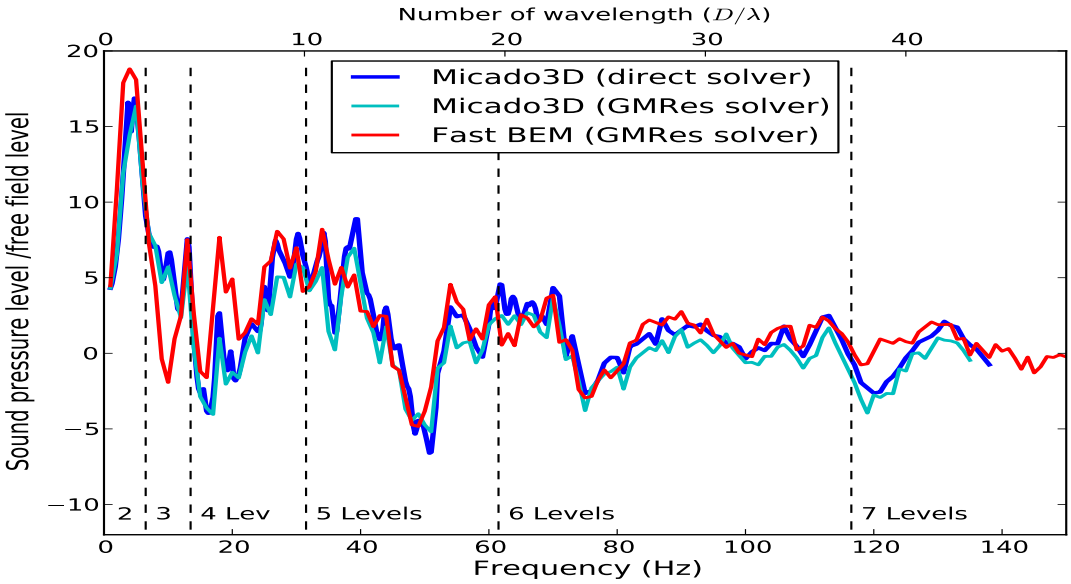

(a) opened court yard

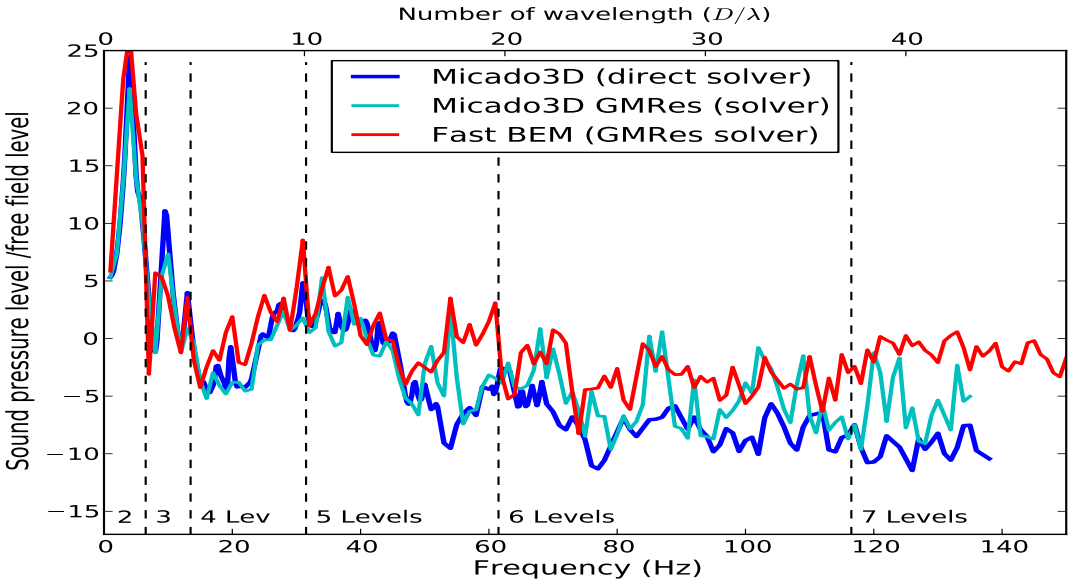

(b) closed court yard

FIGURE 7.5: *Pressure levels averaged on all the 19 × 19 receivers with respect to frequency for both studied areas computed by Micado3D with direct solver (blue lines), Micado3D with the GMRes solver (cyan lines) and the FMBEM with the GMRes solver (red lines). The pressure levels are normalized by the free field pressure levels.*

subsequently chosen as a reference in a higher frequency range (150 - 300 Hz) to assess the accuracy of the ray tracing method in the opened court yard. It appears that this method is capable to compute the pressure levels in this area with an acceptable accuracy.

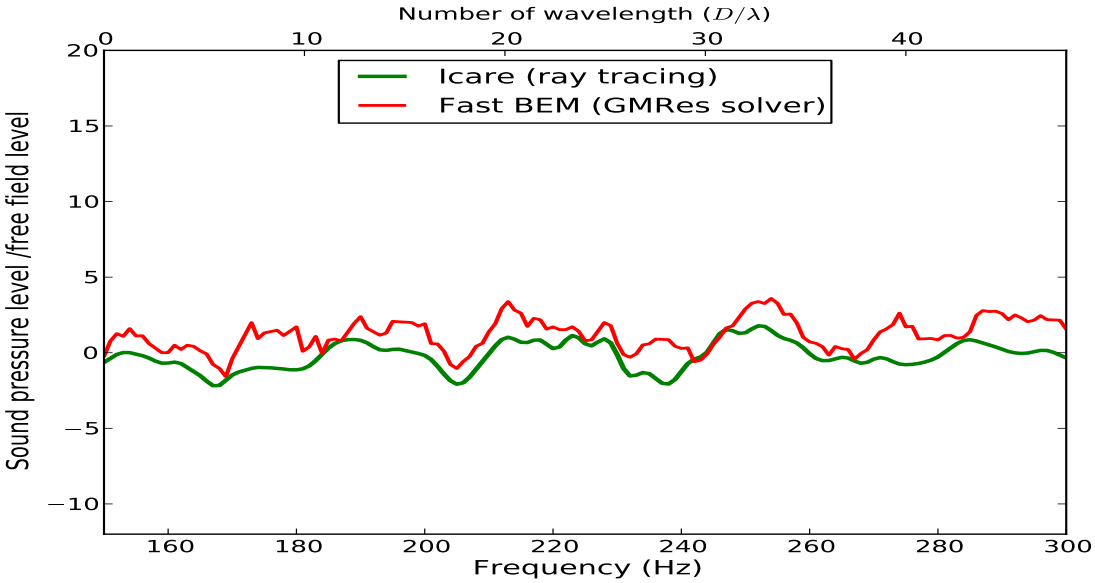

FIGURE 7.6: *Pressure levels averaged on the 19 × 19 receivers with respect to frequency between 150 - 300 Hz in the opened court yard computed by the fast BEM (red lines) and Icare® software (green lines). The pressure levels are normalized by the free field pressure levels.*

Part III: Conclusion

We focus in this part on the application of the fast multipole boundary element algorithm on realistic cases. The first application is a scattering case by a noise barrier located in a front of a building (section 5.1). We performed comparisons of the average pressure level computed with a BEM reference algorithm and the FMBEM algorithm for two frequency ranges. As a result, 98 % of the receivers located on the ground have a discrepancy lower than 3 dB in the first frequency range (90-100 Hz), while 96% of the receivers have a discrepancy lower than 3 dB in the second frequency range (170-190 Hz). We also study a sound propagation problem in a city block made of 5 buildings. Investigation on the weighting parameter in the CHBIE formulation provides a suitable value to minimize the fictitious eigenfrequency problem as well as the number of iterations. We also study the influence of the relative residual on the accuracy of the solution. A value equal to 10^{-2} seems sufficient for a rapid evaluation of the pressure level in this context, except in the sensitive area where 10^{-3} is required to ensure a reliable solution. This problem is solved with a computational time complexity $O(Nlog(N))$, while a standard BEM algorithm based on an iterative solver requires a computation time complexity $O(N^2)$. The computation time can furthermore be improved by performing the direct interactions calculations through a parallel process which can be realized easily thanks to the OpenMP (Open Multi-Processing) library. One can observe a very good agreement between both calculations (i.e. reference BEM algorithm and FMBEM algorithm) up to a dimensionless domain size equal to 32 wavelengths. For higher dimensionless domain sizes, we highlight discontinuities of the surface pressure field and a no convergence of the iterative solver coming from instabilities in the recursive process of the computation of translation matrices. This observation lead us to consider a “stable” recursive process, introduced by Gumerov & Duraiswamy for the computation of rotation matrices coefficients in the RCR decomposition. We describe how a “fast and stable” recursive scheme can be guaranteed for the computation of the rotational matrices entries of large expansion orders and the benefits provided in the case the sound propagation in city blocks. This new improved algorithm is subsequently assessed successfully on a multi scattering problem up to a dimensionless domain size equal to 207 wavelengths. This problem is solved, for 621000 elements, 750 times faster with the FMBEM algorithm than if it was solved with an iterative solver by a standard collocation BEM algorithm, while reducing the required storage memory by 477. Finally, we performed comparisons between a BEM based algorithm *Micado3D*, the FMBEM algorithm and a ray tracing based method, Icare® software, to compute averaged pressure levels in the opened and closed court yards. The fast multipole algorithm allowed to validate the results computed with Icare® in the opened court yards up to 300 Hz ($\simeq 100\lambda$), while in the closed court yards, i.e. a very sensitive

area, further investigations related to the preconditioning seem required to ensure reliable solutions provided by iterative solver based algorithms.

Conclusion of this work

Summary of results

Basically, the boundary integral formulation, basis of the boundary element method, appears to be very attractive in free space as it: (i) eliminates the need to consider the infinite domains normally associated with radiation problems; (ii) reduces the dimensionality of the problem by one (i.e., from a three dimensional partial differential equation, to a two dimensional surface integral equation); (iii) can readily handle arbitrary geometries and boundary conditions. All these properties are very advantageous from a computational viewpoint, as the first two significantly reduce the computer storage requirement for outdoor wave propagation problems. For these reasons, the BEM based algorithms are commonly used to provide reference solutions for problems governed by linear partial differential equations in homogeneous media including a broad scope of applications in physics: Laplace's or Poisson's problems, frequency or time wave equation, elastostatics or elastodynamics... The major drawback of this formalism is the dense system of equations generated, leading to a heavy computational resources dependency (time and memory), which so far limit the application of the boundary element method to a few number of degrees of freedom.

Described as one of the best ten algorithms of the 20th century, the fast Multipole formalism allows to accelerate the multiplication of $N \times N$ matrices and decreases the complexity of boundary element based algorithms by an order of magnitude. Handling several hundreds of thousands or millions of degrees of freedom through the boundary elements method on a common workstation is now possible. It allows to handle larger scale models which was unconceivable few years ago. Thus the motivation of the present work was to assess the ability of this formalism for solving sound propagation problems and providing reference results, as well as the benefits in terms of computational resources, in a three dimensional dense urban environments, with the aim of assessing or improving faster numerical tools.

Since the boundary element algorithm represents a crucial aspect of the fast multipole formalism, a prior assessment, by comparison with the analytical solution, of a successful implementation of the BEM was required. Thus, we investigated, in the first part, the robustness of the conventional & hypersingular boundary integral formulation when solving scattering problems by a spherical body, even at fictitious eigen-frequencies, for both rigid and impedant boundary conditions. Problems related to the hypersingularities have been overcame through the subtraction technique. As a result, the boundary element

algorithm was found to be reliable to compute the *near interactions* in the framework of the fast multipole boundary element algorithm.

We have introduced, in the second part of this manuscript, the fast multipole formalism. The elementary solution of the Helmholtz equation is expanded on spherical basis, derived from Bessel functions, Hankel functions and spherical harmonic series. We have discussed about the RCR-decomposition principle, coming from Gumerov & Duraiswamy's work and the high-frequency formulation, coming from Rokhlin's work, as well as the main stages from a numerical viewpoint required to perform calculations, including the moment to moment step, the moment to local step and the local to local step. We have estimated the theoretical computational complexity of the fast multipole algorithm as $O(N) \simeq O(p^2)$. We have proven the accuracy of the fast multipole formalism for both rigid and impedant boundary conditions, by comparison with the analytical solution at regular frequencies. We have also assessed the conventional & hyper-singular boundary integral formulation to tackle the fictitious eigenfrequency problem. We have first emphasized, as for the BEM algorithm, that the B&M formulation dramatically reduces the number of iterations as the frequency increases, regardless of the boundary conditions. We have also proven the efficiency of this formulation to provide reliable results for soft boundary conditions, while for rigid cases, it leads to a loss of accuracy with increasing number of levels at low frequency. Thus this formulation does not seem to be recommended for small scale models, and further investigations may be needed to work out this problem in order to guarantee an optimum reliability of the algorithm. Because of the presence of the ground in urban context, the full space problem requires to mesh the symmetrical geometry to simulate the reflections on the ground. This drawback has been tackled by the implementation of the half space problem with the addition of the infinite rigid baffle, which provides improvements in terms of computation time and memory, compared to its equivalent problem in full space. This half space problem has been subsequently used in an urban context in the remainder of the document.

The third part of this manuscript represents, as far as the author knows, the original work of this PhD thesis. We have intended to assess the ability of the fast multipole algorithm to provide reference solutions of sound propagation problems when applied to realistic urban geometries. The first realistic application is a scattering case by a noise barrier located in front of a building. We have performed comparisons of the average pressure level computed with a BEM reference algorithm and the FMBEM algorithm for two frequency ranges. As a result, 98 % of the value on the receivers located on the ground are lower than 3 dB in the first frequency range (90-100 Hz) while 96 % of the value on the receivers are lower than 3 dB in the second frequency range (170-190 Hz). We have also studied a sound propagation problem in a city block made of 5 buildings. An investigation on the influence of the weighting parameter in the CHBIE formulation has provided a suitable value to minimize the fictitious eigenfrequency problem as well as the number of iterations. We have also studied the influence of the relative residual on the accuracy of the solution. A value equal to 10^{-2} seems sufficient for a rapid evaluation of the pressure level in this context, except in the sensitive areas where 10^{-3} is required to ensure a reliable solution. This problem has been solved with a computational time dependency $O(Nlog(N))$, while a standard BEM algorithm based on an iterative solver requires a computation time dependency $O(N^2)$. We have also reduced the computation time, by performing

the direct interactions calculations through a parallel process, which can be realized easily thanks to the OpenMP (Open Multi-Processing) library. One has observed a very good agreement between the BEM reference calculation and the FMBEM algorithm up to a dimensionless domain size of 32 wavelengths. For higher dimensionless domain sizes, we have highlighted discontinuities of the surface pressure field and a failed convergence of the iterative solver coming from instabilities in the recursive computation of translation matrices. This observation led us to consider a "stable" recursive process, introduced very recently by Gumerov & Duraiswamy, for the computation of rotation matrices coefficients in the RCR decomposition. Thus, we have explained how a "stable" recursive computation of the rotational matrices entries can be guaranteed for an absolute error equal to 10^2 above the numerical precision up to an expansion order $p = 10^4$. This corresponds to an error equal to 10^{-13} when a double precision is used to store the numerical data, which is an acceptable accuracy for many practical problems. This new improved algorithm has subsequently been assessed on a multi scattering problem up to a dimensionless domain size equal to 207 wavelengths. This problem has been solved, for 621000 elements, 750 times faster with the FMBEM algorithm than if it had been solved with an iterative solver by a standard collocation BEM algorithm, while reducing the required memory by 477. We have finally performed comparisons between a BEM algorithm, *Micado3D*, the FMBEM algorithm and a ray tracing algorithm, Icare® software, to compute averaged pressure levels in an opened and a closed court yards. The fast multipole algorithm allowed to validate the results computed with Icare® in the opened court yard up to 300 Hz ($\simeq 100\lambda$), while in the closed court yards, i.e. a very sensitive area, further investigations related to the preconditioning seem required to ensure reliable solutions provided by iterative solver based algorithms.

Perspectives of this work

We have pointed out, through this manuscript, some important issues which could require further research in order to guarantee an optimum reliability of the algorithm. It is nevertheless important to underline that, besides numerical instability previously emphasized, these issues are not directly related to the fast multipole formalism, but are however crucial for an efficient fast multipole boundary element algorithm. Thus, even if the fictitious eigen-frequency problem has been overcame for a spherical geometry, thanks to the CHBIE formulation, its efficiency on an arbitrary geometry or for a large range of frequency is not so obvious. Another crucial point, which fast multipole algorithms are based on, concerns the use of iterative solvers. Indeed, the computation time, as well as the required memory to solve a given scattering problem, are closely related to the convergence of the iterative solver. Thus, as already highlighted in the manuscript, the numerical resources could be dramatically reduced through the use of an efficient preconditioner. These transformations of the matrix system have not been considered in the framework of this thesis and, even if preconditioners have been the purpose of a large number of papers, they seem to still be a subject of investigations. We have furthermore pointed out that consistent results, between a problem solved by a direct solver and an iterative solver, can be a difficult task in the more sensitive areas, and it would be important to check that the preconditioners can lead to reliable solutions, even inside sensitive areas. We have

only implemented in the framework of this thesis, a parallelization process carried on the *near interactions* through the OpenMP library. It is noteworthy that savings, regarding the computation time, can be obtained, through a parallelization process of the iterative steps, thanks to a Message Passing Interface (MPI) but this improvement requires deep knowledge in programming.

Regarding the fast multipole formalism, the fast adaptive multipole algorithm can be several times faster than the classical algorithm [Cheng 1999, Shen 2006]. This improvement suggests not dividing a cell which respect the cell-size criterion. This method, involving leaves on several levels, has a significant influence only for a large number of degrees of freedom and brings a significant advantage in terms of computation time as the number of levels (i.e. elements) increases. Fast multipole algorithms may also be coupled with others numerical methods such as the FEM, already implemented in the seismic waves domain [Grasso 2012]. The computation of noise maps can be an expensive task as frequency increases. Indeed, the calculation of interactions between N elements and M receivers requires $O(N \times M)$ operations. It is however possible to realize this task through the fast multipole principle. Two different hierarchical trees would be required and two successive fast multipole calculations as well, one for the solution vector on the mesh and another one to radiate this solution on the receivers' maps. As a result, this radiation step could be realized with $O(N + M)$ operations. Several geometries have been considered in this thesis, a spherical body, a noise barrier located in a front of a building, a city block made of 5 buildings or a square array of cubic scatterers, and further studies on realistic geometries must be investigated to generalize, in years to come, the application of the fast multipole formalism to the boundary element method in acoustics.

Appendix A

RCR decomposition

A.1 Rotation Matrices coefficients

The first step consists in the commutation of rotational matrices, by computing the set of expansion coefficients expressed over basis functions, oriented towards the new target expansion center. The new components $\tilde{C}_n^m$ of translation matrices **C** can be performed according to the following formula:

$$\tilde{C}_n^m \equiv \mathbf{Rot}(Q(\alpha,\beta,\gamma))C_n^m = \mathrm{e}^{-im'\gamma}\sum_{m=-n}^{n} H_n^{m',m}(\beta)\mathrm{e}^{im\alpha}C_n^m, \tag{A.1}$$

$$n = 0, 1, \cdots, p-1, \qquad m = -n, \cdots n \tag{A.2}$$

where for each subspace of degree n, components of dense $(2n+1)\times(2n+1)$ matrix $H_n^{m',m}(\beta)$ are computed recursively using:

$$H_{n-1}^{\nu,m+1}(\beta) = \frac{1}{b_n^m}\left\{\frac{1}{2}\Big[\, b_n^{-\nu-1}\,(1-\cos\beta)\,H_n^{\nu+1,m} - b_n^{\nu-1}\,(1\cos\beta)\,H_n^{\nu-1,m}\,\Big] - a_{n-1}^{\nu}\sin(\beta)H_n^{\nu,m}\right\} \tag{A.3}$$

$$n = 2, 3, \cdots, \qquad \nu = -n+1, \cdots, n+1, \qquad m = 0, \cdots, n-2,$$

with the initial values

$$H_n^{\nu,0}(\beta) = (-1)^{\nu}\sqrt{\frac{(n-|\nu|)!}{(n+|\nu|)!}}P_n^{|\nu|}(\cos\beta) \tag{A.4}$$

$$n = 0, 1, \cdots, \qquad \nu = -n, \cdots, n.$$

We note that the rotation matrices can be performed with indifferent γ angles and it turns out that γ can be taken to zero.

A.2 Coaxial translation coefficients

Now z-axis is oriented toward the next expansion center, the second step is to translate the expansion coefficients $\tilde{C}_n^m$. We can determine the new components of the translated matrices $\tilde{\tilde{C}}_n^m$ by using the following formula:

$$\tilde{\tilde{C}}_n^m \equiv (\mathbf{E}|\mathbf{F})_{coax}(t)\tilde{C}_n^m = \sum_{n=|m|}^{p-1} (E|F)_{n',n}^m(t) C_n^m \tag{A.5}$$

$$m = 0, \pm 1, \cdots, \pm(min(p, p') - 1) \qquad n' = 0, 1, \cdots, p' - 1, \qquad E, F = S, R \tag{A.6}$$

All the entries $(E|F)_{n',n}^m$ of the matrix $(\mathbf{E}|\mathbf{F})_{coax}(t)$ can be computed recursively with a complexity $O(p^3)$ using the following recursion property:

$$a_n^m (E|F)_{n',n+1}^m = a_{n-1}^m (E|F)_{n',n-1}^m - a_{n'}^m (E|F)_{n'+1,n}^m + a_{n'-1}^m (E|F)_{n'-1,n}^m \tag{A.7}$$

$$n = m, m + 1, \cdots, \qquad E, F = S, R, \tag{A.8}$$

with the coefficients a given in 3.15, where for each subspace n' recursive procedure start with the following values for the two kinds of translations :

- **Moment to moment (M2M) and Local to local (L2L) translations**: In the case of the Helmholtz equation, we have identical moment to moment $(\mathbf{R}|\mathbf{R})_{coax}$ and local to local $(\mathbf{S}|\mathbf{S})_{coax}$ coaxial translation. For these operators (eq. 3.20 or eq. 3.22), the recursive computations start with the initial values:

$$(R|R)_{n',0}^0(t) = (-1)^{n'} \sqrt{2n' + 1}\, j_{n'}(kt). \tag{A.9}$$

- **Moment to local translations**: For this operator (eq. 3.21), the recursive computation starts with the initial values:

$$(S|R)_{n',0}^0(t) = (-1)^{n'} \sqrt{2n' + 1} h_{n'}(kt). \tag{A.10}$$

A.3 Inverse rotation Matrices coefficients

Finally, we need to rotate the expansion coefficients backward. Since the direct rotation matrix $Q(\alpha, \beta, \gamma)$ is an orthogonal rotation matrix, it satisfies $Q^{-1}(\alpha, \beta, \gamma)) = Q^T(\alpha, \beta, \gamma)) = Q(\gamma, \beta, \alpha)$ (the reader can refer to chapter 3 in [Gumerov 2004]). So, we can obtain the final expansion coefficients $\tilde{\tilde{C}}_n^m$ using:

$$\tilde{\tilde{C}}_n^m \equiv \mathbf{Rot}(Q(\gamma, \beta, \alpha))\tilde{\tilde{C}}_n^m = \mathrm{e}^{-im'\alpha} \sum_{m=-n}^{n} H_n^{m',m}(\beta)\mathrm{e}^{im\gamma}\tilde{\tilde{C}}_n^m, \tag{A.11}$$

$$n = 0, 1, \cdots, p - 1, \qquad m = -n, \cdots n \tag{A.12}$$

with the same recursive methods (eq. A.3 and eq. A.4) as for the direct rotation transform.

Appendix B

Appendixes related to the spherical body

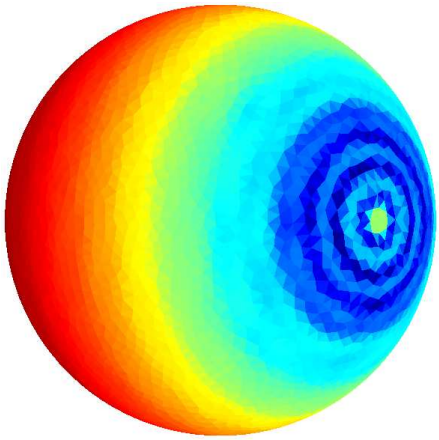

FIGURE B.1: *Sound pressure level obtained on the mesh at a frequency equal to 1100 Hz for spherical body discretized with 7932 constant planar triangular elements.*

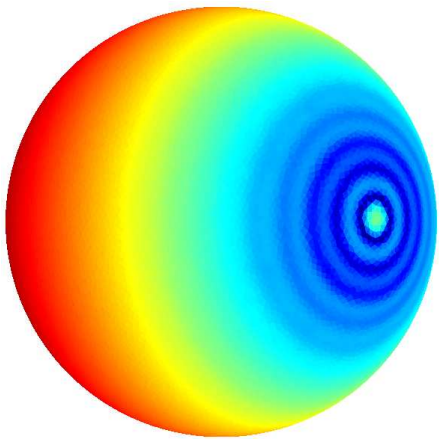

FIGURE B.2: *Sound pressure level obtained on the mesh at a frequency equal to 1082 Hz for spherical body discretized with 31696 constant planar triangular elements.*

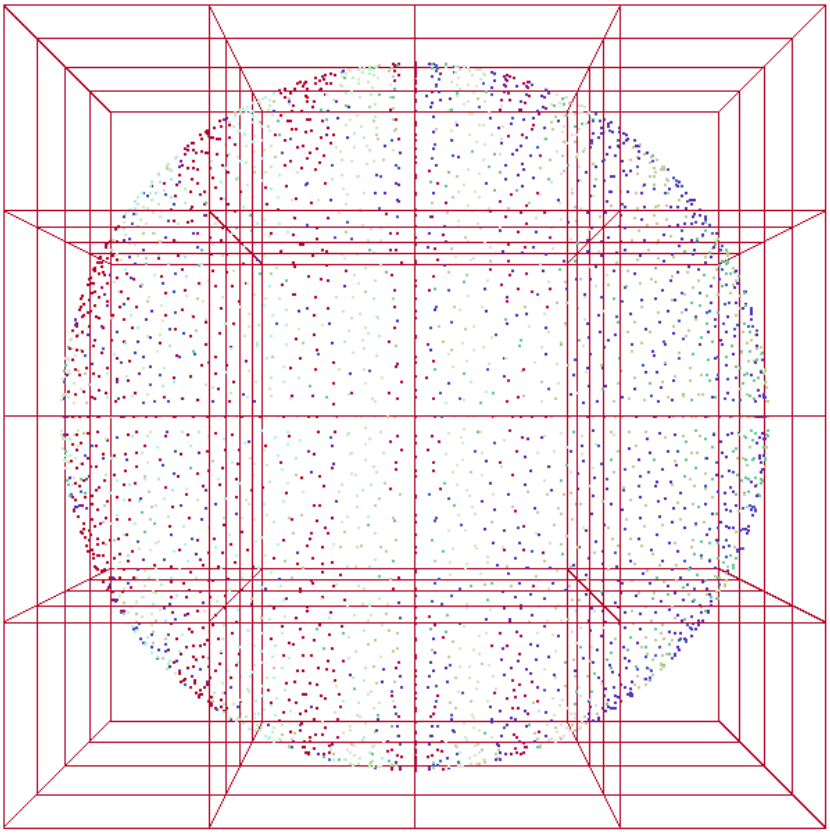

FIGURE B.3: *Space partitionning for a spherical body at the* 2^{nd} *level.*

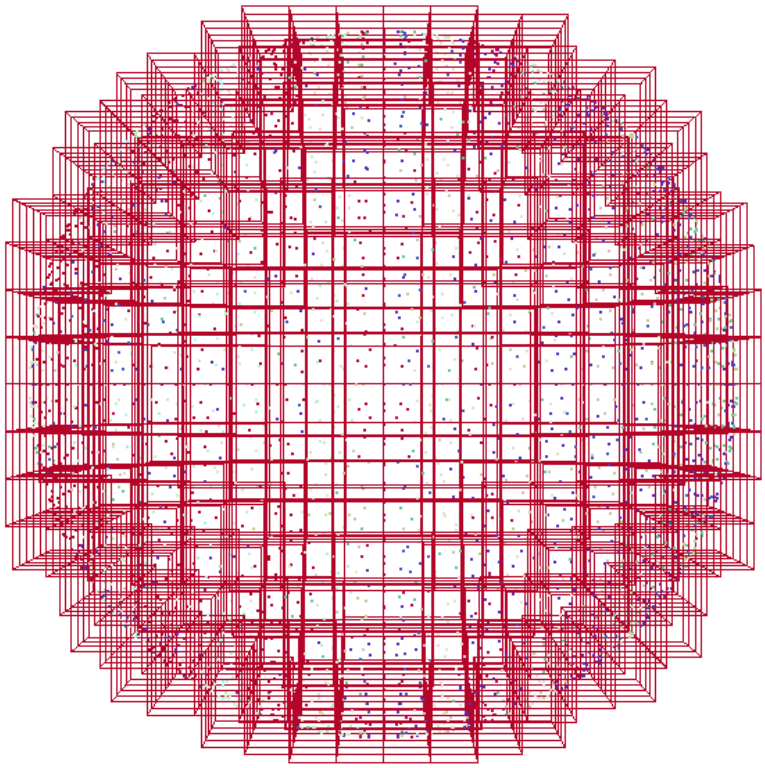

FIGURE B.4: *Space partitionning for a spherical body at the* 4^{th} *level.*

Appendix C

Appendixes related to the sound barrier

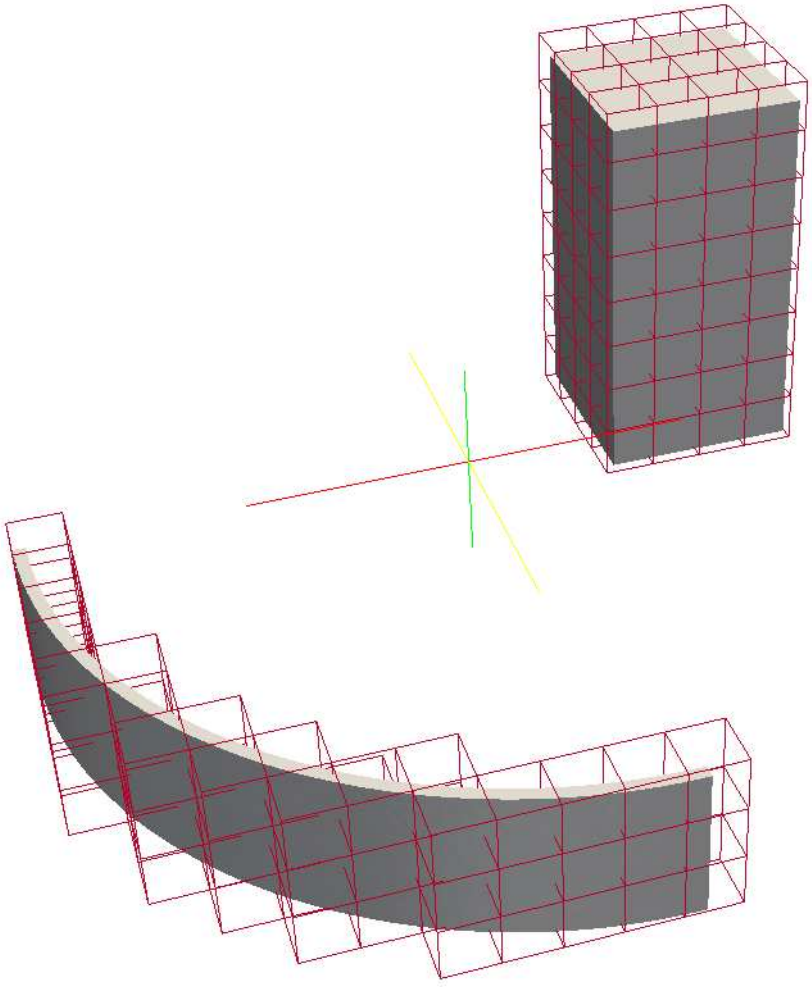

FIGURE C.1: *Space partitionning for the sound barrier at the 4^{th} level.*

Appendix D

Appendixes related to the city block

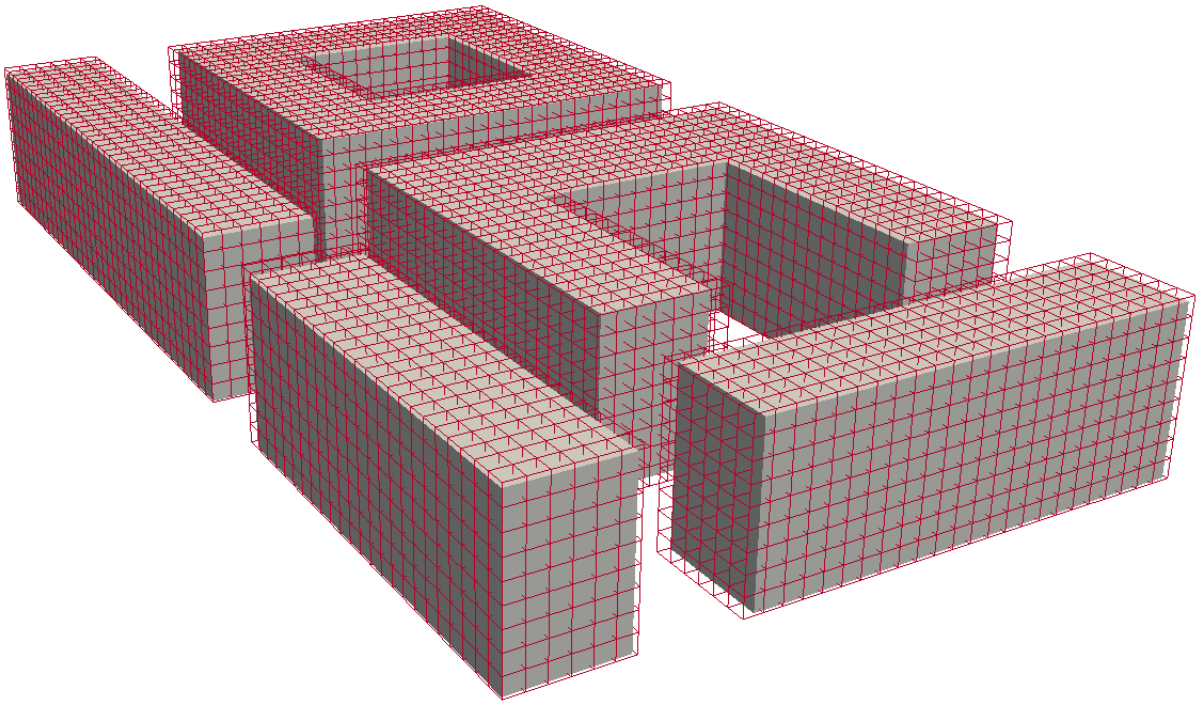

FIGURE D.1: *Space partitionning for the city block at the* 6^{th} *level.*

Appendix E

Benefits provided by a parallelization process

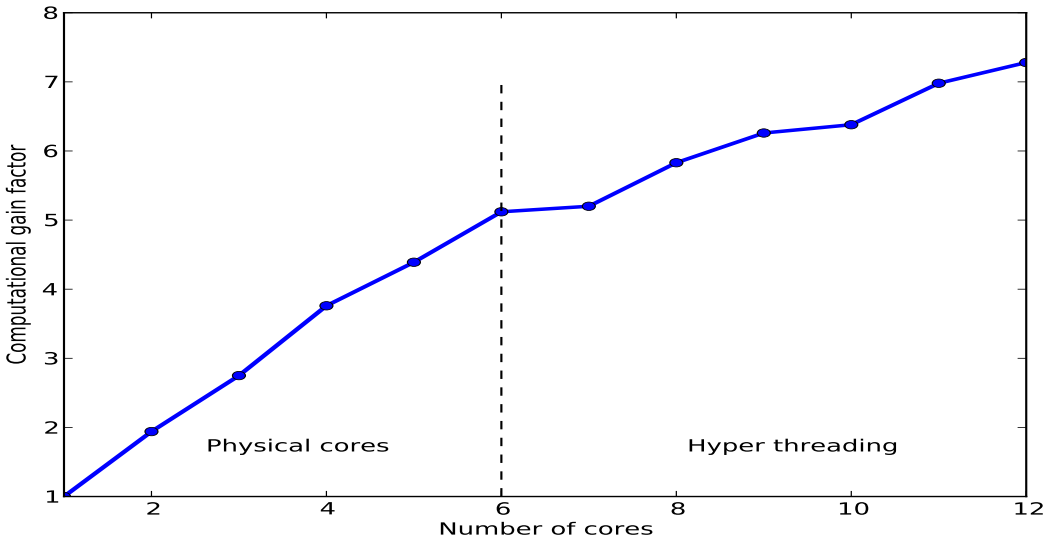

FIGURE E.1: *Benefits of the computational time provided by a parallelization process of direct interactions with respect to the number of cores which the computation is carried on.*

Appendix F

Multi scattering problem by cubic bodies

We provide here complementary information related to additional calculations which have been performed for the multi scattering problem by cubic bodies. We can see in figures F.1 the meshes used to perform these calculations. The meshes are obtained for geometric parameters related to $\lambda = 5.67m$ (60 Hz):

- figure F.1(a): length of the cubic scatterers 0.35λ, the distance between two successive scatterers 7λ and the maximal length of the problem 92 m (16.5λ);
- figure F.1(b): length of the cubic scatterers 0.35λ, the distance between two successive scatterers 7λ and the maximal length of the problem 192 m (33.9λ);
- figure F.1(c): length of the cubic scatterers 0.35λ, the distance between two successive scatterers 7λ and the maximal length of the problem 292 m (52λ).

The comparison of the pressure level between the reference algorithm, *Micaco3D* and the fast multipole method taken along the receivers' line (red lines figures F.1) is display figure F.2 for three cases: 16.5λ figure F.2(a), 33.9λ figure F.2(b) and 52λ figure F.2(c).

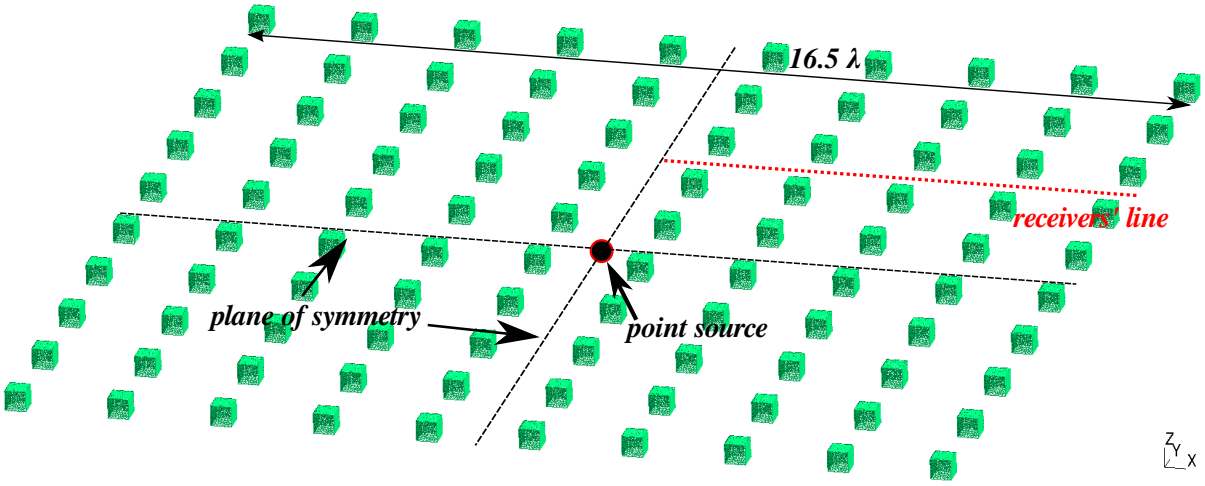

(a)

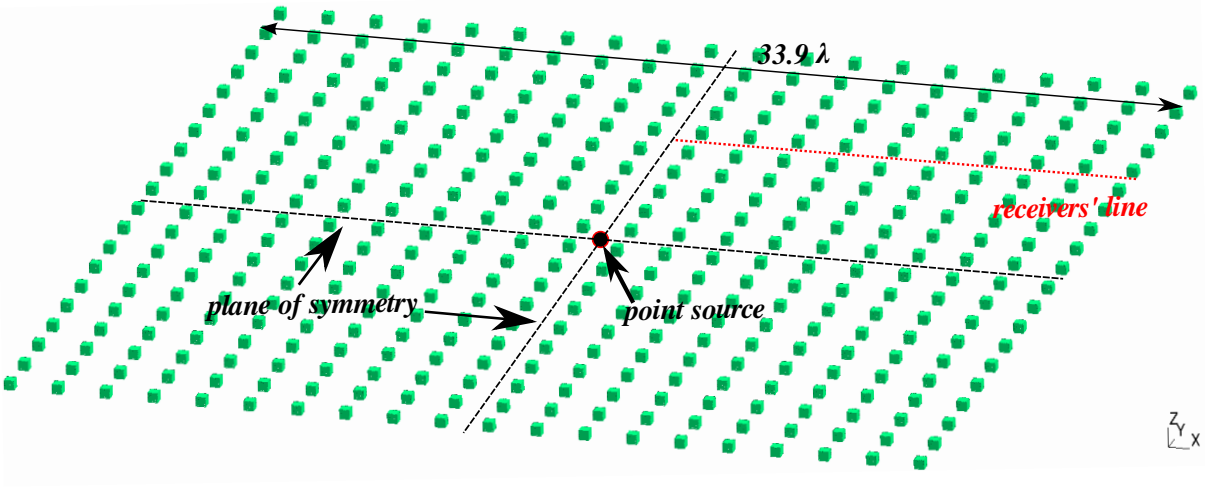

(b)

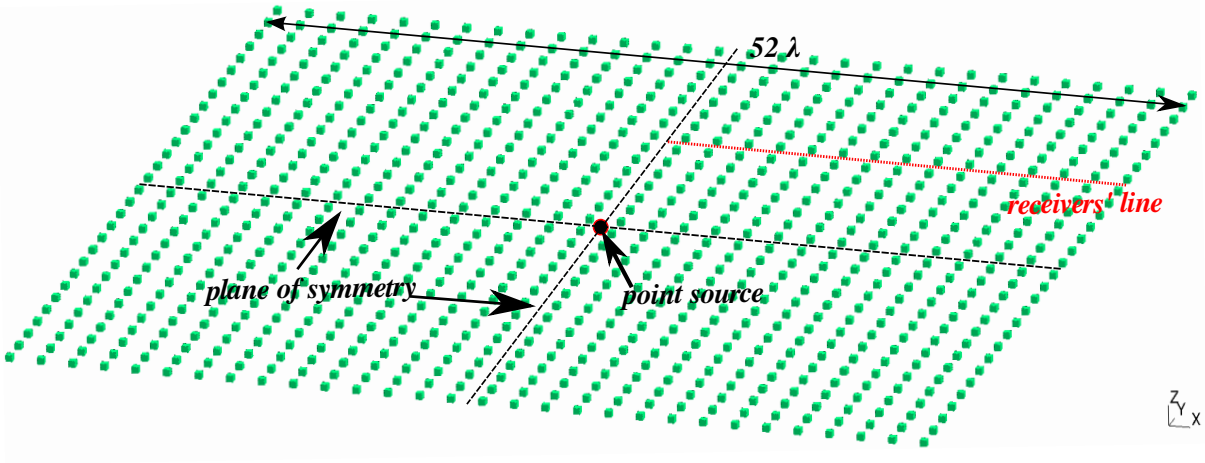

(c)

FIGURE F.1: *Multi scattering problem meshes for a dimensionless domain size equal to 16.5λ F.1(a), 33.9λ* F.1(b) and 52*λ* F.1(c).

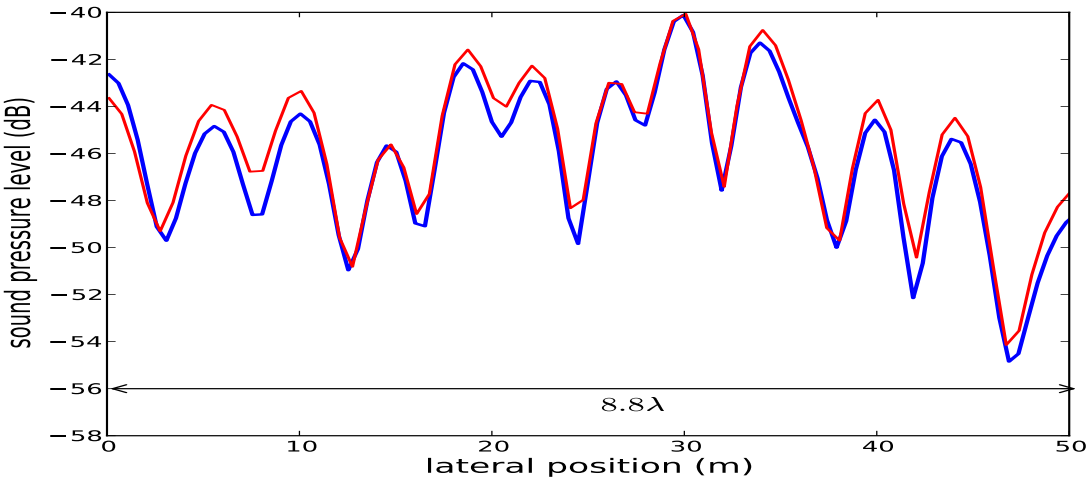

(a)

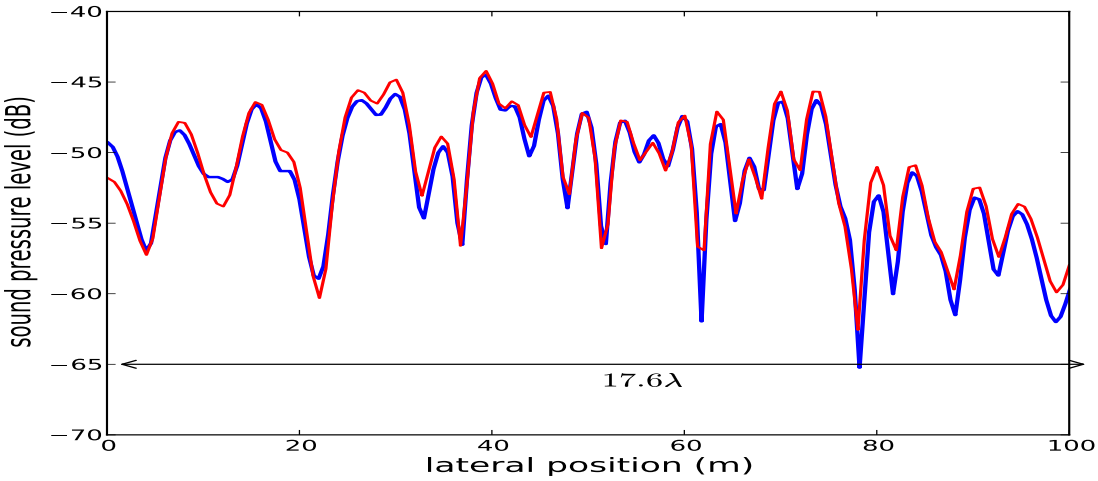

(b)

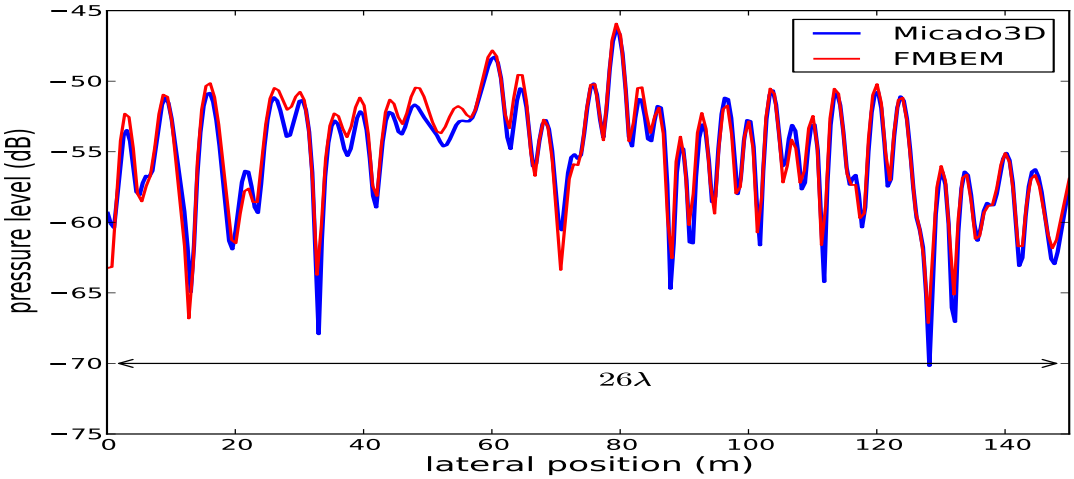

(c)

FIGURE F.2: *Sound pressure level (dB) along the receivers' lines (red dotted lines) for a dimensionless domain size equal to 16.5λ F.2(a), 33.9λ* F.2(b) and 52*λ* F.2(c).

Bibliography

[2001/C 148/02] 2001/C 148/02. *Opinion of the Committee of the Regions on the "Proposal for a Directive of the European Parliament and the Council relating to the Assessment and Management of Environmental Noise"*. http://eur-lex.europa.eu/legal-content/EN/TXT/?uri=uriserv:OJ.C_.2001.148.01.0007.01.ENG.

[Aballéa 2004] F. E. Aballéa and J. Defrance. *Propagation acoustique en milieu extérieur : Application de l'équation parabolique rapide au couplage d'effets météorologiques et de topographies complexes*. PhD thesis, Université du Maine, 2004.

[Abramowitz 1964] M. Abramowitz and I. A. Stegun. Handbook of Mathematical Functions. National Bureau of Standards, Washington, DC, 1964.

[Alves-Pereira 2007] M. Alves-Pereira and N. A. A. Castelo-Branco. *Vibroacoustic disease: biological effects of infrasound and low-frequency noise explained by mechanotransduction cellular signalling*. Progress in biophysics and molecular biology, vol. 93, no. 1-3, pages 256–279, 2007.

[Amini 1987] S. Amini. *An iterative method for the boundary element solution of the exterior acoustic problem*. J. Comput. Appl. Math., vol. 20, pages 109–117, 1987.

[Amini 1990a] S. Amini. *On the choice of the coupling parameter in boundary integral formulations of the exterior acoustics problem*. Applicable Anal., vol. 35, pages 75–92, 1990.

[Amini 1990b] S. Amini, C. Ke and P. J. Harris. *Iterative solution of boundary element equations for the exterior Helmholtz problem*. J. Vib. Acoust., vol. 112, pages 257–262, 1990.

[Attenborough 2006] K. Attenborough, K. Li and K. Horoshenkov. Predicting Outdoor Sound. CRC Press, 2006.

[Autrique 2006] J.-C. Autrique and F. Mougalès. *Studies of an infinite element method for acoustical radiation*. Applied Mathematical Modelling, vol. 30, pages 641–655, 2006.

[Balay 1997] Satish Balay, William D. Gropp, Lois Curfman McInnes and Barry F. Smith. *Efficient Management of Parallelism in Object Oriented Numerical Software Libraries*. In E. Arge, A. M. Bruaset and H. P. Langtangen, editeurs, Modern Software Tools in Scientific Computing, pages 163–202. Birkhäuser Press, 1997.

[Balay 2014a] Satish Balay, Shrirang Abhyankar, Mark F. Adams, Jed Brown, Peter Brune, Kris Buschelman, Victor Eijkhout, William D. Gropp, Dinesh Kaushik, Matthew G. Knepley, Lois Curfman McInnes, Karl Rupp, Barry F. Smith and Hong Zhang. *PETSc Web page*. http://www.mcs.anl.gov/petsc, 2014.

[Balay 2014b] Satish Balay, Shrirang Abhyankar, Mark F. Adams, Jed Brown, Peter Brune, Kris Buschelman, Victor Eijkhout, William D. Gropp, Dinesh Kaushik, Matthew G. Knepley, Lois Curfman McInnes, Karl Rupp, Barry F. Smith and Hong Zhang. *PETSc Users Manual*. Rapport technique ANL-95/11 - Revision 3.5, Argonne National Laboratory, 2014.

[Banaugh 1963] R. P. Banaugh and W. Goldsmith. *Diffraction of steady acoustic waves by surfaces of arbitrary shape.* J. Acoust. Soc. Am., vol. 35, pages 1590–1601, 1963.

[Banerjee 1981] P. K. Banerjee and R. Butterfield. Boundary Element Methods in Engineering Science. Mc Graw-Hill, 1981.

[Bapat 2009] M. S. Bapat, L. Shen and Y. Liu. *Adaptive fast multipole boundary element method for three-dimensional half-space acoustic wave problems*. Engineering Analysis with Boundary Elements, vol. 33, pages 1113–1123, 2009.

[Barrett 1994] R. Barrett, M. Berry, Chan T. F., J. Demmel, J. M. Donato, J. Dongarra, V. Eijkhout, R. Pozo, C. Romine and H. Van der Vorst. Templates for the Solution of Linear Systems: Building Blocks for Iterative Methods. SIAM, 1994.

[Berman 1975] J. M. Berman. *Behavior of sound in a bounded space*. J. Acoust. Soc. Am., vol. 57, no. 6, pages 1275–1291, 1975.

[Bertoni 1993] D. Bertoni, A. Franchini, M. Magnoni, P. Tartoni and M. Vallet. *Reaction of people to urban traffic noise in Modena, Italy.* In 6th Congress on Noise as a Public Health Problem, Noise, and Man, France, 1993.

[Bonnet 1999] M. Bonnet. Boundary Integral Equation Methods for Solids and Fluids. Wiley, 1999.

[Bottledooren 1994] D. Bottledooren. *Acoustical finite-difference time-domain simulation in a quasi-Cartesian grid*. J. Acoust. Soc. Am., vol. 95, pages 2313–2319, 1994.

[Brebbia 1978] C. A. Brebbia. The Boundary Element Method for Engineers. Pentech Press, London, 1978.

[Bristow 2005] A. L. Bristow and M. Wardman. *Valuing aircraft noise: influential variables*. In Proceedings of Inter-Noise, Brazil, 2005.

[Bullen 1977] R. Bullen and F. Fricke. *Sound propagation at a street intersection in an urban environment*. Journal of Sound and Vibration, vol. 54, no. 1, pages 123–129, 1977.

[Burgschweiger 2013] R. Burgschweiger, I. Schäffer, M. Ochmann and B. Nolte. *The Combination of a Multi-Level Fast Multipole Algorithm with a Source-Clustering Method for higher expansion orders*. In AIA-DAGA 2013, Merano, 2013.

[Burton 1971] A. J. Burton and G. F. Miller. *The application of the integral equation methods to the numerical solution of some exterior boundary value problems*. Proc. R. Soc. London, no. Ser. A 323, pages 201–210, 1971.

[Cao 2013] Y. Cao, L. Wen, J. Xiao and Y. Liu. *A fast directional BEM for large-scale acoustic problems based on the Burton-Miller formulation*. Comput. Mechanics, 2013.

[Chaillat 2008] S. Chaillat, M. Bonnet and J. F. Semblat. *A multi-level fast multipole BEM for 3-D elastodynamics in the frequency domain*. Comput. Method Appl. Mech. Engrg, no. 197, pages 4233–4249, 2008.

[Chaillat 2012] S. Chaillat, J. F. Semblat and M. Bonnet. *A preconditioned 3-D multi-region fast multipole solver for seismic wave propagation in complex geometries*. Commun. Comput. Phys., vol. 11, pages 594–609, 2012.

[Chaillat 2013] S. Chaillat and M. Bonnet. *Recent advances on the fast multipole accelerated boundary element method for 3D time-harmonic elastodynamics*. Wave Motion, vol. 50, pages 1090–1104, 2013.

[Chen 1992] G. Chen. Boundary Element Methods. Academic Press, 1992.

[Cheng 1999] H. Cheng, L. Greengard and V. Rokhlin. *A Fast Adaptive Multipole Algorithm in Three Dimensions*. Journal of Computational Physics, vol. 155, no. 2, pages 468–498, 1999.

[Cheng 2006] H. Cheng, W. Y. Crutchfield, Z. Gimbutas, L. F. Greengard, J. F. Ethridge, J. Huang, V. Rokhlin, N. Yarvin and J. Zhao. *A wideband fast multipole method for the Helmholtz equation in three dimensions.* J. Comput. Phys., no. 216, pages 300–325, 2006.

[Chew 1992] W.C. Chew. *Recurrence relations for three-dimensional scalar addition theorem.* J. Electromagn. Waves Appl., vol. 6, no. 1-6, pages 133–142, 1992.

[Chew 1997] W.C. Chew, J.-M. Jin, C.-C. Lu, E. Michielssen and J. Song. *Fast Solution Methods in Electromagnetics*. IEEE Trans. Antennas Propag, vol. 45, no. 3, pages 533–543, 1997.

[Coifman 1993] R. Coifman, V. Rokhlin and S. Wandzura. *the fast multipole method*. IEEE Trans Antennas Propagat., no. 35, pages 7–12, 1993.

[Collins 1993] M. D. Collins. *A split-step Padé solution for the parabolic equation method*. J. Acoust. Soc. Am., vol. 93, no. 4, pages 1736–1742, 1993.

[Cruse 1969] T. A. Cruse. *Numerical solutions in three dimensional elastostatics*. Int. J. Solids Struct., vol. 5, pages 1259–1274, 1969.

[Cruse 1974] T. A. Cruse. *An improved boundary-integral equation method for three-dimensional elastic stress analysis*. Computers Structures, vol. 4, pages 741–754, 1974.

[Dangla 2005] P. Dangla, J. F. Semblat, H. Xiao and N. Delépine. *A Simple and Efficient Regularization Method for 3D bem: Application to Frequency-Domain Elastodynamics*. Bulletin of the Seismological Society of America, no. 95, pages 1928–1939, october 2005.

[Darve 2000] E. Darve. *The fast multipole method I: Error analysis and asymptotic complexity*. Journ. Numeric. Anal., vol. 38, no. 1, pages 98–128, 2000.

[Directive 2002/49/EC] Directive 2002/49/EC. *Directive 2002/49/EC of the European parliement and of the council of 25 June 2002 relating to the assessment and management of environmental noise*. http://eur-lex.europa.eu/legal-content/EN/TXT/?uri=CELEX:32002L0049.

[Dongarra 2000] J. Dongarra and F. Sullivan. *The top ten algorithms*. Comput. Sci. Eng., vol. 2, pages 22–23, 2000.

[Driscoll 1994] J. R. Driscoll and D. M. Healy. *Computing Fourier Transforms and Convolutions on the 2-Sphere.* Adv. Appl. Math., vol. 15, pages 202–250, 1994.

[Engquist 2007] B. Engquist and L. Ying. *Fast directional multilevel algorithms for oscillatory kernels*. SIAM J. Sci. Comput., vol. 29, no. 4, pages 1710–1737, 2007.

[Epton 1995] M. A. Epton and B. Dembart. *Multipole translation theory for the three-dimensional Laplace and Helmholtz equations.* Journal on Scientific Computing., vol. 16, no. 4, pages 865–897, 1995.

[Ergül 2008] Ö. Ergül and L. Gürel. *Efficient parallelization of the multilevel fast multipole algorithm for the solution of large-scale scattering problems*. IEEE Trans. Antennas Propag, vol. 56, no. 8, pages 2335–2345, august 2008.

[Ergül 2009] Ö. Ergül and L. Gürel. *A Hierarchical Partitioning Strategy for an Efficient Parallelization of the Multilevel Fast Multipole Algorithm*. IEEE Trans. Antennas Propag, vol. 57, no. 6, pages 1740–1750, june 2009.

[FastBEM software 2014] FastBEM software. *FastBEM Acoustics® version 4.0*. Advanced CAE Research, Cincinnatti, Ohio, USA, 2014.

[Fischer 2004] M. Fischer, U. Gauger and L. Gaul. *A multipole Galerkin boundary element method for acoustics*. Engineering Analysis with Boundary Elements, vol. 28, pages 155–162, 2004.

[Gauvreau 2002] B. Gauvreau, M. Bérangier, P. Blanc-Benon and C. Depollier. *Traffic noise prediction with the parabolic equation method: Validation of a split-step Padé approach in complex environments*. J. Acoust. Soc. Am., vol. 112, no. 6, 2002.

[Gilbert 1989] K. E. Gilbert and M. J. White. *Application of the parabolic equation to sound propagation in a refracting atmosphere*. J. Acoust. Soc. Am., vol. 85, no. 2, pages 630–637, 1989.

[Gimbutas 2009] Z. Gimbutas and L. Greengard. *A fast and stable method for rotating spherical harmonic expansions*. Journal of Computational Physics, vol. 228, pages 5621–5627, 2009.

[Glassner 1989] A. S. Glassner. An introduction to ray tracing. Academic Press, London, 1989.

[Gomez 1997] J. E. Gomez and H. Power. *A multipole direct and indirect BEM for 2D cavity flow at low Reynolds number*. Engineering Analysis with Boundary Elements, vol. 19, pages 17–31, 1997.

[Grasso 2012] E. Grasso. *Modelling visco-elastic seismic wave propagation: a fast-multipole boundary element method and its coupling with finite elements*. PhD thesis, Paris-Est University, 2012.

[Greengard 1987] L. Greengard and V. Rokhlin. *A fast algorithm for particle simulations.* Journal of Comput. Phys., no. 73, pages 325–348, 1987.

[Gumerov 2001] N. A. Gumerov and R. Duraiswami. *Fast, exact, and stable computation of multipole translation and rotation coefficients for the 3-D Helmholtz equation*. Rapport technique CS-TR-4264, Institute for Advanced Computer Studies, University of Maryland, september 2001.

[Gumerov 2003] N. A. Gumerov and R. Duraiswami. *Recursions for the computation of multipole translation and rotation coefficients for the 3-d helmholtz equation*. SIAM (Soc. Ind. Appl. Math.) J. Sci. Comput., vol. 25, no. 4, pages 1344–1381, 2003.

[Gumerov 2004] N. A. Gumerov and R. Duraiswami. Fast multipole methods for the Helmholtz equation in three dimensions. Elsevier, 2004.

[Gumerov 2009] N. A. Gumerov and R. Duraiswami. *A broadband fast multipole accelerated boundary element method for the three dimensional Helmholtz equation*. J. Acoust. Soc. Am., vol. 125, no. 1, pages 191–205, 2009.

[Gumerov 2012] N. A. Gumerov, K. Berlin, D. Fushman and R. Duraiswami. *A hierarchical algorithm for fast Debye summation with application to small angle scattering.* Journal of Computational Chemistry, vol. 33, no. 25, pages 1981–1996, 2012.

[Gumerov 2014] Nail A. Gumerov and R. Duraiswami. Recursive computation of spherical harmonic rotation coefficients of large degree, arXiv: 1403.7698. 2014.

[Hamdi 1982] M. A. Hamdi. *Formulation variationnelle par équations intégrales pour le calcul de champs acoustiques linéaires proches et lointains*. PhD thesis, Université de Technologie de Compiègne, juin 1982.

[Hanish 1981] S. Hanish. *A treatise on Acoustical Radiation*. Naval Research Laboratory, Washington DC, 1981.

[Heimann 2007] D. Heimann. *Three dimensional linearised Euler model simulations of sound propagation in idealised urban situations with wind effects*. Applied Acoustics, vol. 68, pages 217–237, 2007.

[Hornikx 2012] M Hornikx, Y Smyrnova, T Van Renterghem, C Cheal and J Kang. *Acoustic simulation tools for urban streets, squares and road-side courtyards integrating vegetation*. Rapport technique FP7 HOSANNA Deliverable 5.3, 2012.

[Huijssen 2012] J. Huijssen, P. Fiala, R. Hallez, S. Donders and W. Desmet. *Numerical evaluation of source–receiver transfer functions with the Fast Multipole Boundary Element Method for predicting pass-by noise levels of automotive vehicles*. Journal of Sound and Vibration, vol. 331, pages 2080–2096, 2012.

[ISO 9613-2: 1996] ISO 9613-2:. *Acoustique – Atténuation du son lors de sa propagation à l'air libre – Partie 2: Méthode générale de calcul*. 1996.

[Jakob-Chien 1997] R. Jakob-Chien and B. Alpert. *A fast spherical filter with uniform resolution.* J. Comput. Phys., vol. 136, no. 2, pages 580–584, 1997.

[Jaswon 1963] M. A. Jaswon. *Integral equation methods in potential theory. I.* Proc. R. Soc. London A, vol. 275, pages 23–32, 1963.

[Jean 1998] P. Jean. *A variational approach for the study of outdoor sound propagation and application to railway noise*. Journal of Sound and Vibration, vol. 212, pages 275–294, 1998.

[Jean 2008] P. Jean, N. Noé and F. Gaudaire. *Calculation of tyre noise radiation with a mixed approach*. Acta Acustica, vol. 93, no. 1, pages 91–103, 2008.

[Joyce 1974] W. B. Joyce. *Classical-particle description of photons and phonons*. Physical Review D., vol. 9, no. 12, pages 3234–3256, 1974.

[Kang 2001] J Kang. *Sound propagation in interconnected urban streets: a parametric study*. Environment and Planning B: Planning and design, vol. 28, pages 281–294, 2001.

[Kang 2002a] J Kang. *Numerical Modelling of the Sound Fields in Urban Streets With Diffusely Reflecting Boundaries*. Journal of Sound and Vibration, vol. 258, no. 5, pages 793–813, 2002.

[Kang 2002b] J Kang. *Numerical modelling of the speech intelligibility in dining spaces*. Applied Acoustics, vol. 63, pages 1315–1333, 2002.

[Kang 2005] J Kang. *Numerical modeling of the sound fields in urban squares.* J. Acoust. Soc. Am., vol. 117, no. 6, pages 3695–3706, 2005.

[Kang 2007] J Kang. Urban Sound Environment. Taylor & Francis, 2007.

[Kirkup 2007] S. Kirkup. The boundary element method in acoustics. Integrated Sound Software, 2007.

[Kupradze 1979] V. D. Kupradze. Three-dimensional problems of the mathematical theory of elasticity and thermoelasticity. North-Holland, 1979.

[Lambert 1984] J. Lambert, F. Simonnet and M. Vallet. *Patterns of behaviour in dwellings exposed to road traffic noise*. Journal of Sound and Vibration, vol. 92, pages 159–172, 1984.

[Le Pollès 2003] T. Le Pollès. *Modélisation des champs diffus en acoustique architecturale par la théorie des transport : Application aux milieu urbain*. PhD thesis, Université du Maine, le Mans, France, 2003.

[Lercher 1998] P. Lercher. *Deviant dose-response curves for traffic noise in sensitive areas*. In Proceedings of Inter-Noise, New Zealand, 1998.

[Lewers 1993] T. Lewers. *A Combined Beam Tracing and Radiant Exchange Computer Model of Room Acoustics*. Applied Acoustics, vol. 38, pages 161–178, 1993.

[Li 2010] S. Li and Q. Huang. *An improved form of the hypersingular boundary integral equation for exterior acoustic problems*. Engineering Analysis with Boundary Elements, vol. 34, pages 189–195, 2010.

[Li 2011a] S. Li and Q. Huang. *A fast multipole boundary element method based on the improved Burton–Miller formulation for three-dimensional acoustic problems*. Engineering Analysis with Boundary Elements, vol. 35, pages 719–728, 2011.

[Li 2011b] S. Li and Q. Huang. *A new fast multipole boundary element method for two dimensional acoustic problems*. Comput. Method Appl. Mech. Engrg, vol. 200, pages 1333–1340, 2011.

[Lihoreau 2006] B. Lihoreau, B. Gauvreau, M. Bérangier, P. Blanc-Benon and I. Calmet. *Outdoor sound propagation modeling in realistic environments: Application of coupled parabolic and atmospheric models*. J. Acoust. Soc. Am., vol. 120, no. 1, 2006.

[Liu 1991] Y. Liu and T. J. Rudolphi. *Some identities for fundamental solutions and their applications to weakly-singular boundary element formulations*. Engineering Analysis with Boundary Elements, vol. 8, no. 6, 1991.

[Liu 2008] Y. J. Liu. *A new fast multipole boundary element method for solving 2-D Stokes flow problems based on a dual BIE formulation,*. Engineering Analysis with Boundary Elements, vol. 32, pages 139–151, 2008.

[Liu 2009] Y. Liu. Fast multipoles boundary element method : Theory and applications in engineering. Cambridge, 2009.

[Marburg 2003] S. Marburg and S. Schneider. *Performance of iterative solvers for acoustic problems. Part I. Solvers and effect of diagonal preconditioning*. Engineering Analysis with Boundary Elements, vol. 27, pages 727–750, 2003.

[Marburg 2005] S. Marburg and S. Amini. *Cat's eye radiation with boundary elements: comparative study on treatement of irregular frequencies*. Journal of Comput. Ac., vol. 13, no. 1, pages 21–45, 2005.

[Markovic 1998] V. Markovic. *Efficient numerical solution for nonuniform field in a rectangular room*. Acta Acustica, vol. 84, pages 570–572, 1998.

[Marquis-Favre 2005] C. Marquis-Favre, E. Premat and D. Aubrée. *Noise and its effects - a review on qualitative aspects of sound. Part II: noise and annoyance.* Acta Acustica united with Acustica, vol. 91, pages 622–642, 2005.

[Matsumoto 2010] T. Matsumoto, C. Zheng, S. Harada and T. Takahashi. *Explicit evaluation of hypersingular boundary integral equation for 3-D Helmholtz equation discretized with constant triangular element*. Journal of Comput. Sc. and Tech., vol. 4, pages 194–206, 2010.

[Meyer 1978] W. L. Meyer, W. A. Bell and B. T. Zinn. *Boundary integral solutions of three dimensional acoustic radiation problems*. Journal of Sound and Vibration, vol. 59, no. 2, pages 245–262, 1978.

[Morse 1936] P.M. Morse. Vibration and sound. Mc graw-hill, new york édition, 1936.

[Morse 1968] P.M. Morse and K. U. Ingard. Theoretical acoustics. Mc graw-hill, new york édition, 1968.

[Nelson 1980] J. P. Nelson. *Airport and property values: a survey of recent evidence.* Journal of Transport Economics and Policy, vol. 14, pages 37–52, 1980.

[Nelson 1982] J. P. Nelson. *Highway noise and property values: a survey of recent evidence*. Journal of Transport Economics and Policy, vol. 16, pages 117–138, 1982.

[Noé 2011] N. Noé, N. Hermant, C. Rougier and I. Schmich. *A Hybrid Beam and Particle Tracing Solution for Accurate Time Response Prediction of Rooms*. In Proceedings of the Forum Acusticum 2011 Aalborg, Aalborg, Denmark, 2011. Forum Acusticum.

[Ochmann 2002] M. Ochmann and F. P. Mechel. Analytical and numerical methods in acoustics, chapitre O, pages 930–1023. F. P. Michel, 2002.

[Ochmann 2004] M. Ochmann. *The complex equivalent source method for sound propagation over an impedance plane*. J. Acoust. Soc. Am., vol. 116, no. 6, pages 3304–3311, 2004.

[Ochmann 2008] M. Ochmann and H. Brick. Acoustical radiation and scattering above an impedance plane, volume Computational Acoustics of Noise Propagation in Fluids. Finite and Boundary Element Methods. Springer-Verlag, Berlin, 2008.

[Osetrov 2005] A. Osetrov and M. Ochmann. *A fast and stable numerical solution for acoustic boundary element method equations combined with the Burton and Miller method for models consisting of constant elements*. JCA, vol. 13, pages 1–20, 2005.

[Picaut 1997] J. Picaut, J.-D. Polack and L. Simon. *A mathematical model of diffused sound field based on a diffusion equation*. Acta Acustica, vol. 83, no. 4, pages 614–621, 1997.

[Picaut 1998] J. Picaut. *Modélisation des champs diffus par une équation de diffusion. Application à l'acoustique des salles et à l'acoustique urbaine*. PhD thesis, Université du Maine, le Mans, France, 1998.

[Picaut 1999] J. Picaut and L. Simon. *Sound field in long rooms with diffusely reflecting boundaries*. Applied Acoustics, vol. 56, pages 217–240, 1999.

[Picaut 2005] J. Picaut, T. Le Pollès, P. L'Hermite and V. Gary. *Experimental study of sound propagation in a street*. Applied Acoustics, vol. 66, pages 149–173, 2005.

[Picaut 2006] J. Picaut. *Modélisation des champs diffus en acoustique architecturale et urbaine par un processus de diffusion de l'énergie sonore*. Habilitation a diriger des recherches, 2006.

[Pierce 1981] A. Pierce. Acoustics. An introduction to its physical principles and applications. Mc Graw-Hill, 1981.

[Rayleigh 1904] J. W. Strutt Lord Rayleigh. *On the acoustic shadow of a sphere*. Phil. Trans. R. Soc. Lond. Ser., vol. 203, pages 87–89, 1904.

[Rego Silva 1994] J. J. Rego Silva. Acoustic and elastic wave scattering using boundary elements. Computational Mechanics Publications, 1994.

[Rizzo 1967] F. J. Rizzo. *An integral equation approach to boundary value problems of classical elastostatics*. Quart. Appl. Math., vol. 25, pages 83–95, 1967.

[Rizzo 1977] F. J. Rizzo and D. J. Shippy. *An advanced boundary integral equation method for three-dimensional thermoelasticity*. Int. J. Numer. Methods Eng, vol. 11, pages 1753–1768, 1977.

[Rokhlin 1985] V. Rokhlin. *Rapid solution of integral equations of classical potential theory.* Journ. of Comput. Phys., vol. 60, no. 3, pages 187–207, 1985.

[Rokhlin 1993] V. Rokhlin. *Diagonal forms of translation operators for the Helmholtz equation in three dimensions*. Applied and Computational Harmonic Analysis, vol. 1, pages 82–93, 1993.

[Rosen 1995] E. M. Rosen, F. X. Canning and L. S. Couchman. *A sparse integral equation method for acoustic scattering*. J. Acoust. Soc. Am., vol. 98, pages 599–610, 1995.

[Saad 1986] Y. Saad and M. Shultz. *GMRES: A generalized minimal residual algorithm for solving non-symmetric linear systems*. SIAM Journal on Scient. and Stat. Comput., vol. 7, no. 3, 1986.

[Saad 2003] Y. Saad. Iterative methods for sparse linear system. SIAM, 2nd édition, 2003.

[Sakuma 2002] T. Sakuma and Y. Yasuda. *Fast multipole boundary element method for large-scale steady-state sound field analysis. Part I: setup and validation*. Acta Acustica united with Acustica, vol. 88, pages 513–525, 2002.

[Salomons 2001] E. M. Salomons. Computational atmospheric acoustics. Kluwer Academic Publisher, 2001.

[Salomons 2002] E. M. Salomons, R. Blumrich and D. Heimann. *Eulerian time-domain model for sound propagation over a finite-impedance ground surface*. Acta Acustica united with Acustica, vol. 88, pages 483–492, 2002.

[Sarabandi 2004] K. Sarabandi and I-S. Koh. *Fast multipole representation of Green's function for an impedance half-space*. IEEE Trans. Antennas Propag, vol. 52, no. 1, pages 296–301, 2004.

[Schenck 1967] H. A. Schenck. *Improved integral formulation for acoustic radiation problems*. J. Acoust. Soc. Am., vol. 44, pages 41–58, 1967.

[Schneider 2003] S. Schneider. *Application of fast methods for acoustic scattering and radiation problems*. Journal of Computational Acoustics, vol. 11, pages 387–401, 2003.

[Shen 2006] L. Shen and Y. Liu. *An adaptive fast multipole boundary element method for three-dimensional acoustic wave problems based on the Burton-Miller formulation*. Comput. Mechanics, vol. 40, no. 3, pages 461–472, 2006.

[Shen 2007] L. Shen. *Adaptive Fast Multipole Boundary Element Methods for three-dimensional potential and acoustic wave problems*. PhD thesis, University of Cincinnati, 2007.

[Siegel 2001] R. Siegel and J. Howell. Thermal Radiation Heat Transfer, fourth Edition. CRC Press, 2001.

[Song 1997] J. Song, C.-C. Lu and W.C. Chew. *Multilevel Fast Multipole Algorithm for Electromagnetic Scattering by Large Complex Objects*. IEEE Trans. Antennas Propag, vol. 45, no. 10, pages 1488–1493, 1997.

[Swarztrauber 2000] P. N. Swarztrauber and W. F. Spotz. *Generalized discrete spherical harmonic transforms*. J. Comput. Phys., vol. 159, no. 2, pages 213–230, 2000.

[Sylvand 2002] S. Sylvand. *La méthode multipôle rapide en électromagnétisme. Performances, parallélisation, applications. In French.* PhD thesis, école nationale des ponts et chaussées, juin 2002.

[Symm 1963] G. T. Symm. *Integral equation methods in potential theory. II*. Proc. R. Soc. London A, vol. 275, pages 33–46, 1963.

[Terai 1980] T. Terai. *On calculation of sound fields around three dimensional objects by integral equation methods*. Journal of Sound and Vibration, vol. 69, no. 1, pages 71–100, 1980.

[Terrasse 2007] I Terrasse and T Abboud. *Modélisation des phénomènes de propagation d'ondes*. Département de mathematiques appliquées, École polytechnique, 2007.

[Thierry 2011] B. Thierry. *Analysis and Numerical Simulations of Time Reversal and Multiple Scattering*. PhD thesis, Université Henri Poincaré, Nancy I, 2011.

[Van Maercke 1993] D. Van Maercke and J. Martin. *The prediction of echograms and impulse responses within the Epidaure software*. Applied Acoustics, vol. 38, pages 93–114, 1993.

[Van Renterghem 2003] T. Van Renterghem and D. Bottledooren. *Numerical simulation of the effect of trees on downwind noise barrier performance*. Acta Acustica united with Acustica, vol. 89, pages 764–778, 2003.

[Van Renterghem 2005] T. Van Renterghem, E. M. Salomons and D. Bottledooren. *Efficient FDTD-PE model for sound propagation in situations with complex obstacles and wind profiles*. Acta Acustica united with Acustica, vol. 91, pages 671–679, 2005.

[Van Renterghem 2006] T. Van Renterghem, E. M. Salomons and D. Bottledooren. *Parameter study of sound propagation between city canyons with coupled FDTD-PE model*. Applied Acoustics, vol. 67, pages 487–510, 2006.

[Walters 1975] A. A. Walters. Noise and prices. London: Oxford University Press, 1975.

[White 1989] M. J. White and K. E. Gilbert. *Application of the Parabolic Equation to the Outdoor Propagation of Sound*. Applied Acoustics, vol. 27, pages 227–238, 1989.

[WHO 2011] *Burden of disease from environmental noise. Quantification of healthy life years lost in Europe*. http://www.euro.who.int/en/health-topics/environment-and-health/noise/publications, World Health Organization, 2011.

[WHO 2014] *World Health Organization website*. http://www.who.int/topics/urban_health/en/, 2014.

[Wilson 1978] R. B. Wilson and T. A. Cruze. *Efficient implementation of anisotropic three-dimensional boundary integral equation stress analysis*. Int. J. Numer. Methods Eng, vol. 12, pages 1383–1397, 1978.

[Yasuda 2005] Y. Yasuda and T. Sakuma. *A technique for plane-symmetric sound field analysis in the fast multipole boundary element method*. Journal of Computational Acoustics, vol. 13, pages 71–85, 2005.

[Yasuda 2007] Y. Yasuda, S. Sakamoto, Y. Kosaka, T. Sakuma, N. Okamoto and T. Oshima. *Numerical analysis of large-scale sound fields using iterative methods part I: application of Krylov subspace methods to boundary element analysis*. Journal of Computational Acoustics, vol. 15, pages 449–471, 2007.

[Yasuda 2012] Y. Yasuda, K. Higuchi and T. Oshima. *Efficient technique in low-frequency fast multipole boundary element method for plane-symmetric acoustic problems*. Engineering Analysis with Boundary Elements, vol. 36, pages 1493–1501, 2012.

Publication lists

- X. Vuylsteke, T. Leissing, P. Jean and J.-F. Semblat. *Fast multipole boundary element method applied to acoustic waves propagation in urban environments for a realistic geometry.* Wave Motion, under review.
- X. Vuylsteke, T. Leissing, P. Jean and J.-F. Semblat. *Computing resources to solve acoustic propagation problems in urban environments with the fast multipole boundary element method.* In Proceedings of the Forum Acusticum 2014 Krakow, Krakow, Poland, 2014. Forum Acusticum.
- X. Vuylsteke, T. Leissing, P. Jean and J.-F. Semblat. *Méthode multipolaire rapide des éléments de frontière appliquée aux problémes de propagation acoustique en espace urbain.* In Proceedings of the Congrès Français d'acoustique 2014 Poitiers, Poitiers, France, 2014. Congrès Franąis d'acoustique.
- X. Vuylsteke, T. Leissing, P. Jean and J.-F. Semblat. *Fast multipole boundary element method applied to acoustic propagation in urban area.* In Proceedings of Internoise 2013 Innsbruck, Innsbruck, Austria, 2013. Internoise

Résumé

Décrit comme l'un des algorithmes les plus prometteurs du 20ème siècle, le formalisme multipolaire appliqué à la méthode des éléments de frontière, permet de nos jours de traiter de larges problèmes encore inconcevables il y a quelques années. La motivation de ce travail de thèse est d'évaluer la capacité, ainsi que les avantages concernant les ressources numériques, de ce formalisme pour apporter une solution de référence aux problèmes de propagation sonore tri-dimensionnels en environnement urbain, dans l'objectif d'améliorer les algorithmes plus rapides déjà existants.
Nous présentons la théorie nécessaire à l'obtention de l'équation intégrale de frontière pour la résolution de problèmes non bornés. Nous discutons également de l'équation intégrale de frontière conventionnelle et hyper-singulière pour traiter les artefacts numériques liés aux fréquences fictives, lorsque l'on résout des problèmes extérieurs. Nous présentons par la suite un bref aperçu historique et technique du formalisme multipolaire rapide et des outils mathématiques requis pour représenter la solution élémentaire de l'équation de Helmholtz. Nous décrivons les principales étapes, d'un point de vue numérique, du calcul multipolaire.
Un problème de propagation sonore dans un quartier, composé de 5 bâtiments, nous a permis de mettre en évidence des problèmes d'instabilités dans le calcul par récursion des matrices de translations, se traduisant par des discontinuités sur le champ de pression de surface et une non convergence du solveur. Ceci nous a conduit à considérer le travail très récent de Gumerov et Duraiswamy en lien avec un processus récursif stable pour le calcul des coefficients des matrices de rotation. Cette version améliorée a ensuite été testée avec succès sur un cas de multi diffraction jusqu'à une taille adimensionnelle de problème de 207 longueur d'ondes.
Nous effectuons finalement une comparaison entre un algorithme d'élément de frontière, *Micado3D*, un algorithme multipolaire et un algorithme basé sur le tir de rayons, Icare®, pour le calcul de niveaux de pression moyennés dans une cour ouverte et fermée. L'algorithme multipolaire permet de valider les résultats obtenus par tir de rayons dans la cour ouverte jusqu'à 300 Hz (i.e. 100 longueur d'ondes), tandis que concernant la cour fermée, zone très sensible par l'absence de contributions directes ou réfléchies, des études complémentaires sur le préconditionnement de la matrice semblent requises afin de s'assurer de la pertinence des résultats obtenus à l'aide de solveurs itératifs.

Mots-clés : Méthode des éléments de frontière, méthode multipolaire rapide, acoustique urbaine, propagation des ondes, Équation d'Helmholtz, acoustique numérique.

Abstract

Described as one of the best ten algorithms of the 20th century, the fast multipole formalism applied to the boundary element method allows to handle large problems which were inconceivable only a few years ago. Thus, the motivation of the present work is to assess the ability, as well as the benefits in term of computational resources provided by the application of this formalism to the boundary element method, for solving sound propagation problems and providing reference solutions, in three dimensional dense urban environments, in the aim of assessing or improving fast engineering tools.
We first introduce the mathematical background required for the derivation of the boundary integral equation, for solving sound propagation problems in unbounded domains. We discuss the conventional and hyper-singular boundary integral equation to overcome the numerical artifact of fictitious eigen-frequencies, when solving exterior problems. We then make a brief historical and technical overview of the fast multipole principle and introduce the mathematical tools required to expand the elementary solution of the Helmholtz equation and describe the main steps, from a numerical viewpoint, of fast multipole calculations.
A sound propagation problem in a city block made of 5 buildings allows us to highlight instabilities in the recursive computation of translation matrices, resulting in discontinuities of the surface pressure and a no convergence of the iterative solver. This observation leads us to consider the very recent work of Gumerov & Duraiswamy, related to a "stable" recursive computation of rotation matrices coefficients in the RCR decomposition. This new improved algorithm has been subsequently assessed successfully on a multi scattering problem up to a dimensionless domain size equal to 207 wavelengths.
We finally performed comparisons between a BEM algorithm, *Micado3D*, the FMBEM algorithm and a ray tracing algorithm, Icare®, for the calculation of averaged pressure levels in an opened and closed court yards. The fast multipole algorithm allowed to validate the results computed with Icare in the opened court yard up to 300 Hz, (i.e. 100 wavelengths), while in the closed court yard, a very sensitive area without direct or reflective fields, further investigations related to the preconditioning seem required to ensure reliable solutions provided by iterative solver based algorithms.

Keywords: Boundary element method, fast multipole method, urban acoustics, wave propagation, Helmholtz equation, computational acoustics.